



AFS-09-0276

August 6, 2009

ATTN: Document Control Desk  
Director, Spent Fuel Project Office  
Office of Nuclear Material Safety and Safeguards  
**U.S. Nuclear Regulatory Commission**  
Washington, DC 20555-0001

**Subject:** RESPONSE TO REQUEST FOR ADDITIONAL INFORMATION DATED JUNE 29, 2009 FOR THE BRR PACKAGE, REVISION 1, DOCKET No. 71-9341

Dear Sirs:

AREVA Federal Services LLC hereby submits responses to the NRC request for additional information (RAI), letter dated June 29, 2009, and the corresponding revised Safety Analysis Report (SAR) pages. The individual responses to each RAI are given in Attachment A to this letter. Revised page remove/replace instructions are given in Attachment B. Also included with this letter are the following documents:

- One paper copy of the revised pages of the Safety Analysis Report for updating the three ring binder containing revision 0.
- One electronic copy of Revision 1 of the SAR is provided in PDF format.
- Thermal analysis computer input and output files and a PDF of the thermal calculation which supports Chapter 3 of the SAR.
- Source term calculation packages (as PDF files) prepared by the MURR, MITR-II, and ATR reactor sites.

The electronic copy of the SAR and other computer files are contained on two CDs in an envelope labeled, "BRR Package Docket 71-9341 Rev. 1 Electronic Copy of Documents". The contents of the CDs are provided in the table below.

If there are any questions or comments please contact me at (253) 552-1367 or by email at [charles.temus@areva.com](mailto:charles.temus@areva.com).

AREVA Federal Services LLC

1102 Broadway Plaza, Suite 300, Tacoma, WA 98402-3526 – USA – Tel: 1 253.383.9000 – Fax: 1 253.383.9002

71-9341  
NM 5501  
Received w/o CDs.  
Process as is  
per Michelle  
deBose.



Very Truly Yours,  
Areva Federal Services LLC

A handwritten signature in black ink, appearing to read 'Charles J. Temus'.

Charles J. Temus  
Project Manager

Encl: as noted

cc: Chris Staab, NRC-NMSS

Files on the attached CDs:

File name	Description
<b>CD #1</b>	
001 BRR Package SAR R1 Complete.pdf	Entire BRR Package SAR, Revision 1
(Folder) Thermal Analysis Files	Reference files useful in Chapter 3 review
<b>CD #2</b>	
(Folder) Source Term Calculation Files	Source term calculations for MURR, MITR-II, and ATR fuel

## ATTACHMENT A

### Docket No. 71-9341, Model No. BRR Package Responses to NRC Request for Additional Information

#### General Information

- 1-1 Revise Section 1.2.2 to clarify that only one fuel element is allowed per basket port. Revise Sections 1.2.2.1, 1.2.2.2, and 1.2.2.3 to clarify the maximum U-235 depletion percentage.

The TRIGA Fuel Parameter table clearly indicates maximum U-235 depletion percentages for each TRIGA fuel type. However, the MURR, MITR-II, and ATR fuel details do not. The applicant should compare the presentation of fresh fuel characteristics for all fuel types to determine whether additional inconsistencies exist and revise as appropriate.

This information is needed to determine compliance with 10 CFR 71.33.

**Response:** Section 1.2.2 has been revised to clarify that only one fuel element is allowed per basket location. The maximum U-235 depletion percentage has been added for the MURR, MITR-II, and ATR fuel types. No other inconsistencies were identified.

- 1-2 On page 1.2-1 of the application, add description of the package containment boundary to section 1.2.1.1, "Cask Body," by identifying the associated metal structural components that must be evaluated to meet the proposed Category I package fabrication criteria, per NUREG/CR-3854, "Fabrication Criteria for Shipping Containers."

Section 1.2.1.1 of the application is unclear as to what the package containment boundary is composed of. Section 2.1.2 provides that the BRR package is designated a Category I container.

10 CFR 71.33(a)(4) requires that package containment boundary be properly identified in the application.

**Response:** A description of the containment boundary has been added to Chapter 1 in Section 1.2.1.1, including Figure 1.2-12. This information is also found in Section 4.1.1.

- 1-3 Revise Section 1.2.1.1 and others, alike, of the application, to recognize that the American Society of Mechanical Engineers (ASME), Section III, Subsection NB, pedigree materials must be used for metal components for fabricating the containment boundary of the package.

Use of the ASME pedigree materials, such as SA182, rather than ASTM A182, Type 304 for the body inner shell is necessary to meet the NUREG/CR-3854 guidelines for Category I shipping containers.

This information is needed to determine conformance with the guidelines provided in NUREG-1609, "Standard Review Plan for Transportation Packages for Radioactive Material."

**Response:** According to the ASME B&PV Code, a material specification which is prefixed by "SA-" (such as, for example, SA-240) consists of a material specification found in Section II, Part A (for ferrous materials), and a quality assurance "pedigree", as specified in Section III, Subsection NCA, paragraph NCA-3800.

## ATTACHMENT A

ASME B&PV Code, Section II, Part A specifications are generally identical to the ASTM specifications having the same number; for example, specification SA-240 from Section II, Part A, 2007 edition is noted in the heading as "Identical with ASTM Specification A240 / A240M-04". This is true for all of the materials used in the BRR package. Therefore, ASME SA- material is identical to ASTM A- material.

In addition, all of the materials used in the BRR package will be procured under a Part 71, Subpart H quality program. This program is required by the NRC in lieu of the Section III, Subsection NCA, paragraph NCA-3800 quality assurance provisions. Therefore, the use of ASTM A- materials in the BRR package is acceptable.

- 1-4 Revise Drawing 1910-01-01-SAR, as appropriate, (1) to allow use of only the ASME pedigree materials for the containment boundary components, and (2) to list also material alternatives, which have been evaluated as equivalents.

The specifications for materials and their equivalents, as described in Section 1.2.1.1 of the application must be properly captured in the licensing drawings.

This information is needed to determine compliance with 10 CFR 71.31(a).

**Response:** (1) The use of ASTM A- materials in the BRR package is acceptable, as discussed in the response to RAI 1-3. (2) The drawing has been revised to show all material alternatives in the "Specification" column. Flag notes are used as necessary to specify the inspection requirements that apply to each material type.

Additional changes were made to Drawing 1910-01-01-SAR: 1) Three circumferential welds have been corrected to include the "all-around" symbol which was lacking; 2) The seal weld of the thermal shield to the cask body was clarified.

- 1-5 Add edge design details, such as chamfer dimensions and corner radii, to the rib support disks of the fuel baskets depicted in Drawing 1910-01-03-SAR, sheets 2 and 3, of the application.

Sharp edges at support disk rims (e.g., Section F-F of sheet 2 and detail G of sheet 3) should be avoided or their bearing stress effects on the inner shell containment boundary be evaluated.

This information is needed to determine compliance with 10 CFR 71.31(a).

**Response:** Drawing 1910-01-03-SAR has been revised to show the size of the chamfer on each rib support plate for the applicable baskets. Section 2.7.1.5 of the application has been revised to show that, for the worst case basket (the ATR), at the bounding side drop impact of 120g and bounding temperature of 400 °F, the bearing stress between the basket and the inner shell of the cask is well below the yield point of the cask and basket materials. Therefore, a sharp corner on a support rib will have no effect on the integrity of the containment boundary.

An additional change was made to Drawing 1910-01-03-SAR: For tube material (item nos. 1, 2, 3, and 4), a material option of ASTM A511, Grade MT304, has been added. This material has the same strength as the existing material options.

## ATTACHMENT A

### Structural

- 2-1 Revise the third bullet in Section 2.1.2 of the application by removing the impact limiter shells from the cask components being classified and stipulated to meet the ASME Section III, Subsection NF requirements. Similar citations of the same code provision in the application should also be revised.

The impact limiter shells are configured primarily for confining the polyurethane foam for ensuring that the package will meet the 10 CFR 71.73(c)(4) thermal test requirements. The permissible performance as a sacrificial structural entity, including large deformations and buckling, is not recognized in the Subsection NF code.

This information is needed to determine compliance with 10 CFR 71.31(a).

**Response:** It is acknowledged that Subsection NF does not in itself recognize the large deformations or buckling which is an integral part of the safety function of the impact limiter shells. However, Subsection NF is used for the impact limiter shells of many licensed packages, such as the TRUPACT-II Outer Containment Assembly (Docket 71-9218), the 72-B (71-9212), or the MFFP (71-9295). We note that Table 4.1 of NUREG/CR-3854 indicates Subsection NF for use in "Other Safety" structures, specifically including impact limiters. Furthermore, there is no published guidance from the NRC suggesting an alternative to Subsection NF that would be more acceptable. As shown on drawing 1910-01-02 SAR, the impact limiter welds are inspected per Article NF-5000. Therefore, classification of the impact limiter shells as Subsection NF components is appropriate and should be retained.

- 2-2 Revise Section 2.1.3 and Table 2.1-2 of the application to include information on weights and centers of gravity for all four loaded fuel baskets.

Weights of the loaded baskets vary substantively and their distributions also appear to be non-uniform along the axial direction of the package.

The "bounding" summary description does not meet the intent of the 10 CFR 71.33 requirements.

**Response:** Table 2.1-2 has been revised to include the individual weight and c.g. of each loaded basket, and the weight and c.g. of the BRR package when transporting each loaded basket.

- 2-3 In Section 2.3.1 of the application, justify the use of ASME Code, Subsection NE, Article NE-4220, for fabricating the containment shell.

Section 2.1.2, "Design Criteria," of the application designates the BRR package as Category I container. As such, the Subsection NB, Article NB-4200, fabrication provisions should be used to satisfy the NUREG/CR-3854 guidance.

This information is needed to determine conformance with the 10 CFR 71.31(a) requirements.

**Response:** The choice of ASME B&PV Code, Section III, Subsection NE, Article NE-4220 is based on the fact that the package cylindrical shells are verified for buckling performance using the ASME Code Case N-284-2. This Code Case is for Section III, Division 1, Class MC construction, and as stated in Section -1120 of the Code Case, "The basic Code buckling rules as well as the rules of this Code Case are based on the fabrication requirements of NE-4222." Therefore, it is appropriate to fabricate the BRR

## ATTACHMENT A

package using shell tolerances from NE-4220, rather than NB-4220. Incidentally, the tolerance requirements of NE-4220 and NB-4220 are identical for the BRR package shells. Section 2.3.1 has been revised to include a justification for using NE-4220.

- 2-4 For Section 2.7.1.6, "Fuel Impact Deformation," of the application, provide sketches and calculations to demonstrate that all relevant sections and parts of the fuel elements are considered in estimating the applicable cross-section areas,  $A_{xc}$ , for determining maximum fuel element axial deformations. Revise Table 2.7-5, "Fuel Impact Deformation Results," accordingly.

It's unclear whether the "side plates" as depicted in Figures 1.2-8 and 1.2-10 for the respective MURR and ART fuel are considered in calculating applicable cross-sectional areas. The section views suggest that large segments of the side plates are devoid of fuel plates, which will lead to markedly reduced  $A_{xc}$  to result in a much larger fuel deformation estimates for criticality control evaluation.

This information is needed to determine compliance with the requirements of 10 CFR 71.31(2) and 71.73 (c)(1).

**Response:** The analysis presented in Section 2.7.1.6 is intended to show that the deformation of the fuel-bearing region of the fuel elements is negligibly small under HAC. The fuel elements as manufactured include end structures that do not contain fissile material and are considered sacrificial under accident conditions. The criticality analysis considers only the active length of the fuel, which corresponds to the uniform cross-sectional areas denoted as  $A_{xc}$  in the structural evaluation. As part of the criticality evaluation, the active length of the fuel is moved to different positions in order to find the most reactive configuration, without regard to the presence of any end structures of the fuel. Since the end structures play no role in the criticality evaluation, it is not necessary to evaluate them structurally. The relevant structural response of the fuel is that of the active fuel region, which is part of the criticality evaluation. Therefore, the areas  $A_{xc}$  used in Section 2.7.1.6, and the results given in Table 2.7-5, are sufficient to demonstrate the criticality safety of the fuel assembly contents. Section 2.7.1.6 has been revised to include a justification for neglecting the fuel assembly end structures.

- 2-5 Compared to the deceleration response traces presented on pages 2.12.3-43 and 2.12.3-44 of the application, verify that the listed decelerations in Section 2.12.3.5.3 for the cask secondary end are properly reduced from test data for evaluating the HAC free drop accidents.

The listed peak decelerations may mistakenly lead to an impression that the impact limiters have undergone higher rigid body decelerations than they actually withstood. Even with some vibratory components superimposed on the rigid body motions, the response traces still show peak decelerations of less than about 100 g, which is below the listed maximum average of 107 g.

This information is needed to determine compliance with 10 CFR 71.31(a).

**Response:** The peak accelerations given in Section 2.12.3.5 are correct. Section 2.12.3.4.1 has been revised to clarify that the peak filtered accelerometer results are adjusted using the accelerometer calibration constants. This explanatory information had been mistakenly omitted from the initial submittal. The peak acceleration values shown in the text of Section 2.12.3.5 already include the calibration adjustments, and do not change. The adjustment is only made to the peak value of the accelerometer output, and

## ATTACHMENT A

not to the entire output, thus, the filtered accelerometer plots do not show the effect. Since the calibration constants are all between 0.89 and 0.97mV/g, the adjusted peak acceleration values given in Section 2.12.3.5 are up to approximately 10% higher than the peak value shown on the plots. A new table has been added to give the calibration constant for each accelerometer, and text has been added to explain how the adjustment was made.

- 2-6 With respect to the linearized stresses plotted in Figures 2.12.4-11, -16, and -22 of the application, (1) provide definition for the "total" stress intensity category, and (2) explain how the total stress intensity is considered in evaluating stress performance of the inner shell containment boundary, per the Table 2.1-1 stress limits.

It's unclear how the total stress intensity is computed and considered for the inner shell containment boundary. Table 2.1-1 does not identify a total stress intensity category for evaluating stress performance of the inner shell.

This information is needed to determine compliance with 10 CFR 71.73(c)(1).

**Response:** There are three stresses identified on the subject stress plots: membrane, membrane-plus-bending, and total. These stresses apply along a path which has been defined by the stress analyst to represent the worst case in critical regions of the structure. The membrane stress is the average, uniform stress across the cross-section that is necessary to maintain translational equilibrium; the bending stress is the non-uniform stress which is necessary to maintain moment equilibrium. The total stress is the actual stress in the cross-section, which when linearized produces the membrane and bending stresses. The difference between the total stress and the sum of membrane-plus-bending stress is the peak stress. The membrane and membrane-plus-bending stresses are evaluated against the stress criteria defined in Table 2.1-1. Total stress is conservatively evaluated in Section 2.7.4.3 by utilizing the ultimate stress,  $S_u$ , in lieu of the smaller total stress, in the evaluation of the extreme range of stress.

- 2-7 With respect to Section 2.12.5.1 of the application, provide CASKDROP calculations to demonstrate that the LAST-A-FOAM "lock-up" strain at 70% (per the General Plastics data sheets) is restricted only to local regions of the BRR impact limiters. Revise text, tables, and figures of Section 2.12.5, "Impact Limiter Performance Evaluation," as appropriate, to ensure that technical justifications are adequately substantiated for the following evaluations:

- (a) Criteria for acceptable percentage size of local regions to ensure that impact limiter lock-up effects will not result in unacceptable package structural performance.

Tables 2.12.5-11 through 2.12.5-14 report a maximum calculated strain of 82.7% for HAC drop test results. The lock-up strain and its acceptance criteria are generally BRR impact limiter-specific and the criteria need to be addressed for the expected level of strain, if justifiable.

- (b) Cask drop test response traces showing no large deceleration spikes possibly associated with occurrence of impact limiter lock-up.

Appropriate, unfiltered raw test data such as those described in Section 2.12.3.4 should be used to demonstrate that the impact limiters did not experience any

## ATTACHMENT A

lock-up for the test series. If lock-up did occur, its effects on the package structural performance must be evaluated.

- (c) Crush strengths at strain levels above 70%, in Tables 2.12.5-1 through 2.15.5-8, which are not part of LAST-A-FOAM data sheets.

Crush strength data, including those at a 95% strain, that are not part of the BRR evaluation should not be included in the application.

- (d) Impact limiter force-deflection curves, plotted in Figures 2.12.5-3 through 2.12.5-9, for various cask drop orientations.

The force-deflection curves are misleading, considering the geometry and dimensions, in Figure 2.12.5-2, for the impact limiter CASKDROP analysis. The force-deflection curves in all cases are shown to be applicable for "deflection" levels up to 100%, which is physically unattainable.

The above information is needed to determine compliance with 10 CFR 71.31(a) and 71.73(c)(1).

**Response:** In response to this question, several changes have been made to the impact limiter analytical evaluation given in Section 2.12.5:

1. The maximum foam bulk average temperature has been reduced from 180 °F to 150 °F, and all hot case results recalculated. As shown in Table 3.1-1 and Figure 3.3-2, the bulk average temperature of the polyurethane foam in the impact limiters under NCT hot conditions is a maximum of 146 °F. Thus, a bounding bulk average temperature of 150 °F is appropriate, especially considering that the foam typically crushed is on the outside of the limiter where the temperature is cooler than this value. The 180 °F value used in the original application was based on a very conservative temperature estimate made during the early design development.
2. Besides the change to the hot temperature, minor corrections to the package weight and center of gravity in the SLAPDOWN analysis models were made which corrected errors in the original analysis. These changes have a very small effect on the impact and crush deformation results at both temperature extremes.
3. Since the recalculated maximum foam strain is approximately 80% in the worst case (and is typically much less), the foam stress-strain property extrapolation is limited to a maximum strain of 80%. In the single case where strain exceeds 80% (the 15° slapdown orientation at hot temperature), the stress at a strain of 80% is used for the maximum strain of 83.2%, which conservatively maximizes the crush strain result.
4. The impact limiter force-deflection curves have, for the same reason, been limited to a limiter strain of approximately 80%.
5. A comparison of the foam stress-strain curve as extrapolated between a strain of 70% and 80% has been made with prior data published by the foam manufacturer, General Plastics, which carried out the curve explicitly to a strain of 80%. It is important to note that a strain of 70% does not constitute "lock up" for polyurethane foam. The stress-strain curve is becoming steeper at a strain of 70%, but because polyurethane foam is a cellular polymer, more deformation and energy absorption is possible. General Plastics published stress-strain data up to 80% strain until a few years ago. They have since revised the published data to a maximum of 70% strain because, per General Plastics, the foam is not efficient above this value. The behavior of foam may be contrasted to that of aluminum honeycomb, which



## ATTACHMENT A

has an almost vertical rise in force when it reaches a discrete "lock up". The compaction of foam is more gradual, and lacks a discrete "lock up" point.

The plot below shows the comparison between the foam data used in the application (obtained from General Plastics and shown in Figure 2.12.5-1 of the application) and the prior data published by General Plastics going up to 80% strain (both at 150 °F). Note that between zero and 70% strain, the two curves are quite similar, demonstrating that foam behavior has not changed significantly over time. The lower curve represents the data used in the application, and is extrapolated above 70% strain. The extrapolated region shows a relatively slow rise in stress compared to the upper curve, which represents the prior data. This is conservative, since it will tend to overestimate the total strain in the impact limiter. The prior data, since the stress in the 70% to 80% range is higher, would produce less strain and a higher resulting impact. To show the maximum possible force which would be expected in the hot (150 °F) case, the governing orientation (15° slakedown) was run using the prior data, increased by 10% to cover possible manufacturing variation. It is compared to the hot case result using the current foam stress-strain data, reduced by 10%. The result, as expected, is less strain and higher impact for the prior data, as shown in the table below:

Temperature: 150 °F Orientation: 15° slakedown	Impact (g)	Impact Limiter Deformation, in.
Current foam data, extrapolated, reduced by 10%* (maximum hot strain)	83.6	15.9
Prior foam data, increased by 10%* (minimum hot strain)	90.2	15.2

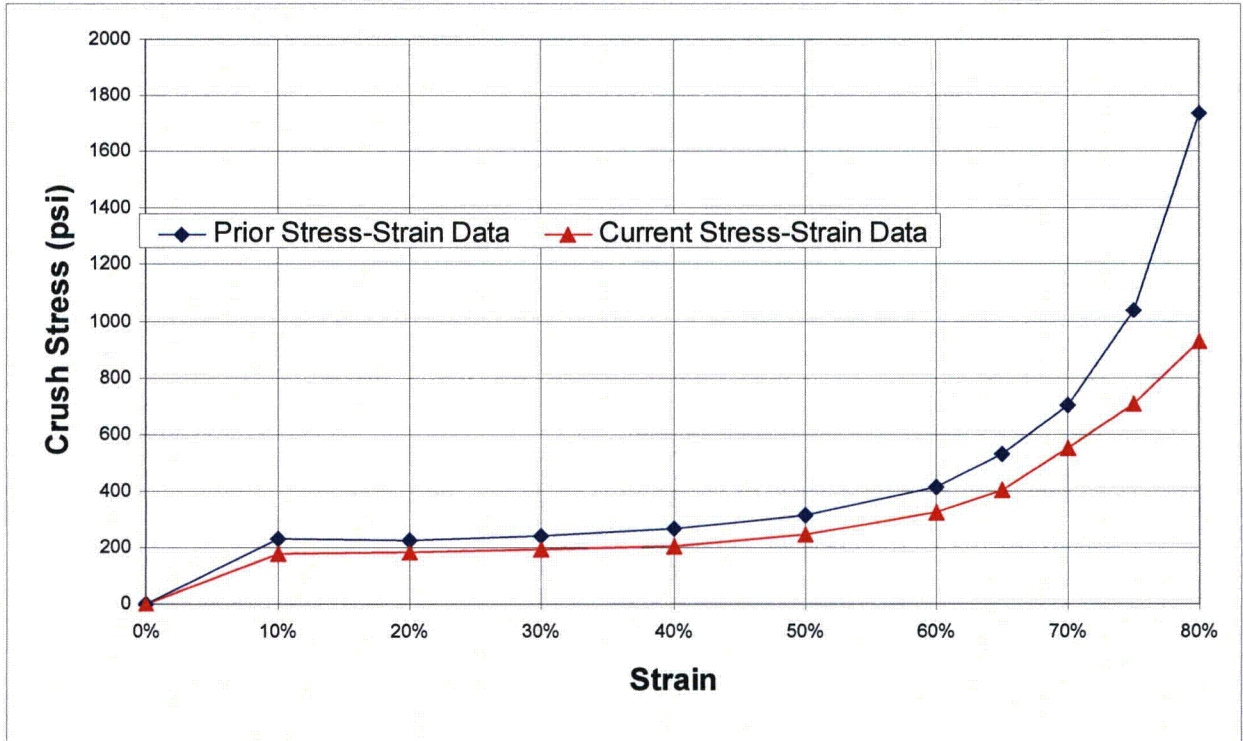
\*Stated percentage reduction or increase is applied to the entire curve, not just to the 70-80% strain region.

Note that these considerations have no effect on the maximum strain in the cold (-20 °F) case, since the cold case maximum strain is always below 70%. Note that the bounding value used for all package stress calculations is 120g, which is 33% higher than the largest calculated impact. Therefore it is concluded that the hot case foam stress-strain curve extrapolation up to 80% as used in the application is acceptable. Specific responses to the other questions are given below.

- a) **Response:** The CASKDROP program does not produce output which permits evaluation of the crush configuration over specific regions of the impact limiter. However, as discussed above, since "lock up" does not occur even at the maximum strain of approximately 80%, "hard contact" of the impact limiter is not of concern.
- b) **Response:** The correct interpretation of unfiltered accelerometer outputs is extremely difficult, since a great deal of extraneous information is present in an unfiltered trace. As discussed above, "lock up" does not occur at a discrete value of strain, but the stress-strain curve steepens as the strain reaches higher values. Since the drop testing was performed at cold temperatures, the strain level reached on the half-scale test unit did not exceed 50%, which is well within the working range of the foam. Therefore lock-up did not occur during certification testing.

## ATTACHMENT A

- c) **Response:** The foam stress-strain curves have been revised to extrapolate only as far as necessary, which is a strain of 80%.
- d) **Response:** The force-deflection curves have been revised to end at an approximate impact limiter strain of 80%. The force-deflection curves are based on one-half inch increments of deformation; the curves end at the first increment which falls beyond an impact limiter strain of 70% for the cold cases and 80% for the hot cases.



2-8 Correct the underscored typographical or editorial errors as follows

In Section 2.12.5.3 of the application, "[T]he test results for the HAC end, side, and slapdown orientations are shown in Table 2.12.5-23."

The 1/2-scale package did not go through any side-drop tests.

This information is needed to meet the 10 CFR 71.31(a) requirements.

**Response:** The referenced section has been revised to read, "The test results for the HAC end, slapdown, and c.g.-over-corner orientations are shown in Table 2.12.5-23."

2-9 Provide further detail concerning the suffix letter "Z" and the term "Trace Element" as part of the "line call-out ASTM D2000 M4AA 710 A13 B13 F17 F48 Z Trace Element."

The closure lid includes two O-ring seals made from butyl rubber of 3/8-inch cross sectional diameter. The inner O-ring is the containment seal and the outer is the test seal. The seals are retained in dovetail grooves machined in the lid. The O-ring material is made from Rainier Rubber R0405-70 or equivalent material meeting ASTM D2000 M4AA 710 A13 B13 F17 F48 Z Trace Element. See paragraph 1.2.1.1, Cask Body, of the application.

## ATTACHMENT A

Specification ASTM D2000, Standard Classification System for Rubber Products, provides a method for specifying rubber materials by the use of a simple "line call-out" designation. Suffix letters are defined and utilized as part of the line call-out. For example, Table 3 of the specification defines suffix letter Z as any special requirement, which shall be specified in detail. Further, Table 5 note K states "suffix Z, special requirement, test method to be specified in detail, or via using information in Tables 3, 4, and 5; for example, Z1 = C12, rating 85% retention minimum."

This information is required to ensure compliance with 10 CFR 71.33(a)(4) and 71.39.

**Response:** The "Z Trace Element" refers to a small addition of a compound which may be added by the manufacturer to uniquely identify the origin of the O-ring. The presence of the specific chemical used for this purpose identifies the O-ring as belonging to that particular manufacturer. It has no other purpose, and does not affect the elastomer properties in any way.

However, the application has been revised to remove the option to use the ASTM D2000 equivalent material, as that is not considered necessary for this package. The O-ring material will be Rainier Rubber R-0405-70 material only. The material tests as stated in Section 8.1.5.2 will still be performed, and the material must pass these tests.

2-10 Provide results for the required Butyl rubber O-ring tests as follows:

- (a) Low Temperature Resistance (Suffix F17) shall be determined in accordance with Method A, 9.3.2 of ASTM D2137. After 3 minutes at -40°C, each lot of butyl rubber material shall be non-brittle.
- (b) Low Temperature Resistance (Suffix F48) (TR) shall be determined in accordance with the test of ASTM D1329, 38mm die, 50% elongation and retraction 50% minimum. Each lot of butyl rubber material shall be resilient at a test temperature of -50°C or less.

The BRR package Butyl O-ring material is tested in accordance with Rainier Rubber test report R0405-70 or equivalent and states that the specifications met or exceeded are ASTM D2000 4AA, 710, A13, B13, and F17. See paragraph 1.2.1.1, Cask Body, of the SAR.

Physical characteristics of the Butyl rubber containment O-ring seals and sealing washers shall be determined for each lot based conforming to the following ASTM D2000 designation: M4AA 710 A13 B13 F17 F48 Z Trace Element. See Butyl Rubber O-rings, paragraph 8.1.5.2 of the application.

The test report R0405-70 (06-15-2001) linked by the application provides results for all required tests with the exception of the low temperature tests listed above. In addition, AREVA should note that the criteria listed on the Test Report for Heat Resistance (Suffix A13) is incorrect. The required criteria are listed on Table 6 of ASTM D2000 supplemental requirements for available suffix Grade 4 as follows: Each lot of butyl rubber material shall experience a maximum 10 Shore A durometer hardness increase, a maximum reduction in tensile strength of 25% and a maximum reduction in ultimate elongation of 25%, when tested at 70°C. The criteria currently listed on the test report noted above are for available suffix Grade 2. Furthermore, the actual results documented on the test report are acceptable based on the Grade 4 criteria.

This information is required to ensure compliance with 10 CFR 71.33(a)(4) and 71.39.

**Response:** The O-rings will conform to the specification Rainier Rubber R-0405-70 and must pass the tests specified in Section 8.1.5.2. The requirements established by Suffix

## ATTACHMENT A

F17 and Suffix F48 must be met for the O-rings to be acceptable for use in the BRR package. This material is routinely procured for use in the TRUPACT-II, and is certified to meet the requirements of Suffix F17 and Suffix F48. In addition, the behavior of the R-0405-70 material at both low and high temperatures has been established by extensive laboratory testing that is described in detail in Section 2.12.7.

No use is made in the BRR package application of the test report 06-15-2001, which is found on the Rainier Rubber website. We have passed this RAI on to Rainier Rubber for their use in correcting their website if they desire to do so.

- 2-11 Provide Charpy impact energy absorption results for Type L43 Socket Head Cap Screws (SHCS) 1-8UNC-2A X 2.5-inches long in accordance with ASTM A320. See I/N 12 on sheet 1 of drawing 1910-01-01-SAR. ASTM A320 covers alloy steel bolting materials for pressure vessels, valves, flanges, and fittings for low temperature service.

Grade L43 shall show minimum impact energy absorption of 20 ft lbf [27 J] at the test temperature when tested by the procedure specified in the applicable portions of Sections 19 to 28 of Test Methods and Definitions ASTM A370. Table 3 lists applicable test temperatures for the various ferritic grades identified in ASTM A320. Exceptions to this requirement are permissible and the impact tests may be made at specified temperatures different than those shown in Table 3, provided the test temperature is at least as low as the intended service temperature and the bolting is suitably marked to identify the reported test temperature. See paragraph 6.2.1.1, Material of Grades, ASTM A320.

Table 2 prescribes impact test requirements for standard and sub-size Charpy test specimens for all grades with the exception of grade L1. See paragraph 6.2.1.2 of ASTM A320.

This information is required to ensure compliance with 10 CFR 71.33(a)(4) and 71.39.

**Response:** Material certified to meet ASTM A320 Grade L43 must meet all of the requirements stated in the specification. Therefore, the bolting material is certified to have a minimum Charpy impact energy per Table 4 of the specification, tested at the applicable temperature given in Table 3. The results are reported in the material certification.

### Thermal

- 3-1 Perform the analysis of the regulatory thermal test with values specified in 10 CFR 71.73(c)(4).

The applicant's analysis of HAC based on a lower fire temperature (1425°F) is not in compliance with 10 CFR Part 71.73(c)(4) which partly states: "Thermal Exposure of the specimen fully engulfed, except for a simple support system, in a hydrocarbon fuel/air fire of sufficient extent, and in sufficiently quiescent ambient conditions, to provide an average emissivity coefficient of at least 0.9, with an average flame temperature of at least 800°C (1475°F) for a period of 30 minutes, or any other thermal test that provides the equivalent total heat input to the package and which provides a time averaged environmental temperature of 800°C." Although the current method may essentially provide an equivalent level of heat input, the applicant needs to perform the analysis for the regulatory prescribed temperature of 1475°F. The applicant should update the temperatures of the O-ring seals (vent port seal and drain port seal) and other components as necessary. The applicant should also submit all thermal analysis (input and output) files concerning this case.

## ATTACHMENT A

This information is needed to determine compliance with 10 CFR 71.73(c)(4).

**Response:** As noted by the RAI, the methodology for modeling the radiation input from the HAC fire was chosen to yield the equivalent level of heat input, while simplifying the modeling effort since the modeling approach used did not allow for the direct input of an emissivity coefficient for the fire that is less than 1.0. It should be noted that a fire temperature of 800 °C (1475 °F) was used as the temperature basis for the convective input from the HAC fire.

Although a different modeling approach could be used to allow for an average emissivity coefficient for the fire of less than 1 (i.e., 0.90) together with a 800 °C (1475 °F) temperature basis for the radiation portion, implementation of that approach would entail a fairly significant change to the thermal model setup. Therefore, to simplify the review process and to conservatively bound the level of heat input to the package, the HAC fire modeling has been revised to use a temperature level of 1475°F for both the convective and radiation portions of the heat input and to assume a conservatively high average emissivity coefficient of 1.0 vs. the minimum 0.9 specified by 10 CFR Part 71.73(c)(4).

The results of the revised HAC flame definition of 1475 °F with an average emissivity coefficient of 1.0 results in a 7 to 41 °F increase in the noted peak temperatures with the largest temperature increase occurring for the exterior package components and the minimum for the enclosed MURR fuel elements. The decrease in thermal margin for the majority of package components is considered insignificant. The greatest impact occurs for the drain port seal where the thermal margin is decreased from 35 to 27 °F. Given the conservatism assumed in the level of impact limiter damage and the location of the damage, this level of thermal margin is still considered adequate to cover for modeling uncertainties for this component.

Section 3.4 of the application has been revised to reflect the revised basis and results of the HAC evaluations.

- 3-2 Verify the convection heat transfer coefficient used for the analysis of the 30-minute fire by comparing to previously accepted values obtained from reliable reports such as "Thermal Measurements in a Series of Large Pool Fires," Sandia Report SAND85 –0196 TTC – 0659 UC 71, (August 1971)."

Section 3.4.2 of the application states the convection heat transfer coefficients between the package and the ambient during the 30-minute fire event are based on an average gas velocity of 10 m/sec. The actual convection heat transfer coefficient used during the analysis is not provided in the application. Typical values obtained from measurements reported on the above Sandia report are on the order of 4.5 BTU/ft<sup>2</sup>-h-°F). The applicant should verify the convection heat transfer coefficient used during the 30-minute fire analysis of the BRR package is on the order of this value.

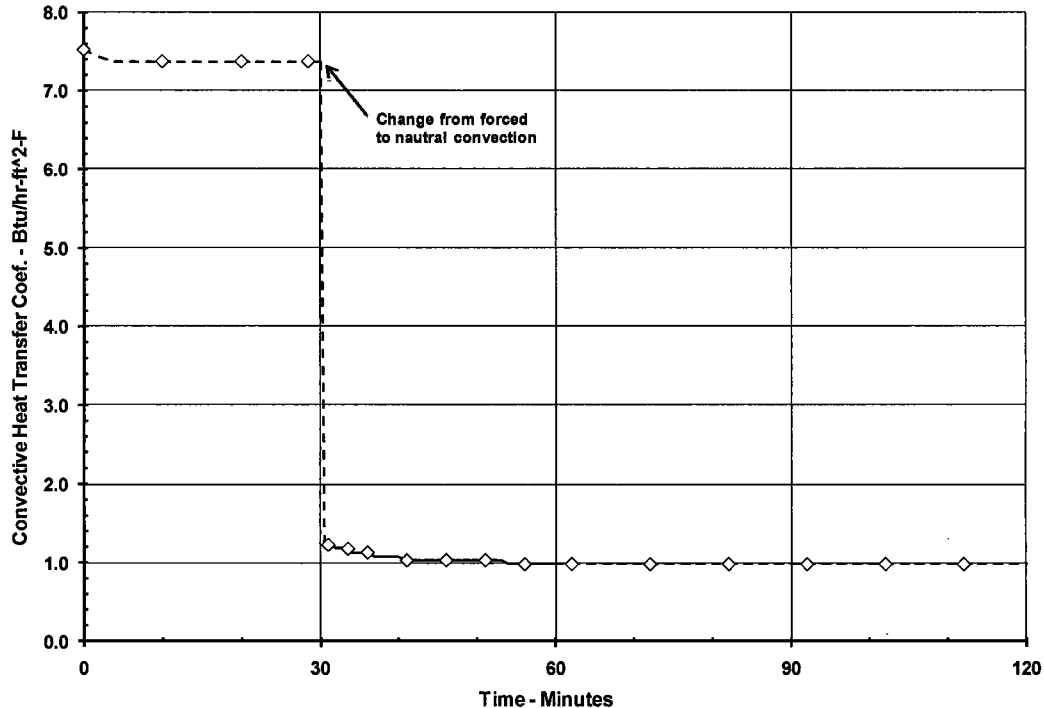
This information is needed to determine compliance with 10 CFR 71.73(c)(4).

**Response:** As documented in Chapter 3.0, the convection heat transfer coefficients between the package and the ambient are not defined as a fixed number, but are continuously re-computed during the HAC transient based on the mean gas temperature. The variation in the computed convection coefficient with time is shown below for the first 120 minutes of the HAC transient. As seen, the convection heat transfer coefficient is approximately 7.4 BTU/ft<sup>2</sup>-h-°F during the fire portion of the transient and then drops to approximately 1.0 BTU/ft<sup>2</sup>-h-°F during the initial phase of the package cool-down. The predicted heat transfer coefficient is approximately 60% higher

## ATTACHMENT A

than the values in the Sandia report due to the selection of a conservatively short characteristic length of 0.25 feet. This characteristic length was purposely selected to over-state the level of turbulence in the fire in order to maximize the convective heat transfer coefficients.

The figure below is provided as Figure 3.5 14 in the revised SAR text.



- 3-3 Perform thermal analysis for the vacuum drying operations to demonstrate maximum temperatures remain within allowable limits.

No thermal analysis is provided in Chapter 3.0 for moisture removal operations. When performing vacuum drying, the cask heat transfer capabilities are limited which may result in maximum temperatures higher than the allowable limits.

This information is needed to determine compliance with 10 CFR 71.71.

**Response:** Evaluation of the proposed vacuum drying operation has been added to Chapter 3, Section 3.3.3. The results demonstrate that adequate time and thermal margin exists to allow the necessary vacuum drying operations to be completed without exceeding the maximum allowable component temperature limits.

- 3-4 Clarify why a temperature survey is not needed in preparation for transport of the BRR package.

10 CFR 71.43(g) states a package must be designed, constructed, and prepared for transport so that in still air at 38°C (100°F) and in the shade, no accessible surface of a package would have a temperature exceeding 50°C (122°F) in a nonexclusive use shipment, or 85°C (185°F) in an exclusive use shipment.

This information is needed to determine compliance with 10 CFR 71.43(g).

**Response:** The text in Section 3.3.1.1 of the application that referred to a very limited area on the cask impact limiter attachment lugs possibly exceeding the 85 °C (185 °F) criteria by

## ATTACHMENT A

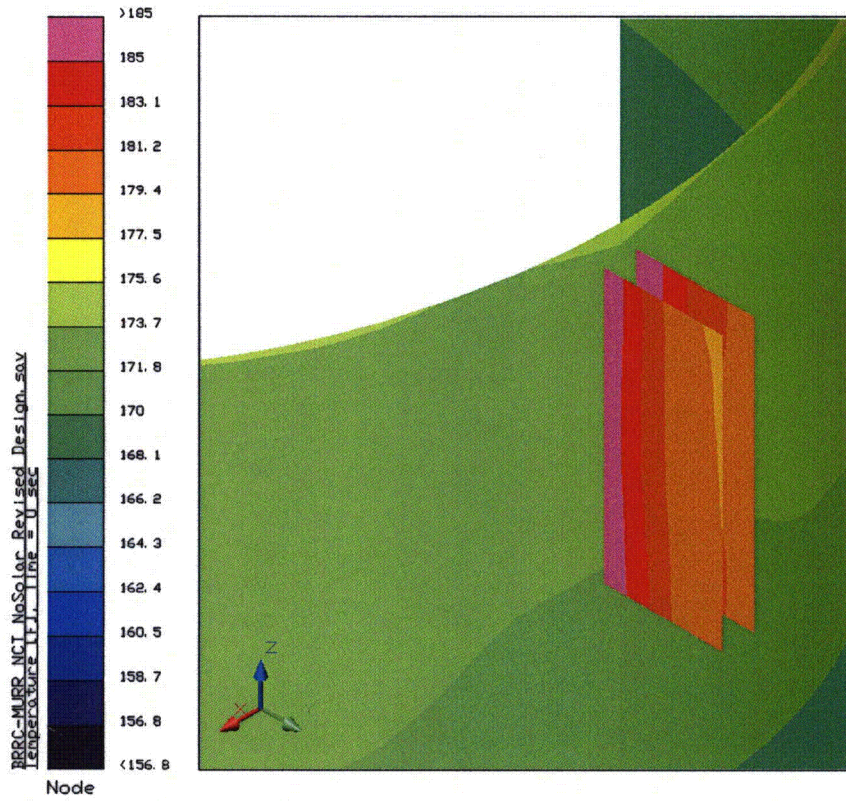
a few degrees was based on a conservative model of the region of the attachment lugs. As described in SAR Section 3.5.3.1, the increased number and size of the re-designed impact limiter attachment lugs was not implemented in the NCT thermal model since the changes represented an increased surface area for heat rejection. As such, the NCT thermal model was judged to provide a conservatively high estimate of the NCT package temperatures. However, as illustrated by the figure on the left below, this original thermal modeling also erroneously predicts that a small length of the cask impact limiter attachment lug near the cask body area could exceed 185 °F by approximately 5 °F.

To verify that no accessible surface temperature would exceed the 85 °C (185 °F) criteria, a revised sensitivity analysis has been conducted wherein the increased size of the attachment lugs was addressed. For simplicity and conservatism, the increase in the number of attachment points from six to eight is ignored. Besides the change in the attachment lug design, this revised modeling also included credit for the seal welded joints between the thermal shield and the attachment lugs. The resulting temperature distribution is presented in the right hand figure below. As seen, no accessible surface will exceed 185 °F.

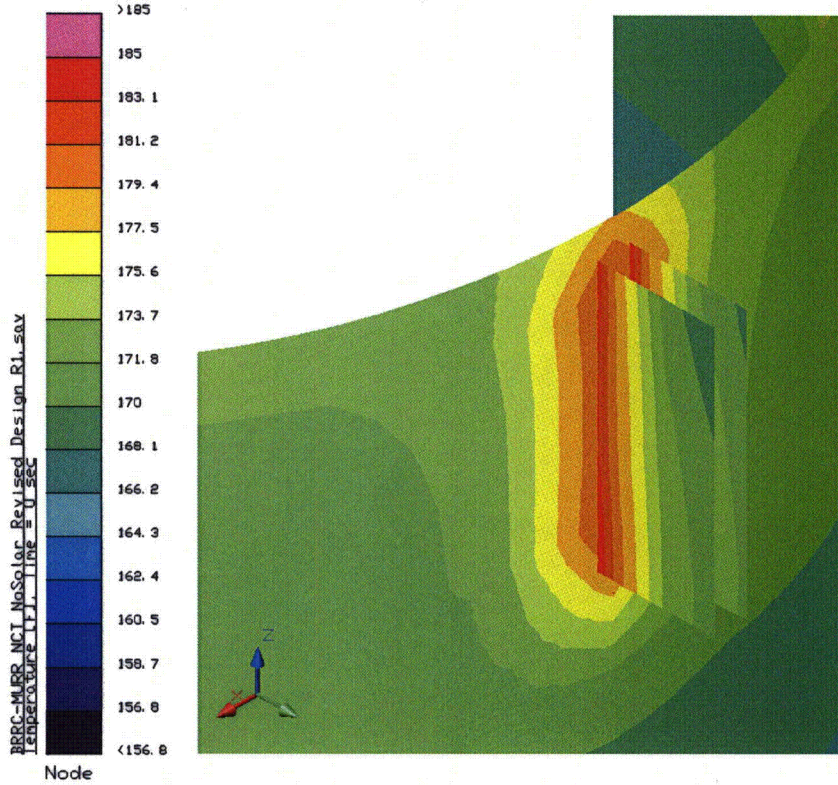
It should be noted that the revised NCT thermal model still contains the following conservatisms: 1) the modeling is based on six instead of eight attachment points per limiter, 2) the potential for convective heat transfer from the inside surface of each attachment lug is ignored due to the assumed flow blockage by the blade portion of the impact limiter attachment (a nominal 1/8-inch gap will exist on either side of the blade), 3) no credit is taken for conduction into the attachment pin and then dissipation to the ambient via convection and radiation from the attachment pins. As such, the actual peak temperature is expected to be lower.

The text in SAR Section 3.3.1.1 and the temperature results in SAR Table 3.3 1 for 'NCT Hot without Solar' have been updated to reflect the results of the revised NCT thermal model. No changes have been made to the 'NCT Hot' results since, as explained earlier, the base NCT thermal model generates conservatively high package temperatures.

# ATTACHMENT A



Original NCT Model in Vicinity of Attachment Lugs



Revised NCT Model for Current Attachment Lug Design



## ATTACHMENT A

### Containment

- 4-1 Provide the allowable compression limits of the O-ring containment seals under NCT and HAC.

In SAR 4.1.3, the applicant performed the calculation of compression acting on the O-ring containment seal, and calculated a minimum compression of 22% and a maximum compression of 26%, based on groove depth and O-ring cross-sectional diameter. The application needs to document the safety limits of compression on the O-ring seals to verify that the calculated compression on the O-ring containment seals falls below the safety limits.

This information is required by the staff to access compliance with 10 CFR 71.33, 71.35, 71.51(a), and 71.51(b).

**Response:** The Parker O-ring Handbook recommends a minimum compression of 16%. The limit for maximum compression is when the O-ring cross-section, adjusted for maximum temperature, fills the cross sectional area of the dovetail groove. This occurs for the BRR package closure O-ring at a compression of 31.2%. The compression range reported in Section 4.1.3 of the application of 22% to 26% is 6% above the recommended minimum value and 5% below the recommended maximum value, and is therefore acceptable. This applies to HAC as well as NCT. Section 4.1.3 of the application has been revised to include the recommended limits of compression.

### Shielding

- 5-1 Pertaining to Section 5.2.2, "Radiation Source," provide verification of the accuracy of the information and calculations provided by the host Reactor staff.

On page 5.2-1 of the SAR, the applicant states: "The source specification for the four fuels is provided in the following sections. Note that the sources MURR, MITII, and ATR fuel were developed and provided by the host Reactor staff. The source for TRIGA was derived from information in INEL-96/0482."

This information is needed pursuant to the requirements of 10 CFR 71.39.

**Response:** In response to this RAI, the reactor staff at the three reactor sites (MURR, MITR-II, and ATR) have prepared formal calculations to document the source term calculations. Both MURR and MITR-II operate their reactors under an NRC-approved QA program, while ATR is operated by under an equivalent DOE-approved QA program. The calculations are overchecked by the reactor staff. AFS also reviewed the calculations and consider them to be acceptable.

- 5-2 Pertaining to Section 5.2.2.1, "Gamma Source," provide justifications for the use of computer codes, to generate gamma source terms which are no longer supported by the code developer.

On page 5.2-1 of the SAR, the applicant states: "The MURR gamma source term was generated by the ORIGEN 2.2 computer program. The MITR-II gamma source term was generated by the ORIGEN 2.2 computer program. The ATR gamma source term was generated by the ORIGEN 2.1 computer program." From the abstract for ORIGEN2 V.2.2, Oak Ridge National Laboratories (ORNL) states that "No significant updates have

## ATTACHMENT A

been made to Origen2 in more than 10 years, and it is no longer supported by ORNL. We recommend that new users obtain CCC-750/SCALE 6 that includes the latest version of ORIGEN-ARP, which is supported by ORNL and has the latest nuclear data." Also in the same abstract, ORNL states that "ORIGEN is a computer code system for calculating the buildup, decay, and processing of radioactive materials. ORIGEN2 is a revised version of ORIGEN and incorporates updates of the reactor models, cross sections, fission product yields, decay data, and decay photon data, as well as the source code. ORIGEN2.1 replaces ORIGEN2 and includes additional libraries for standard and extended-burnup PWR and BWR calculations, which are documented in ORNL/TM-11018. ORIGEN2.1 was first released in August 1991 and was replaced with ORIGEN2 Version 2.2 in June 2002. Version 2.2 was the first update to ORIGEN2 in over 10 years and was stimulated by a user discovering a discrepancy in the mass of fission products calculated using ORIGEN2 V2.1. Code modifications, as well as reducing the irradiation time step to no more than 100 days/step, reduced the discrepancy from ~10% to 0.16%. The bug does not noticeably affect the fission product mass in typical ORIGEN2 calculations involving reactor fuels because essentially all of the fissions come from actinides that have explicit fission product yield libraries. Thus, most previous ORIGEN2 calculations that were otherwise set up properly should not be affected." (See: <http://rsicc.ornl.gov/codes/ccc/ccc3/ccc-371.html>)

As a result of a telephone call between NRC and the applicant on June 2, 2009, (telephone call is documented in ADAMS under Docket No. 71-9341), the applicant submitted ORIGEN2 input and output files for MURR, MITII, and ATR. The staff reviewed these files and found that they were out dated. Also, staff found that an updated library is needed to ensure that the source term is accurate

This information is needed pursuant to the requirements of 10 CFR 71.65.

**Response:** The ORIGEN 2.1 bug does not affect any of the fuels used in the BRR package. The ORIGEN 2.1 bug affects only exotic fuel mixtures that contain large quantities of actinides other than uranium and plutonium. To confirm this, the ATR input file was rerun using ORIGEN 2.2. Most of the results were identical, and all deviations were less than 0.1%. Because the differences were negligible, the ATR source presented in the application has not been updated.

The NRC noted in the telephone call (documented in ADAMS under Docket No. 71-9341) that the confirmatory calculation using ORIGEN-ARP for MURR fuel resulted in a gamma source term 20% larger than the gamma source term computed by ORIGEN2. A possible cause of this discrepancy is the irradiation and decay assumptions used in the ORIGEN-ARP input file. In Revision 0 of the application, Section 5.2.1.1, second paragraph, it was incorrectly stated in that the MURR source was generated using a one week in/one week out pattern. (The first paragraph correctly stated two weeks between cycles.) The actual reported MURR source was generated using a one week in/two week out pattern. It is unknown to AFS if the NRC confirmatory model used one or two weeks between cycles. AFS estimates the difference (in total photons/s) between the gamma source computed with correct and incorrect decay assumptions to be about 28%, which is agreement with the NRC observations. NRC should verify that two weeks decay between cycles was used in the ORIGEN-ARP confirmatory model.

Given the long history of ORIGEN 2.2, results may be considered reasonable. For example, at MITR-II, ORIGEN 2.2 has been used in conjunction with MCNP to compute reactivities to within 0.2%. Also, MURR routinely produces certain isotopes, and

## ATTACHMENT A

ORIGEN 2.2 conservatively bounds the generated activities. Based upon the long use of ORIGEN 2.2 at the reactor sites, the program has been shown to be reliable.

In any case, the calculated dose rate margins in Revision 0 of the application were quite large. The maximum calculated side surface dose rate was 10.7 mrem/hr, compared against a limit of 200 mrem/hr, which is 189.3 mrem/hr below the limit. A 20% variation in the computed dose rate is 2.1 mrem/hr, and 2.1 mrem/hr << 189.3 mrem/hr. While AFS concurs that ORIGEN 2.2 is an older program and is no longer supported, there is a wealth of accumulated experience using the ORIGEN 2.2 program that confirms the program generates reasonable results. Given the large margins, computing the source terms using ORIGEN-ARP was not performed because fluctuations in the source term are expected to be <25%, which is a very small fraction of the margin. Rather, all reported dose rates have been increased by 25% in Revision 1 of the application as a penalty for using ORIGEN 2.2.

In addition to the 25% penalty, a number of assumptions are made to generate conservative source terms. For all reactors, the source terms are inherently high for the stated maximum burnups because the burnups are achieved using irradiation times much shorter than the irradiation times that would be used to achieve the burnup in actual practice. For example, for MITR-II, the fuel element is modeled with 900 days of continuous operation, although the reactor runs approximately 300 days per year, with the rest of the time consumed by refueling outages and other down time. Likewise, the MURR fuel element is modeled with a one week in/two week out irradiation scheme, which never happens in actual practice, as fuel elements are typically out of the core many weeks at a time. For ATR, a fuel element power of 10 MW is assumed and down time between cycles is neglected, although the actual element power is in the range of 2.25-3.25 MW. For TRIGA, a 4-year continuous irradiation is modeled, although TRIGA reactors tend to operate in a sporadic manner rather than continuous, and TRIGA elements often have in-core residence times greater than 10 years.

For these reasons, there is sufficient margin in the reported dose rates to ensure safe operation of the BRR package.

### Criticality

- 6-1 Provide clarification as to whether the criticality design is credited with maintaining the cask leaktight under all HAC scenarios.

Section 1.1 of the SAR states that "The package is designed to provide leaktight containment of the radioactive contents under all NCT and HAC." However, Section 6.3.1 only makes reference to credit being taken for the leaktight nature of the package for NCT cases.

This information is needed to determine compliance with 10 CFR 71.31 and 71.33.

**Response:** The package has been demonstrated to remain leaktight under HAC. However, it is standard practice to conservatively allow flooding in the HAC criticality analysis. This assumption is not meant to imply that the actual package will leak under HAC. Section 6.3.1 has been modified to state that the package remains leaktight under HAC, but that flooding was modeled to be conservative.

- 6-2 Describe the function of the samarium trioxide and molybdenum discs and the justification for excluding them in the TRIGA criticality model.

## ATTACHMENT A

Section 6.2.4 describes samarium trioxide discs and molybdenum discs which are located between the active fuel regions and reflector material. Section 6.2.4 states that these discs were ignored in the model for simplicity. No details were provided as to the justification for excluding these in the model.

This information is needed to determine compliance with 10 CFR 71.31 and 71.33.

**Response:** The samarium trioxide discs are used as a burnable poison, so neglecting this item is conservative. The function of the molybdenum discs is not entirely clear, so an additional case was prepared in which the molybdenum disc was modeled explicitly (see Section 6.9.2.4, *TRIGA Fuel Parametric Evaluation*). The molybdenum disc has a thickness of only 0.031-in, so the effect on the reactivity is within the statistical uncertainty of the method. Justification for neglecting the samarium trioxide and molybdenum discs has been added to the application, as well as the additional case using the molybdenum disc.

- 6-3 Provide information (e.g., isotopic form, physical quantity, etc.) regarding the solid form plutonium material expected as a result of fuel irradiation.

Section 1.2.3 states that "the BRR package may contain plutonium in excess of 20 Ci as a consequence of irradiation of the reactor fuel." However, no other information concerning this expected plutonium was found.

This information is needed to determine compliance with 10 CFR 71.31 and 71.33.

**Response:** The quantity of plutonium for each of the four fuel types has been added to Section 1.2.3 in Table 1.2-3. Note that RAI 6-3 is unrelated to the criticality chapter, as the criticality analysis was conservatively performed using fresh fuel (no plutonium), which is more reactive than burned fuel.

### Operating Procedures, Acceptance Criteria, and Maintenance Tests

- 7-1 Clarify "sufficient to impair containment integrity" in steps 18 and 21 in the loading procedure.

The application should define containment integrity impairment in order to provide for an adequate inspection to ensure no loss or dispersal of radioactive contents. The applicant should review other procedural steps in Chapters 7 and 8 in which the passing criteria for an inspection or test is not specified or lacks specificity and revise as appropriate.

This information is needed to determine compliance with 10 CFR 71.51 and 71.35(a).

**Response:** Clarification has been added to the appropriate operational steps in Chapter 7.0 where inspection is specified by providing examples of defects that could impair containment integrity. These examples include cuts, tears, and/or joint separation in the seal material, or scratches, and/or indentations in the sealing surface areas. As noted in Chapter 7.0, any seal that is determined to be damaged will be replaced, and repair of the sealing areas is specifically addressed in Section 8.2.3.2, *Sealing Area Routine Inspection and Repair*, of the application. Any replacement of a damaged seal and/or sealing area repair will be completed prior to shipment, as noted in the operational steps. Any repair of a sealing area and/or a seal replacement will comply with the requirements specified on the General Arrangement Drawings in Appendix 1.3.3 of the application. As suggested, all sections in Chapter 8.0 have been reviewed to ensure that adequate specificity for any inspection or test is noted.

## ATTACHMENT A

In addition, the appropriate steps in Section 7.1 have been revised in accordance with the vacuum drying procedure which has been added (see RAI 3-3).

## ATTACHMENT B

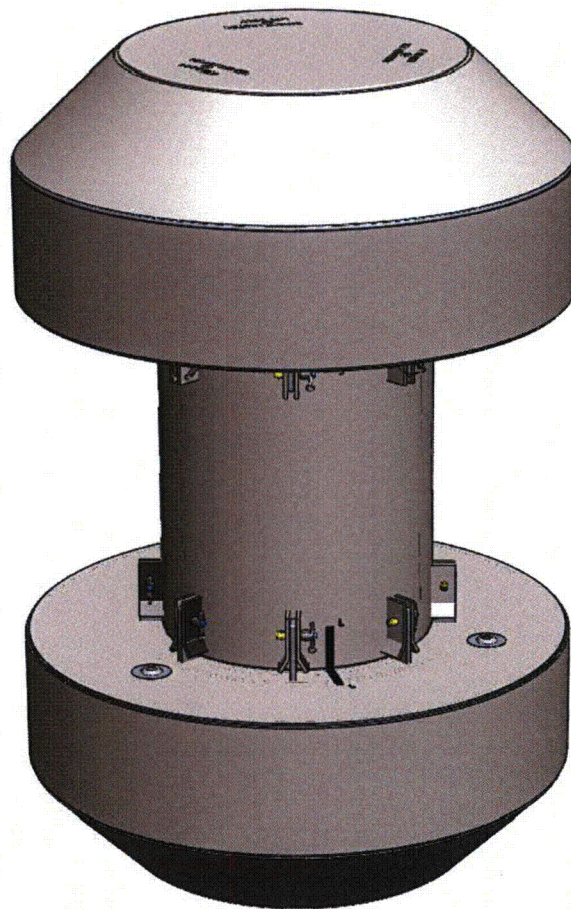
### Revised Pages

<b>Page Changes</b>	
<b>Remove Rev. 0</b>	<b>Insert Rev. 1</b>
Cover page & spine i to v	Cover page & spine i to v
1.2-2 – 1.2-7	1.2-2 – 1.2-7
1.2-9	1.2-9
	1.2-20
1910-01-01-SAR R0	1910-01-01-SAR R1
1910-01-03-SAR R0	1910-01-03-SAR R1
2.1-6	2.1-6
2.1-8	2.1-8
2.3-1 – 2.3.2	2.3-1 – 2.3.2
2.6-1	2.6-1
2.7-2	2.7-2
2.7-15 – 2.7-29	2.7-15 – 2.7-30
2.12.1-3	2.12.1-3
2.12.3-3 – 2.12.3-11	2.12.3-3 – 2.12.3-11
2.12.3-13	2.12.3-13
2.12.5-1 – 2.12.5-20	2.12.5-1 – 2.12.5-33
2.12.7-1 – 2.12.7-2	2.12.7-1 – 2.12.7-2
2.12.7-4 – 2.12.7-6	2.12.7-4 – 2.12.7-6
2.12.8-1	2.12.8-1
2.12.8-12	2.12.8-12
3.1-5 – 3.1-6	3.1-5 – 3.1-6
3.2-3	3.2-3
3.3-2 – 3.3-13	3.3-2 – 3.3-17
3.4-1 – 3.4-6	3.4-1 – 3.4-6
3.5-3	3.5-3
3.5-5 – 3.5-8	3.5-5 – 3.5-8
3.5-10 – 3.5-14	3.5-10 – 3.5-14
3.5-27 – 3.5-36	3.5-27 – 3.5-37
4.1-2	4.1-2
4.5-1	4.5-1
5.1-2 – 5.2-9	5.1-2 – 5.2-10
5.4-2 – 5.4-3	5.4-2 – 5.4-3
5.4-5 – 5.4-10	5.4-5 – 5.4-10
5.5-1 – 5.5-8	5.5-1 – 5.5-8
6.2-5	6.2-5
6.3-1 – 6.3-2	6.3-1 – 6.3-2
6.9-5	6.9-5
6.9-11	6.9-11
7.1-1 – 7.1-5	7.1-1 – 7.1-5



DOCKET 71-9341

# BEA Research Reactor Package



## *Safety Analysis Report*

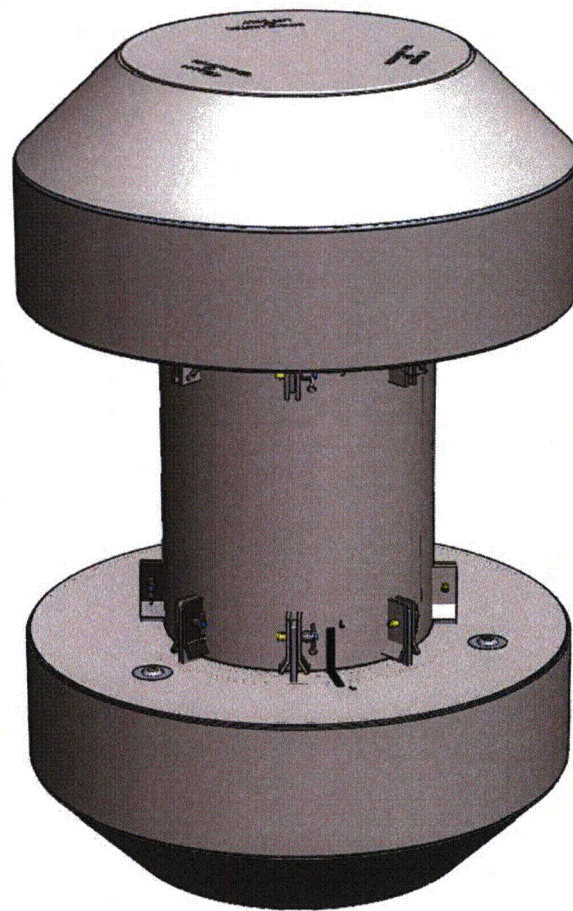
AREVA Federal Services LLC

Revision 1  
August 2009



DOCKET 71-9341

# BEA Research Reactor Package



## *Safety Analysis Report*

AREVA Federal Services LLC

Revision 1  
August 2009



**TABLE OF CONTENTS**

1.0 GENERAL INFORMATION ..... 1.1-1

1.1 Introduction..... 1.1-1

1.2 Package Description..... 1.2-1

1.2.1 Packaging..... 1.2-1

1.2.2 Contents ..... 1.2-5

1.2.3 Special Requirements for Plutonium ..... 1.2-7

1.2.4 Operational Features ..... 1.2-7

1.3 Appendices..... 1.3-1

1.3.1 References..... 1.3-1

1.3.2 Glossary of Terms and Acronyms ..... 1.3-2

1.3.3 Packaging General Arrangement Drawings..... 1.3-4

2.0 STRUCTURAL EVALUATION ..... 2.1-1

2.1 Structural Design ..... 2.1-1

2.1.1 Discussion..... 2.1-1

2.1.2 Design Criteria..... 2.1-2

2.1.3 Weights and Centers of Gravity..... 2.1-6

2.1.4 Identification of Codes and Standards for Package Design..... 2.1-6

2.2 Materials ..... 2.2-1

2.2.1 Material Properties and Specifications ..... 2.2-1

2.2.2 Chemical, Galvanic, or Other Reactions ..... 2.2-1

2.2.3 Effects of Radiation on Materials ..... 2.2-2

2.3 Fabrication and Examination ..... 2.3-1

2.3.1 Fabrication ..... 2.3-1

2.3.2 Examination ..... 2.3-1

2.4 General Standards for All Packages ..... 2.4-1

2.4.1 Minimum Package Size ..... 2.4-1

2.4.2 Tamper-Indicating Feature ..... 2.4-1

2.4.3 Positive Closure ..... 2.4-1

2.4.4 Valves ..... 2.4-1

2.4.5 Package Design..... 2.4-1

2.4.6 External Temperatures ..... 2.4-1

2.4.7 Venting..... 2.4-2

2.5 Lifting and Tie-down Standards for All Packages ..... 2.5-1

2.5.1 Lifting Devices..... 2.5-1

2.5.2 Tie-down Devices ..... 2.5-1

2.6 Normal Conditions of Transport..... 2.6-1

2.6.1 Heat ..... 2.6-1

2.6.2 Cold..... 2.6-7

2.6.3 Reduced External Pressure ..... 2.6-9

2.6.4 Increased External Pressure ..... 2.6-9

2.6.5 Vibration ..... 2.6-10

2.6.6 Water Spray ..... 2.6-11

2.6.7 Free Drop ..... 2.6-11

2.6.8 Corner Drop ..... 2.6-15

2.6.9 Compression ..... 2.6-15

2.6.10 Penetration ..... 2.6-15

2.7 Hypothetical Accident Conditions ..... 2.7-1

2.7.1 Free Drop ..... 2.7-1

2.7.2 Crush ..... 2.7-18

2.7.3 Puncture ..... 2.7-18

2.7.4 Thermal ..... 2.7-20

2.7.5 Immersion – Fissile ..... 2.7-22

2.7.6 Immersion – All Packages ..... 2.7-22

2.7.7 Deep Water Immersion Test ..... 2.7-22

2.7.8 Summary of Damage ..... 2.7-23

2.8 Accident Conditions for Air Transport of Plutonium ..... 2.8-1

2.9 Accident Conditions for Fissile Material Packages for Air Transport ..... 2.9-1

2.10 Special Form ..... 2.10-1

2.11 Fuel Rods ..... 2.11-1

2.12 Appendices ..... 2.12-1

2.12.1 References ..... 2.12.1-1

2.12.2 Certification Test Plan ..... 2.12.2-1

2.12.3 Certification Test Results ..... 2.12.3-1

2.12.4 Stress Analysis Finite Element Models ..... 2.12.4-1

2.12.5 Impact Limiter Performance Evaluation ..... 2.12.5-1

2.12.6 Analysis Software Descriptions ..... 2.12.6-1

2.12.7 Seal Performance Tests ..... 2.12.7-1

2.12.8 Fuel Basket Stress Analysis ..... 2.12.8-1

3.0 THERMAL EVALUATION ..... 3.1-1

3.1 Description of Thermal Design ..... 3.1-1

3.1.1 Design Features ..... 3.1-1

3.1.2 Content’s Decay Heat ..... 3.1-3

3.1.3 Summary Tables of Temperatures ..... 3.1-4

3.1.4 Summary Tables of Maximum Pressures ..... 3.1-4

3.2 Material Properties and Component Specifications ..... 3.2-1

3.2.1 Material Properties ..... 3.2-1

3.2.2 Technical Specifications of Components ..... 3.2-3

3.3 Thermal Evaluation for Normal Conditions of Transport ..... 3.3-1

3.3.1 Heat and Cold ..... 3.3-1

3.3.2 Maximum Normal Operating Pressure ..... 3.3-3

3.3.3 Vacuum Drying Operations ..... 3.3-4

3.4 Thermal Evaluation for Hypothetical Accident Conditions ..... 3.4-1

3.4.1 Initial Conditions ..... 3.4-1

3.4.2 Fire Test Conditions ..... 3.4-2

3.4.3 Maximum Temperatures and Pressure ..... 3.4-2

3.4.4 Maximum Thermal Stresses ..... 3.4-3

3.5 Appendices ..... 3.5-1

3.5.1 References ..... 3.5-2

3.5.2 Computer Analysis Results ..... 3.5-4

3.5.3	Analytical Thermal Model.....	3.5-4
3.5.4	'Last-A-Foam' Response under HAC Conditions.....	3.5-35
4.0	CONTAINMENT .....	4.1-1
4.1	Description of the Containment System .....	4.1-1
4.1.1	Containment Boundary .....	4.1-1
4.1.2	Containment Penetrations .....	4.1-1
4.1.3	Seals .....	4.1-1
4.1.4	Welds .....	4.1-2
4.1.5	Closure .....	4.1-2
4.2	Containment Under Normal Conditions of Transport .....	4.2-1
4.3	Containment Under Hypothetical Accident Conditions .....	4.3-1
4.4	Leakage Rate Tests for Type B Packages.....	4.4-1
4.4.1	Fabrication Leakage Rate Tests .....	4.4-1
4.4.2	Maintenance/Periodic Leakage Rate Tests .....	4.4-1
4.4.3	Preshipment Leakage Rate Tests .....	4.4-1
4.5	Appendix.....	4.5-1
4.5.1	References.....	4.5-1
5.0	SHIELDING EVALUATION .....	5.1-1
5.1	Description of Shielding Design.....	5.1-1
5.1.1	Design Features.....	5.1-1
5.1.2	Summary Table of Maximum Radiation Levels.....	5.1-1
5.2	Source Specification .....	5.2-1
5.2.1	Gamma Source.....	5.2-1
5.2.2	Neutron Source .....	5.2-4
5.3	Shielding Model.....	5.3-1
5.3.1	Configuration of Source and Shielding .....	5.3-1
5.3.2	Material Properties.....	5.3-2
5.4	Shielding Evaluation.....	5.4-1
5.4.1	Methods.....	5.4-1
5.4.2	Input and Output Data.....	5.4-1
5.4.3	Flux-to-Dose Rate Conversion .....	5.4-2
5.4.4	External Radiation Levels.....	5.4-2
5.5	Appendices.....	5.5-1
5.5.1	References.....	5.5-1
5.5.2	Detailed TRIGA Results .....	5.5-1
5.5.3	Sample Input File.....	5.5-8
6.0	CRITICALITY EVALUATION.....	6.1-1
6.1	Description of Criticality Design.....	6.1-1
6.1.1	Design Features.....	6.1-1
6.1.2	Summary Table of Criticality Evaluation.....	6.1-1
6.1.3	Criticality Safety Index .....	6.1-2
6.2	Fissile Material Contents .....	6.2-1
6.2.1	MURR Fuel Element .....	6.2-1
6.2.2	MITR-II Fuel Element .....	6.2-2
6.2.3	ATR Fuel Element .....	6.2-3
6.2.4	TRIGA Fuel Element.....	6.2-4

6.3	General Considerations.....	6.3-1
6.3.1	Model Configuration.....	6.3-1
6.3.2	Material Properties.....	6.3-2
6.3.3	Computer Codes and Cross-Section Libraries.....	6.3-2
6.3.4	Demonstration of Maximum Reactivity .....	6.3-3
6.4	Single Package Evaluation.....	6.4-1
6.4.1	Configuration .....	6.4-1
6.4.2	Results.....	6.4-3
6.5	Evaluation of Package Arrays under Normal Conditions of Transport.....	6.5-1
6.5.1	Configuration .....	6.5-1
6.5.2	Results.....	6.5-1
6.6	Package Arrays under Hypothetical Accident Conditions .....	6.6-1
6.6.1	Configuration .....	6.6-1
6.6.2	Results.....	6.6-2
6.7	Fissile Material Packages for Air Transport.....	6.7-1
6.8	Benchmark Evaluations .....	6.8-1
6.8.1	Applicability of Benchmark Experiments .....	6.8-1
6.8.2	Bias Determination .....	6.8-2
6.9	Appendices.....	6.9-1
6.9.1	References.....	6.9-1
6.9.2	Parametric Evaluations to Determine the Most Reactive Fuel Geometries .....	6.9-1
6.9.3	Sample Input Files .....	6.9-14
7.0	PACKAGE OPERATIONS.....	7.1-1
7.1	Procedures for Loading the Package.....	7.1-1
7.1.1	Preparation for Loading .....	7.1-1
7.1.2	Loading of Contents.....	7.1-1
7.1.3	Preparation for Transport.....	7.1-4
7.2	Procedures for Unloading the Package.....	7.2-1
7.2.1	Receipt of Package from Carrier.....	7.2-1
7.2.2	Removal of Contents.....	7.2-1
7.3	Preparation of an Empty Package for Transport.....	7.3-1
7.4	Preshipment Leakage Rate Test.....	7.4-1
7.4.1	Gas Pressure Rise Leakage Rate Test Acceptance Criteria .....	7.4-1
7.4.2	Determining the Test Volume and Test Time.....	7.4-1
7.4.3	Performing the Gas Pressure Rise Leakage Rate Test.....	7.4-2
7.4.4	Optional Preshipment Leakage Rate Test.....	7.4-2
7.5	Appendix.....	7.5-1
7.5.1	References.....	7.5-1
8.0	ACCEPTANCE TESTS AND MAINTENANCE PROGRAM.....	8.1-1
8.1	Acceptance Tests .....	8.1-1
8.1.1	Visual Inspection and Measurements .....	8.1-1
8.1.2	Weld Examinations.....	8.1-1
8.1.3	Structural and Pressure Tests .....	8.1-1
8.1.4	Fabrication Leakage Rate Tests .....	8.1-2
8.1.5	Component and Material Tests .....	8.1-6

8.1.6 Shielding Integrity Tests ..... 8.1-13  
8.1.7 Thermal Tests..... 8.1-14  
8.2 Maintenance Program ..... 8.2-1  
8.2.1 Structural and Pressure Tests ..... 8.2-1  
8.2.2 Maintenance/Periodic Leakage Rate Tests ..... 8.2-1  
8.2.3 Component and Material Tests ..... 8.2-3  
8.2.4 Thermal Tests..... 8.2-4  
8.3 Appendix..... 8.3-1  
8.3.1 References..... 8.3-1

**BRR Package Safety Analysis Report**

in-place through the upper end structure, and is nominally 8 inches thick. The shield at the bottom is made from lead sheet material that is packed firmly into place, and is 7.7 inches thick. The bottom lead cavity is closed using a one inch thick plate secured with a full penetration groove weld, see Zone A6/7 of sheet 3 of drawing 1910-01-01-SAR.

The removable shield plug is located at the top of the payload cavity. The outer shell is made from Type 304 plate material of 1/2-inch, 3/8-inch, 1-inch, and 1 1/2-inch thickness. See Zone D2 of sheet 4 of drawing 1910-01-01-SAR. The cavity is filled with lead sheet material that is packed firmly into place. The total thickness of the plug is 11.2 inches, and the lead thickness is 9.7 inches. The plug rests on a shoulder located approximately half way along the length of the plug. A corresponding shoulder is located in the upper end structure of the cask body to support the shield plug. A 3/4-inch diameter pipe passes through the plug to ensure proper draining and drying of the cask. The pipe is oriented approximately diagonally to prevent a deleterious shine path. The shield plug is lifted using a central, 1/2-13 UNC threaded hole.

The closure lid is made from 2-inch thick, ASTM A240, Type 304 stainless steel plate. It is attached to the cask using 12, 1-8 UNC bolts made of ASTM A320, Grade L43 material, with hardened steel washers. The bolts are plated with electroless nickel per MIL-DTL-26074 Rev. F Class 1 Grade B, and tightened to a torque of  $220 \pm 20$  ft-lb. The mating holes in the cask body may be optionally fitted with heavy duty thread inserts. The mating surface of the lid features a step relief located at the bolt circle. This relief prevents any contact from occurring between the lid and the body outside of the bolt circle, thus preventing prying loads from being applied to the closure bolts. The closure lid includes two O-ring seals made from butyl rubber of 3/8-inch cross sectional diameter. The inner O-ring is the containment seal, and the outer is the test seal. The seals are retained in dovetail grooves in the lid. The O-ring material (including the sealing washers, see below) is made from Rainier Rubber R-0405-70, and subject to the tests given in Section 8.1.5.2.

The BRR package provides a single level of leaktight containment. The containment boundary of the BRR package consists of the following elements. Unless noted, all elements are made of ASTM Type 304 stainless steel in various product forms.

- The lower massive end structure (including the passage to the drain port)
- The inner cylindrical shell
- The upper massive end structure
- The containment O-ring seal (the inner seal in the closure lid)
- The closure lid
- The vent port in the closure lid
- The drain port in the lower end structure

The containment boundary is shown in Figure 1.2-12.

As noted above, the BRR package features two ports that are part of the containment boundary: a vent port in the closure lid, and a drain port in the lower end structure. Both ports are closed with threaded plugs made of ASTM B16 brass and sealed with butyl rubber sealing washers. A

threaded brass cover is used to protect the port plugs. A seal test port is located between the containment O-ring seal and test O-ring seals, and is not part of containment.

### **1.2.1.2 Impact Limiters**

Impact limiters are attached to each end of the BRR package, having essentially identical design, and are shown in drawing 1910-01-02-SAR. Each limiter is 78 inches in diameter and 34.6 inches long overall, with a conical section 15 inches long towards the outer end. The impact limiter design consists of Type 304 stainless steel shells and approximately 9 lb/ft<sup>3</sup> polyurethane foam. The external shells (except for the end plate) are 1/4 inches thick, and the internal shells (that interface with the cask body) are 1/2 inches thick. The outer end plate is 1/2 inches thick. The closure end impact limiter features three reinforced, 1/2-13UNC holes for lifting of the impact limiter only. The polyurethane foam is rigid, closed-cell, and is poured in place. On the side that mates with the cask, the annular sheet features three plastic melt-out plugs designed to relieve pressure in the HAC fire event. The attachment of the impact limiters to the cask body is described in Section 1.2.1.1, *Cask Body*.

### **1.2.1.3 Baskets**

There are four baskets used with the BRR package, one for each type of fuel transported, and are shown in drawing 1910-01-03-SAR. The baskets are made from welded construction using Type 304 stainless steel in plate, bar, pipe, and tubular forms. Each basket has a diameter of 15.63 inches and a length of 53.45 inches, and features a number of cavities that fit the size and shape of the fuel. The cavities are sized to minimize free play between the fuel and the basket, while ensuring free insertion and removal of the elements. The baskets are open on the top, and the fuel is located at the top end, nearest the shield plug. The baskets are designed to freely drain water when the cask is lifted out of the spent fuel pool.

#### **1.2.1.3.1 MURR**

The MURR basket consists of an outer rolled shell, an inner pipe, and thick radial plates that form eight pie-shaped cavities for the fuel in a circular array. The bottom of the fuel cavities is formed by a 3/8-inch thick plate that is welded to the inside of the shell. The lifting bar divides the interior of the inner tube in half and prevents loading any fuel within the inner tube. The MURR basket is shown in Figure 1.2-4.

#### **1.2.1.3.2 MITR-II**

The MITR-II basket consists of eleven diamond-shaped tubes that match the shape and size of the fuel. Three tubes are arranged side-by-side in the center, and eight tubes are arrayed around the outside. Tubes are held in place by a top plate, a bottom support plate, and a central support plate. The bottom support plate is 1/2-inches thick. A 14-inch diameter, 1/4-inch thick circular shell forms the lower portion of the basket. The MITR-II basket is shown in Figure 1.2-5.

## **BRR Package Safety Analysis Report**

### **1.2.1.3.3 ATR**

The ATR basket consists of a rolled outer shell, an inner pipe, and radial plates that form eight pie-shaped cavities for the fuel in a circular array. Since the outer shell is somewhat smaller than the cask cavity, the ATR basket features four circular ribs having an outer diameter of 15.63 inches. The bottom support plate is 1/2-inch thick. The lifting bar divides the interior of the inner tube in half and prevents loading any fuel within the inner tube. The ATR basket is shown in Figure 1.2-6.

### **1.2.1.3.4 TRIGA**

The TRIGA basket consists of an array of 19 tubes having a 2-inch outer diameter and an 11-gauge wall thickness. The tubes are held in place by a top plate, a bottom support plate, and a central support plate. A 13-inch diameter, 1/4-inch thick circular shell forms the lower portion of the basket. The short spacer pedestal and the adjustable spacer pedestal are used to customize the fuel cavity for various TRIGA fuel lengths. The TRIGA basket is shown in Figure 1.2-7.

### **1.2.1.4 Gross Weight**

The gross weight of the BRR package, including the cask, impact limiters, and maximum payload, is 32,000 lb. A summary of overall component weights is shown in Table 2.1-2 and discussed in Section 2.1.3, *Weights and Centers of Gravity*.

### **1.2.1.5 Neutron Moderation and Absorption**

The BRR package maintains criticality control by means of limitation of the quantity of fissile material present and by maintaining a safe configuration of the material under all NCT and HAC. The design of the BRR package does not include any components whose principal purpose is the absorption of neutrons. A more detailed description of the package criticality control functions is given in Chapter 6, *Criticality Evaluation*.

### **1.2.1.6 Receptacles, Valves, Testing and Sampling Ports**

The BRR package closure lid contains a vent port and a containment seal test port. A body drain port is located on the side of the lower end of the cask. There are no valves or receptacles used in the BRR package.

### **1.2.1.7 Heat Dissipation**

The dissipation of heat from the BRR package is entirely passive. The impact limiters are painted white to reduce the absorption of solar heat. A thermal shield is used on the cask body to limit the temperature of the lead gamma shield in the HAC fire event. A more detailed description of the package thermal design is given in Chapter 3, *Thermal Evaluation*.

### **1.2.1.8 Lifting and Tie-down Devices**

Other than the threaded holes in the top of the cask body, there are no lifting or tie-down devices that are a structural part of the BRR package. The package is secured to the transport vehicle



## **BRR Package Safety Analysis Report**

using structures that interface with the surfaces of the upper and lower impact limiters. The package rests on a lower frame that is attached to the vehicle. An upper frame contacts the upper impact limiter and is attached to the vehicle using cables or the equivalent. There are no provisions to lift the package with the impact limiters installed.

### **1.2.1.9 Pressure Relief System**

There is no pressure relief system in the BRR package.

### **1.2.1.10 Shielding**

Biological shielding of gamma radiation is provided by a combination of lead and the thick steel shells of the BRR package. Hydrogenous neutron shielding is not necessary and none is included in the package design. Details of the gamma shielding are provided in Section 1.2.1.1, *Cask Body*. A full assessment of the shielding design is provided in Chapter 5, *Shielding Evaluation*.

## **1.2.2 Contents**

The BRR package may contain up to 8 irradiated MURR fuel elements, up to 11 irradiated MITR-II fuel elements, up to 8 irradiated ATR fuel elements, and up to 19 irradiated TRIGA fuel elements. Only one fuel element is allowed per basket location. Details for each fuel type are provided in the following paragraphs.

### **1.2.2.1 MURR**

The MURR fuel element may be irradiated to a maximum burnup of 180 MWD (216,346 MWD/MTU, or a U-235 depletion of 28.3%). The minimum cooling time is 180 days after reactor shutdown.

Each fresh MURR element contains  $775.0 \pm 7.8$  g U-235, enriched up to 93 wt.%. The weight percents of the remaining uranium isotopes are 1.2 wt.% U-234, 0.7 wt.% U-236, and 5.0 – 7.0 wt.% U-238. The MURR fuel element fissile material is uranium aluminide ( $UAl_x$ ).

Each MURR fuel element contains 24 curved fuel plates. Fuel plate 1 has the smallest radius, while fuel plate 24 has the largest radius, as shown in Figure 1.2-8. The fuel “meat” is a mixture of uranium metal and aluminum, while the cladding and structural materials are an aluminum alloy. The fuel plates are rolled to shape and swaged into the two fuel element side plates. The fissile material (uranium aluminide) is nominally 0.02-in thick for all 24 plates. Fuel element side plates are fabricated of ASTM B 209, aluminum alloy 6061-T6 or 6061-T651 and are approximately 0.15-in thick. The fuel plates are typically spaced with a 0.08-in gap between plates.

The MURR element overall length, including irradiation growth, is 32.75 inches. The bounding weight of one assembly is 15 lb. The maximum decay heat per fuel element is 158 W.

### 1.2.2.2 MITR-II

The MITR-II fuel element may be irradiated to a maximum burnup of 225 MWD (411,498 MWD/MTU, or a U-235 depletion of 55.6%). The minimum cooling time is 30 days after reactor shutdown.

Each fresh MITR-II element contains  $510.0 \pm 3.0/-10.0$  g U-235, enriched up to 93 wt.%. The weight percents of the remaining uranium isotopes are 1.2 wt.% U-234, 0.7 wt.% U-236, and 5.0 – 7.0 wt.% U-238. Like the MURR fuel element, the MITR-II fuel element fissile material is uranium aluminide ( $UAl_x$ ).

Each MITR-II fuel element contains 15 flat fuel plates, as shown in Figure 1.2-9. The fuel plates are fabricated and swaged into the two fuel element side plates. The fuel “meat” is a mixture of uranium metal and aluminum, while the cladding and structural materials are an aluminum alloy. The fissile material (uranium aluminide) is nominally 0.03-in thick and the cladding is nominally 0.025-in thick. Fuel element side plates are fabricated of ASTM B 209, aluminum alloy 6061-T6 and are approximately 0.19-in thick. The fuel plates are nominally 0.08 inches apart.

The MITR-II element overall length, including irradiation growth, is 26.52 inches. The bounding weight of one assembly is 10 lb. The maximum decay heat per assembly is 30 W.

### 1.2.2.3 ATR

The ATR fuel element may be irradiated to a maximum burnup of 350 MWD (302,768 MWD/MTU, or a U-235 depletion of 40.9%). The minimum cooling time is 1,280 days (3.5 years) after reactor shutdown.

There are two general classes of ATR fuel element, XA and YA. The XA fuel element has a fresh fuel loading of  $1,075 \pm 10$  g U-235. The weight percents of the remaining uranium isotopes are 1.2 wt.% U-234 (max), 0.7 wt.% U-236 (max), and 5.0 – 7.0 wt.% U-238. Like the MURR and MITR-II fuel elements, the fuel element fissile material is uranium aluminide ( $UAl_x$ ).

The XA fuel element is further subdivided into fuel element types 7F, 7NB, 7NBH. In the 7F fuel element, all 19 fuel plates are loaded with enriched uranium in an aluminum matrix with the eight outer plates (1 through 4 and 16 through 19) containing boron as a burnable poison. The fuel element with the greatest reactivity is the 7NB that contains no burnable poison. The 7NBH fuel element is similar to the 7NB fuel element except that it contains one or two borated plates. The YA fuel element is identical to the 7F fuel element except that plate 19 of the YA fuel element is an aluminum alloy plate containing neither uranium fuel nor boron burnable poison. The YA fuel element has a fresh fuel loading of  $1,022.4 \pm 10$  g U-235. A second YA fuel element design (YA-M) has the side plate width reduced by 15 mils.

The ATR fuel elements contain 19 curved fuel plates. A section view of an ATR fuel element is given in Figure 1.2-10. Note that an intact ATR fuel element has end boxes (as shown on Figure 1.2-10), although these end boxes are removed prior to insertion in the BRR package. The fuel plates are rolled to shape and swaged into the two fuel element side plates. Fuel plate 1 has the smallest radius, while fuel plate 19 has the largest radius. The fissile material (uranium aluminide) is nominally 0.02-in thick for all 19 plates. Fuel element side plates are fabricated of

ASTM B 209, aluminum alloy 6061-T6 or 6061-T651 and are approximately 0.19-in thick. The fuel plates are typically spaced with a 0.08-in gap between plates.

The ATR element overall length, after removal of the end box structures, 51.0 inches max. The bounding weight of one assembly is 25 lb. The maximum decay heat per assembly is 30 W.

#### **1.2.2.4 TRIGA**

Many different types of TRIGA fuel elements have been fabricated over the past several decades. TRIGA fuel elements utilize a zirconium hydride fuel matrix. The BRR package is limited to five specific TRIGA fuel types:

1. 8 wt.% uranium aluminum clad element (General Atomics catalog number 101)
2. 8.5 wt.% uranium stainless steel clad element (General Atomics catalog number 103)
3. 8.5 wt.% uranium stainless steel clad element, high enriched uranium (General Atomics catalog number 109). This fuel element is sometimes referred to in the literature as a Fuel Life Improvement Program (FLIP) element.
4. 20 wt.% uranium stainless steel clad element (General Atomics catalog number 117). This fuel element is sometimes referred to in the literature as a FLIP-LEU-I element.
5. 8.5 wt.% uranium stainless steel clad element, instrumented (General Atomics catalog number 203).

Basic fresh fuel data used to describe the various TRIGA fuel elements are summarized in Table 1.2-1. The maximum length of an element, including irradiation growth, is 45.50 inches. Non-instrumented fuel elements are somewhat shorter. For all fuel elements, spacers are utilized within the TRIGA baskets.

The maximum burnup and minimum cooling time varies for the five fuel element types and is summarized in Table 1.2-2. The two FLIP elements have significantly higher U-235 loadings and hence much larger burnups and longer cooling times. The bounding weight of any TRIGA fuel element is 10 lb. The maximum decay heat per element is 20 W.

#### **1.2.3 Special Requirements for Plutonium**

The BRR package may contain plutonium in excess of 20 Ci as a consequence of irradiation of the reactor fuel. As such, the plutonium is in solid form within the fuel matrix. Table 1.2-3 summarizes the plutonium activity for each of the four fuel types, both on a per-element and per-cask basis. The maximum quantity of plutonium for the BRR package is 872.5 Ci.

#### **1.2.4 Operational Features**

The BRR package is of conventional design and is not complex to operate. Operational features are depicted on the drawings provided in Appendix 1.3.3, *Packaging General Arrangement Drawings*. Operating procedures and instructions for loading, unloading, and preparing an empty package for transport are provided in Chapter 7, *Package Operations*.

**Table 1.2-2 – TRIGA Fuel Parameters**

Fuel Type	Maximum U-235 depletion (%)	Maximum Burnup (MWD/MTU)	Minimum Decay Time
GA Cat. # 101 (Aluminum-clad standard)	22.42	36,953	28 days
GA Cat. # 103/203 (Stainless steel-clad standard)	20.72	34,111	28 days
GA Cat. # 109 (FLIP)	59.74	339,368	1 year
GA Cat. # 117 (FLIP-LEU-I)	43.81	75,415	1 year

**Table 1.2-3 – Plutonium Activity**

Plutonium Activity per Fuel Element (Ci)				
Isotope	MURR	MITR-II	ATR	TRIGA
Pu-238	1.74E-02	7.17E+00	3.01E+00	7.19E-01
Pu-239	3.74E-03	1.34E-02	1.65E-01	2.33E-01
Pu-240	9.07E-04	1.38E-02	7.95E-02	1.70E-01
Pu-241	1.66E-02	1.67E+00	2.27E+01	4.48E+01
Pu-242	3.02E-08	1.02E-05	1.02E-04	2.44E-04
Total	0.04	8.9	25.9	45.9
Plutonium Activity per BRR Package (Ci)				
Isotope	MURR	MITR-II	ATR	TRIGA
Pu-238	1.39E-01	7.88E+01	2.40E+01	1.37E+01
Pu-239	2.99E-02	1.47E-01	1.32E+00	4.42E+00
Pu-240	7.26E-03	1.52E-01	6.36E-01	3.23E+00
Pu-241	1.33E-01	1.83E+01	1.81E+02	8.51E+02
Pu-242	2.42E-07	1.12E-04	8.18E-04	4.64E-03
Total	0.3	97.5	207.3	872.5

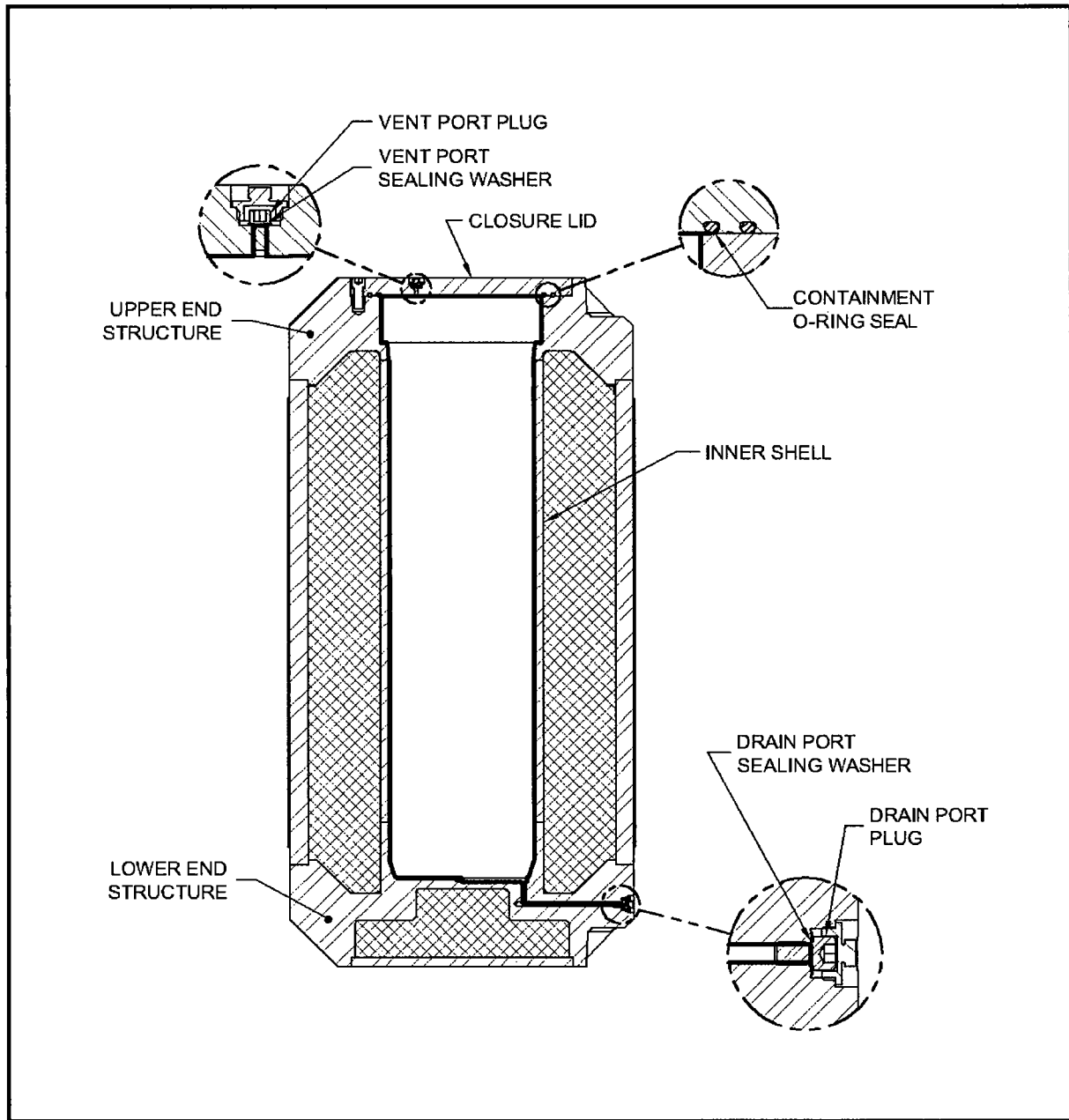



Figure 1.2-12 – BRR Package Containment Boundary

DWG NO	1910-01-01-SAR	REV	1	SHT	1
--------	----------------	-----	---	-----	---

Figure Withheld Under 10 CFR 2.390

		AREVA Federal Services LLC Packaging Projects Tacoma, WA 98402	
DWG TITLE BRR PACKAGE ASSEMBLY SAR DRAWING			
SCALE SHOWN		WT. - LBS	
REV. 1		SHEET 1 OF 4	
DWG NO.	1910-01-01-SAR		
SIZE	D		
CADFILE: 19100101.SAR.dwg			

---

Figure Withheld Under 10 CFR 2.390

---

Figure Withheld Under 10 CFR 2.390




---

Figure Withheld Under 10 CFR 2.390

DWG NO	1910-01-03-SAR	REV	1	SHEET	1
--------	----------------	-----	---	-------	---

Figure Withheld Under 10 CFR 2.390

		AREVA Federal Services LLC Packaging Projects Tacoma, WA 98402	
DWG TITLE			
BRR PACKAGE FUEL BASKETS SAR DRAWING			
SCALE: SHOWN		WT. - LBS	
REV: 1		SHEET 1 OF 3	
DWG SIZE		DWG NO.	
D		1910-01-03-SAR	
CAD FILE: 19100103SAR1.DWG			

---

Figure Withheld Under 10 CFR 2.390

---

Figure Withheld Under 10 CFR 2.390

### **2.1.2.3.3 Buckling Assessment**

Buckling, per Regulatory Guide 7.6, is an unacceptable failure mode for the containment vessel. The intent of this provision is to preclude large deformations that would compromise the validity of linear analysis assumptions and quasi-linear stress allowable limits, as given in Paragraph C.6 of Regulatory Guide 7.6.

Buckling investigations contained herein consider the outer shell of the BRR package. The outer and inner shells of the cask are closely connected through the massive end structures, thus, the two shells act to strengthen each other. One shell cannot buckle independently of the other. However, the strength of the inner shell for buckling considerations is conservatively ignored.

The shell buckling analysis is performed using the methodology of ASME B&PV Code Case N-284-2 [13]. Consistent with Regulatory Guide 7.6 philosophy, factors of safety corresponding to ASME Boiler and Pressure Vessel Code, Level A and Level D service conditions are employed. For NCT (Service Level A), the factor of safety is 2.0, and for HAC (Service Level D), the factor of safety is 1.34. Buckling analysis details are provided in Section 2.6.4, *Increased External Pressure*, Section 2.7.1, *Free Drop*, and Section 2.7.6, *Immersion – All Packages*.

### **2.1.3 Weights and Centers of Gravity**

The maximum gross weight of the BRR package is 32,000 lb. The packaging component weights are summarized in Table 2.1-2, and the fuel basket and fuel weights in Table 2.1-3. The center of gravity (CG) of the package is located 38.7 inches from the bottom outside surface of the cask body. Note that this is directly on the geometric center of the package. The mass moment of inertia of the cask about a transverse axis through the center of gravity (including impact limiters, as prepared for transport) is 63,246 in-lb-s<sup>2</sup>.

### **2.1.4 Identification of Codes and Standards for Package Design**

The BRR package, without regard to content, is conservatively designated a Category I package. Per the guidance of NUREG/CR-3854, the appropriate design criteria for the containment is Section III, Subsection NB of the ASME B&PV Code. Consequently, the design of the containment boundary is based on the methodology of Regulatory Guide 7.6, and load cases are applied and combined according to Regulatory Guide 7.8. The outer shell is conservatively included under the NB criteria. The closure bolts are designed using the guidance of NUREG/CR-6007.

For the design of the baskets as criticality control components, the criteria is taken from Section III, Subsection NG of the ASME B&PV Code. For other structures such as the thermal shield, impact limiter shells, and impact limiter attachments, the criteria is taken from Section III, Subsection NF of the ASME B&PV Code.

**Table 2.1-2 – BRR Package Component Weights**

Item	Weight, lb	CG, inches
Cask body <sup>①</sup>	25,400	---
Removable shield plug	950	---
Closure lid	280	---
Upper impact limiter	2,300	---
Lower impact limiter	2,300	---
<b>Total empty package</b>	<b>31,230</b>	<b>38.6<sup>④</sup></b>
MURR Fuel basket <sup>②</sup> (loaded)	770	32.7 <sup>③</sup>
MITR-II Fuel basket <sup>②</sup> (loaded)	400	32.7 <sup>③</sup>
ATR Fuel basket <sup>②</sup> (loaded)	650	27.1 <sup>③</sup>
TRIGA Fuel basket <sup>②</sup> (loaded)	480	28.1 <sup>③</sup>
<b>Total package, including MURR fuel (maximum)</b>	<b>32,000</b>	<b>38.7<sup>④</sup></b>
Total package, including MITR-II fuel	31,630	38.6 <sup>④</sup>
Total package, including ATR fuel	31,880	38.6 <sup>④</sup>
Total package, including TRIGA fuel	31,710	38.6 <sup>④</sup>

**Notes:**

1. Includes all shells, end structures, and lead.
2. Individual basket and fuel weights are given in Table 2.1-3. Although ATR fuel is the heaviest at 200 lb, the MURR basket plus fuel weight is greatest overall.
3. Measured from the bottom surface of the basket.
4. Measured from the bottom outside surface of the cask body.

**Table 2.1-3 – BRR Package Basket and Fuel Weights**

Design	Weight (lb)			
	Empty Basket	Fuel Element × Quan.	Combined Fuel	Total
MURR	650	15 × 8	120	770
MITR-II	290	10 × 11	110	400
ATR	450	25 × 8	200	650
TRIGA	290	10 × 19	190	480

## 2.3 Fabrication and Examination

### 2.3.1 Fabrication

The BRR package is fabricated using conventional metal forming and joining techniques. All welding procedures and welding personnel must be qualified in accordance with Section IX of the ASME Boiler and Pressure Vessel Code [14]. Containment boundary welds, as well as the welds at each end of the outer shell, are full penetration joints. All non-containment joints are fabricated in accordance with the requirements delineated on the drawings in Appendix 1.3.3, *Packaging General Arrangement Drawings*. The containment shell and outer shell fabrications shall comply with the tolerance requirements of the ASME Code, Subsection NE, Article NE-4220 [15]. Article NE-4220 is selected because the package cylindrical shells are verified for buckling performance using the ASME Code Case N-284-2. This Code Case is for Section III, Division 1, Class MC construction, and is based on the fabrication requirements of NE-4222, as stated in Section 1120 of the Code Case. Therefore, it is appropriate to fabricate the BRR package using shell tolerances from NE-4220, rather than NB-4220.

The polyurethane foam and butyl rubber O-rings are procured using written procedures. See Section 8.1.5, *Component Tests*, for details of the fabrication and performance requirements of these components.

### 2.3.2 Examination

Each of the materials performing a significant safety function must meet the ASTM specifications delineated on the drawings in Appendix 1.3.3, *Packaging General Arrangement Drawings*. Safety-significant materials not having an ASTM designation are controlled by means of written procedures whose requirements are summarized in Section 8.1.5, *Component Tests*.

Forgings are subject to ultrasonic and liquid penetrant inspection per the ASME Code, Subsection NB, Article NB-2540 [16]. Castings are subject to radiographic and liquid penetrant inspection per the ASME Code, Subsection NB, Article NB-2570 [17].

All welds are subject to visual examination per AWS D1.6 [18]. The welds between the inner containment shell and either end structure, the welds between the outer shell and either end structure, and the longitudinal weld(s) in the outer shell, if any, are examined by ultrasonic inspection in accordance with the ASME Code, Subsection NB, Article NB-5000, and Section V, Article 4 [20]. Optionally, the weld between the inner containment shell and the lower end structure may be examined by radiographic inspection in accordance with the ASME Code, Subsection NB, Article NB-5000, and Section V, Article 2 [19]. All welds on the BRR package, except seal welds, are liquid penetrant inspected on the final pass in accordance with the ASME Code, Subsection Nx, Article Nx-5000, and Section V, Article 6 [21]. The appropriate Subsection for the containment welds and outer shell welds is NB; for other cask body welds and the impact limiter shells, NF; and for the fuel baskets, NG.

Each BRR package will also be subjected to the following tests:

- An internal pressure test, in which the containment boundary is pressurized to 125% of the design pressure per the ASME Code [22], or 150% of the MNOP, per 10 CFR §71.85(b),

whichever is greater. The pressure test requirements are described in Section 8.1.3.2, *Containment Boundary Pressure Testing*.

- Containment boundary leakage rate test, which includes helium leakage rate tests of the containment boundary, the closure lid containment O-ring seal, the vent port containment O-ring seal, and the drain port containment O-ring seal. The leakage rate test requirements are described in Section 8.1.4, *Fabrication Leakage Rate Tests*.
- A test to ensure the integrity of the lead gamma shielding. The gamma test requirements are described in Section 8.1.6, *Shielding Integrity Test*.



## 2.6 Normal Conditions of Transport

When subjected to normal conditions of transport (NCT) as specified in 10 CFR §71.71, the BRR package meets the performance requirements specified in Subpart E of 10 CFR 71. This is demonstrated in the following subsections where each NCT condition is addressed and shown to meet the applicable design criteria. Load combinations used in this section are consistent with Regulatory Guide 7.8.

### 2.6.1 Heat

The normal heat condition, as defined in 10 CFR §71.71(c)(1), is evaluated in Section 3.0, *Thermal Evaluation*. The bounding temperatures and pressures for use in structural analyses are summarized in the following section. Material properties and stress limits, consistent with the design criteria shown in Table 2.1-1, are summarized for the relevant bounding temperatures in Table 2.6-1.

#### 2.6.1.1 Summary of Pressures and Temperatures

The bounding maximum temperatures for the 100 °F ambient NCT condition of the BRR package are presented in Table 3.1-1 of Chapter 3, *Thermal Evaluation*. For purposes of structural evaluation, the bounding fuel basket temperature is 400 °F. All components of the cask body, including the end structures, shells, shield plug, lead, closure lid and bolts, and elastomer seals, are bounded by a temperature of 250 °F. The bulk average polyurethane foam in both limiters is bounded by a temperature of 150 °F.

The initial pressure in the package at assembly is ambient, i.e., 14.7 psia. As determined in Section 3.3.2, *Maximum Normal Operating Pressure*, the maximum normal operating pressure (MNOP) can be conservatively defined to be 10 psig. The design pressure of the BRR package is 25 psig, which is significantly higher than the MNOP.

#### 2.6.1.2 Differential Thermal Expansion

Acceptable minimum clearances are maintained, including consideration of worst-case tolerances, between the cask, the fuel baskets, and the fuel.

##### 2.6.1.2.1 Baskets

The baskets for each fuel type have a nominal length of 53.45 inches with a tolerance of  $\pm 0.12$  inches, giving a maximum length of 53.57 inches. The cask cavity, with the shield plug installed, has a nominal length of 54.0 inches, with a tolerance of  $\pm 0.1$  inches, for a minimum length of  $L_{\text{Cask-min}} = 53.9$  inches. The length of the basket at a bounding temperature of 400 °F is:

$$L_{\text{Bsk}} = 53.57[1 + \alpha(400 - 70)] = 53.74 \text{ inches}$$

where the coefficient of thermal expansion,  $\alpha$ , is taken from Table 2.6-1 for Type 304 stainless steel at 400 °F as  $9.5(10^{-6})$  in/in/°F, and the reference temperature is 70 °F. The cask cavity thermal expansion is conservatively ignored. The minimum axial clearance at the NCT hot temperature is:

predicted hot case crush distances downward. The maximum predicted hot case crush distance occurs in the 15° oblique secondary impact event, and amounts to 15.9 inches, or 83.2% of the available crush distance. Not only is the majority of the foam in the limiter at a lower value of strain than this maximum value, the value is well within the range in which strain energy absorption is effective. The bounding bulk average foam temperature used for the analysis of 150 °F conservatively bounds the temperature predicted in the thermal analysis.

The final requirement is that the impact limiter structures and attachments to the cask maintain sufficient integrity subsequent to the HAC free drop and puncture drop events so that the containment O-ring seal is protected from excessive temperature in the subsequent HAC fire event. As documented in Appendix 2.12.3, *Certification Test Results*, while the original design did not meet this requirement, the final design of the attachment structures did meet it, as demonstrated by half-scale test. Section 2.7.1.7, *Impact Limiter Attachments*, shows that the final design is stronger than the successfully tested design. In addition, the worst-case damage to the impact limiter shells as a result of the puncture tests is fully accounted for in the thermal model, as discussed in Chapter 3, *Thermal Evaluation*.

For these reasons, the performance of the impact limiters is considered acceptable.

### 2.7.1.2 End Drop

The HAC end orientation free drop is evaluated using a combination of computer and manual calculations using an acceleration of 120g as discussed in Section 2.7.1.1, *Impact Forces and Deformations*. Stresses in the cask body are evaluated using the finite element model described in Appendix 2.12.4, *Stress Analysis Finite Element Models*. Both bottom down and top down impact orientations are considered. Including manual calculations, eight analyses of the HAC end drop are performed:

- Cask body stress
- Closure bolt stress
- Closure lid stress
- Lower closure plate weld stress
- Shield plug shell stress
- Buckling evaluation
- Lead slump evaluation
- Fuel basket stress is discussed in Section 2.7.1.5, *Basket Stress Analysis*.

**Cask body stress.** From Section 2.12.4.4.5, *Case No. 5, HAC Bottom-down End Drop*, the maximum stress intensity resulting from the bottom-down impact of 120g is 45,681 psi, located at the outside surface of the bottom end structure, as shown in Figure 2.12.4-10. The stress is linearized through the lower massive end structure cross section, Figure 2.12.4-11, and the maximum primary membrane stress is 22,680 psi. From Table 2.1-1, the limit on primary membrane stress is the lesser of  $2.4S_m$  and  $0.7S_u$ , which for Type 304 cast or forged material (see Table 2.2-2) is  $0.7S_u = 44,835$  psi at 250 °F. The margin of safety is:

In the HAC side drop impact orientation, the fuel baskets apply a load to the inside of the inner shell. The heaviest basket is for MURR fuel, but this basket has no ribs and the load is well distributed. The next-heaviest basket, for ATR fuel (650 lb), has four ribs. The top rib is a 0.5-inch thick plate with a 0.19-inch chamfer, for a land width of 0.31 inches. The middle two ribs are made from 0.38-inch thick plate with 0.19-inch chamfers, for a land width of 0.19 inches each. The lowest rib is made from 0.50-inch thick plate with a 0.13-inch step and a 0.19-inch chamfer, for a land width of 0.18 inches. The diameter of each rib is 15.63 inches. The projected bearing area of the ribs against the inner shell is:

$$A = 15.63(0.31 + 0.19 + 0.19 + 0.18) = 13.60 \text{ in}^2$$

The side load, using the bounding side drop impact of 120g, is:

$$P = 650(120) = 78,000 \text{ lb}$$

The bearing stress is:

$$\sigma = \frac{P}{A} = 5,735 \text{ psi}$$

The other two baskets, the MITR-II and the TRIGA, are considerably lighter and not bounding. At the bounding fuel basket temperature of 400 °F, the minimum yield strength of the inner shell material, from Table 2.2-2, is 20,700 psi. Since this stress is over three times larger than the bearing stress, bearing yield of the basket ribs or of the inner shell will not occur.

### 2.7.1.6 Fuel Impact Deformation

During the end drop, the fuel elements may experience a separate, internal impact with the cask or basket structures. This impact could occur if, during the period of package free fall, the fuel was in contact with the upper end of its cavity, which would be possible due to the zero-g environment of free fall. When the package strikes the ground, the velocity of the cask would begin to decrease, but the fuel would continue to fall freely until impact with the lower end occurred. When the gap between the fuel and the cask was traversed, the fuel would hit the cavity end. The fuel would have the full free drop velocity,  $v_o$ , but the cask cavity would be traveling in the same direction with a lower velocity. See Figure 2.7-1.

To simplify calculations, it will be conservatively assumed that, at the moment of impact with the fuel, the cask inner contact surface is motionless and unyielding. Further, it will be assumed that the deceleration of the package during the period of fuel traversing the gap is constant and equal to the maximum bounding deceleration of 120g. The fuel will therefore experience an equivalent free drop. This analysis will determine the magnitude of the free drop impact and determine the effect on the fuel elements.

At the moment of impact with the ground, both the cask and fuel have a velocity of  $v_o$ . The cask immediately begins to decelerate according to:

$$v(t) = at + v_o$$

The distance the cask travels until the moment of impact with the fuel is:

$$x_c = a \int_0^T t dt = \frac{1}{2} at^2 + v_o t \Big|_0^T = \frac{1}{2} aT^2 + v_o T$$

where  $T$  is the time of fuel impact, and  $x_c = 0$  at  $t = 0$  (the time of package impact). Note that during time  $T$ , the fuel has traveled the distance the cask has traveled, plus the initial gap between the fuel and cask. Alternately, it can be stated that the fuel has traveled  $v_o T$ , since its velocity is unchanged during this interval. Therefore:

$$x_c + \text{GAP} = v_o T, \quad \text{or}$$

$$x_c = v_o T - \text{GAP}$$

Substituting this into the formula for  $x_c$  above,

$$x_c = \frac{1}{2} aT^2 + v_o T = v_o T - \text{GAP}$$

Simplifying,

$$T = \left( \frac{-2\text{GAP}}{a} \right)^{1/2}$$

Since the difference in velocity between the fuel and the cask at time  $T$  is equal to the decay in velocity over the interval, equal to  $(aT)$ , the difference can be written as:

$$\Delta v = aT = a \left( \frac{-2\text{GAP}}{a} \right)^{1/2} = (-2a\text{GAP})^{1/2}$$

(Note that since the acceleration is negative (deceleration), the quantity under the square root will be positive.) The energy associated with a change in velocity,  $\Delta v$ , is equivalent to the energy of a free drop height,  $h$ . Since:

$$h = \frac{\Delta v^2}{2g_g}$$

then the equivalent free drop height of the fuel element in the BRR package impact is:

$$h = \bar{g}\text{GAP}$$

where  $g_g$  is the acceleration due to gravity, and the deceleration in  $g$ -units,  $\bar{g} = a/g_g = 120g$ . The energy to be dissipated during the impact of the fuel is equal to  $Wh$ , or:

$$E = W\bar{g}\text{GAP}$$

where  $W$  is the weight of a fuel element. If this energy is absorbed in the fuel structure by volumetric plastic flow, the energy absorbed is related to the volume of flow according to:

$$E = V\sigma_f$$

where  $\sigma_f$  is the flow stress of the material, equal to the average of the yield and ultimate tensile strengths. Solving this for the volume,

$$V = \frac{W\bar{g}\text{GAP}}{\sigma_f}$$

Since the material flow is assumed to occur on the fuel cross section, the deformation length is equal to the volume divided by the cross-sectional area of the fuel element,  $L = V/A_{xc}$ , or:

$$L = \frac{W\bar{g}GAP}{\sigma_f A_{xc}}$$

This formula will be evaluated for the bounding fuel case. The fuel is made from 6061-T6 aluminum material. From the ASME B&PV Code, Section II, Part D, Table Y-1, the yield strength at a temperature of 400 °F is equal to 13.3 ksi. Since this material does not appear in Table U, an ultimate tensile strength at temperature is not readily available. Conservatively, the yield strength will be used for the flow strength as defined above. Therefore,  $\sigma_f = 13,300$  psi.

The total gap value, GAP, consists of a) the free space between the fuel element and the basket cavity length, plus b) the difference between the cask cavity and the basket length. Parameter a), denoted as  $L_{FB}$ , is calculated by subtracting the fuel length from the basket cavity length, and is listed in Table 2.7-5. Parameter b) is found by subtracting the basket length (equal to 53.45 inches in all cases) from the cask cavity length of 54.0 inches, and is equal to 0.55 inches. The total fuel gap is therefore:

$$GAP = L_{FB} + 0.55$$

Due primarily to its larger gap and weight, the ATR fuel is the governing case. The maximum deformation length of any fuel element is therefore:

$$L = \left( \frac{W}{A_{xc}} \right) \frac{\bar{g}GAP}{\sigma_f} = 0.096 \text{ inches}$$

The fuel bounding weights, cross-sectional areas, and  $W/A_{xc}$  ratios are presented in Table 2.7-5. The bounding fuel weights are taken from Table 2.1-3. The areas are calculated from CAD drawings of the fuel active region cross section, and do not consider the end structures. The end structures are considered sacrificial since a) they do not contain any fissile material and b) the criticality analysis discussed in Section 6.3.1 does not model the end structures, and determines the most reactive axial position of the active length of the fuel as if the end structures were absent. Since the fuel end structures do not serve a safety function, they are ignored in the axial deformation analysis.

This maximum deformation length, which is just below 1/10<sup>th</sup> of an inch, is negligible from a structural, shielding, or criticality perspective. Therefore fuel behavior in the HAC end drop is acceptable.

### 2.7.1.7 Impact Limiter Attachments

As reported in Appendix 2.12.3, *Certification Test Results*, the initial design of the impact limiter attachments was not adequate, since they did not securely retain the primary impact limiter in the 15° oblique slapdown free drop impact. The redesigned attachments are shown in the drawings in Appendix 1.3.3, *Packaging General Arrangement Drawings*. One half-scale certification test limiter was refurbished, as far as possible, to incorporate the revised design and retested to confirm its adequacy. The attachment load path of the refurbished test article, when converted to full-scale, was conservatively less strong than the revised design, as shown by the comparison

shown in Table 2.7-6. Note: in the table, the blade is the attachment component integral to the impact limiter, and the receptacle is the pair of plates, attached to the cask, that accept the blade.

As detailed in Section 2.12.3.6, *Confirmatory Test of Attachments*, the 15° oblique slapdown free drop was repeated, followed by a puncture test. The attachments that experienced the greatest loads from the puncture test were the same ones that experienced the greatest loads in the free drop test. The result was that the impact limiter was securely retained on the test cask. The only measurable change to the refurbished attachment hardware was a negligible elongation of one of the blade holes by 0.07 inches (full-scale). Other than that slight deformation, there were no signs of distress or impending failure in any other feature located in the attachment load path. Of note, no other free drop or puncture drop test orientation caused any significant damage to the original, smaller design of the attachments. Therefore the impact limiter attachments are adequate to securely retain the impact limiter in the worst-case series of free drop and puncture events.

## 2.7.2 Crush

Since the weight of the BRR package exceeds 1,100 lb, the crush test specified in 10 CFR §71.73(c)(2) does not apply.

## 2.7.3 Puncture

The BRR package is evaluated for puncture resistance under HAC as defined in 10 CFR §71.73(c)(3). The puncture event is defined as a free drop from a height of 40 inches onto a vertical, cylindrical mild steel bar, 6 inches in diameter, in an orientation and in a location for which maximum damage is expected. Puncture performance of the BRR package is divided into two categories: puncture on the impact limiters, which was evaluated by half-scale certification test, and puncture of the package body, which is evaluated by analysis.

### 2.7.3.1 Puncture on the Impact Limiters

Appendix 2.12.2, *Certification Test Plan*, discusses the strategy used to evaluate the puncture performance of the impact limiters under the worst-case conditions, including the test objectives and success criteria. Section 2.12.2.4.1, *Test Sequence and Damage Accumulation*, identifies the five puncture tests that were performed on the half-scale certification test unit. The results of these tests is summarized below. Details are to be found in Appendix 2.12.3, *Certification Test Results*. The configuration of each test is shown schematically in Figure 2.12.3-2.

**Test P1.** This test was designed to show that the puncture bar would not penetrate beyond the impact limiter shell located on the flat bottom. This protects the closure lid from direct puncture bar loading, and prevents possible excessive loss of foam for protection in the HAC fire event. This test was performed subsequent to the end free drop test. The bar impacted the shell at an oblique angle through the cask c.g., which would enhance its ability to perforate the plate. The result shown in Figure 2.12.3-12 demonstrates that the impact limiter shell prevents perforation by the bar.

**Test P2.** This test was designed to show that the puncture bar would not create a significant exposure of foam adjacent to the cask (and containment seal) or dislodge the impact limiter from

the end of the cask. Although Figure 2.12.3-2 shows the impact occurring on the same side as the slapdown free drop primary damage, it was found that it would be much more challenging to impact the side opposite to this damage, since that is the azimuth location where the attachments experienced the greatest loading in the free drop. This test was successfully repeated (test P2C) after the redesign of the impact limiter attachments, and subsequent to the repeated 15° oblique slapdown free drop (test D2C). As shown in Figure 2.12.3-40, the impact with the bar did not perforate the shell or expose any foam, and the discussion in Section 2.12.3.6.4, *Examination of Attachments*, documents that the impact limiter was not dislodged by the impact.

**Test P3.** This test was designed to show that the puncture bar would not enter the impact limiter through a side impact on the limiter shell (in this case, the secondary slapdown damage area caused by the 15° oblique slapdown free drop) and rip open a large area that could compromise the performance in the subsequent HAC fire event. As shown in Figure 2.12.3-34, no perforation of the shell occurred.

**Test P4.** This test was designed to show that the puncture bar damage from impact on the c.g.-over-corner free drop damage would be acceptable. The bar impacted the thinner shell material (formerly the conical portion of the limiter shell, before the free drop deformation occurred), adjacent to the thicker bottom plate material. As shown in Figure 2.12.3-29, the exposure of foam from this test was modest, and is bounded by a large margin by the exposure of foam from test P5.

**Test P5.** This test was originally designed to apply an oblique impact on a damaged portion of the shell to determine that the exposure of foam would be acceptable. When it was determined that the limiter shell corner joint between the top flat annular portion and the cylindrical side had developed a crack in the secondary 15° oblique slapdown free drop, this test was used to accumulate the maximum amount of damage in that area. The orientation of the test is shown in Figure 2.12.3-30. The impact with the bar opened up the cracked region and peeled back part of the annular plate, exposing the underlying foam. The final configuration is shown in Figure 2.12.3-31 and Figure 2.12.3-32. Since this test is clearly governing above the other puncture tests regarding the HAC fire event, it is used in modeling the fire event as discussed in Section 3.4, *Thermal Evaluation for Hypothetical Accident Conditions*. It is worth noting that a design change was made subsequent to this test, aimed at preventing this breach of the joint from recurring. The design shown in Appendix 1.3.3, *Packaging General Arrangement Drawings*, includes the stronger joint. The details of the change are discussed in Section 2.12.3.3, *Test Unit Configuration*. However, as just noted, in spite of the design change, the result from the half-scale puncture test P5 was conservatively used for the HAC fire event analysis.

### 2.7.3.2 Puncture on the Cask Body

The puncture resistance of the outer surface of the cask body is evaluated using Nelms' Equation [27], which is used to determine the resistance to puncture of lead-backed stainless steel shells. For the NCT hot case temperature of 250 °F, the ultimate strength of the Type 304 outer shell (assuming the lower strength cast or forged option) is  $S_u = 64,050$  psi from Table 2.2-2. The bounding weight of the BRR package, including impact limiters, is  $W = 32,000$  lb. The required thickness of the outer shell to resist puncture is:

$$t = \left( \frac{W}{S_u} \right)^{0.71} = 0.61 \text{ inches}$$

The thickness of the outer shell is 2 inches. The margin of safety on the cask outer shell thickness is:

$$MS = \frac{2.0}{0.61} - 1 = +2.28$$

Therefore, puncture of the BRR package is not of concern.

## 2.7.4 Thermal

The BRR package is designed to withstand the HAC 30 minute fire specified in 10 CFR §71.73(c)(4). The thermal evaluation is presented in Section 3.4, *Thermal Evaluation under Hypothetical Accident Conditions*.

### 2.7.4.1 Summary of Pressures and Temperatures

As shown in Table 3.1-2, the maximum internal cask pressure as a result of the HAC fire event is 8.8 psig. This is lower than the bounding value of MNOP of 10 psig, and significantly lower than the design pressure of 25 psig stated in Section 2.6.1.1, *Summary of Temperatures and Pressures*. Package component stresses were calculated for an internal pressure of 25 psig in Section 2.6.1.3, *Stress Calculations*, and are compared to allowable stress at the higher HAC temperature in Section 2.7.4.3, *Stress Calculations*.

From Table 3.1-1, as a result of the HAC fire event, the maximum temperature of any part of the cask (except closure bolts) may be bounded by a temperature of 710 °F. The maximum temperature of the closure bolts is considered to be the same as that of the closure lid, bounded by a temperature of 350 °F. Conservatively, all stainless steel components will be assumed to be made from cast or forged Type 304 material, which has a lower ultimate strength than plate material. From Table 2.2-2,  $S_u = 59,140$  psi at 710 °F. The value of  $S_u$  for the closure bolts at 350 °F is equal to 125,000 psi, from Table 2.2-3.

### 2.7.4.2 Differential Thermal Expansion

Differential expansion under NCT is evaluated in Section 2.6.1.2.1, *Baskets*. In that case, the basket was given a uniform bounding temperature of 400 °F, and the thermal expansion of the cask was conservatively neglected. The resulting minimum axial clearance is shown as 0.16 inches, and the minimum diametral clearance is 0.10 inches. In the HAC fire event, from Table 3.1-1, the peak basket temperature is given as 437 °F. Since the basket temperature is locally only 37 °F hotter than the uniform NCT assumption, and in consideration of the significant thermal expansion of the cask cavity dimensions (for example, the inner shell peak temperature is 393 °F), the clearance between the basket and the cask will not be significantly affected by the cask temperatures resulting from the fire event.

Similarly, the fuel axial clearance was evaluated using a uniform bounding temperature of 400 °F in Section 2.6.1.2.2, *Fuel*, and found to have a minimum value of 0.19 inches. Given that the local peak fuel temperature, from Table 3.1-1 is only 451 °F, and that the NCT evaluation again



neglected the thermal expansion of the cask components, the clearance between the fuel and the basket will not be significantly affected by the cask temperatures resulting from the fire event.

### 2.7.4.3 Stress Calculations

Cask stress due to the internal design pressure of 25 psig is presented in Section 2.6.1.3.1, *Stresses Due to Pressure Loading*, as equal to 1,002 psi. This corresponds to the stress in the outer fiber of the closure lid, and is classified as a membrane plus bending stress. This stress clearly bounds the stress generated under an internal pressure in the HAC fire event of 8.8 psig, and the margin of safety may be conservatively calculated using this stress along with the lower fire case allowable stress determined in Section 2.7.4.1, *Summary of Temperatures and Pressures*. The margin of safety is:

$$MS = \frac{59,140}{1,002} - 1 = +58.0$$

The primary load on the closure bolts is governed by the preload force, calculated in Section 2.6.1.5, *Closure Bolts*, as equal to 19,200 lb. The stress is:

$$S_{bs} = 1.2732 \frac{19,200}{D_{ba}^2} = 31,711 \text{ psi}$$

where the stress diameter,  $D_{ba} = 0.878$  inches from Section 2.6.1.5. From Table 2.1-1, the allowable average tensile stress intensity for HAC is the lesser of  $0.7S_u$  or  $S_y$ , which for the ASTM A320 L43 bolting material is  $0.7S_u = 87,500$  psi at 350 °F. The margin of safety is:

$$MS = \frac{87,500}{31,711} - 1 = +1.76$$

Per Regulatory Guide 7.6, paragraph C.7, the extreme range of stress must be considered. Of all the various allowable stresses corresponding to the different conditions evaluated (including fabrication stresses and normal conditions of transport), the largest allowable stress is equal to the material ultimate strength,  $S_u$ . It is therefore conservative to assume that  $S_u$  bounds all stresses actually developed in the structure. For Type 304 stainless steel,  $S_u = 75,000$  psi at 70 °F. The maximum possible stress intensity range is twice this value, or 150,000 psi.

Applying a factor of four to account for possible stress concentrations at structural discontinuities gives a total elastic stress range of 600,000 psi. The alternating component is one-half of this value, or 300,000 psi. To account for temperature effects, this value of alternating stress is factored by the ratio of modulus of elasticity. This ratio is formed between the modulus of elasticity at room temperature (at which the test data applies directly) and the modulus of elasticity at the maximum temperature, conservatively bounded by a temperature of 710 °F for any structural part of the package. The adjusted stress is

$$S_{alt} = 300,000 \frac{E_{70^\circ F}}{E_{710^\circ F}} = 343,725 \text{ psi}$$

where  $E_{70^\circ F} = 28.3(10^6)$  psi and  $E_{710^\circ F} = 24.7(10^6)$  psi. Per Figure I-9.2.1 and Table I-9.1 of the ASME Code [9], the allowable value for  $S_{alt}$  at 10 cycles is 708,000 psi. The margin of safety is

$$MS = \frac{708,000}{343,725} - 1 = +1.06$$

Considering the significant conservatism used in the underlying assumptions (e.g., use of allowable stress rather than smaller actual stresses, assuming worst case stresses are fully reversing, use of the maximum factor of stress concentration), it is apparent that the actual margin of safety is larger than 1.06. Thus, the requirement of paragraph C.7 of Regulatory Guide 7.6 is met.

### 2.7.5 Immersion – Fissile

An immersion test for fissile material packages is required by 10 CFR §71.73(c)(5). The criticality evaluation presented in Chapter 6, *Criticality Evaluation*, assumes optimum hydrogenous moderation of the contents, thereby conservatively addressing the effects and consequences of water in-leakage.

### 2.7.6 Immersion – All Packages

An immersion test for all packages is required by 10 CFR §71.73(c)(6), in which a separate, undamaged specimen must be subjected an equivalent pressure of 21.7 psig. Since the BRR package is evaluated to the much greater hydrostatic pressure of the deep immersion test (see the next section), this test does not need to be evaluated.

### 2.7.7 Deep Water Immersion Test (for Type B Packages Containing More than $10^5 A_2$ )

For Type B packages containing an activity of more than  $10^5 A_2$ , 10 CFR §71.61 requires that an undamaged containment system withstand an external pressure of  $p_o = 290$  psig for a period of not less than one hour without collapse, buckling, or inleakage of water. This test will not have a significant effect on the BRR package. Although a temperature is not specified for this test, a lead shrinkage (fabrication) stress corresponding to a temperature of  $-40$  °F, taken from Section 2.6.2, *Cold*, will be conservatively applied in addition to the specified hydrostatic pressure. The lead shrinkage pressure is  $p_c = 787$  psi. Conservatively, the inner shell is evaluated neglecting the outer shell, even though the external pressure would be applied to the much stronger outer shell.

The internal pressure in the cask is assumed to be ambient, thus the net external pressure across the inner shell on its outer cylindrical surface is equal to a sum of the applied hydrostatic pressure of 290 psig and the lead shrinkage pressure of 787 psi, or a total of:

$$p_{cyl} = 290 + 787 = 1,077 \text{ psi}$$

The compressive hoop stress is:

$$\sigma_{\theta} = p_{cyl} \frac{r_{avg}}{t} = 9,155 \text{ psi}$$

where the mean inner shell radius,  $r_{avg} = 8.5$  inches, and the thickness,  $t =$  one inch. The compressive axial stress, obtained by supporting the hydrostatic pressure load,  $p_o$ , from the entire cask end cross section over the inner shell cross section, is:

$$\sigma_{\phi} = \frac{p_o \pi r_{\text{cask}}^2}{2 \pi r_{\text{avg}} t} = 6,289 \text{ psi}$$

where  $r_{\text{cask}} = 38.4/2 = 19.2$  inches. Using Mohr's circle, the maximum shear stress is:

$$\sigma_{\phi\theta} = \frac{1}{2}(\sigma_{\theta} - \sigma_{\phi}) = 1,433 \text{ psi}$$

The possibility of buckling of the inner shell is evaluated using [13]. Consistent with Regulatory Guide 7.6, a factor of safety corresponding to ASME Code, Service Level D is employed. In this case, the applicable factor of safety is 1.34 for hypothetical accident conditions, as specified in [13]. The analysis used a modulus of elasticity of  $28.3(10^6)$  psi, corresponding to 70 °F. Buckling analysis geometry and loading parameters are listed in Table 2.7-7 and results of the analysis in Table 2.7-8. As shown, all interaction parameters, including the maximum value of 0.4286, are less than unity, as required. Thus, the deep water immersion test is not of concern for the BRR package.

### 2.7.8 Summary of Damage

From the analyses presented, it is shown that the HAC sequence does not result in significant damage to the BRR package, and that all stress criteria established for HAC in Section 2.1.2, *Design Criteria*, are satisfied. The margins of safety resulting from the analyses performed in this section are shown in Table 2.7-9.

The BRR cask body and internal components were evaluated primarily by analysis, and the impact limiters and attachments were evaluated by test. The test results confirmed that the impact acceleration of 120g used in the analyses was bounding for all free drop orientations. The tests are summarized below.

The analysis of the cask body and internal components under free drop impact included the cask body structure, the closure lid, the closure bolts, and the shield plug shell. Bounding orientations of end and side drop were evaluated. A demonstration that the side drop governs over the worst-case slapdown is provided in Section 2.7.1.4, *Oblique Drop*. The cask body was analyzed using finite element analysis, in which the cask was loaded by self-weight and contents weight, and supported by the impact limiters. Conservatively, the lead shielding was considered to act as a fluid, having no structural strength. The minimum margin of safety from the finite element analysis, which corresponded to the side drop impact case, was +0.23. All of the manual evaluations resulted in larger margins of safety, as shown in Table 2.7-9. The end drop buckling analysis of the package shells, performed using ASME Code Case N-284-2, resulted in a maximum check value of 0.4024, which is well below the limit of unity, as required by the Code Case. An evaluation of lead slump in the end drop orientation was performed, and resulted in a bounding value of 1.185 inches. This value was used in the shielding evaluation documented in Chapter 5.0, *Shielding Evaluation*. An analysis of the fuel baskets was performed as documented in Appendix 2.12.8, *Fuel Basket Stress Analysis*. Each basket was evaluated for governing modes of failure, with a minimum margin of safety of +0.12. A summary of the margins of safety for the fuel baskets is provided in Table 2.7-4. An analysis of the puncture test on the cask body was performed using Nelms' equation, and resulted in a margin of safety of +2.28. Therefore, since all margins of safety are positive, the criteria of Section 2.1.2, *Design Criteria*, are satisfied for the BRR package.

The impact limiter design was tested using half-scale, prototypic certification test units and a dummy cask body. The impact limiters successfully performed their role in limiting the impact acceleration to a value considerably lower than the value of 120g used for stress analysis. In addition, the test showed that the calculated maximum strain in the energy-absorbing polyurethane foam of 83.2% was conservative. Some exposure of the foam was produced by the worst-case sequence of free drop and puncture tests. The final configuration of the impact limiter shell and of the exposed foam was included in the HAC fire event thermal model as described in Section 3.5.3.7, *Description of Thermal Model for HAC Conditions*. The impact limiter attachments, subsequent to a redesign and retest under the worst-case free drop and puncture conditions, successfully retained the impact limiters on the cask. Therefore the impact limiters satisfy their design criteria established in Section 2.1.2.2, *Other Structures*.

**Table 2.7-1 – HAC Free Drop Buckling Evaluation: Geometry and Loads**

	<b>Outer shell dimensions, inches</b>	<b>Applied stress, psi</b>	
Inner Dia.	34.0	$\sigma_{\phi}$	7,117
Outer Dia.	38.0	$\sigma_{\theta}$	0
Length (bounding)	55.0	$\sigma_{\phi\theta}$	0

Table 2.7-2 – HAC Free Drop: N-284-2 Results

Parameter	Value	Remarks
<b>Capacity Reduction Factors (-1511)</b>		
$\alpha_{\phi L} =$	0.2279	
$\alpha_{\theta L} =$	0.8000	
$\alpha_{\phi\theta L} =$	0.8000	
<b>Plasticity Reduction Factors (-1610)</b>		
$\eta_{\phi} =$	0.0568	
$\eta_{\theta} =$	0.0850	
$\eta_{\phi\theta} =$	0.0232	
<b>Theoretical Buckling Values (-1712.1.1)</b>		
$C_{\phi} =$	0.6050	
$\sigma_{\phi eL} =$	1,831,806 psi	
$C_{\theta r} =$	0.1150	
$\sigma_{\theta eL} = \sigma_{reL} =$	348,340 psi	
$C_{\theta h} =$	0.1078	
$\sigma_{\theta eL} = \sigma_{heL} =$	326,534 psi	
$C_{\phi\theta} =$	0.2527	
$\sigma_{\phi\theta eL} =$	765,157 psi	
<b>Elastic Interaction Equations (-1713.1.1)</b>		
$\sigma_{xa} =$	311,567 psi	
$\sigma_{ha} =$	194,946 psi	
$\sigma_{ra} =$	207,964 psi	
$\sigma_{\tau a} =$	456,810 psi	
Axial + Shear $\Rightarrow$ Check (c):	0.0228	<1 $\therefore$ OK (see note*)
Hoop + Shear $\Rightarrow$ Check (d):	0.0000	<1 $\therefore$ OK
<b>Inelastic Interaction Equations (-1714.2.1)</b>		
$\sigma_{xc} =$	17,687 psi	
$\sigma_{rc} =$	17,687 psi	
$\sigma_{\tau c} =$	10,612 psi	
Max(Axial,Hoop) $\Rightarrow$ Check (a):	0.4024	<1 $\therefore$ OK
Axial + Shear $\Rightarrow$ Check (b):	0.4024	<1 $\therefore$ OK
Hoop + Shear $\Rightarrow$ Check (c):	0.0000	<1 $\therefore$ OK

\*Note: Elastic interaction checks (a), (b), (e), and (f) are not applicable.

**Table 2.7-3 – Cask Shell Force and Stress Comparison**

Case	Impact Limiter Force, lb	Axial Force, R, lb	Shear Force, V, lb	Bending Moment, M, in-lb	Relative Stress Intensity, psi
Side Drop	1.920(10 <sup>6</sup> )	0	1.920(10 <sup>6</sup> )	33.600(10 <sup>6</sup> )	164,077*
15°, Primary	1.049(10 <sup>6</sup> )	271,501	1.013(10 <sup>6</sup> )	10.508(10 <sup>6</sup> )	59,940*
15°, Secondary	1.143(10 <sup>6</sup> )	0	1.143(10 <sup>6</sup> )	11.853(10 <sup>6</sup> )	62,441*

\*Stress for comparison purposes only; not actual inner shell stress.

**Table 2.7-4 – Fuel Basket Stress Analysis Results**

Analysis Description	Reference Section <sup>①</sup>	Margin of Safety
<b>MURR Basket</b>		
Fuel Support Plate Bending		+8.32
Outer Shell Slot Welds		+3.00
Buckling of Lower Shell		Pass <sup>②</sup>
<b>MITR-II Basket</b>		
Buckling of Lower Shell		Pass <sup>②</sup>
Buckling of Fuel Tubes		+5.71
Side Drop Bending		+4.90
<b>ATR Basket</b>		
Fuel Support Plate Bending		+10.2
Outer Shell Slot Welds		+1.02
Side Drop Bending		+4.16
<b>TRIGA Basket</b>		
Fuel Support Plate Bending		+0.65
Shear Load on Spacer Screw		+0.12
Buckling of Fuel Tubes		Pass <sup>②</sup>
Side Drop Bending		+1.81

**Notes:**

1. Calculational details are presented in Appendix 2.12.8, *Fuel Basket Stress Analysis*.
2. Interaction equation checks are less than unity, as required by [13].

**Table 2.7-5 – Fuel Impact Deformation Results**

Fuel Type	W, lb	L <sub>FB</sub>	A <sub>XC</sub> , in <sup>2</sup>	W/A <sub>XC</sub> , lb/in <sup>2</sup>	GAP	L, in
MURR	15	0.38	4.584	3.27	1.18	0.035
MITR-II	10	0.36	3.814	2.62	1.17	0.028
ATR	25	0.38	3.961	6.31	1.68	0.096
TRIGA	10	0.37	1.72*	5.81	1.18	0.062

\*TRIGA fuel has 0.03-inch thick cladding for aluminum clad and 0.02-inch thick cladding for stainless steel clad fuel. Since the entire fuel cross-section is made of a strong material (fuel pellet of UZrH), the area used is that of the entire pellet cross-section of 1.48 inches.

**Table 2.7-6 – Impact Limiter Attachment Comparisons**

Feature Description	Refurbished Test article (Full-scale Equiv.)	Final Production Design (per Appendix 1.3.3)	Remarks
Blade and receptacle material	ASTM Type 304	ASTM Type 304	Same
Blade thickness, in.	3/4	3/4	Same
Blade width, in.	3.0	3.3	Improved
Hole diameter in blade, in.	1.13	1.13	Same
Hole-to-blade edge, in.	0.94	1.06	Improved
Blade weld to limiter inner shell structure	3/8-in. fillet on both sides	3/8-in. fillet on both sides	Same
Receptacle plate thickness, in.	3/8	1/2	Improved
Ball lock pin diameter, in.	1.0	1.0	Same
Pin material	Carbon steel	Stainless steel	Improved
Pin rated double shear strength, lb	65,600	73,500	Improved
Attachment quantity per limiter	6	8	Improved

**Table 2.7-7 – Deep Immersion Test: Geometry and Loads**

	Inner shell dimensions, inches	Applied stress, psi	
		$\sigma_{\phi}$	$\sigma_{\theta}$
Inner Dia.	16.0	$\sigma_{\phi}$	6,289
Outer Dia.	18.0	$\sigma_{\theta}$	9,155
Length (bounding)	62.0	$\sigma_{\theta\theta}$	1,433

Table 2.7-8 – Deep Immersion Test: N-284-2 Results

Parameter	Value	Remarks
<b>Capacity Reduction Factors (-1511)</b>		
$\alpha_{\phi L} =$	0.2850	
$\alpha_{\theta L} =$	0.8000	
$\alpha_{\phi\theta L} =$	0.8000	
<b>Plasticity Reduction Factors (-1610)</b>		
$\eta_{\phi} =$	0.0523	
$\eta_{\theta} =$	0.2856	
$\eta_{\phi\theta} =$	0.0417	
<b>Theoretical Buckling Values (-1712.1.1)</b>		
$C_{\phi} =$	0.6050	
$\sigma_{\phi eL} =$	2,014,294 psi	
$C_{\theta r} =$	0.0387	
$\sigma_{\theta eL} = \sigma_{reL} =$	128,711 psi	
$C_{\theta h} =$	0.0387	
$\sigma_{\theta eL} = \sigma_{heL} =$	128,711 psi	
$C_{\phi\theta} =$	0.1619	
$\sigma_{\phi\theta eL} =$	539,157 psi	
<b>Elastic Interaction Equations (-1713.1.1)</b>		
$\sigma_{xa} =$	428,445 psi	
$\sigma_{ha} =$	76,843 psi	
$\sigma_{ra} =$	76,843 psi	
$\sigma_{\tau a} =$	321,885 psi	
Axial + Shear $\Rightarrow$ Check (c):	0.0147	<1 $\therefore$ OK (see note*)
Hoop + Shear $\Rightarrow$ Check (d):	0.1192	<1 $\therefore$ OK
<b>Inelastic Interaction Equations (-1714.2.1)</b>		
$\sigma_{xc} =$	22,388 psi	
$\sigma_{rc} =$	21,943 psi	
$\sigma_{\tau c} =$	13,433 psi	
Max(Axial,Hoop) $\Rightarrow$ Check (a):	0.4172	<1 $\therefore$ OK
Axial + Shear $\Rightarrow$ Check (b):	0.2923	<1 $\therefore$ OK
Hoop + Shear $\Rightarrow$ Check (c):	0.4286	<1 $\therefore$ OK

\*Note: Elastic interaction checks (a), (b), (e), and (f) are not applicable.



**Table 2.7-9 – Minimum Margins of Safety from HAC Evaluations**

Component	Loading Condition	Minimum Margin of Safety
<i>Free Drop</i>		
Cask body (FEA)	End drop, bottom down, membrane stress	+0.98
	End drop, bottom down, membrane + bending	+0.49
	End drop, top down, membrane stress	+0.97
	End drop, top down, membrane + bending stress	+0.92
	Side drop, membrane stress	+1.75
	Side drop, membrane + bending stress	+0.23
Lower closure plate	End drop, bottom down, membrane + bending	+0.40
Closure bolts	End drop, top down	+0.83
Closure lid	End drop, top down	+1.65
Shield plug shell lower plate	End drop, bottom down, assuming simple support, stress at center	+0.46
	End drop, bottom down, assuming fixed edge support, stress at edge (weld)	+0.91
Cask outer shell	End drop, buckling (Code Case N-284-2)	0.4024*
<i>Puncture</i>		
Cask outer shell	Nelms' Equation	+2.28
<i>Thermal</i>		
Containment boundary	Internal pressure, fire conditions	+58.0
Closure bolts	Internal pressure, fire conditions	+1.76
Cask	Range of stress	+1.06

\*Maximum check value must be less than unity.

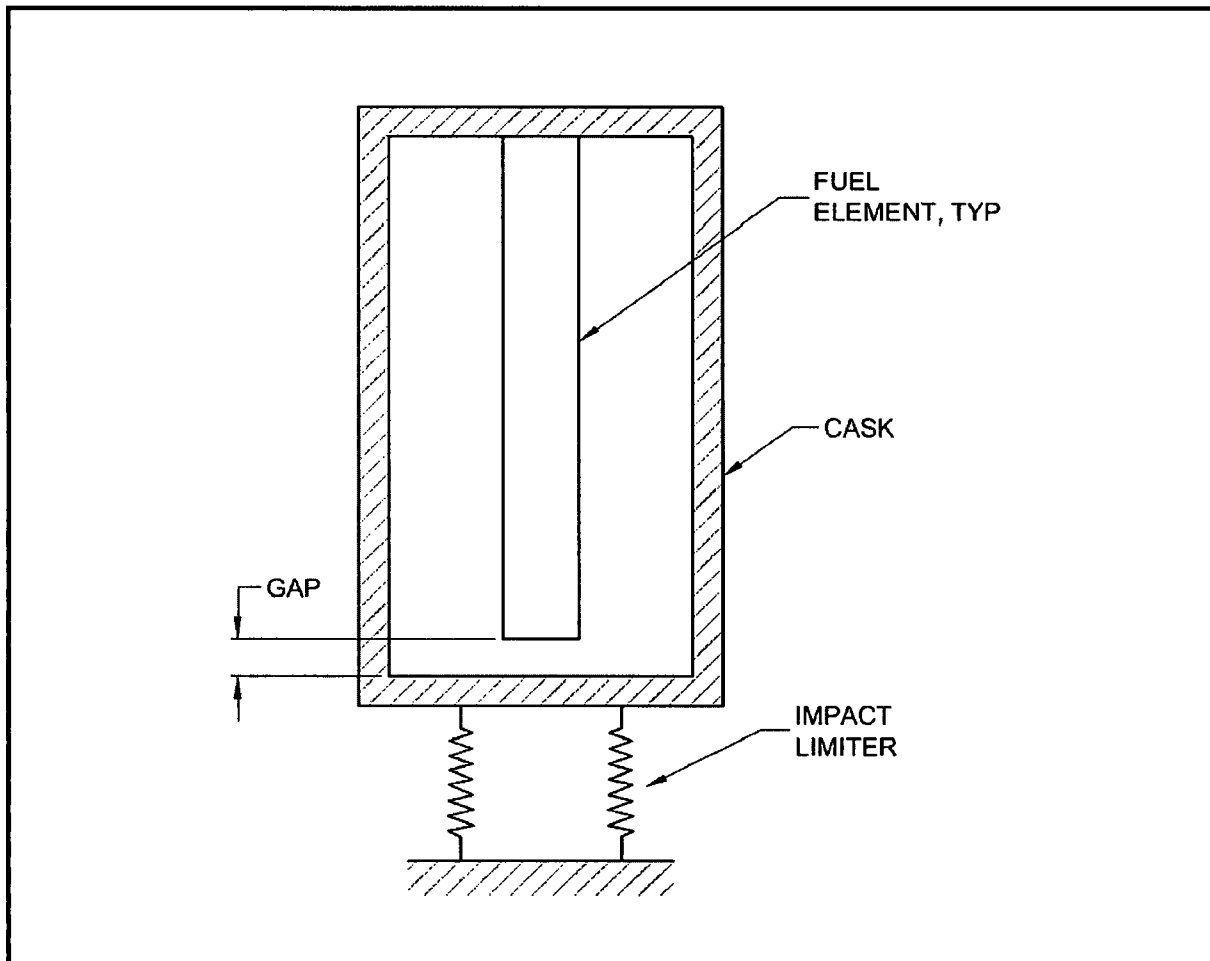


Figure 2.7-1 – Cask Cavity and Fuel During Free End Drop

30. G. D. Sjaardema and G. W. Wellman, *Numerical and Analytical Methods for Approximating the Eccentric Impact Response (Slapdown) of Deformable Bodies*, SAND88-0616 (UC-71), Sandia National Laboratories.
31. **SCANS** (*Shipping Cask ANalysis System*), *A Microcomputer Based Analysis System for Shipping Cask Design Review*, NUREG/CR-4554 (UCID-20674), Lawrence Livermore National Laboratory.
32. American Society of Mechanical Engineers (ASME) Boiler and Pressure Vessel Code, Section III, *Rules for Construction of Nuclear Facility Components*, Division 1 – Subsection NG, *Core Support Structures*, Article NG-3350, 2007 Edition.
33. American Society of Mechanical Engineers (ASME) Boiler and Pressure Vessel Code, Section III, *Rules for Construction of Nuclear Facility Components*, Appendix F, *Rules for Evaluation of Service Loadings with Level D Service Limits*, 2007 Edition.
34. General Plastics Manufacturing Company, *General Plastics Last-A-Foam® FR-3700 For Crash & Fire Protection of Radioactive Material Shipping Containers*, June 1997.

### **2.12.3.4 Instrumentation**

#### **2.12.3.4.1 Accelerometers**

Accelerometers were used to record the impact of each free drop, except drop D2C, which was a confirmatory test for the revised impact limiter attachments. Accelerations of the puncture drops were not recorded. For axial or near-axial drop orientations (D1 – end drop, and D3 – c.g.-over-corner drop), the measurement axis of the accelerometers was axial. For the near-horizontal, 15° slapdown drops (D2 and D2R), the measurement axis was transverse to the cask axis.

Four axial and four transverse mounting positions were provided at each end of the cask. The measurement axes were as close to the cask surface as possible, and the mounting blocks were rigidly welded to the cask. The transverse measurement axis was located 8.68 inches from the flat end of the cask. The mounting location and orientation of each accelerometer is shown in Figure 2.12.3-5 and Figure 2.12.3-6. The transverse accelerometers at each end were all mounted on the same axial plane with their axes parallel.

The raw data was conditioned and low-pass filtered at a level of 1019 Hz. As shown in Section 2.12.3.7, *Accelerometer Plots*, the filtered accelerometer time histories retain a significant vibrational component, indicating that a lower filter cutoff frequency could have been used, which would have lowered the peak values by more than 10%. Thus, use of the stated filter cutoff is conservative. The filtered peak acceleration values are adjusted using the accelerometer calibration constants listed in Table 2.12.3-5 below. The adjustment is only made to the peak value of the accelerometer output, as shown in Section 2.12.3.5, and not to the entire output. Thus, the filtered accelerometer plots, in Section 2.12.3.7, do not show the effect of this adjustment. Since the calibration constants are all between 0.89 and 0.97 mV/g, the adjusted peak acceleration value is approximately 10% higher than the peak value shown on the plots in Section 2.12.3.7. Individual results are discussed in Section 2.12.3.5.

#### **2.12.3.4.2 Thermocouples**

A refrigerated trailer was present onsite to chill the certification test articles prior to assembly onto the dummy cask for testing. Thermocouples were inserted in 1/8-inch diameter holes in each test article, five inches deep, and approximately 6.75 inches from the flat annulus side of the test article. Two thermocouples were used for each test article, located 180° apart. Since the minimum temperature which could be set on the chiller unit was -20 °F, the test articles were generally between -10 °F and -20 °F at the time of test. The temperature of the foam in tests D3, P2, P2C, P3, P4, and P5 was not required to be cold. Temperature of the foam was recorded just prior to the test for the impact limiter(s) experiencing impact or puncture.

#### **2.12.3.5 Test Results**

Results for the initial series of four, 30-ft free drop tests and five puncture drop tests are given in the sections below. (Results for the confirmatory test of the attachments (tests D2C and P2C) are given in Section 2.12.3.6, *Confirmatory Test of Attachments*.) The tests were performed in the order D1, P1, D2, D2R, P2, D3, P4, P5, P3. A description of the tests is given in Table 2.12.3-2. Figures of the tests are shown in Figure 2.12.3-1 and Figure 2.12.3-2. Peak accelerations given in tables below are taken from the accelerometer time histories shown in Section 2.12.3.7, *Accelerometer Plots*. The average of the peak values is then resolved to a value which is

**BRR Package Safety Analysis Report**

perpendicular to the ground, when necessary. Since the data was collected orthogonal to the cask axes, the resolution of the data in the oblique impact cases is as follows.

For test D1, which was a vertical end drop, the accelerometers were mounted with their measurement axes parallel to the dummy cask axis. Therefore, the accelerometer readings require no adjustment.

For tests D2 and D2R, which were identical, 15° slapdown free drops, the accelerometers were mounted with their measurement axes transverse to the dummy cask axis. For the secondary impact, in which the cask axis is essentially parallel to the ground, the accelerometer readings require no adjustment. For the primary impact at 15°, the average accelerometer reading is divided by the cosine of the recorded impact angle to obtain the impact which occurred perpendicular to the ground.

For test D3, which was the c.g.-over-corner free drop, the accelerometers were mounted with their measurement axes parallel to the dummy cask axis. The average accelerometer reading is divided by the cosine of 23°, which corresponds to the recorded angle between the cask axis in the c.g.-over-corner drop and the ground, to obtain the impact perpendicular to the ground.

All puncture drop tests were performed from a height of 40 inches above the top of the puncture bar. All puncture tests except P2 and P2C were performed using a 25-inch long puncture bar. Tests P2 and P2C utilized the 50-inch long bar. The puncture bars remained securely attached to the steel drop pad in all cases.

For each test, the recorded temperature of the polyurethane foam was taken as described in Section 2.12.3.4.2, *Thermocouples*. Note that all data reported in this appendix applies to the half-scale test unless stated otherwise. According to the laws of scaling, the full-scale linear measurements are twice those recorded here, and the full-scale accelerations are half of those recorded here. The tests are documented in the order in which they were performed.

**2.12.3.5.1 Free Drop, Vertical (D1)**

Test D1 was performed using a drop height of 30 feet, oriented with the cask axis vertical, as shown in Figure 2.12.3-1 and Figure 2.12.3-7. The lower impact limiter was serial number 1. The two polyurethane foam temperature readings were -16.4 °F and -15.6 °F. Four accelerometers were used. Results are shown in the table below.

<b>Free Drop Test D1 (End)</b>					
<b>Channel</b>	<b>12</b>	<b>13</b>	<b>14</b>	<b>15</b>	<b>Avg.</b>
<b>Peak Value</b>	110g	121g	113g	118g	<b>116g</b>

The impact deformation was a combination of outside-in and inside-out. The outside-in crush depth is calculated from the diameter of the scuff mark (contact area) on the bottom of the limiter. Two orthogonal diameter measurements showed a scuff diameter of 27-1/2 and 27-5/8 inches, or an average of 27.6 inches. Since the original diameter of the bottom of the impact limiter was 24.0 inches, and the tapered portion had an angle of 45°, the outside-in crush distance is:

$$(D_{\text{scuff}} - D_{\text{orig}}) / 2 = 1.8 \text{ inches}$$

**BRR Package Safety Analysis Report**

The inside-out crush distance is calculated from the dimension from the top of the dummy cask (with the upper impact limiter removed) to the outside rim of the lower impact limiter. Since the outside rim of the limiter is undeformed, this measurement will reveal how far the dummy cask has "sunk" into the lower impact limiter. Measurements of this distance, taken in four quadrants, were 29-7/8, 29-7/8, 30-1/2, and 30-7/16 inches. The average value is 30.2 inches. In an undeformed limiter, the top surface of the cask would stand  $(38.6 - 6.8) = 31.8$  inches above the outer rim of the lower limiter, given that the cask is 38.6 inches long, and the center pocket of the limiter is 6.8 inches deep. The inside-out crush is therefore  $(31.8 - 30.2) = 1.6$  inches. The sum of the outside-in and inside-out crush distances is therefore  $1.8 + 1.6 = 3.4$  inches.

The impact limiter was securely attached following the test. Of the six impact limiter attachment pins, one failed by bending and shear, and others showed signs of bending without failure. At least two had no noticeable damage. The shells of the limiter deformed without any tearing or exposure of foam. The post-test configuration is depicted in Figure 2.12.3-8 and Figure 2.12.3-9.

**2.12.3.5.2 Puncture Drop Test P1**

Puncture test P1 was performed immediately after drop test D1. The test was a c.g.-over-corner impact on the thicker bottom plate of the impact limiter, near the outer edge of the thicker plate, as shown in Figure 2.12.3-2 and Figure 2.12.3-10. The impact took place on the crush damage from free drop test D1, on serial number 1. The angle of the cask axis was  $73^\circ \pm 3^\circ$  to the horizontal. The two polyurethane foam temperature readings were  $-3.8^\circ\text{F}$  and  $-5.0^\circ\text{F}$ .

The bar impact was located approximately one inch from the outer edge of the thicker bottom plate (i.e., the center of the 3-inch bar was approximately 2-1/2 inches in from the edge). The impact created a dent approximately 1-3/4 inches deep. One or two rebound impacts having negligible deformation also occurred. There were no signs of cracking in the dent or in the nearby weld seam. The post-test configuration is depicted in Figure 2.12.3-11 and Figure 2.12.3-12.

**2.12.3.5.3 Oblique Slapdown Free Drop Test D2**

Test D2 was performed using a drop height of 30 feet, oriented with the cask axis at  $16^\circ$  to the horizontal, as shown in Figure 2.12.3-1 and Figure 2.12.3-13. The primary (lower) impact limiter was serial number 2, and the secondary (upper) impact limiter was serial number 3. The polyurethane foam temperature reading in the primary limiter was  $-15.6^\circ\text{F}$  (only one thermocouple was functioning), and in the secondary limiter, the readings were  $-13.8^\circ\text{F}$  and  $-16.4^\circ\text{F}$ . Four accelerometers were used at each end. Results are shown in the table below.

Free Drop Test D2 (15° Oblique)					
Channel	16	17	18	19	Avg., Primary End
Peak Value, g	Severed wire	133g	137g	135g	140g $\perp$ to ground*
Channel	12	13	14	15	Avg., Secondary End
Peak Value, g	102g	108g	110g	108g	107g

\*Equal to  $(133 + 137 + 135)/3/\cos(16^\circ)$ .

The general post-test configuration is shown in Figure 2.12.3-14. Comparing the measurements of the undeformed and deformed impact limiters, as shown in Figure 2.12.3-15, the crush

**BRR Package Safety Analysis Report**

distance, perpendicular to the ground, was 3.9 inches for the primary impact limiter and 4.0 inches for the secondary impact limiter.

In the test, all of the attachment pins on the primary impact limiter sheared off. The limiter remained attached to the cask, although after coming to rest, it was displaced approximately 1-1/2 inches at the top, as shown in Figure 2.12.3-16. None of the pins failed on the secondary impact limiter. There was some incipient cracking of the weld seam on the secondary limiter, but the cracks were of insignificant size and no foam was exposed. The impact surfaces of the impact limiters are shown in Figure 2.12.3-17.

**2.12.3.5.4 Repeated Oblique Slapdown Free Drop Test D2R**

Test D2R was designed as a repeat of test D2, made after increasing the size of the attachment pins from the original diameter of 1/4 inches to 1/2 inches. To accommodate this increase, the hole through the cask attachment lugs was increased to 1/2 inches and the hole in the impact limiter blade was increased to 5/8 inches. The effect of increasing the blade hole size was to reduce the ligament width on both sides of the hole, but especially on the inner side (toward the cask body). These changes were made to all three impact limiter test articles. Due to the small size of these ligaments, the inner ligament width on serial numbers 1 and 3 were enhanced after drilling by application of a Type 308 weld overlay. Serial number 2 ligaments were not enhanced after drilling. The average ligament widths of the three impact limiters are as follows:

- S/N 001: 0.306 inches (weld overlay enhanced)
- S/N 002: 0.243 inches (not welded)
- S/N 003: 0.320 inches (weld overlay enhanced)

The attachment pins were Carr-Lane part no. CL-8-BLPT-2.00, 1/2-inch diameter carbon steel ball lock pins, having a rated load of 16,000 lb, or four times that of the 1/4-inch pins.

Test D2R was performed using a drop height of 30 feet, oriented with the cask axis at 17° to the horizontal, as shown in Figure 2.12.3-1 and Figure 2.12.3-18. The primary (lower) impact limiter was serial number 2, rotated 180° from its orientation in test D2. The secondary (upper) impact limiter was serial number 1. The polyurethane foam temperature readings in the primary limiter were -13.4 °F and -12.8 °F, and in the secondary limiter, the readings were -13.0 °F and -13.4 °F. Four accelerometers were used at each end. Results are shown in the table below.

<b>Free Drop Test D2R (15° Oblique)</b>					
<b>Channel</b>	<b>16</b>	<b>17</b>	<b>18</b>	<b>19</b>	<b>Avg., Primary End</b>
<b>Peak Value, g</b>	111g	116g	106g	106g	<b>115g ⊥ to ground*</b>
<b>Channel</b>	<b>12</b>	<b>13</b>	<b>14</b>	<b>15</b>	<b>Avg., Secondary End</b>
<b>Peak Value, g</b>	113g	111g	106g	124g	<b>114g</b>

\*Equal to  $(111 + 116 + 106 + 106)/4/\cos(17^\circ)$ .

The general post-test configuration is shown in Figure 2.12.3-19. Comparing the measurements of the undeformed and deformed impact limiters, as shown in Figure 2.12.3-20, the crush distance, perpendicular to the ground, was 4.0 inches for the primary impact limiter and 3.9 inches for the secondary impact limiter. Note that the measurements of the crush in test D2 are very similar to these (3.9 inches primary and 4.0 inches secondary). This is to be expected since

**BRR Package Safety Analysis Report**

the tests are essentially identical. However, since this test had prior damage on both of the impact limiters, the results of test D2 will be taken as the official crush results for this orientation.

In the test, none of the attachment pins failed, but four out of six of the blades of the primary limiter failed by tensile failure of the inner ligaments, as shown in Figure 2.12.3-21. The limiter remained attached to the cask, although after coming to rest, it was displaced approximately 2 inches at the top, as shown in Figure 2.12.3-19. None of the pins or ligaments failed on the secondary impact limiter, although the holes were elongated up to 0.854 inches.

In addition, the corner joint between the top annular plate and the outer cylindrical shell of the secondary impact limiter (serial number 1) failed in the impact region, as shown in Figure 2.12.3-22. This limiter had been tested in the 30-foot end drop (D1) and the subsequent puncture (P1), and the torn joint may have been the result of over-testing. The tear had a maximum opening of 1/2 inches. It appeared to start at the outer edges of the impact zone and travel inward. The length of the torn joint on one side was 7-1/2 inches, and on the other side 10-1/4 inches, with approximately 4-3/4 inches of sound material in the center. The tear appeared in both the weld as well as in the leg of the corner angle located on the top surface. However, the tear did not occur in the outer cylindrical shell side of the joint, where the thickness is double by virtue of the lap joint used in that position.

**2.12.3.5.5 Puncture Drop Test P2**

Puncture test P2 was performed immediately after drop test D2R. The longer puncture bar was used to impact the top annular surface of the damaged primary impact limiter (serial number 2), as shown in Figure 2.12.3-2 and Figure 2.12.3-23. The orientation could not be over the center of gravity due to the desired impact location. The impact occurred just to the inside of the bulge, in approximately the radial center of the annular plate. The two polyurethane foam temperature readings were -0.2 °F and -3.0 °F.

The impact dent on the annular plate was negligible, but the impact limiter became significantly dislodged from the cask end due to the failure of the impact limiter attachment blades, as shown in Figure 2.12.3-24. By inspection of the conventional-speed video record, the impact limiter was displaced by a greater amount than is shown in the figure, before it was driven partially back on by a secondary impact with the safety wall.

**2.12.3.5.6 CG-Over-Corner Free Drop Test D3**

Test D3 was performed from a drop height of 30 feet, with the cask axis oriented at 67° to the horizontal, or essentially center of gravity over corner, as shown in Figure 2.12.3-1 and Figure 2.12.3-25. The lower impact limiter was serial number 3, rotated 180° from its orientation in test D2. The polyurethane foam temperature reading in the lower limiter was -2.2 °F (the other thermocouple was not functioning). Four accelerometers were used at each end, oriented parallel to the cask axis. Results are shown in the table below. Note, since channels 16 – 17 exhibited excess noise, only channels 12 – 15 are used.

Free Drop Test D3 (CG Over Corner)					
Channel	12	13	14	15	Avg.
Peak Value, g	106g	111g	110g	103g	117g $\perp$ to ground*



\*Equal to  $(106 + 111 + 110 + 103)/4/\cos(23^\circ)$ .

The general post-test configuration is shown in Figure 2.12.3-26. Comparing the measurements of the undeformed and deformed impact limiters, as shown in Figure 2.12.3-27, the crush distance perpendicular to the ground was 5.5 inches.

None of the pins or ligaments failed the test, although the holes were elongated up to 0.725 inches. There were no shell failures and no exposure of foam.

#### **2.12.3.5.7 Puncture Drop Test P4**

Puncture test P4 was performed on the damage incurred in free drop test D3, on serial number 3. The bar impacted just outside the thicker bottom plate, on the 0.12-inch thick material which once constituted the tapered region of the shell. The orientation is shown in Figure 2.12.3-2 and Figure 2.12.3-28. The cask axis was oriented at  $74^\circ$  to the horizontal. The line of action was nearly, but not completely, c.g.-over-corner. The polyurethane foam temperature readings in the lower limiter were  $17.6^\circ\text{F}$  and  $5.0^\circ\text{F}$ .

As expected, the puncture bar penetrated the shell, and entered the foam to a depth of 2-1/4 inches. The width of the hole was 4 inches, and the length of the hole/torn flap was 5 inches. The impact limiter attachments were not affected. A close-up view of the damage is shown in Figure 2.12.3-29.

#### **2.12.3.5.8 Puncture Drop Test P5**

Puncture test P5 was performed on the damaged corner joint created in free drop test D2R on serial number 1 (the secondary impact end). The orientation is shown in Figure 2.12.3-2 and Figure 2.12.3-30. The puncture bar was oriented at approximately  $45^\circ$  to the package axis, and contacted a fold which was adjacent to the damaged corner joint. Since the test was carried out shortly after puncture test P4, the polyurethane foam temperature is considered to be essentially the same as that recorded for test P4.

The bar caught the fold and tore the damaged joint open as shown in Figure 2.12.3-31 and Figure 2.12.3-32. The total length of the damage, measured as a chord, was approximately 26 inches. At the location of the bar (i.e., the center of the damage), the width was 5 inches. On either side the width of the opening was approximately 2-1/2 inches, tapering to zero at the ends. Only negligible amounts of foam were lost from the shells as shown in Figure 2.12.3-32.

#### **2.12.3.5.9 Puncture Drop Test P3**

Puncture test P3 was performed on the secondary slapdown damage incurred by serial number 3 in free drop test D2. The orientation is shown in Figure 2.12.3-2 and Figure 2.12.3-33. The bar struck the damaged area approximately in the center. The cask axis was at a small angle to the horizontal. Since the test was carried out shortly after puncture tests P4 and P5, the polyurethane foam temperature is considered to be essentially the same as that recorded for test P4.

The depth of the impact dent was approximately one inch. There was no sign of cracking or tearing of the impact limiter shell, as shown in Figure 2.12.3-34.

## BRR Package Safety Analysis Report

### 2.12.3.6 Confirmatory Test of Attachments

The confirmatory tests were performed on February 17, 2009 at Hiline, in order to demonstrate the adequacy of the redesigned impact limiter attachments. The test used the existing dummy cask and impact limiters, which had been altered to enhance the strength of the attachments. The revisions made to the test articles resulted in attachments which, in full-scale, were not stronger than the attachment design used on the production hardware.

None of the other tests will be invalidated by the increase in the strength of the attachments. In all of the other tests, the attachments did not fail, therefore, making the attachments stronger had no effect on the prior tests.

The tests that were selected to demonstrate the attachments were the D2 free drop and P2 puncture drop configurations. The D2 drop was chosen since that is the orientation in which the primary impact limiter attachments consistently failed. Attachment failures did not occur in any other impacts. The P2 puncture was chosen since a) a puncture subsequent to free drop is required by 10 CFR 71, and b) it is the puncture test that places the greatest load on the attachments. The test article having the greatest remaining capacity for an additional impact was serial no. 2, which was the primary limiter in tests D2 and D2R. The secondary limiter in the confirmatory tests was serial no. 3, which was less damaged than serial no. 1. The confirmatory tests were designated D2C and P2C.

Prior damage required that the CTU be rotated 90° about its axis. Since the attachment pattern has only one plane of symmetry, this meant that instead of one worst-case loaded attachment at 12 o'clock (relative to the impact at 6 o'clock), there were two attachments at approximately 11 and 1 o'clock, which were loaded somewhat less than in the prior drops. However, since the production redesign now features eight attachments, the load developed in each of the two maximum-loaded attachments in this test was greater than the maximum load which would develop in the production design.

#### 2.12.3.6.1 Description of Design Changes

The configuration of the attachments was increased in capacity as much as possible given the limitations of the existing hardware. In no case did the revised test hardware have a greater strength than the revised full-scale design. A detailed comparison of the test configuration and the full-scale design is given in Section 2.7.1.7, *Impact Limiter Attachments*. The revised CTU attachment is depicted in Figure 2.12.3-35. The nominal thickness of the blades, made of ASTM Type 304 material, was 3/8 inches. The width of the blades was increased to 1.5 inches, and their inner edge was set at 1/8 inches from the inner diameter of the impact limiter. The new blades were attached to the original blade roots using a full penetration weld, and the region between the top surface of the limiter and the new blade (approximately 1/2-inches) was buttered with weld metal to approximately the dimensions of the new blade. The hole in the blade was match-drilled from the existing hole in the cask attachments, and drilled out to 9/16 inches in diameter. The thickness, width, hole diameter, and hole-to-inner edge dimension for each blade before testing are given in Table 2.12.3-3. Serial no. 2 was mated with end A of the dummy cask, at the existing orientation marks.

Since the secondary impact limiter attachments did not fail in either prior slapdown drop, the refurbishment to serial no. 3 was minimal. The existing 3/16-inch thick blade was cut off and replaced with the same thickness material by a full penetration weld, match drilled to the existing

**BRR Package Safety Analysis Report**

holes on cask end B, and drilled out to 9/16-inch diameter. Both limiters were attached using 1/2 inch diameter carbon steel ball lock pins (the same specification as used in test D2R).

Since the test articles had both received two prior 30-ft drop impacts, and since good data was collected in the same orientation in tests D2 and D2R, test D2C was not instrumented with accelerometers. Both impact limiters were cold for the free drop test. Foam temperature was not recorded for the secondary limiter since the purpose of this test was not related to the secondary impact event.

**2.12.3.6.2 Oblique Slapdown Free Drop Test D2C Results**

Test D2C was performed using a drop height of 30 feet, oriented with the cask axis at 17° to the horizontal, as shown in Figure 2.12.3-1 and Figure 2.12.3-36. The primary (lower) impact limiter was serial no. 2, and the secondary (upper) impact limiter was serial no. 3. The polyurethane foam temperature readings in the primary limiter were -8.8 °F and -5.6 °F. The primary limiter was oriented so that blade nos. 5 and 6 were directly opposite the impact, where experience showed that the attachment loads are the highest.

The crush deformations were very similar to those obtained in tests D2 and D2R on the same limiter. All of the attachments, both primary and secondary, remained completely intact. Figure 2.12.3-37 and Figure 2.12.3-38 show the post-test configuration of the two most highly loaded attachments, at locations #5 and #6, respectively. All welds attaching the blades to the impact limiter appeared in good condition without failure. The attachments were examined in further detail following the puncture test.

**2.12.3.6.3 Puncture Drop P2C Results**

Puncture test P2C was performed immediately after drop test D2C. The longer puncture bar was used to impact the top annular surface of the damaged primary impact limiter (serial no. 2), as shown in Figure 2.12.3-2 and Figure 2.12.3-39. The orientation could not be over the center of gravity due to the desired impact location. The impact occurred adjacent to the outside edge of the limiter, halfway between attachment locations #5 and #6, thus maximizing the moment arm and loading of those attachments. The polyurethane foam temperature reading closest to the impact was lower than -3.0 °F.

The impact caused the long puncture bar to bend somewhat, but the attachment to the steel drop pad plate remained intact. The impact dent on the annular plate was negligible, without any cracking or tearing of the steel shell, and no exposure of foam. The attachments all appeared to be in good shape following the test. Figure 2.12.3-40 shows the impact dent and the attachment at location #5.

**2.12.3.6.4 Examination of Attachments**

After removal of the impact limiters from the dummy cask, the attachments were examined in detail. There was very little evidence of plastic deformation in the attachments, except that the holes of the most highly loaded blades were very slightly elongated. There was no evidence of bearing yielding in the hole, and no evidence of bending or cracking in the attachment pins. There was no evidence of weld cracking or deformation, except in one case, part of the weld between the blade and the annular sheet showed some shear. This was due to deformation of the annular plate in the puncture test, and this weld has no role in the impact limiter attachment load

path. Table 2.12.3-4 shows the measurements of the blade after test. Comparing Table 2.12.3-3 and Table 2.12.3-4, the largest increase in the hole dimension (measured in-line with the attachment loading direction, parallel to the cask axis) was 0.034 inches for blade no. 5, which is negligible. A comparison of the hole-to-edge dimension indicates that this distance appeared to increase slightly in several cases (ranging between a 0.016-inch decrease in width to a 0.010-inch increase), but as this goes against reason, it is assumed to be caused by measuring error on the rough surfaces. Figure 2.12.3-41 shows the blade configuration at location #5, and Figure 2.12.3-42 shows location #6, after all testing. Figure 2.12.3-43 shows a view of all of the pins used to retain the primary impact limiter. These photographs demonstrate that the attachments were essentially unchanged by the test loads.

The cask receptacle plate holes were somewhat elongated from prior testing (they were not refurbished). After the tests, the holes did not appear to have deteriorated any further.

**Table 2.12.3-3 - Attachment Pretest Data (Serial No. 2 Before D2C), inches**

No.	Blade Thick	Blade Width	Hole Dia.	Hole-to-Edge
1	0.376	1.515	0.565	0.376
2	0.375	1.517	0.565	0.353
3	0.375	1.520	0.563	0.375
4	0.377	1.519	0.565	0.471
5	0.376	1.519	0.565	0.420
6	0.377	1.519	0.565	0.396

**Table 2.12.3-4 - Attachment Post-test Data (Serial No. 2 After D2C), inches**

No.	Hole Axial* Diameter	Hole Lateral** Diameter	Hole-to-Edge
1	0.573	0.567	0.360
2	0.569	0.565	0.354
3	0.568	0.565	0.375
4	0.567	0.566	0.472
5	0.599	0.566	0.430
6	0.585	0.569	0.400

Note: Blade thickness and width were unchanged from the pre-test measurements.

\*Parallel to cask axis

\*\*Taken at right angle to axial diameter

**Table 2.12.3-5 - Accelerometer Calibration Constants**

Accelerometer Channel	Calibration Constant (mV/g)
12	0.935
13	0.926
14	0.930
15	0.941
16	0.916
17	0.889
18	0.905
19	0.973

## 2.12.5 Impact Limiter Performance Evaluation

This appendix presents the analytical evaluation of the impact and crush performance of the BRR package impact limiters. The impact magnitude and crush deformation of the limiters in several impact orientations, and at hot and cold bounding temperatures, is presented. Each step of the analysis is presented in detail, including the establishment of the crush properties of the polyurethane energy-absorbing foam, the calculation of the impact limiter force-deflection curves using the CASKDROP computer program, and the calculation of the impact response of the package using the SLAPDOWN computer program. A description of CASKDROP and SLAPDOWN are given in Appendix 2.12.6, *Analysis Software Descriptions*.

This appendix concludes with a reconciliation between the analysis results and test results, which shows that the analysis results are generally bounding. Of note, the impact magnitude used for stress analysis of 120g is nearly 50% greater than the highest test or analysis result.

### 2.12.5.1 Introduction

The analysis procedure of the impact limiter performance proceeds in three steps:

1. Calculate the effective stress-strain properties of the 9 lb/ft<sup>3</sup> polyurethane foam used within the limiter to absorb energy. The analysis begins with the room temperature, quasi-static stress-strain curves obtained from the foam manufacturer, and then adjusts the curves for minimum (-20 °F) and maximum (150 °F) temperature, for manufacturing tolerance ( $\pm 10\%$  on the bulk average strength property), for a dynamic (strain rate) effect, for the difference between the crush axis and the axes of material orthotropy, and for the effect of the outer steel shell.
2. Calculate the overall force-deflection relation for the limiter in each orientation, using the fully adjusted stress-strain curve established above and the geometry of the limiter. The result is a force-deflection curve for each orientation at each extreme temperature.
3. Calculate the overall response of the cask and impact limiters, modeling the cask as a rigid rod and the impact limiters as non-linear springs. The result is the impact magnitude and crush deformation of each impact limiter. If the impact orientation is not stable (i.e., a "slapdown"), calculate the acceleration at the end of the payload cavity farthest from the c.g. of the package.

These steps will now be presented in detail. The impact limiter geometry is found on drawing 1910-01-02-SAR in Appendix 1.3.3, *Packaging General Arrangement Drawings*. The basic, room temperature, quasi-static polyurethane foam stress-strain properties are taken from the database provided by the foam manufacturer, General Plastics Manufacturing Co. of Tacoma, WA. Pertinent pages from their web site are shown in Figure 2.12.5-1. Both limiters are taken to be identical, since the only actual difference is the presence of lifting bosses in the upper limiter. The maximum foam temperature of 150 °F is established in Section 2.6.1.1, *Summary of Pressures and Temperatures*. The minimum temperature is -20 °F as defined in [1].

The polyurethane foam is introduced into the impact limiter steel shells as a liquid, which then solidifies. During solidification, orthotropy of properties is established along an axis perpendicular to the ground ("parallel-to-rise") and on the orthogonal axis ("perpendicular-to-rise"). The parallel-to-rise direction is the same as the axis of the package.

**BRR Package Safety Analysis Report**

**2.12.5.1.1 Foam Stress-Strain Determination**

The foam stress-strain curves are a function of the given strain, temperature, manufacturing tolerance, dynamic crush factor, drop orientation, and a steel shell adjustment. This procedure is illustrated by means of example calculations for 10% strain and a drop orientation of 15° from the horizontal. The static crush strength at ambient temperature (75 °F) for both perpendicular and parallel-to-foam rise are calculated using the method and formulas given in Tables 7 and 8 of the manufacturer's data sheet shown in Figure 2.12.5-1. The resulting static, room temperature crush strengths are shown in the left-hand columns of Table 2.12.5-1 (parallel-to-rise) and Table 2.12.5-2 (perpendicular-to-rise). The basic equation for static crush strength is:

$$\sigma = Y\rho^S$$

where  $\sigma$  is the crush strength in psi,  $\rho$  is the foam density in lb/ft<sup>3</sup>, and Y and S are constants which depend on the strain level. As an example, for 10% strain,

$$\sigma_{\text{Para}}(\epsilon = 10\%) = Y\rho^S = (7.3058)(9)^{1.6590} = 280 \text{ psi}$$

$$\sigma_{\text{Perp}}(\epsilon = 10\%) = Y\rho^S = (6.3841)(9)^{1.7182} = 278 \text{ psi}$$

The static crush strength is modified by a temperature coefficient and a manufacturing tolerance for both the hot (150 °F) and cold (-20 °F) conditions. The manufacturing tolerance is included by entering a  $\pm 10\%$  variation in the crush strength. These two effects are conservatively combined such that the -10% manufacturing tolerance is applied to the hot temperature case (both tend to reduce crush strength) and the +10% manufacturing tolerance is applied to the cold temperature case (both tend to increase crush strength).

Static crush strength using the  $C_T$  values found in Tables 7 and 8 of Figure 2.12.5-1 combining the cold (-20 °F) temperature with the plus manufacturing tolerance is illustrated by the following example for 10% strain:

$$\sigma_{\text{Para}}(\epsilon = 10\%) = C_T(\sigma_{\text{Para}})(1 + \text{Bias}) = 1.29(280)(1 + 0.1) = 397 \text{ psi}$$

$$\sigma_{\text{Perp}}(\epsilon = 10\%) = C_T(\sigma_{\text{Perp}})(1 + \text{Bias}) = 1.32(278)(1 + 0.1) = 404 \text{ psi}$$

Similarly, static crush strength at the hot (150 °F) temperature with the minus manufacturing tolerance gives:

$$\sigma_{\text{Para}}(\epsilon = 10\%) = C_T(\sigma_{\text{Para}})(1 - \text{Bias}) = 0.71(280)(1 - 0.1) = 179 \text{ psi}$$

$$\sigma_{\text{Perp}}(\epsilon = 10\%) = C_T(\sigma_{\text{Perp}})(1 - \text{Bias}) = 0.72(278)(1 - 0.1) = 180 \text{ psi}$$

The manufacturer's data extends as far as a strain of 70%. In some drop orientations at the hot temperature, local strains are expected to exceed this value. In order to account for this, the manufacturer's data was extrapolated between 70% and 80% strain. To demonstrate the validity of this approach, the extrapolated curve is compared to data up to 80% strain that has been previously published [34] by the same manufacturer, in Figure 2.12.5-18<sup>1</sup>. The curves shown in Figure 2.12.5-18 are for a temperature of 150 °F and parallel to rise. Note that between zero and

<sup>1</sup> Note from Figure 2.12.5-18 that polyurethane foam does not have a discrete "lock up" point. While the foam becomes much stiffer at high strains, this occurs relatively gradually compared to other materials such as aluminum honeycomb.

70% strain, the two curves are quite similar, which demonstrates that foam behavior has not changed significantly since the previous data was published. As shown in the figure, the lower curve (current data, extrapolated above 70%) has a slower rise in stress with increasing strain than the upper (previously published) data curve. Use of the extrapolated curve (according to the procedure used in this appendix) will result in a conservatively greater crush deformation prediction than the upper curve. Since the actual foam behavior may tend to be more in line with the upper stress-strain curve, a calculation of package impact acceleration was made using the upper curve, according to the procedure described in Section 2.12.5.1, *Introduction*. This calculation results in the largest impact acceleration that would be expected from the hot case utilizing foam stress-strain behavior like that previously published in the region beyond 70% strain. Since the largest impact was desired, the stress-strain curve was conservatively increased by 10% for manufacturing variability. The results are given in Table 2.12.5-25, which compare the results of the two curves utilizing the governing 15° slapdown orientation. The results, as expected, show less strain and higher impact for the previously published stress-strain data. Although the maximum impact of 90.2g is slightly higher than the cold case maximum value of 86.8g, it is still far below the bounding value used in stress calculations of 120g. Therefore, the method of extrapolating the hot case foam stress-strain values is acceptable. Note that in the one case where a strain of up to 83.2% is needed (see Table 2.12.5-14), the stress for 80% is used, adding further conservatism to the maximum impact limiter deformation strain result.

The resulting static crush strengths at the temperature extremes are shown in the right-hand columns of Table 2.12.5-1 (parallel-to-rise) and Table 2.12.5-2 (perpendicular-to-rise).

The static crush strength is further modified to account for the dynamic loading of the impact limiter. Table 9 in the manufacture's datasheet (reproduced in Figure 2.12.5-1) provides the method used to calculate the dynamic crush strength. The formula used is:

$$\sigma_{\text{Dynamic}} = Y_{\text{int}} (\sigma_{\text{Static}})^S$$

where  $Y_{\text{int}}$  and  $S$  are different values than those defined above, and  $\sigma_{\text{Static}}$  is the static crush strength given on the right-hand side of Table 2.12.5-1 and Table 2.12.5-2. Examples for 10% strain at room temperature and the two temperature extremes are given as follows:

Dynamic crush strength at room temperature:

$$\sigma_{\text{Para}} (\epsilon = 10\%) = Y \sigma_{\text{Para}}^S = (1.2971)(280)^{1.0330} = 437 \text{ psi}$$

$$\sigma_{\text{Perp}} (\epsilon = 10\%) = Y \sigma_{\text{Perp}}^S = (1.2971)(278)^{1.0330} = 434 \text{ psi}$$

Dynamic crush strength at the cold temperature:

$$\sigma_{\text{Para}} (\epsilon = 10\%) = Y \sigma_{\text{Para}}^S = (1.2971)(397)^{1.0330} = 627 \text{ psi}$$

$$\sigma_{\text{Perp}} (\epsilon = 10\%) = Y \sigma_{\text{Perp}}^S = (1.2971)(404)^{1.0330} = 639 \text{ psi}$$

Dynamic crush strength at the hot temperature:

$$\sigma_{\text{Para}} (\epsilon = 10\%) = Y \sigma_{\text{Para}}^S = (1.2971)(179)^{1.0330} = 276 \text{ psi}$$

$$\sigma_{\text{Perp}} (\epsilon = 10\%) = Y \sigma_{\text{Perp}}^S = (1.2971)(180)^{1.0330} = 277 \text{ psi}$$



Table 9 does not provide values for the dynamic crush strength for strains above 70%. The values for S and Y for 70% strain are used to extend the curve up to 80% for the hot case (the room temperature case must also be extended in order to perform the adjustment for the steel shell as shown below). This keeps the dynamic crush strength dependence on the static crush strength similar to that of the highest strain in Table 9. If the value of either variable (S or Y) is modeled too high, the dynamic crush strength will be greatly increased resulting in much lower deformation. Since much of the energy from the crush will be dissipated in the initial 70% strain, small variations of the dynamic crush strength at the highest strains are negligible. The effect of this assumption will be compared against the test data. Table 2.12.5-3 and Table 2.12.5-4 show the result of the dynamic crush adjustment.

The variation in crush strength due to drop orientation is calculated based on the angle of the drop test with respect to the horizontal plane and the axis of the cask. The rise direction of the polyurethane foam is assumed to be parallel to the axis of the cask. An ellipse function is used to combine the parallel and perpendicular crush strength curves to obtain the crush curve for a particular drop orientation. The example for 10% strain and an impact orientation of 15° is carried out below.

Room temperature crush strength adjusted for orientation:

$$\sigma_{\text{Ambient}} = \frac{1}{\sqrt{\left(\frac{\sin \theta}{\sigma_{\text{Para}}}\right)^2 + \left(\frac{\cos \theta}{\sigma_{\text{Perp}}}\right)^2}} = \frac{1}{\sqrt{\left(\frac{\sin(15^\circ)}{437}\right)^2 + \left(\frac{\cos(15^\circ)}{434}\right)^2}} = 434 \text{ psi}$$

Cold crush strength adjusted for orientation:

$$\sigma_{\text{Cold}} = \frac{1}{\sqrt{\left(\frac{\sin \theta}{\sigma_{\text{Para}}}\right)^2 + \left(\frac{\cos \theta}{\sigma_{\text{Perp}}}\right)^2}} = \frac{1}{\sqrt{\left(\frac{\sin(15^\circ)}{627}\right)^2 + \left(\frac{\cos(15^\circ)}{639}\right)^2}} = 638 \text{ psi}$$

Hot crush strength adjusted for orientation:

$$\sigma_{\text{Hot}} = \frac{1}{\sqrt{\left(\frac{\sin \theta}{\sigma_{\text{Para}}}\right)^2 + \left(\frac{\cos \theta}{\sigma_{\text{Perp}}}\right)^2}} = \frac{1}{\sqrt{\left(\frac{\sin(15^\circ)}{276}\right)^2 + \left(\frac{\cos(15^\circ)}{277}\right)^2}} = 277 \text{ psi}$$

Table 2.12.5-5, Table 2.12.5-6, and Table 2.12.5-7 show the stress-strain values adjusted for dynamic loading.

Finally, the stress-strain curves generated by this method were biased upward to account for the steel shell of the impact limiter. A bias equivalent to a 47 percent strength increase was applied to the foam crush strength at ambient (75 °F) temperature. This bias is based on results obtained in engineering tests of the MOX Fresh Fuel Package (MFFP, NRC Docket 71-9295, Appendix 2.12.1). The bias was applied by adding 47% of the room temperature adjusted crush strength (see Table 2.12.5-5) to either the cold or hot adjusted crush strengths (Table 2.12.5-6 and Table 2.12.5-7, respectively). Following the example,

Crush strength biased for steel shell, cold (10% strain, 15° orientation):

**BRR Package Safety Analysis Report**

$$\sigma(\epsilon) = 0.47(\sigma_{\text{Ambient}}) + \sigma_{\text{Cold}} = .47(434) + 638 = 842 \text{ psi}$$

Crush strength biased for steel shell, hot (10% strain, 15° orientation):

$$\sigma(\epsilon) = 0.47(\sigma_{\text{Ambient}}) + \sigma_{\text{Hot}} = .47(434) + 277 = 481 \text{ psi}$$

Table 2.12.5-8 presents the complete set of stress-strain data that supports the calculation of impact limiter force-deflection curves. These values represent a summary of the adjustments to the static, room temperature data for temperature extremes, manufacturing tolerance, dynamic effect, impact orientation, and steel shell bias.

**2.12.5.1.2 Force-Deflection Curves**

The force-deflection curves are calculated using the computer program CASKDROP. Given an impact limiter external geometry, orientation to the impacting surface, and crush strength corresponding to that orientation, CASKDROP calculates the total crush force for each increment of deflection. The calculational technique is described in detail in Appendix 2.12.6, *Analysis Software Descriptions*. In summary, CASKDROP divides the crush area into small regions, and for each differential element, calculates the strain and, by means of the stress-strain table, the corresponding stress. Multiplying the stress times the differential area and summing all of the individual forces results in the total force at a given level of crush deformation. Repeating this process at a range of crush deformations results in the complete force-deflection curve.

The geometry shown in Figure 2.12.5-2 is utilized with CASKDROP. There are very small differences between the geometry shown and the drawings given in Appendix 1.3.3, *Packaging General Arrangement Drawings*, but the effect on the force-deflection curves is negligible.

The drop angle formed when the package center of gravity is directly over the conical diameter corner of the impact limiter is of particular interest. This angle is known as the center of gravity over corner, or cg-over-corner. At this angle, the impact limiter will absorb all of the drop kinetic energy on the primary impact. This angle is calculated as:

$$\theta_{\text{cg}} = \text{Tan}^{-1} \frac{L}{d_c} = \text{Tan}^{-1} \left[ \frac{119.5}{48.1} \right] = 68^\circ$$

where L is the total height of the cask, and  $d_c$  is the conical diameter.

CASKDROP was used to generate force-deflection curves for drop orientations of 0°, 15°, 30°, 45°, 60°, 68° and 90° from a horizontal cask orientation. Since the cg-over-corner drop orientation is considered critical for the calculation, that angle was selected instead of 75° in the sequence. Table 2.12.5-9 summarizes the input data used with the CASKDROP program for this solution. Note: because CASKDROP actually solves for the total crush in stable orientations using an energy approach, the program requires inputs of package weight and drop height. However, since only the force-deflection output is relevant here, the weight and drop height are not listed in the table.

Force-deflection curves are taken directly from the CASKDROP output files, except for the case of the horizontal side drop. Since CASKDROP outputs a single force-deflection curve, the result must be divided by 2 in this case, since two limiters are in contact with the ground. The force-deflection curves for the stated orientations, for hot and cold conditions, are shown in Figure 2.12.5-3 through Figure 2.12.5-9.

### 2.12.5.1.3 Impact Acceleration and Crush Deformation

The SLAPDOWN program, as described in Appendix 2.12.6, *Analysis Software Descriptions*, was used to analyze the impact response of the BRR package with the unyielding surface. It is particularly useful when the center of gravity is not directly over the impact point. Under these circumstances, the package will generally hit, begin to rotate, and strike the ground a second time as a "slapdown" impact. SLAPDOWN conducts a time-integration analysis using a model of the package as a rigid rod, and of the impact limiters as non-linear springs. Given a drop height, the package has an initial velocity at impact. The energy is absorbed first by the primary spring/impact limiter ('nose'), which imparts a rotational force to the model, until the secondary spring/impact limiter ('tail') comes in contact. Most of the energy absorbed by the springs is lost, except the portion that is restored by springback. The position, angle, velocity, and acceleration in both linear and rotational modes are calculated for each time step.

The force-deflection curves calculated by CASKDROP were input into SLAPDOWN to produce the results listed in this analysis. The primary impact limiter non-linear spring data was equal to the force-deflection curve created for the corresponding impact orientation. The secondary impact limiter non-linear spring was equal to the force-deflection curve for the zero degree orientation (i.e., horizontal) in each case. Additional input variables used in SLAPDOWN are summarized in Table 2.12.5-10, and briefly described below.

**Length, Nose-to-CG** – the distance along the cask axis from the location of impact to the CG of the cask. The impact location is dependent on the drop angle and ranges from one-half the total span between impact limiter springs of  $77.13/2 = 38.565$  inches for the side drop, to zero for the cg-over-corner drop ( $68^\circ$ ) and end drop ( $90^\circ$ ). Note that the discrete location of the impact limiter springs has been taken as coincident with the flat ends of the cask body.

**Length, Tail-to-CG** – the distance from the location of the secondary impact to the CG. This value remains the same as the secondary impact is considered to be a horizontal impact in all cases.

**Radius, Nose Limiter** – the radius of the primary impact limiter.

**Radius, Tail Limiter** – the radius of the secondary impact limiter.

**Body Mass** – the total mass of the cask and impact limiters expressed in  $\text{lb}_m\text{-s}^2/\text{in}$ , equivalent to the bounding package weight of 32,000 lb from Table 2.1-2.

**Rotational Moment of Inertia** – the rotational moment of inertia of the cask and assembly, calculated using the weight and geometry of the package.

**Drop Height** – the initial height of the cask prior to free drop measured in feet.

**Impact Angle** – the orientation of the primary impact, measured to the horizontal.

### 2.12.5.2 Results

The results of the analysis include the maximum crush and acceleration values for the given orientations. For unstable, i.e., slapdown orientations, the acceleration output is taken at a distance of 29.565 inches from the c.g. of the cask, which is conservatively further from the c.g. than either end of the payload cavity, and it is the maximum acceleration that the payload will experience.

The calculated impact limiter strain is determined as a percentage of the maximum allowable crush. The allowable crush is the distance between the point of impact on the limiter and the closest point of the internal shell of the limiter, and is calculated from the drawings for each orientation of primary impact. The allowable crush for secondary impact is the same for all cases, since the orientation is assumed to be horizontal in each case. The actual crush distance is the value provided as part of the SLAPDOWN output. The impact limiter strain is:

$$\varepsilon_{IL} = \frac{\text{Actual Crush}}{\text{Allowable Crush}}(100\%)$$

#### **2.12.5.2.1 HAC Free Drop Results**

Table 2.12.5-11 through Table 2.12.5-14 summarize the HAC free drop results. Note that maximum accelerations are governed by the cold case, and maximum impact limiter strain by the hot case. Figure 2.12.5-10 and Figure 2.12.5-11 show the maximum impact limiter strain developed for the primary and secondary impacts for the specified impact orientations. From a comparison of the two plots, the overall maximum impact limiter strain occurs in the secondary impact, hot case, for a primary impact orientation of 15°. Figure 2.12.5-12 and Figure 2.12.5-13 show the maximum acceleration of the cask for the specified drop orientations. The overall maximum impact acceleration occurs in the secondary impact, cold case, for a primary impact orientation of 15°.

#### **2.12.5.2.2 NCT Free Drop Results**

The NCT test requires the cask to be dropped from a height of two feet, per 10 CFR §71.71(c)(7). Table 2.12.5-15 through Table 2.12.5-18 summarize the NCT free drop results, using the same orientations and force-deflection curves as for the HAC cases.

Figure 2.12.5-14 and Figure 2.12.5-15 show the maximum impact limiter strain developed for the NCT primary and secondary impacts for the specified impact orientations. The maximum strain for the primary impact occurs at 68°, while the maximum strain for the secondary impact is seen to occur at a primary impact orientation of 15°. In both cases, the maximum strain is bounded by all the HAC strains for both primary and secondary impacts.

Figure 2.12.5-16 and Figure 2.12.5-17 show the maximum acceleration of the cask for the specified drop orientations. The maximum impact acceleration occurs in the 45° slapdown orientation. As expected, all NCT impact cases are bounded by the HAC cases.

#### **2.12.5.2.3 Combined HAC and NCT Free Drop Results**

Since 10 CFR 71 requires that the NCT free drop precede the HAC free drop, the effect of the combination of both drops is next considered. Since the impact acceleration is a function of the crush of the limiter, and the crush of the limiter is a function of the energy absorbed, a 2-foot free drop followed by a 30-foot free drop (taken in the same orientation on the same spot) may be modeled as a single 32-foot free drop. This is a conservative assumption, which neglects the effect of material springback which will occur after the initial NCT impact.

A sample of selected cold impact cases, where the acceleration was shown to be the highest, as shown in Table 2.12.5-19 and Table 2.12.5-20 demonstrates that the maximum increase in acceleration is less than 5 percent. A sample of selected hot impact cases, where the strain was

shown to be greater than the cold impact cases, is shown in Table 2.12.5-21 and Table 2.12.5-22. From the results of the combined NCT and HAC drop, it is clear that the effect of the NCT free drop on the HAC free drop is negligible.

### 2.12.5.3 Reconciliation with Certification Test Results

To verify the BRR Package functions as intended, a half-scale CTU was tested in three drop orientations as described in Appendix 2.12.3, *Certification Test Results*. The results of the test indicate that the results predicted in this calculation are conservative. The test results for the HAC end, slapdown, and c.g.-over-corner orientations are shown in Table 2.12.5-23. To convert the half-scale results to full-scale, the acceleration is divided by 2, and the crush distance is multiplied by 2.

The transverse accelerometers were located 8.68 inches from the end of the cask, or 17.36 inches in the equivalent full-scale, whereas the SLAPDOWN calculations correspond to the end of the cask cavity at the bottom, bounded by a distance of 29.565 inches from the cask c.g. This difference does not affect the stable impact orientations such as the end (D1) and c.g. over corner (D3), but for the slapdown impact, an adjustment of the test results must be made before comparison to the SLAPDOWN calculations.

The acceleration at any point along the axis in an oblique impact can be found from:

$$a_i = a_{c.g.} + \alpha L$$

where  $a_{c.g.}$  is the acceleration of the center of gravity ( $\text{in/s}^2$ ),  $\alpha$  is the rotational acceleration in  $\text{rad/s}^2$ , and  $L$  is the distance of the point  $i$  from the c.g. in inches. Since  $a_{c.g.}$  was not measured in the test, it must be calculated using the known location of the transverse accelerometers and the rotational acceleration calculated using SLAPDOWN. At the moment of maximum primary impact, the rotational acceleration is calculated by SLAPDOWN to be  $\alpha_P = 535 \text{ rad/s}^2$ . The full scale equivalent location of the accelerometers from the cask c.g. was:

$$L_{\text{accel}} = \frac{L_{\text{cask}}}{2} - 17.36 = 21.21 \text{ in}$$

where  $L_{\text{cask}} = 77.13$  inches, and the full scale equivalent location of the accelerometers from the cask end was 17.36 inches. The full-scale acceleration of the cask c.g. for the primary event in the test therefore can be computed as:

$$a_{\text{test c.g.-P}} = a_{\text{accel-P}} - \alpha_P L_{\text{accel}} = 15,701 \text{ in/s}^2$$

where the full-scale measured acceleration from Table 2.12.5-23 for the primary impact of test D2,  $a_{\text{accel-P}} = 70g$  (i.e.,  $27,048 \text{ in/s}^2$ ), and the location of the accelerometers,  $L_{\text{accel}} = 21.21$  inches from the cask c.g. The acceleration of the test cask at the location of used for the SLAPDOWN runs (i.e., the bottom end of the payload cavity) is therefore:

$$a_{\text{adj-P}} = a_{\text{test c.g.-P}} + \alpha_P L_{\text{adj}} = 31,518 \text{ in/s}^2 = 81.6g$$

where the distance from the cask c.g. to the location of the SLAPDOWN output is  $L_{\text{adj}} = 29.565$  inches. The corresponding SLAPDOWN calculated output acceleration for the primary impact is equal to  $71.0g$  from Table 2.12.5-11.

**BRR Package Safety Analysis Report**

Similarly, at the moment of maximum secondary impact, the rotational acceleration is calculated by SLAPDOWN to be  $\alpha_S = 687 \text{ rad/s}^2$ . The full-scale acceleration of the cask c.g. for the secondary event in the test can be computed as:

$$a_{\text{test c.g.-S}} = a_{\text{accel-S}} - \alpha_S L_{\text{accel}} = 6,101 \text{ in/s}^2$$

where the full-scale measured acceleration from Table 2.12.5-23 for the secondary impact of test D2,  $a_{\text{accel-S}} = 53.5g$  (i.e.,  $20,672 \text{ in/s}^2$ ), and  $L_{\text{accel}}$  is the same as above. The acceleration of the test cask at the location used for the SLAPDOWN runs (i.e., the bottom end of the payload cavity) is therefore:

$$a_{\text{adj-S}} = a_{\text{test c.g.-S}} + \alpha_S L_{\text{adj}} = 26,412 \text{ in/s}^2 = 68.4g$$

The corresponding SLAPDOWN calculated output acceleration for the secondary impact is equal to 86.8g from Table 2.12.5-12.

The results show that the corrected test accelerations are still below the maximum acceleration used in stress analysis of 120g. The maximum secondary acceleration of 68.3g is lower than the calculated value of 86.8g. The corrected primary acceleration of 81.6g is somewhat above the calculated value of 71.0g, but observation of the corresponding filtered accelerometer time histories given in Appendix 2.12.3, *Certification Test Results* shows a significant residual vibrational component for all impacts, but particularly this impact. Removal of the conservatism would be very likely to lower the test result to approximately the calculated value. This indicates that the calculation is essentially bounding for all cases. The principal conclusion, however, is that the actual accelerations of the BRR package are well below the bounding value of 120g used in the stress calculations.

As stated in Section 2.12.3.3, *Test Unit Configuration*, the weight of the test cask was 3,181 lb, or when properly adjusted for scale, approximately 7% below the maximum equivalent full-scale weight of 32,000 lb. This had the effect of conservatively increasing the recorded accelerations of the CTU. Correspondingly, the crush deformations were slightly underestimated in the test, since there was less kinetic energy in the drop.

The force-deflection curves discussed in Section 2.12.5.1.2, *Force-Deflection Curves*, show that the strain increases nonlinearly with an increase in applied load. Therefore, although an increase in weight will result in an increased deformation, each succeeding crush strain increment becomes smaller as a greater force is applied, particularly as the end of crush is neared. Thus the percent change in the crush distance will be smaller in magnitude than the percent change in weight. Since the increase in the crush distance will be less than the weight increase, and since the weight increase is small in magnitude, the crush distance is bounded by the values in the calculation. This holds true for both the cold and hot temperature conditions developed in this calculation. The bounding crush strain corresponds to the 15° secondary impact in the hot case. As shown in Table 2.12.5-14, the predicted crush is 15.9 inches. Since, as shown in Table 2.12.5-24, the cold secondary crush was measured to be 34% lower than the prediction, then the small increase in weight of 7% will not invalidate the hot case maximum predicted crush. Thus the predictions are conservative.

A comparison of the calculated ('Calc') and full-scale equivalent test ('Actual') impact limiter performance is given in Table 2.12.5-24. A negative sign in the '% Less' columns indicates that the test result was lower than the calculated value.

#### **2.12.5.4 Conclusion**

The impact limiter evaluation is used to establish a bounding impact magnitude for stress analysis in other sections of this SAR. The maximum impact occurs in the cold temperature case. For NCT, the maximum overall impact is equal to 33.0g in the 45° slapdown drop orientation, from which a bounding impact for all orientations of 40g is taken. For HAC, the maximum overall impact is 86.8g in the 15° secondary slapdown impact, and a very conservative value of 120g is used as a bounding impact for all orientations.

The maximum strain occurs under HAC in the hot temperature case, and equals 83.2% in the 15° secondary slapdown case.

**Table 2.12.5-1 - Parallel-to-Rise Static Compressive Strength (psi)**

Strain	Room Temperature (75 °F)				-20 °F		150 °F	
	Y, int	density	S	Crush Str	C <sub>T</sub>	Crush Str	C <sub>T</sub>	Crush Str
10%	7.3058	9	1.6590	280	1.29	397	0.71	179
20%	6.7276	9	1.7021	283	1.36	423	0.73	186
30%	6.4961	9	1.7350	294	1.32	427	0.74	196
40%	6.9137	9	1.7255	306	1.29	434	0.75	207
50%	5.6711	9	1.8877	359	1.26	498	0.76	246
60%	5.3279	9	2.0431	474	1.28	667	0.76	324
65%	5.9871	9	2.0870	587	1.29	833	0.76	402
70%	6.2085	9	2.1868	758	1.37	1142	0.81	553
75%				952				710
80%				1,204				928

**Table 2.12.5-2 - Perpendicular-to-Rise Static Compressive Strength (psi)**

Strain	Room Temperature (75 °F)				-20 °F		150 °F	
	Y, int	density	S	Crush Str	C <sub>T</sub>	Crush Str	C <sub>T</sub>	Crush Str
10%	6.3841	9	1.7182	278	1.32	404	0.72	180
20%	6.5943	9	1.6946	273	1.35	405	0.74	182
30%	6.1154	9	1.7403	280	1.34	413	0.79	199
40%	5.7722	9	1.8023	303	1.32	440	0.77	210
50%	5.3041	9	1.9054	349	1.32	507	0.77	242
60%	5.3181	9	2.0392	470	1.33	688	0.77	326
65%	5.7864	9	2.1002	584	1.34	861	0.77	405
70%	5.7701	9	2.2255	767	1.36	1,147	0.78	538
75%				971				683
80%				1,240				878



**Table 2.12.5-3 - Parallel-to-Rise Dynamic Crush Strength**

Strain	Dynamic Crush Strength Coefficients		Dynamic Crush Strength (psi)		
	Y, int	S	75 °F	-20 °F	150 °F
10%	1.2971	1.0330	437	627	276
20%	1.4397	1.0069	424	635	278
30%	1.5181	0.9941	432	625	288
40%	1.3887	1.0028	432	613	292
50%	1.4419	0.9912	492	680	338
60%	1.4275	0.9831	610	853	419
65%	1.3871	0.9910	769	1088	528
70%	1.4660	0.9586	844	1251	624
75%	1.4660	0.9586	1,051		793
80%	1.4660	0.9586	1,316		1,025

**Table 2.12.5-4 - Perpendicular-to-Rise Dynamic Crush Strength**

Strain	Dynamic Crush Strength Coefficients		Dynamic Crush Strength (psi)		
	Y, int	S	75 °F	-20 °F	150 °F
10%	1.2971	1.0330	434	639	277
20%	1.4397	1.0069	409	608	272
30%	1.5181	0.9941	411	605	293
40%	1.3887	1.0028	428	622	296
50%	1.4419	0.9912	478	692	332
60%	1.4275	0.9831	605	879	422
65%	1.3871	0.9910	765	1124	532
70%	1.4660	0.9586	854	1256	608
75%	1.4660	0.9586	1,071		764
80%	1.4660	0.9586	1,354		972

**Table 2.12.5-5 - Dynamic Strength Adjusted for Impact Angle (75 °F)**

Strain	Angle of Impact (degrees)						
	0	15	30	45	60	68	90
	Compressive Stress (psi)						
10%	434	434	435	435	436	437	437
20%	409	410	413	416	420	422	424
30%	411	412	416	421	426	429	432
40%	428	428	429	430	431	431	432
50%	478	479	481	485	488	490	492
60%	605	605	606	607	609	609	610
65%	765	765	766	767	768	768	769
70%	854	853	851	849	846	845	844
75%	1,071	1,070	1,066	1,061	1,056	1,054	1,051
80%	1,354	1,351	1,344	1,335	1,325	1,321	1,316

**Table 2.12.5-6 - Dynamic Strength Adjusted for Impact Angle (-20 °F)**

Strain	Angle of Impact (degrees)						
	0	15	30	45	60	68	90
	Compressive Stress (psi)						
10%	639	638	636	633	630	629	627
20%	608	610	614	621	628	631	635
30%	605	606	610	615	620	622	625
40%	622	621	620	617	615	614	613
50%	692	691	689	686	683	682	680
60%	879	877	872	866	859	857	853
65%	1,124	1,121	1,115	1,106	1,097	1,093	1,088
70%	1,256	1,256	1,255	1,253	1,252	1,252	1,251

**Table 2.12.5-7 - Dynamic Strength Adjusted for Impact Angle (150 °F)**

Strain	Angle of Impact (degrees)						
	0	15	30	45	60	68	90
	Compressive Stress (psi)						
10%	277	277	277	276	276	276	276
20%	272	272	273	275	276	277	278
30%	293	293	292	290	289	289	288
40%	296	296	295	294	293	293	292
50%	332	332	333	335	336	337	338
60%	422	422	421	420	420	419	419
65%	532	532	531	530	529	529	528
70%	608	609	612	616	620	622	624
75%	764	766	771	778	785	789	793
80%	972	975	984	997	1,011	1,017	1,025

**Table 2.12.5-8 - Fully Adjusted Polyurethane Foam Stress-Strain Data**

Strain	Angle of Impact (degrees)						
	0	15	30	45	60	68	90
<b>-20 °F Stress (psi)</b>							
10%	843	842	840	837	835	834	832
20%	800	803	808	817	825	829	834
30%	798	800	806	813	820	824	828
40%	823	822	822	819	818	817	816
50%	917	916	915	914	912	912	911
60%	1,163	1,161	1,157	1,151	1,145	1,143	1,140
65%	1,484	1,481	1,475	1,466	1,458	1,454	1,449
70%	1,657	1,657	1,655	1,652	1,650	1,649	1,648
<b>150 °F Stress (psi)</b>							
10%	481	481	481	480	481	481	481
20%	464	465	467	471	473	475	477
30%	486	487	488	488	489	491	491
40%	497	497	497	496	496	496	495
50%	557	557	559	563	565	567	569
60%	706	706	706	705	706	705	706
65%	892	892	891	890	890	890	889
70%	1,009	1,010	1,012	1,015	1,018	1,019	1,021
75%	1,267	1,269	1,272	1,277	1,281	1,284	1,287
80%	1,608	1,610	1,616	1,624	1,634	1,638	1,644

**Table 2.12.5-9 - CASKDROP Input Data**

<b>Input Data</b>	<b>Value</b>
Impact Limiter Outside Diameter, in.	78.0
Impact Limiter Overall Length, in.	34.6
Impact Limiter Conical Diameter, in.	48.1
Impact Limiter Conical length, in.	15.0
Impact Limiter End Thickness, in.	21.2
Impact Limiter Hole Diameter, in.	0
Impact Limiter Hole Length, in.	0
Body Outside Diameter, in.	38.0
Body Overall Length, in.	77.13
Frictional Coefficient	0

**Table 2.12.5-10 - SLAPDOWN Input Data**

<b>Input data</b>	<b>Value</b>
Length, Nose-to-C.G., in.	Variable
Length, Tail-to-C.G., in.	38.565
Radius, Nose Limiter, in.	39.0
Radius, Tail Limiter, in.	39.0
Body Mass, lb <sub>m</sub> -s <sup>2</sup> /in.	82.816
Rotational Moment of inertia, in-lb <sub>m</sub> -s <sup>2</sup>	63,246
HAC Drop Height, ft.	30
NCT Drop Height, ft	2
HAC + NCT Drop Height, ft	32
Impact Angle (with Horizontal)	Variable
Force Deflection Curves	Variable
Friction Coefficient	0

**Table 2.12.5-11 - Cold Primary Impact Results, HAC**

Primary Impact Angle	Acceleration	Crush	Allowable Crush	Crush Margin	Limiter Strain
(deg)	(g)	(in)	(in)	(in)	%
0	63.3	11.0	19.1	8.1	57.6
15	71.0	10.6	21.4	10.8	49.5
30	79.4	12.4	22.1	9.7	56.1
45	81.0	10.8	21.4	10.6	50.5
60	83.4	13.0	22.6	9.6	57.5
68	69.6	13.3	22.5	9.2	59.1
90	72.4	7.3	20.2	12.9	36.1

**Table 2.12.5-12 - Cold Secondary Impact Results, HAC**

Primary Impact Angle	Acceleration	Crush	Allowable Crush	Crush Margin	Limiter Strain
(deg)	(g)	(in)	(in)	(in)	%
0	63.3	11.0	19.1	8.1	57.6
15	86.8	12.2	19.1	6.9	63.9
30	65.2	9.2	19.1	9.9	48.2
45	58.2	8.1	19.1	11.0	42.4
60	42.1	5.4	19.1	13.7	28.3

**Table 2.12.5-13 - Hot Primary Impact Results, HAC**

Primary Impact Angle	Acceleration	Crush	Allowable Crush	Crush Margin	Limiter Strain
(deg)	(g)	(in)	(in)	(in)	%
0	55.1	14.5	19.1	4.6	75.9
15	53.4	13.5	21.4	7.9	63.1
30	60.7	15.9	22.1	6.2	71.9
45	66.6	14.4	21.4	7.0	67.3
60	68.6	16.4	22.6	6.2	72.6
68	55.4	16.6	22.5	5.9	73.8
90	54.8	10.5	20.2	9.7	52.0

**Table 2.12.5-14 - Hot Secondary Impact Results, HAC**

Primary Impact Angle	Acceleration	Crush	Allowable Crush	Crush Margin	Limiter Strain
(deg)	(g)	(in)	(in)	(in)	%
0	55.1	14.5	19.1	4.6	75.9
15	83.6	15.9	19.1	3.2	<b>83.2</b>
30	53.2	12.3	19.1	6.8	64.4
45	43.4	10.5	19.1	8.6	55.0
60	31.7	7.5	19.1	11.6	39.3

**Table 2.12.5-15 - Cold Primary Impact Results, NCT**

Primary Impact Angle	Acceleration	Crush	Allowable Crush	Crush Margin	Limiter Strain
(deg)	(g)	(in)	(in)	(in)	%
0	19.7	2.8	19.1	16.3	14.7
15	19.1	4.1	21.4	17.3	19.2
30	21.1	4.7	22.1	17.4	21.3
45	26.3	3.0	21.4	18.4	14.0
60	24.9	5.0	22.6	17.6	22.1
68	15.2	5.2	22.5	17.3	23.1
90	32.9	1.5	20.2	18.7	7.4

**Table 2.12.5-16 - Cold Secondary Impact Results, NCT**

Primary Impact Angle	Acceleration	Crush	Allowable Crush	Crush Margin	Limiter Strain
(deg)	(g)	(in)	(in)	(in)	%
0	19.7	2.8	19.1	16.3	14.7
15	29.7	3.7	19.1	15.4	19.4
30	29.3	3.4	19.1	15.7	17.8
45	<b>33.0</b>	3.5	19.1	15.6	18.3
60	29.0	3.3	19.1	15.8	17.3

**Table 2.12.5-17 - Hot Primary Impact Results, NCT**

Primary Impact Angle	Acceleration	Crush	Allowable Crush	Crush Margin	Limiter Strain
(deg)	(g)	(in)	(in)	(in)	%
0	13.9	3.7	19.1	15.4	19.4
15	15.7	4.9	21.4	16.5	22.9
30	16.8	5.8	22.1	16.3	26.2
45	20.0	3.9	21.4	17.5	18.2
60	19.5	6.1	22.6	16.5	27.0
<b>68</b>	12.4	6.4	22.5	16.1	<b>28.4</b>
90	23.9	2.0	20.2	18.2	9.9

**Table 2.12.5-18 - Hot Secondary Impact Results, NCT**

Primary Impact Angle	Acceleration	Crush	Allowable Crush	Crush Margin	Limiter Strain
(deg)	(g)	(in)	(in)	(in)	%
0	13.9	3.7	19.1	15.4	19.4
15	22.7	5.2	19.1	13.9	27.2
30	21.7	4.5	19.1	14.6	23.6
45	20.8	4.6	19.1	14.5	24.1
60	20.0	4.4	19.1	14.7	23.0

**Table 2.12.5-19 - Cold Primary Impact Results, HAC + NCT**

Primary Impact Angle	HAC Acceleration	HAC+NCT Acceleration	Acceleration Increase	Percent Increase
(deg)	(g)	(g)	(g)	%
15	71.0	73.2	2.2	3.1
68	69.6	71.9	2.3	3.3
90	72.4	73.9	1.5	2.1



**Table 2.12.5-20 - Cold Secondary Impact Results, HAC + NCT**

Primary Impact Angle	HAC Acceleration	HAC+NCT Acceleration	Acceleration Increase	Percent Increase
(deg)	(g)	(g)	(g)	%
15	86.8	90.1	3.3	3.8

**Table 2.12.5-21 - Hot Primary Impact Results, HAC + NCT**

Primary Impact Angle	HAC Crush	HAC+NCT Crush	Crush Increase	Percent Increase
(deg)	(in)	(in)	(in)	%
15	13.5	13.9	0.4	3.0
68	16.6	17.0	0.4	2.4
90	10.5	10.9	0.4	3.8

**Table 2.12.5-22 - Hot Secondary Impact Results, HAC + NCT**

Primary Impact Angle	HAC Crush	HAC+NCT Crush	Crush increase	Percent Increase
(deg)	(in)	(in)	(in)	%
15	15.9	16.3	0.4	2.5

**Table 2.12.5-23 - CTU Test Results**

Test #	Description	Location	Half-Scale		Full-Scale	
			Accel. (g)	Crush Distance (in)	Accel. (g)	Crush Distance (in)
D1	End Drop	Primary	116	3.4	58.0	6.8
D2	Oblique Slapdown	Primary	140	3.9	70.0	7.8
		Secondary	107	4.0	53.5	8.0
D3	CG Over Corner	Primary	116	5.5	58.0	11.0

**Table 2.12.5-24 - CTU Percentage of Predicted Results (Full Scale)**

Test #	Location	Acceleration (g)			Crush Distance (in)		
		Calc	Actual	% Less	Calc	Actual	% Less
D1	Primary	72.4	58.0	-19.9	7.3	6.8	-6.8
D2	Primary	71.0	81.6	+14.9	10.6	7.8	-26
	Secondary	86.8	68.4	-21.2	12.2	8.0	-34
D3	Primary	69.6	58.0	-16.7	13.3	11.0	-17

\* The values for D2 primary and secondary impact have been adjusted as discussed above.

**Table 2.12.5-25 - Comparison of Results Using Previously Published Stress-Strain Data\***

Dataset	Primary Impact		Secondary Impact	
	Deflection, in	Acceleration, g	Deflection, in	Acceleration, g
Current Data	13.5	53.4	15.9	83.6
Previous Data	13.0	57.3	15.2	90.2

\* HAC, 15° slapdown, 150 °F. "Current Data" results correspond to Table 2.12.5-13 and Table 2.12.5-14.

**Design Guide for use of LAST-A-FOAM FR-3700 for Crash and Fire Protection of Radioactive Material Shipping Containers**

**Table 7: Static Nominal Crush Strength, Parallel to Direction of Rise (see Table 8 for Perpendicular to Rise)**

For 4 to 10 lb <sub>m</sub> /ft <sup>3</sup>									
Temp	Correlation Factors	Crush Strength, psi, Parallel to Direction of Rise							
		10%	20%	30%	40%	50%	60%	65%	70%
-20°F	C <sub>T</sub>	1.29	1.36	1.32	1.29	1.26	1.28	1.29	1.37
75°F	Y <sub>int</sub>	7.3058	6.7276	6.4961	6.9137	5.6711	5.3279	5.9871	6.2085
	S	1.6590	1.7021	1.7350	1.7255	1.8877	2.0431	2.0870	2.1868
100°F	C <sub>T</sub>	0.87	0.88	0.89	0.89	0.90	0.91	0.91	0.96
140°F	C <sub>T</sub>	0.73	0.75	0.76	0.77	0.78	0.78	0.79	0.84
180°F	C <sub>T</sub>	0.65	0.66	0.67	0.68	0.69	0.68	0.68	0.71
220°F	C <sub>T</sub>	0.61	0.60	0.60	0.61	0.61	0.59	0.59	0.61
260°F	C <sub>T</sub>	0.45	0.44	0.46	0.47	0.48	0.49	0.49	0.52
For 11 to 40 lb <sub>m</sub> /ft <sup>3</sup>									
Temp	Correlation Factor	Crush Strength, psi, Parallel to Direction of Rise							
		10%	20%	30%	40%	50%	60%	65%	70%
-20°F	C <sub>T</sub>	1.35	1.33	1.32	1.31	1.31	1.30	1.28	1.26
75°F	Y <sub>int</sub>	4.3422	3.8755	3.5241	3.0307	3.0402	3.4889	5.8935	5.6055
	S	1.8809	1.9321	1.9872	2.0755	2.1451	2.2143	2.1041	2.2368
100°F	C <sub>T</sub>	0.86	0.87	0.88	0.88	0.89	0.90	0.90	0.97
140°F	C <sub>T</sub>	0.72	0.74	0.75	0.75	0.75	0.76	0.76	0.81
180°F	C <sub>T</sub>	0.62	0.63	0.65	0.65	0.65	0.65	0.64	0.68
220°F	C <sub>T</sub>	0.56	0.56	0.57	0.57	0.56	0.54	0.54	0.57
260°F	C <sub>T</sub>	0.40	0.40	0.41	0.42	0.41	0.43	0.43	0.47

The room temperature (75°F) foam crush strength is calculated at each %-Crush and is a function of density;  $\sigma = Y_{int}(\rho)^S$ , where Y<sub>int</sub> and S are defined above, ρ is the nominal foam density in lb/ft<sup>3</sup>, and σ in the resulting crush stress in psi at the indicated strain. The foam crush strength at temperatures other than 75°F is calculated at each %-Crush and is a function of the strength at 75°F;  $\sigma = \sigma_{75°F} C_T$ . General Plastics Mfg. Co. is re-investigating the correlations factors at temperatures above and below 75°F. Please contact us for more specific and detailed data, as needed.

GENERAL PLASTICS MANUFACTURING COMPANY



10 ISS004

Figure 2.12.5-1 - General Plastics Data (Page 1 of 3)

**Design Guide for use of LAST-A-FOAM FR-3700 for Crash and Fire Protection of Radioactive Material Shipping Containers**

**Table 8: Static Nominal Crush Strength, Perpendicular to Direction of Rise (see Table 7 for Parallel to Rise)**

For 4 to 10 lb <sub>m</sub> /ft <sup>3</sup>									
Temp	Correlation Factors (see below)	Crush Strength, psi, Perpendicular to Direction of Rise							
		10%	20%	30%	40%	50%	60%	65%	70%
-20°F	C <sub>T</sub>	1.32	1.35	1.34	1.32	1.32	1.33	1.34	1.36
75°F	Y <sub>int</sub>	6.3841	6.5943	6.1154	5.7722	5.3041	5.3181	5.7864	5.7701
	S	1.7182	1.6946	1.7403	1.8023	1.9054	2.0392	2.1002	2.2255
100°F	C <sub>T</sub>	0.85	0.87	0.88	0.89	0.90	0.91	0.91	0.92
140°F	C <sub>T</sub>	0.75	0.77	0.78	0.79	0.79	0.79	0.79	0.80
180°F	C <sub>T</sub>	0.63	0.66	0.68	0.69	0.69	0.70	0.69	0.70
220°F	C <sub>T</sub>	0.59	0.59	0.60	0.61	0.60	0.60	0.59	0.60
260°F	C <sub>T</sub>	0.45	0.45	0.47	0.48	0.48	0.48	0.48	0.48
For 11 to 40 lb <sub>m</sub> /ft <sup>3</sup>									
Temp	Correlation Factors (see below)	Crush Strength, psi, Perpendicular to Direction of Rise							
		10%	20%	30%	40%	50%	60%	65%	70%
-20°F	C <sub>T</sub>	1.34	1.33	1.32	1.33	1.30	1.28	1.24	1.17
75°F	Y <sub>int</sub>	4.1342	3.5581	3.2664	2.8352	2.8988	3.3972	6.5439	5.6464
	S	1.8957	1.9593	2.0109	2.0955	2.1602	2.2242	2.0660	2.2321
100°F	C <sub>T</sub>	0.84	0.85	0.86	0.88	0.87	0.88	0.88	0.90
140°F	C <sub>T</sub>	0.72	0.73	0.74	0.76	0.75	0.76	0.76	0.79
180°F	C <sub>T</sub>	0.62	0.63	0.64	0.65	0.65	0.65	0.65	0.67
220°F	C <sub>T</sub>	0.53	0.53	0.54	0.55	0.54	0.54	0.54	0.56
260°F	C <sub>T</sub>	0.39	0.39	0.40	0.41	0.41	0.40	0.40	0.42

The room temperature (75°F) foam crush strength is calculated at each %-Crush and is a function of density;  $\sigma = Y_{int}(\rho)^S$ , where Y<sub>int</sub> and S are defined above, ρ is the nominal foam density in lb/ft<sup>3</sup>, and σ is the resulting crush stress in psi at the indicated strain. The foam crush strength at temperatures other than 75°F is calculated at each %-Crush and is a function of the strength at 75°F;  $\sigma = \sigma_{75°F} C_T$ . General Plastics Mfg. Co. is re-investigating the correlations factors at temperatures above and below 75°F. Please contact us for more specific and detailed data, as needed.

GENERAL PLASTICS MANUFACTURING COMPANY



11 159004

Figure 2.12.5-1 - General Plastics Data, continued (Page 2 of 3)

**Design Guide for use of LAST-A-FOAM FR-3700 for Crash and Fire Protection of Radioactive Material Shipping Containers**

**Dynamic Crush Strength**

The crush strength of LAST-A-FOAM<sup>®</sup>, like many materials, is modestly sensitive to strain rate. The static to dynamic adjustment shown in Table 9 is based on a significant testing program and included strain rates in the range of 30 sec<sup>-1</sup> to 100 sec<sup>-1</sup>. It is expected that the adjustment will provide good predictions of dynamic impact strength of FR-3700 for most Packaging design conditions. This information is intended to be a guide for designers of impact mitigating devices. The constitutive material models may be useful in targeting a foam density or rage for a particular application. However, each design should be thoroughly analyzed or tested to understand the implications of the complete design.

Table 9: Static to Dynamic Crush Strength Adjustment

Strain	10%	20%	30%	40%	50%	60%	65%	70%
Y <sub>int</sub>	1.2971	1.4397	1.5181	1.3887	1.4419	1.4275	1.3871	1.4660
S	1.0330	1.0069	0.9941	1.0028	0.9912	0.9831	0.9910	0.9586

The dynamic crush strength is calculated at each %-strain and a function of the static crush strength at the same %-strain;

$$\sigma_{\text{Dynamic}} = y_{\text{int}} (\sigma_{\text{Static}})^S$$

CAUTION: Use only units of PSI for input  $\sigma_{\text{Static}}$  value.



**General Plastics Manufacturing Company**  
4910 Burlington Way • P.O. box 9097  
Tacoma, WA 98409

Telephone: (800) 806-6051 or (253) 473-5000  
Facsimile: (253) 473-5104

See our World Wide Web Site at:  
[www.generalplastics.com](http://www.generalplastics.com)  
E-mail address: [sales@generalplastics.com](mailto:sales@generalplastics.com)



Figure 2.12.5-1 - General Plastics Data, continued (Page 3 of 3)

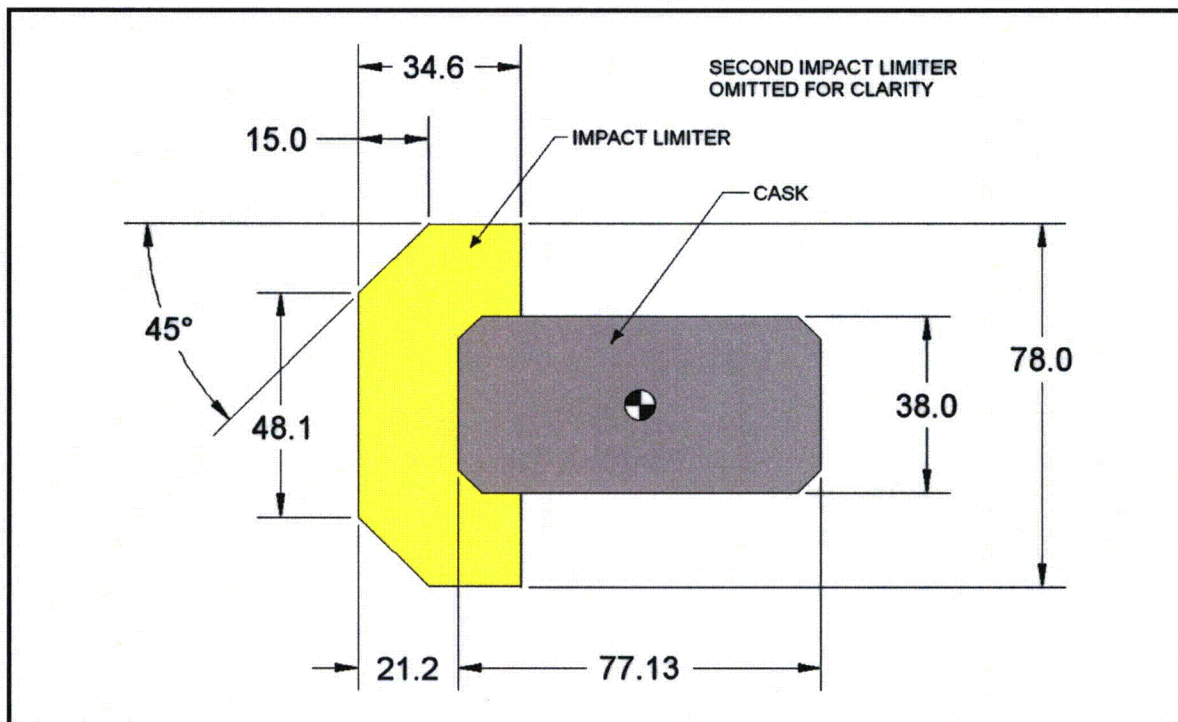


Figure 2.12.5-2 - Dimensions Used in CASKDROP

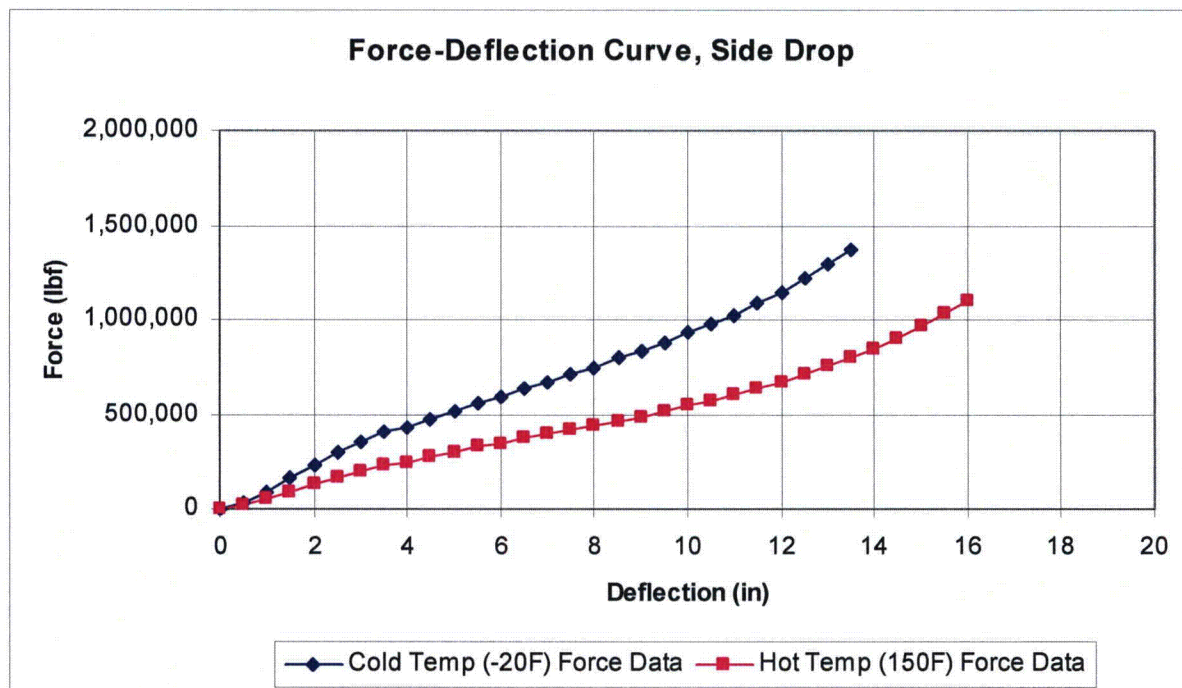


Figure 2.12.5-3 - Force-Deflection Curve, Side Orientation

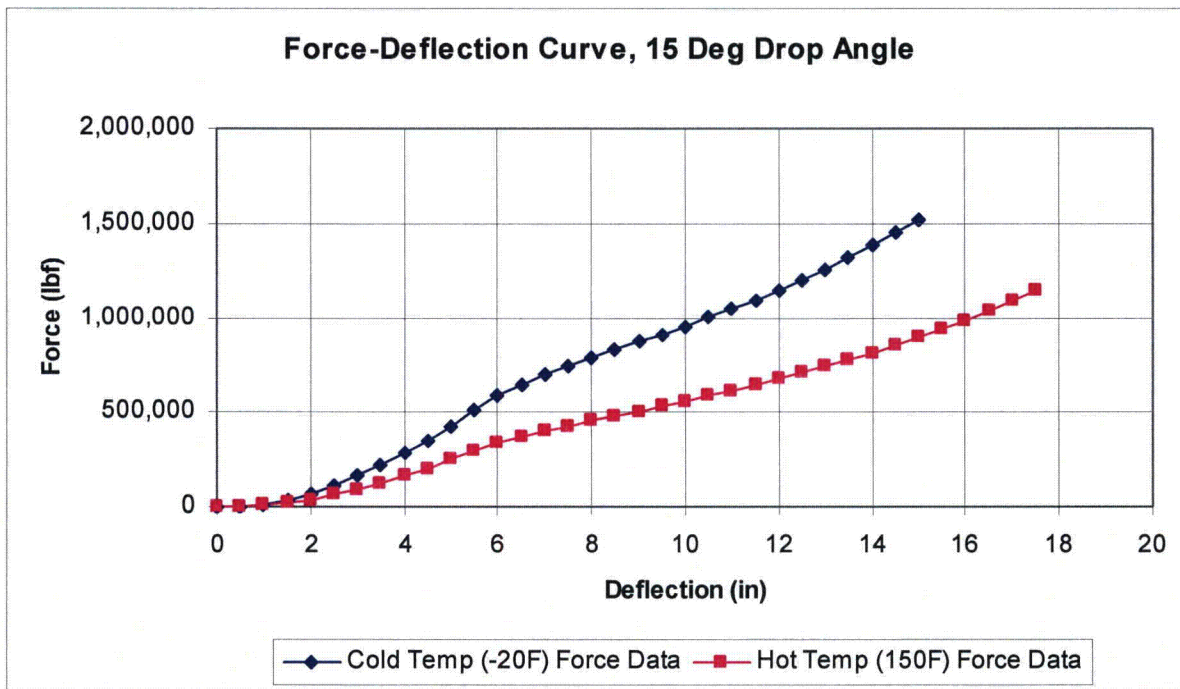


Figure 2.12.5-4 - Force-Deflection Curve, 15° Orientation

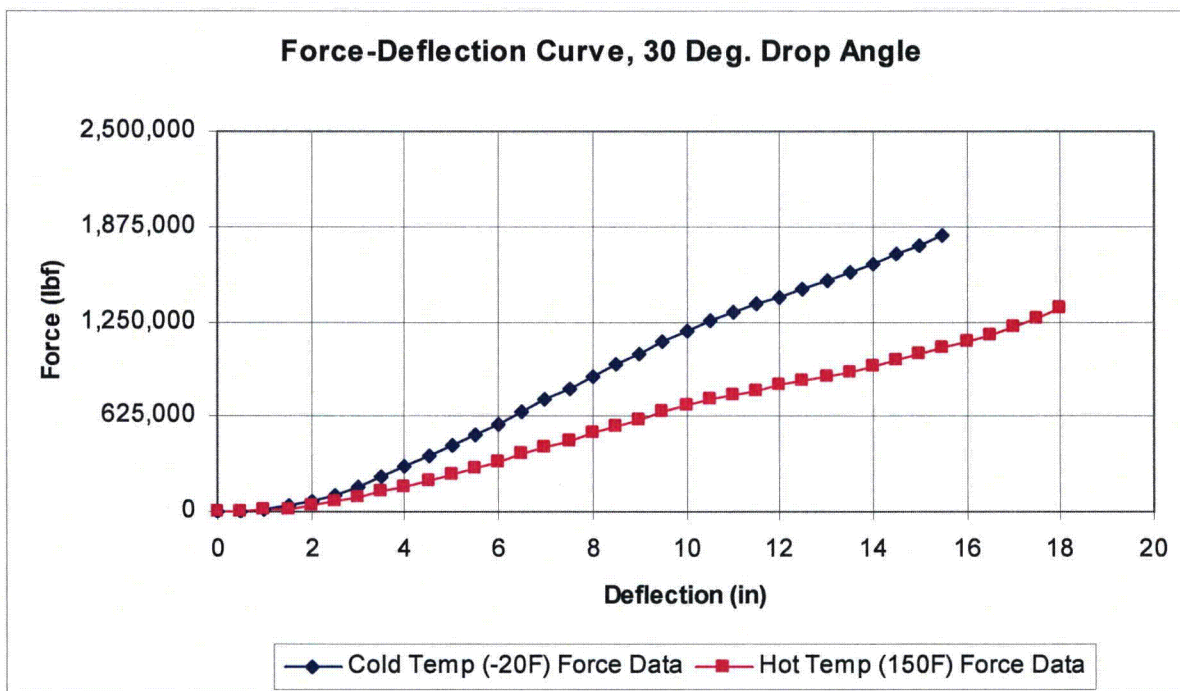


Figure 2.12.5-5 - Force-Deflection Curve, 30° Orientation

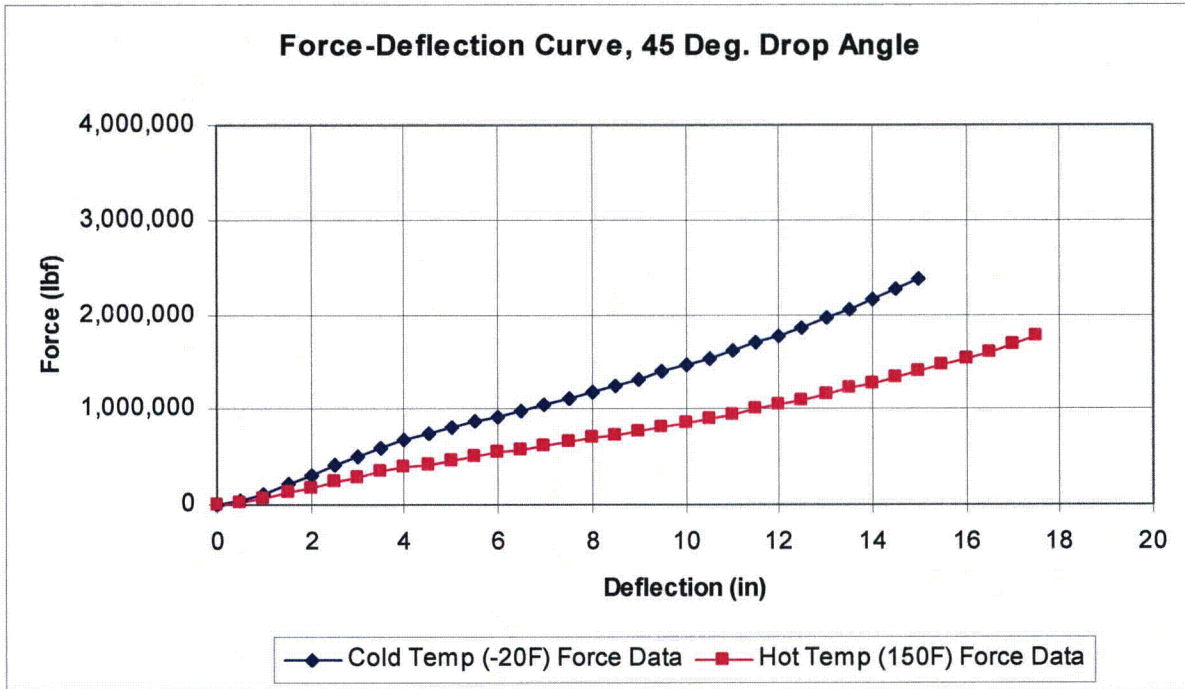


Figure 2.12.5-6 - Force-Deflection Curve, 45° Orientation

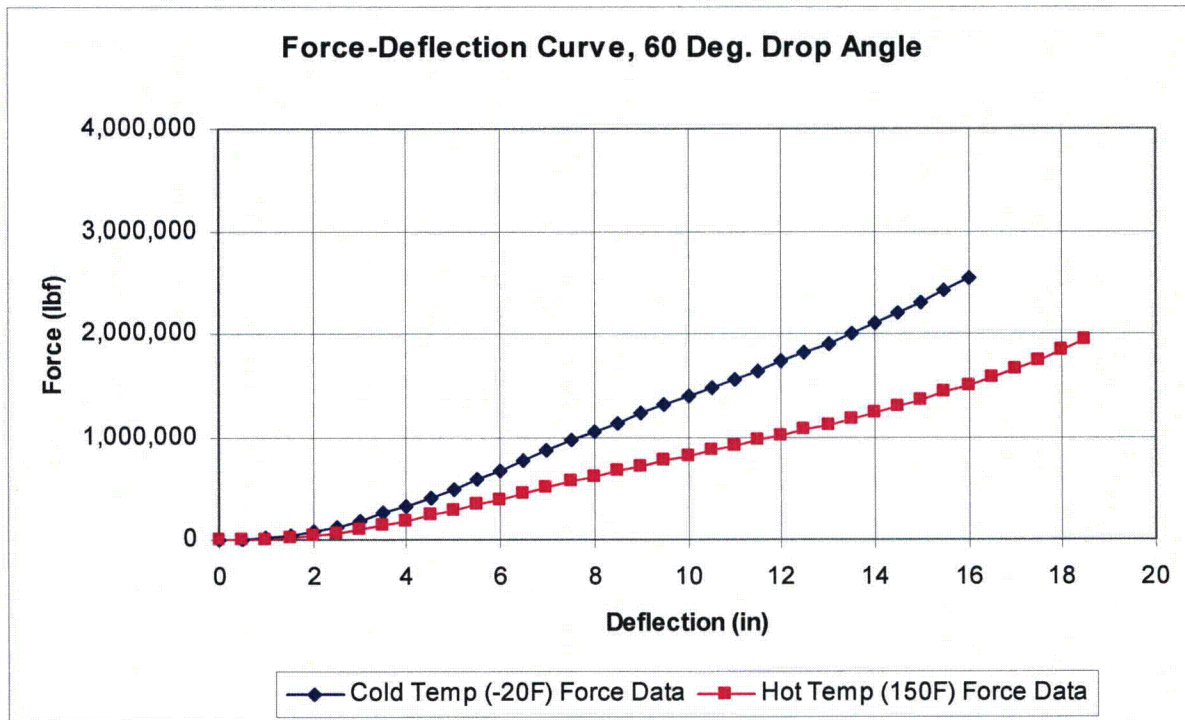


Figure 2.12.5-7 - Force-Deflection Curve, 60° Orientation



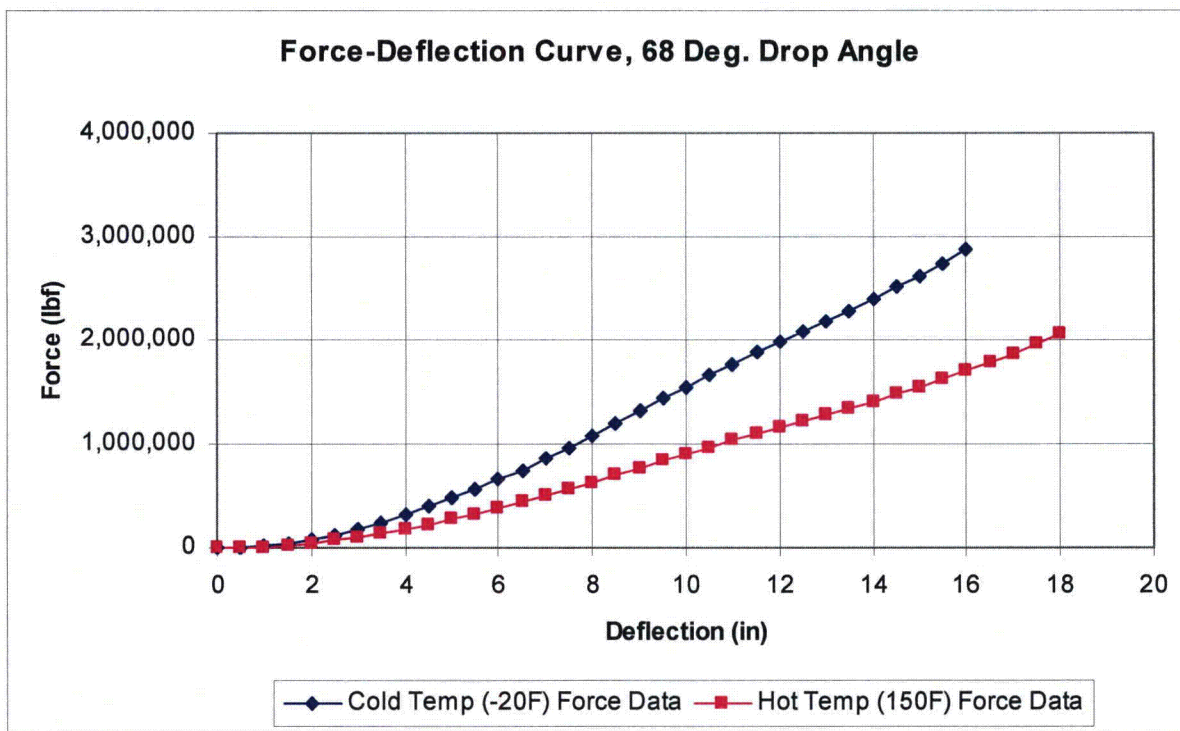


Figure 2.12.5-8 - Force-Deflection Curve, 68° Orientation

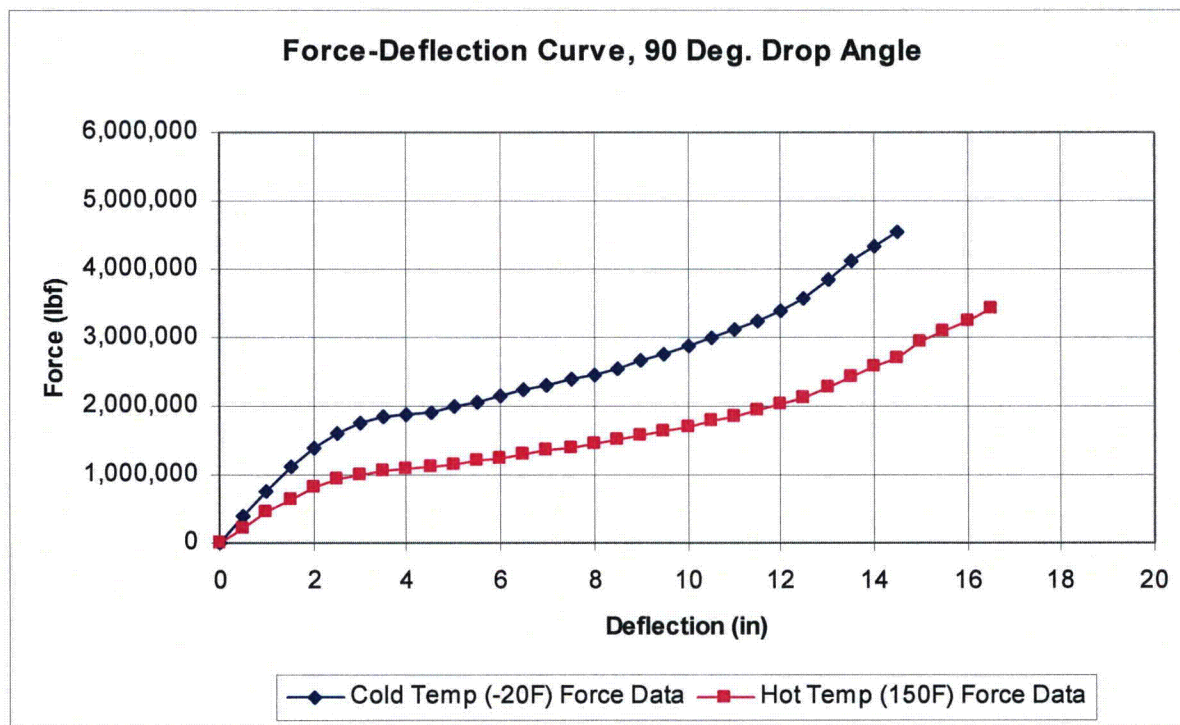


Figure 2.12.5-9 - Force-Deflection Curve, 90° Orientation

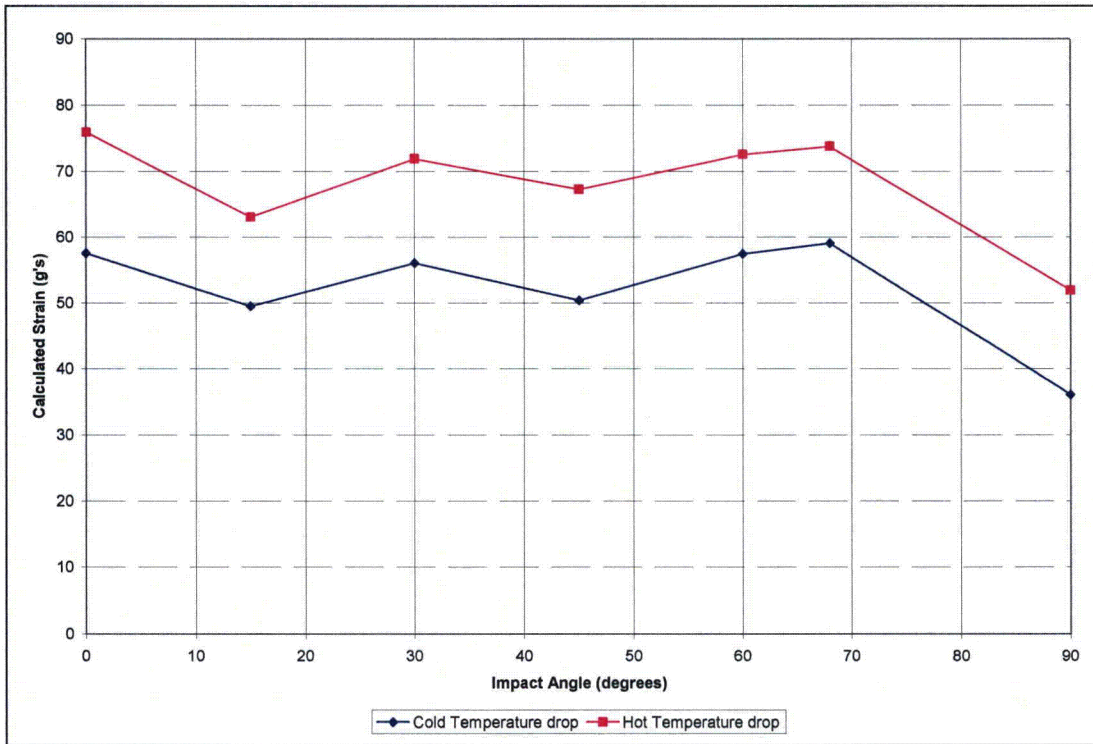


Figure 2.12.5-10 - Primary Impact Limiter Strain, HAC

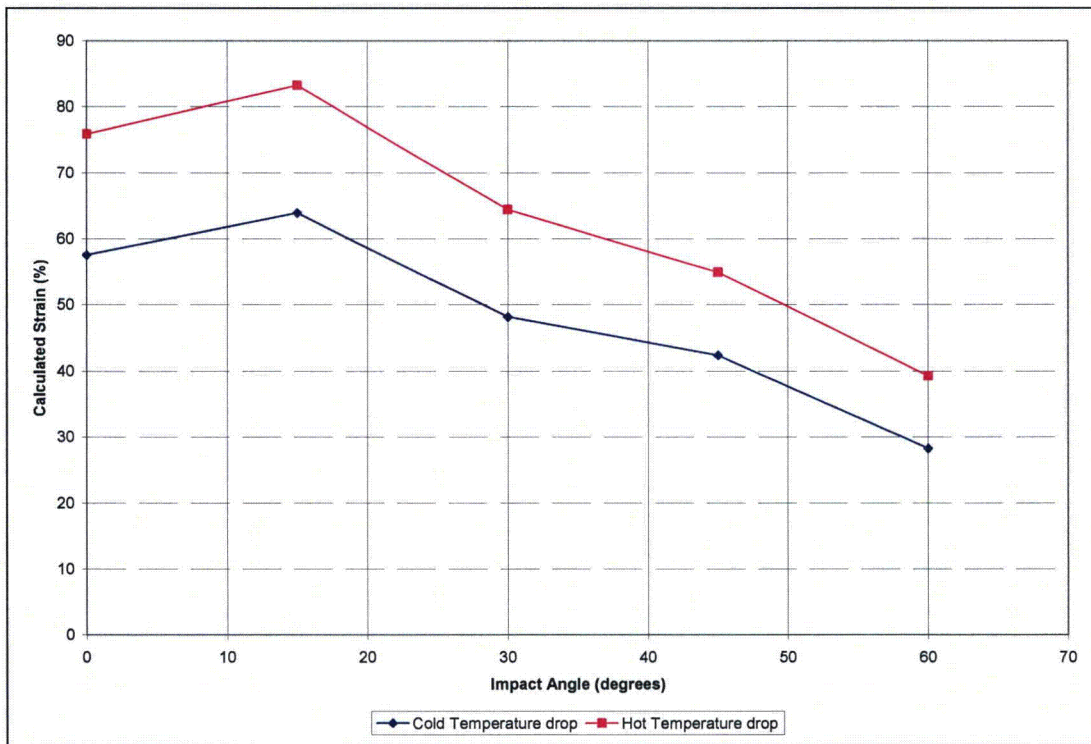


Figure 2.12.5-11 - Secondary Impact Limiter Strain, HAC

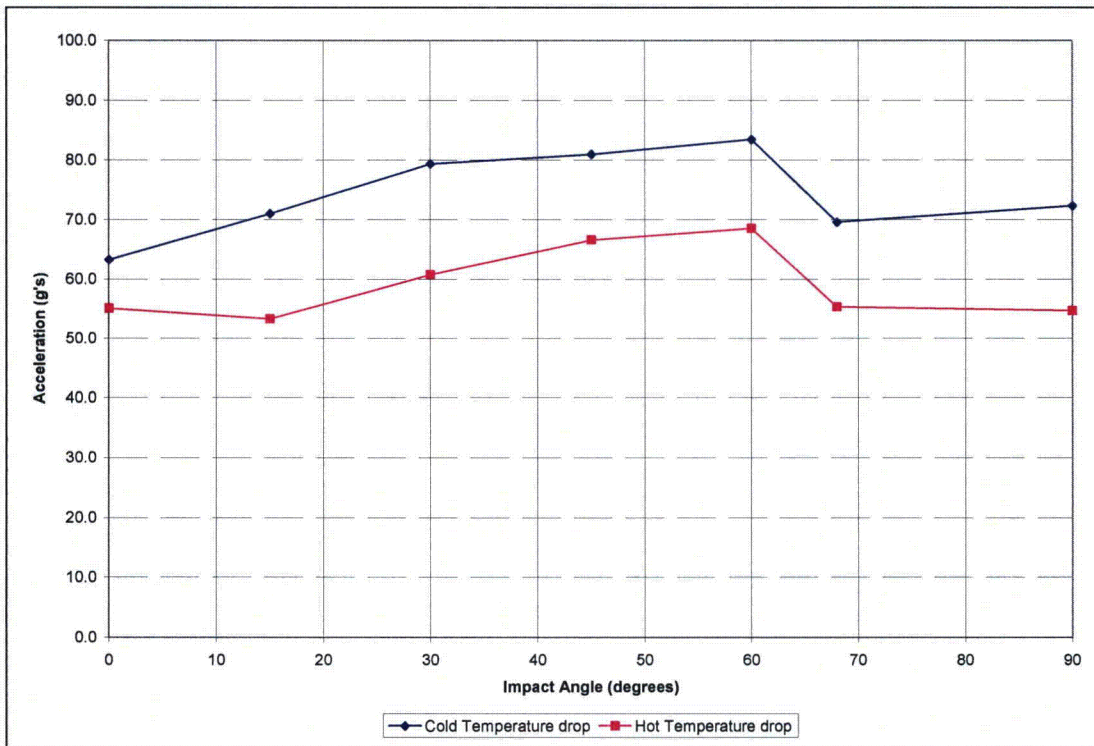


Figure 2.12.5-12 - Primary Impact Acceleration, HAC

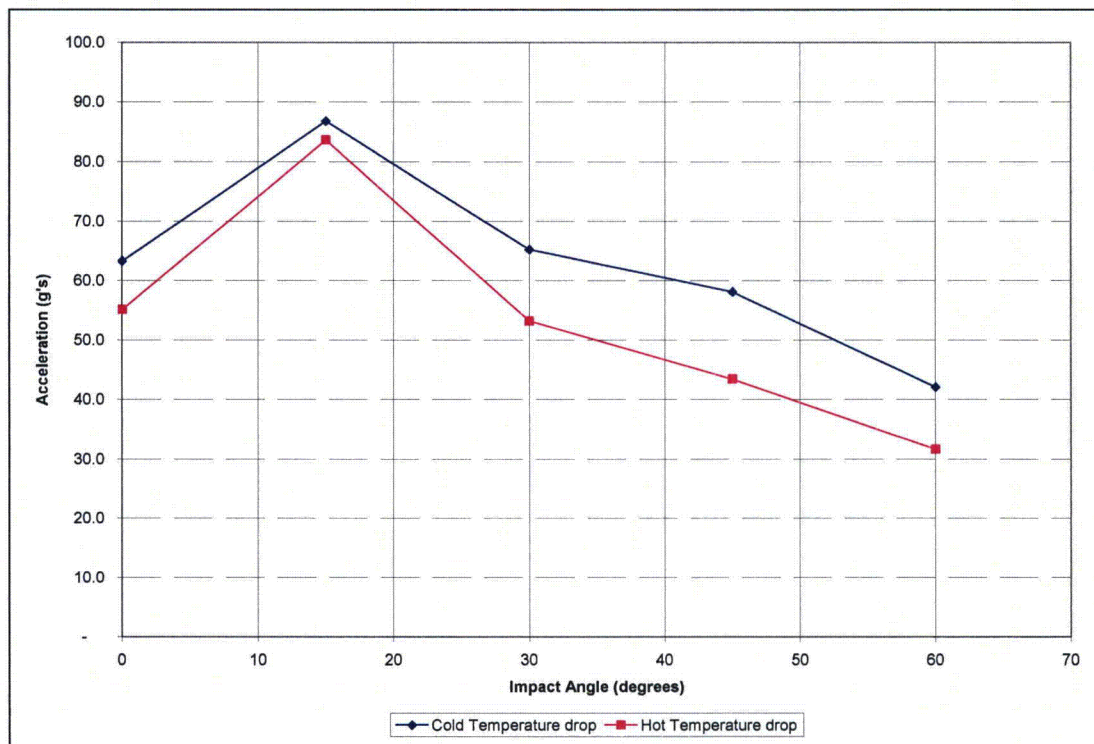


Figure 2.12.5-13 - Secondary Impact Acceleration, HAC

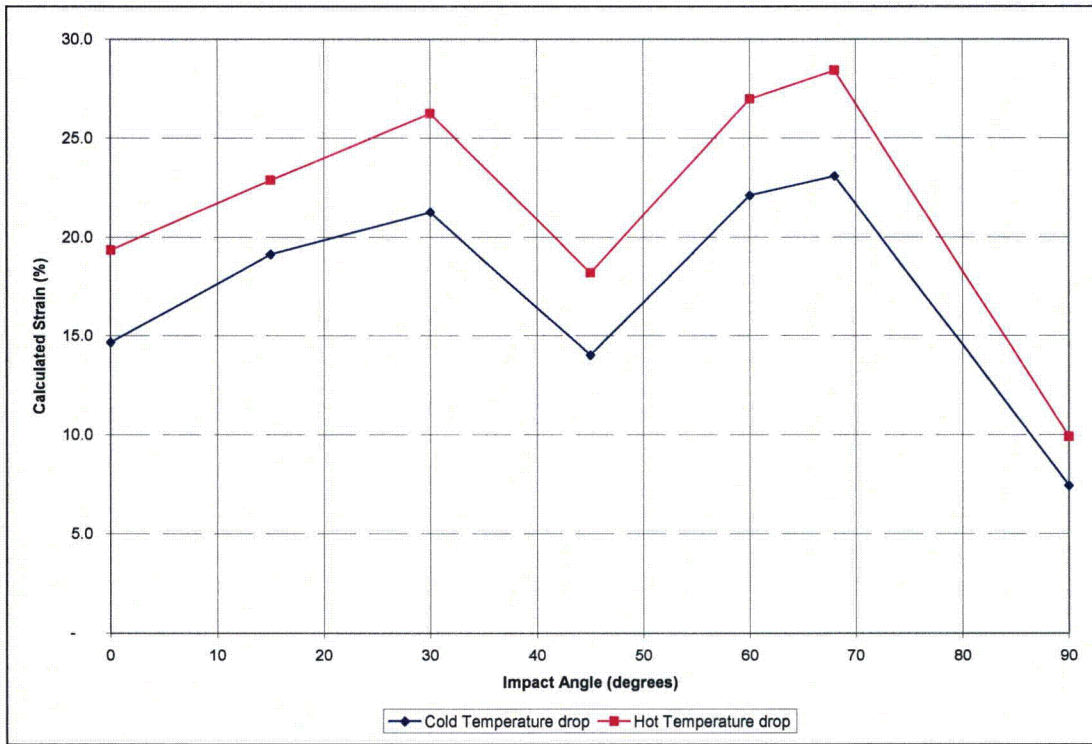


Figure 2.12.5-14 - Primary Impact Limiter Strain, NCT

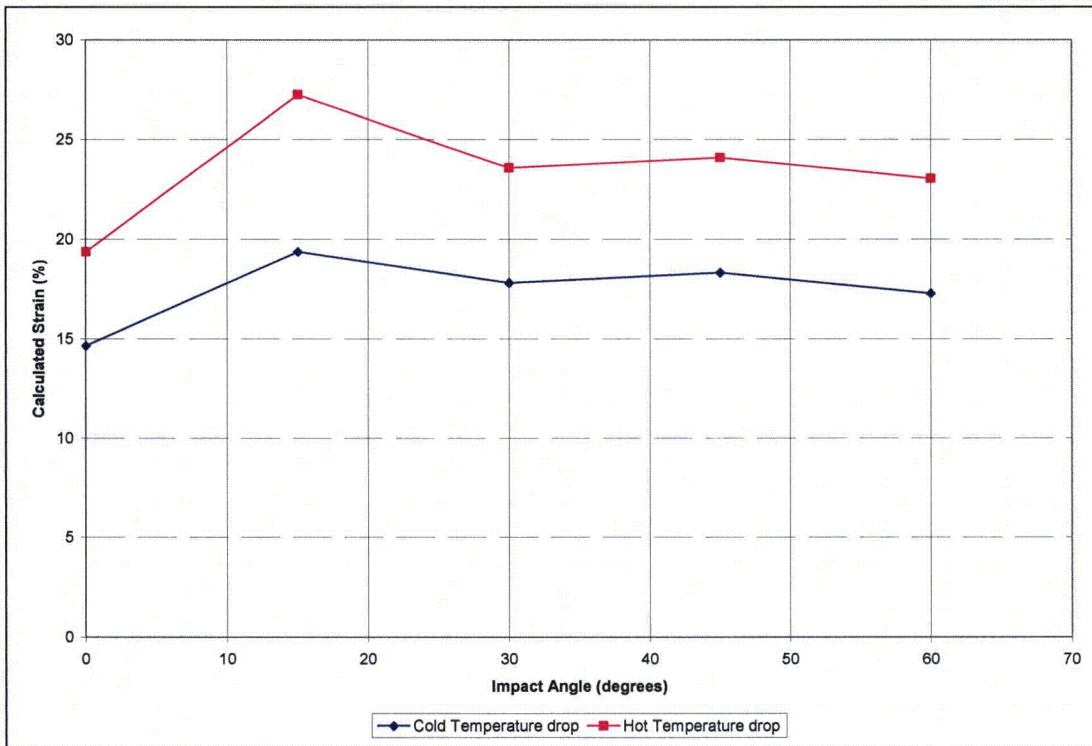


Figure 2.12.5-15 - Secondary Impact Limiter Strain, NCT

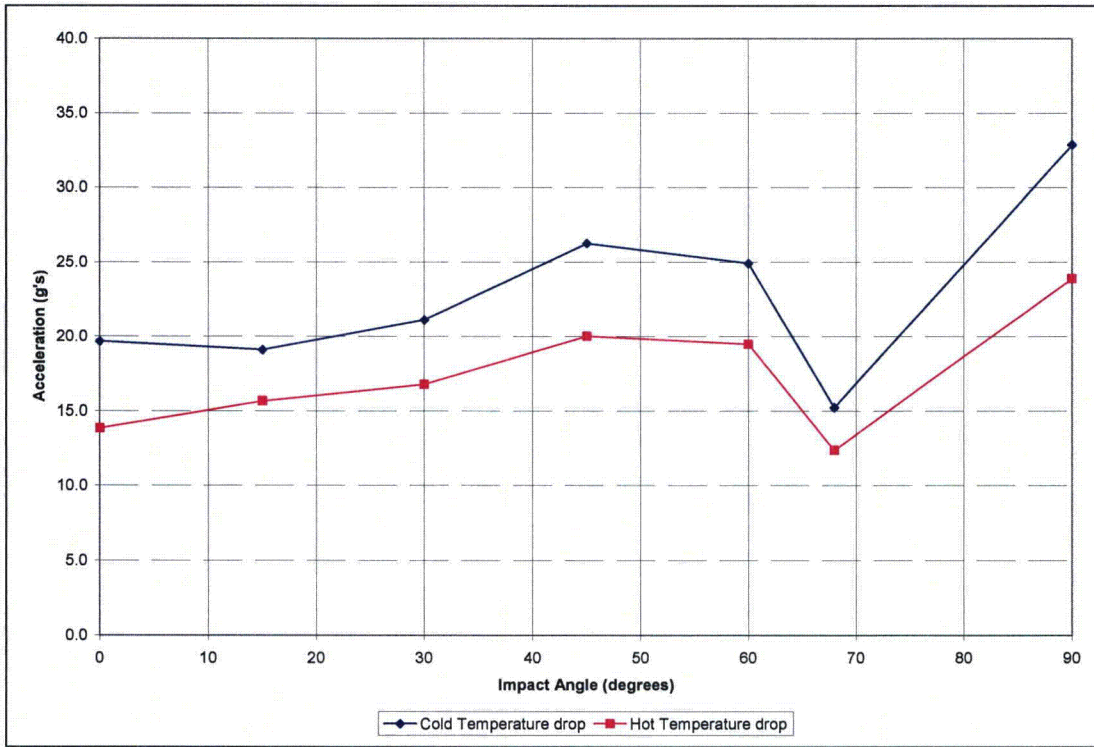


Figure 2.12.5-16 - Primary Impact Acceleration, NCT

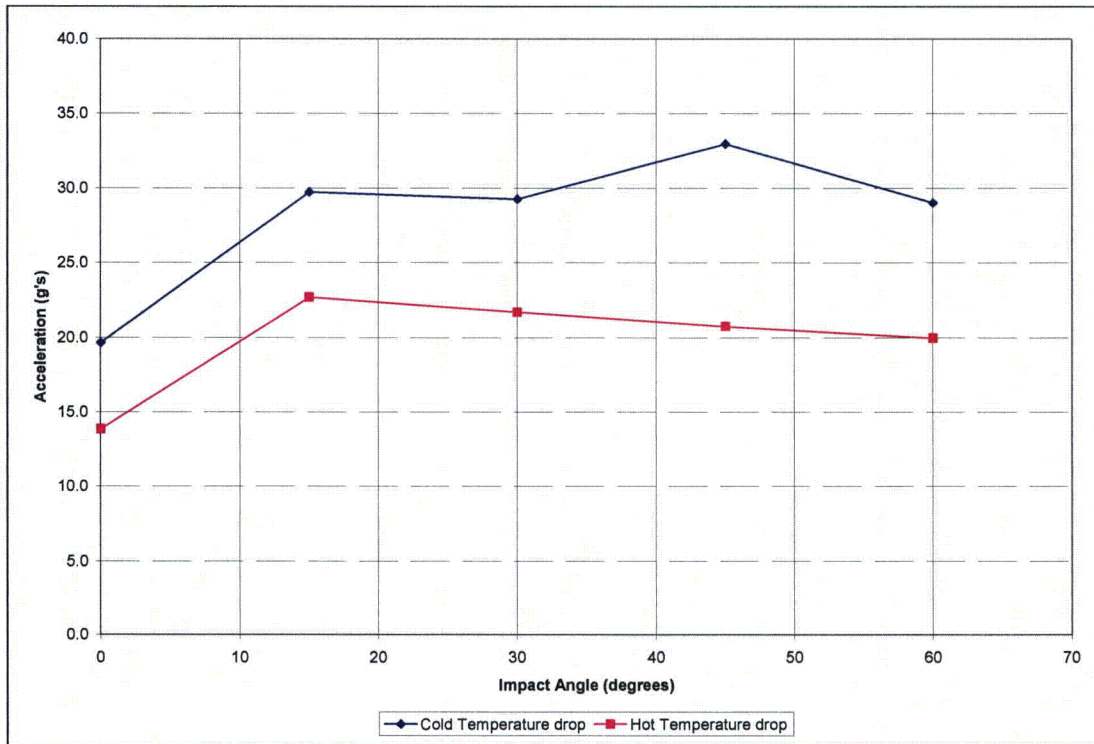


Figure 2.12.5-17 - Secondary Impact Acceleration, NCT

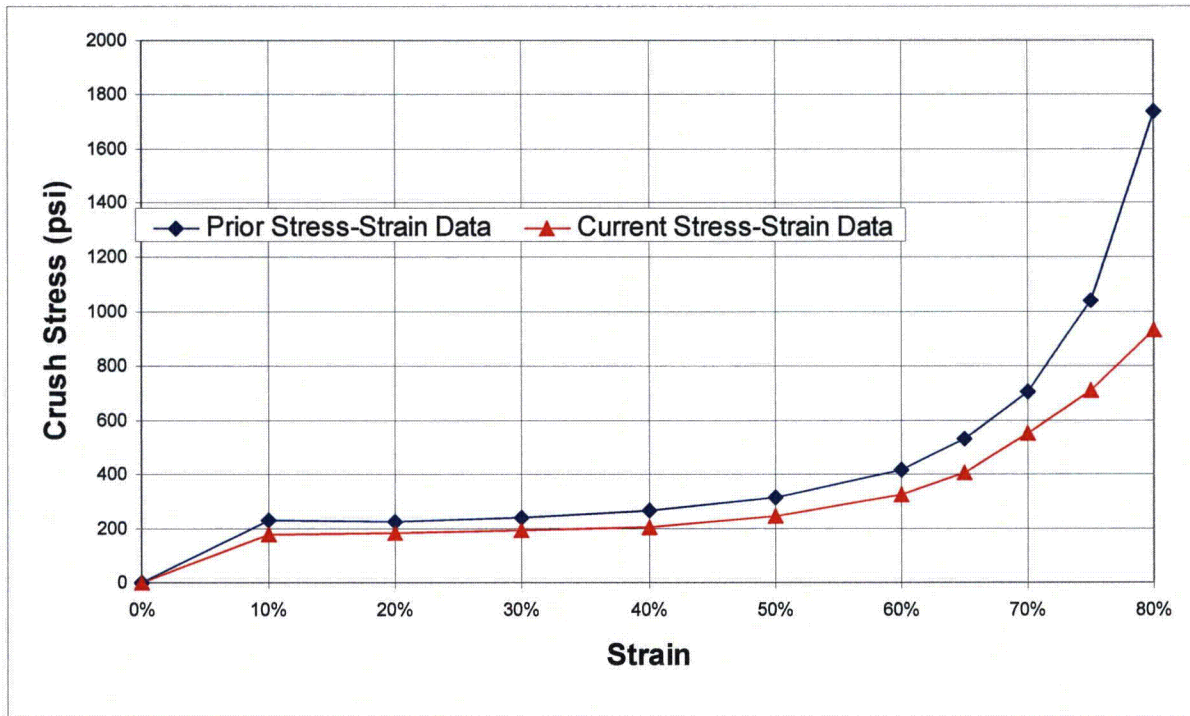


Figure 2.12.5-18 - Previously Published vs. Current Stress-Strain Data (150 °F)

## **2.12.7 Seal Performance Tests**

This appendix contains descriptions of the performance tests which have been run on the butyl rubber compound used for the containment O-ring seal and sealing washers used in the BRR package. The material is designated as Rainier Rubber R-0405-70. The performance tests which will be discussed have demonstrated the ability of this material to maintain a leaktight<sup>1</sup> containment boundary under minimum compression, minimum temperature, and maximum temperature conditions which are beyond those experienced in the BRR package.

### **2.12.7.1 Performance Tests Associated with the TRUPACT-II Package**

Two sets of butyl rubber performance tests have been done in support of the TRUPACT-II package certification (NRC Docket 71-9218). All relevant tests have used a bore-type fixture which is consistent with the configuration of the O-ring seals in the TRUPACT-II.

The test configuration and procedure was similar between the two tests and will now be briefly described. More details are available in Section 2.10.7.4 and Section 2.10.7.4A of [2]. Only the small test fixture is considered, since it was used in both sets of tests. The test fixture consists of an inner ring containing two O-ring grooves on its outer diameter and an outer ring which fits over the inner ring and provides compression of the two test O-rings. The cross-sectional diameter of the test O-rings was nominally 0.400 inches, which is essentially equivalent to the 0.375 nominal dimension of the BRR package containment O-ring seal. To vary the O-ring compression in the test fixture, the radial position of the inner ring was controlled by jacking screws. When the inner ring was shifted to one side within the outer ring, a maximum compression was obtained on the side toward which the inner ring was shifted, and a minimum compression was obtained on the opposite side. The entire fixture could be placed in an environmental chamber and either cooled or heated for a set time. A helium leakage rate test was performed at various stages by testing the leakage rate between the outside of the fixture and the space between the two test O-rings.

The first set of tests was performed in 1989 and is documented in Section 2.10.7.4 of [2]. A typical test sequence consisted of the following steps:

1. Assemble the test fixture at ambient conditions.
2. Perform a leakage rate test with the inner ring centered in the outer ring.
3. Chill the fixture to -40 °F and perform a helium leakage rate test.
4. Allow the fixture to warm to -20 °F.
5. Shift the inner ring laterally within the outer ring to achieve maximum compression on one side and minimum compression on the other side.
6. Perform a helium leakage rate test with the fixture still at -20 °F.
7. Heat to an elevated temperature, maintaining the inner ring in the shifted position.

---

<sup>1</sup> Leaktight is defined as a maximum leakage rate of  $1 \times 10^{-7}$  ref-cc/sec, air, per [1].

**BRR Package Safety Analysis Report**

8. Hold at temperature for 8 hours. Create a hard vacuum between the two test O-rings to confirm their integrity. A helium leakage rate test was not performed due to the tendency toward rapid saturation of the O-rings with helium at elevated temperature.
9. Chill the fixture to -20 °F, maintaining the inner ring in the shifted position.
10. Perform a final helium leakage rate test with the fixture still at -20 °F.

For each test, the maximum and minimum compressions were calculated using the dimensions of the fixture and of the test O-rings. The principal result of these tests was a demonstration that the subject rubber compound is capable of maintaining a leaktight condition at -20 °F with a minimum compression of 14.9% subsequent to an 8 hour soak at 400 °F. Details of the five small fixture tests are given in Table 2.12.7-1, adapted from Table 2.10.7-1 of [2]. Note that the term 'disk' in the table corresponds to the term 'inner ring' used in this description.

The second set of tests was performed in 1999, and are documented in Section 2.10.7.4A of [2]. These tests served to lower the minimum compression value at which a leaktight condition was demonstrated to be maintained. The tests used the same small test fixture, modified to allow it to achieve a lower minimum compression. The same test procedure was followed, except that all tests were run at a temperature of 400 °F. The principal result of these tests was a demonstration that the subject rubber compound is capable of maintaining a leaktight condition at -20 °F with a minimum compression of 12.9% subsequent to an 8 hour soak at 400 °F. Details of the three tests are given in Table 2.12.7-2, adapted from Table 2.10.7.4A-2 of [2].

### **2.12.7.2 Performance Tests Associated with the RTG Package**

O-ring tests were also performed in support of the Radioisotope Thermoelectric Generator (RTG) package certification (DOE Docket 94-6-9904). The results are reported in Section 2.10.6 of [3]. In these tests, a face-type fixture was used which permitted four different compressions to be tested at once. Unlike the TRUPACT-II testing, and consistent with the conditions in a face-type configuration, the O-rings were not mechanically moved or disturbed throughout the test. The fixture consisted of an inner plate having three concentric grooves on each side. Each groove had a different depth and contained an O-ring made from butyl compound R-0405-70 as described above. The inner and outer O-rings on each side were the test specimens; the center O-rings were used only to support leakage rate testing of the test specimens. The O-rings were compressed by outer plates which were set off from the inner plate by shims which, along with the groove depths, controlled the amount of compression of each test O-ring. The nominal test O-ring cross-sectional diameter was 0.275 inches. The minimum compression created by the fixture was 10%, which was uniform around the entire circumference of the fixture. Compressions of 12%, 14%, and 15.5% were tested at the same time. The dimensions of the fixture and of the test specimens, and the resulting compression values, are shown in Table 2.12.7-3.

The time/temperature sequence was as follows:

1. Assemble the test fixture at ambient conditions and perform a helium leakage rate test.
2. Chill the fixture to -40 °F and perform a helium leakage rate test.
3. Heat the fixture to 380 °F, and hold for 24 hours. Confirm integrity of the test O-rings by placing a hard vacuum on the test cavity (less than 0.2 mbar).



**BRR Package Safety Analysis Report**

**Table 2.12.7-1 – TRUPACT-II O-ring Seal Performance Test Results (1989)⑦**

Test Number	O-ring Seal Cross-Sectional Diameter (inches)				Stretch (%)		Maximum Gap (inches)		Minimum Compression (%)				Soak Temperature and Helium Leakage Rate Test Results ④				
	O-ring Seal No. 1		O-ring Seal No. 2		Min	Max	Disk Center	Disk Offset	Disk Centered		Disk Offset		Disk Centered		Disk Offset		
	Min	Max	Min	Max					Min	Max	Min	Max	Ambient	-40 °F	-20 °F	8 hrs⑤	-20 °F
1	0.387	0.397	0.387	0.396	2.0	4.1	0.026	③	22.1	25.6	14.9	20.0	Yes	Yes	Yes	350 °F	Yes
2	0.388	0.398	0.387	0.398	2.0	4.1	0.029	0.050	21.3	25.1	15.7	19.7	Yes	Yes	⑥	450 °F	No
3	0.387	0.397	0.387	0.399	2.0	4.1	0.027	0.052	21.9	25.8	15.2	19.4	Yes	Yes	Yes	400 °F	Yes
4	②	②	②	②	2.0	4.1	0.027	0.053	21.9	25.8	<b>14.9</b>	19.1	Yes	Yes	Yes	<b>400 °F</b>	<b>Yes</b>
5	②	②	②	②	2.0	4.1	0.026	0.050	22.1	26.0	15.7	19.9	Yes	Yes	Yes	400 °F	Yes

Notes:

- ① Material for all O-ring seal test specimens was butyl rubber compound R-0405-70, Rainier Rubber Co., Seattle, WA.
- ② Not measured; calculations assume the worst case range as taken from Tests Numbers 1 - 3 (i.e., Ø0.387 minimum to Ø0.399 maximum).
- ③ Range of values is 0.048 in. minimum to 0.053 in. maximum due to an indirect method of gap measurement (used for this test only).
- ④ A “Yes” response indicates that helium leakage rate testing demonstrated a leaktight condition as defined in [1], i.e., the leakage rate was less than or equal to  $1 \times 10^{-7}$  ref-cc/sec, air. In all cases, measured leak rates were less than or equal to  $2.0 \times 10^{-8}$  ref cc/s, helium, for tests with a “Yes” response.
- ⑤ No helium leakage rate tests were performed at elevated temperatures due to O-ring seal permeation and saturation by helium gas. The ability of the test fixture to establish a rapid, hard vacuum between the O-ring seals was used as the basis for leakage rate test acceptance at elevated temperatures. All tests rapidly developed a hard vacuum, with the exception of Test Number 2 at an elevated temperature of 450 °F, which slowly developed a vacuum.
- ⑥ Initial leakage rate of  $1.0 \times 10^{-5}$  ref cc/s, helium; became leaktight approximately one minute later.
- ⑦ Adapted from Table 2.10.7-1 of [2].

**BRR Package Safety Analysis Report**

**Table 2.12.7-2 – Supplementary TRUPACT–II O-ring Seal Performance Test Results (1999)④**

Test No.	Disk Centered % Comp.		Disk Offset % Comp.		Helium Leak Tight②				
	O-ring #1	O-ring #2	O-ring #1	O-ring #2	Ambient Temp.	-40 °F	-20 °F (Disk Offset)	Hot Soak (Disk Offset)③	-20 °F (Disk Offset)
1	18.5	17.9	12.7	12.0	Yes	Yes	Yes	Held Vacuum	Yes
2	20.8	20.0	12.9	<b>11.9</b>	Yes	Yes	Yes	Held Vacuum	<b>Yes</b>
3	19.2	19.2	12.1	12.1	Yes	Yes	Yes	Held Vacuum	Yes

Notes:

- ① Material for all O-ring seal test specimens was butyl rubber compound R-0405-70, Rainier Rubber Co., Seattle, WA.
- ② Seal is considered to be leaktight if the actual leakage rate is less than or equal to  $8 \times 10^{-8}$  atm-cc/sec.
- ③ Hot soak was 8 hours at a uniform temperature of 400 °F.
- ④ Adapted from Table 2.10.7.4A-2 of [2].

**BRR Package Safety Analysis Report**

**Table 2.12.7-3 – RTG O-ring Seal Performance Test Parameters<sup>③</sup>**

<b>Fixture Side</b>	<b>Outer groove depth, in.</b>	<b>Inner groove depth, in.</b>	<b>Shim Thickness, in.</b>	<b>Outer O-ring X- section, in.</b>	<b>Inner O-ring X- section, in.</b>	<b>Outer O-ring compression, %</b>	<b>Inner O-ring compression, %</b>
Side A	0.2053	0.2000	0.044	0.2770	0.2773	10	12
Side B	0.2075	0.2033	0.031	0.2776	0.2774	14	15.5

Notes:

- ① Material for all O-ring seal test specimens was butyl rubber compound R-0405-70, Rainier Rubber Co., Seattle, WA.
- ② Each of the four test O-ring seals were leaktight per [1] when tested at a temperature of -20 °F following the time/temperature sequence of 380 °F for 24 hours followed by 350 °F for 144 hours.
- ③ Adapted from Table 4.1-1 and Table 4.1-2 of [3].

## 2.12.8 Fuel Basket Stress Analysis

This appendix provides details of the stress analysis evaluations of the four fuel baskets used in the BRR package under HAC free drop conditions. One basket corresponds to each type of fuel, which includes the University of Missouri Research Reactor (MURR), the Massachusetts Institute of Technology Nuclear Research Reactor (MITR-II), Advanced Test Reactor (ATR), and Training, Research, Isotopes, General Atomics (TRIGA) reactors.

The evaluations consist of manual calculations and buckling evaluations using ASME B&PV Code Case N-284-2 [13]. An additional buckling evaluation technique for non-circular sections, used for the MITR-II basket, is referenced below. All buckling evaluations use a minimum factor of safety of 1.34, consistent with [13]. The bounding HAC impact acceleration of 120g is used for all analyses, which include free drops on the package end and on the package side. Basket and fuel weight is taken from Table 2.1-3. All of the material used in the fuel baskets is ASTM Type 304 stainless steel in various product forms including A240 (plate), A249 (tube), A269 (tube) A511 (tube), and A312 (pipe). Material properties are evaluated at the NCT maximum temperature of 400 °F, and taken from Table 2.2-1. Allowable stresses are taken from Table 2.1-1. The numeric values of allowable stress are given in Table 2.12.8-1. The analyses described in this appendix are based on the most critical load paths and demonstrate the structural integrity of the basket. Since each basket has a different design, the analyses which are most critical for each basket will be somewhat different.

Basket analyses do not include a dynamic load factor (DLF), since the impact acceleration used is nearly 50% higher than the maximum test result (see Section 2.12.5.3, *Reconciliation with Certification Test Results*), and because the basket structures are relatively stiff, which would result in a DLF not significantly different from unity.

### 2.12.8.1 MURR Basket

The MURR basket provides positioning and support for up to eight MURR fuel elements. The structure consists of an outer shell, an inner shell, eight radial separation plates, a support plate, and other stiffening components. From Table 2.1-3, the empty basket has a weight of 650 lb, and with eight fuel elements, the bounding weight is 770 lb. A cross sectional view of the basket is shown in Figure 2.12.8-1 and a view of the support plate is shown in Figure 2.12.8-2.

#### 2.12.8.1.1 Fuel Support Plate Bending

The fuel support plate provides lower end support of the fuel elements. In the bottom-down vertical impact, the support plate is loaded by a maximum of eight fuel elements. Since each fuel element slot is supported by welds along three sides as shown in Figure 2.12.8-2, the loading of the plate can be analyzed for a single segment of the plate.

Stresses loading the plate can be modeled using [25], Table 24, Case 27. This is a conservative approach using the simply supported case. This method will ignore the in-plane moment reducing effects of the welds. The effective area of plate for the applied load is:

$$A_p = \frac{\pi}{4}(d_o^2 - d_i^2) - 8 \cdot \frac{\pi}{4}d_H^2 - 8 \cdot A_s = 106.3 \text{ in}^2$$

**Table 2.12.8-1 – Material Properties and Allowable Stress**

Parameter	(ASTM, Type 304) <sup>①④</sup>
NCT Hot Bounding Temperature, °F	400
Elastic Modulus, psi	$26.4 \times 10^6$
Design Stress, $S_m$ , psi	18,600
Yield Stress, $S_y$ , psi	20,700
Ultimate Stress, $S_u$ , psi	64,000
HAC Allowable Stresses	
Primary Membrane Stress Intensity ( $P_m$ ), psi	Lesser of: <b><math>2.4S_m = 44,640</math></b> $0.7S_u = 44,800$
Primary Membrane + Bending Stress Intensity ( $P_m + P_b$ ), psi	Lesser of: <b><math>S_u = 64,000</math></b> $3.6S_m = 66,960$
Pure Shear Stress Intensity, psi	Lesser of: $0.42S_u = 26,880$ <sup>②</sup> <b><math>1.2S_m = 22,320</math></b> <sup>③</sup>

Notes:

1. ASTM A240, A249, A269, A276, A511, and A312.
2. ASME Code, Section III, Appendix F, Paragraph F-1334.2.
3. ASME Code, Section III, Subsection NG, Article NG-3225.
4. Governing values of allowable stress are in bold type.

**Table 3.1-1 – Maximum Temperatures for NCT and HAC Conditions**

Location / Component <sup>①</sup>	NCT Hot Conditions, °F	Accident Conditions, °F	Maximum Allowable	
			Normal	Accident
Fuel Element Plate	350	451	400	1,100
Fuel Element Side Plate	348	449	400	1,100
Fuel Basket	334	437	800	800
Inner Shell	237	393	800	800
Lead	233	482	620	620
Outer Shell	216	704	800	2,700
Thermal Shield	185	1,256	800	2,700
Lower End Structure	205	335	800	800
Upper End Structure	220	485	800	800
Shield Plug	225	317	620 <sup>②</sup>	620 <sup>②</sup>
Cask Lid	216	306	800	800
Closure/Vent Port Seals	216	306	250	400
Drain Port Seal	202	373	250	400
Upper Impact Limiter				
- Max. Foam	215	-	300	N/A
- Avg. Foam	146	-	300	N/A
- Shell	215	1,475	250 <sup>③</sup>	2,700 <sup>④</sup>
Lower Impact Limiter				
- Max. Foam	200	-	300	N/A
- Avg. Foam	142	-	300	N/A
- Shell	200	1,475	250 <sup>③</sup>	2,700 <sup>④</sup>
Max. Accessible Surface without Insolation	185 <sup>⑤</sup>	-	185	N/A
Cask Cavity Bulk Gas	259	388	N/A	N/A

Notes: ① Results assume a payload of eight (8) MURR fuel elements dissipating 158 W each and helium as the backfill gas.

② Temperature criterion based on melting point of the enclosed lead shielding.

③ Temperature criterion based on long term temperature limit for shell coating.

④ Temperature criterion based on melting point for the shell. No criteria for the polyurethane foam since its thermal decomposition serves as its principal means of providing thermal protection during the HAC event.

⑤ Maximum temperature occurs at the root of the upper cask impact limiter attachment lugs.

**Table 3.1-2 – Summary of Maximum Pressures**

Condition	Cask Cavity Pressure
NCT Hot	5.2 psi gauge
HAC Hot	8.8 psi gauge

**Table 3.1-3 – Summary of Permissible BRR Package Fuel Basket Loadings**

Payload	Backfill Gas for Transport	Max. Decay Heat Per Element	Max. Package Decay Heat
MURR Fuel	Helium	158	1,264
MITR-II Fuel	Helium	30	330
ATR Fuel	Helium	30	240
TRIGA Fuel	Helium	20	380

absorptivity of approximately 0.20. For conservatism, an emissivity of 0.9 and a solar absorptivity of 0.30 are assumed by this evaluation.

The char layer associated with the decomposed polyurethane foam has a conservative surface emissivity of approximately 0.95 based on a combination of the material type, color, and surface roughness. No free surfaces will exist for the 'poured in place' foam under NCT conditions.

Under HAC conditions, all exterior surfaces of the package are assumed to attain an emissivity of 0.9. This assumption exceeds the minimum requirements of 10 CFR §71.73(c)(4) [1].

### 3.2.2 Technical Specifications of Components

The materials used in the BRR packaging that are considered temperature sensitive are the lead used for the radiological shielding, the polyurethane foam used in the impact limiters, the epoxy coating used on the impact limiter exterior surfaces, the butyl rubber compound used for the containment boundary seals, and the aluminum cladding and UAl<sub>x</sub> fuel matrix used for the enclosed fuel assemblies. The other materials either have temperature limits above the maximum expected temperatures or are not considered essential to the function of the package.

Type 304 stainless steel has a melting point above 2,700 °F [6], but in compliance with the ASME B&PV Code [3], its allowable temperature is limited to 800 °F if the component serves a structural purpose (e.g., the material's structural properties are relied on for loads postulated to occur in the respective operating mode or accidental free drop condition). As such, the appropriate upper temperature limit under normal conditions is 800 °F for stainless steel components that form the containment boundary or are used in the fuel baskets. The upper limit for all other stainless steel components is 2,700 °F for both normal and accident conditions.

The applicable temperature criterion for the ASTM B29 lead is its melting point of approximately 620 °F [6].

Below 250 °F the variation in the thermal properties of the proprietary polyurethane foam with temperature are slight and reversible. While small variations in the foam properties will occur between 250 and 500 °F as water vapor and non-condensable gases are driven out of the foam, the observed changes are very slight. For conservatism, a long-term limit of 300 °F is assumed for the foam. There is no short term temperature limit for the foam as its decomposition under exposure to high temperatures is part of its mechanism for providing thermal protection during the HAC fire event. A detailed description of the foam's behavior under elevated temperatures is presented in Appendix 3.5.4, '*Last-A-Foam*' *Response under HAC Conditions*.

The exterior surfaces of the impact limiter shells are to be coated in a two step process consisting of a primer coat of polyamide epoxy, followed by an acrylic polyurethane top coat [11]. The color is white. The coating system is resistant to long term temperature exposure up to 250 °F and for intermittent exposure up to 275 °F.

The butyl rubber compound used for the containment seals is fabricated from Rainier Rubber compound R-0405-70 [20]. Butyl rubber has a long term temperature range of -75 °F to 250 °F [21]. Per Appendix 2.12.7, *Seal Performance Tests*, an acceptable short duration limit for this compound is 400 °F for 8 hours, 380 °F for 24 hours, and 350 °F for 144 hours. For conservatism, a long-term limit of 250 °F, a short-term limit of 400 °F for 8 hours, and a low temperature limit of -40 °F are assumed for this analysis.



Aluminum has a melting point of approximately 1,100 °F [6]; however for strength purposes the normal operational temperature of the fuel cladding and the UAl<sub>x</sub> fuel matrix are limited to 400°F based on structural strength considerations for aluminum [3]. The limit under HAC conditions is 1,100°F. The same allowable temperature limits are conservatively used for the TRIGA fuel elements as well.

The minimum allowable service temperature for all BRR package components is below -40 °F.

Figure 3.3-1 to Figure 3.3-4 present the predicted temperature distribution within the BRR package for the NCT Hot condition. The elevation of the MURR fuel payload within the cask cavity is clearly evident from the temperature distribution seen in Figure 3.3-1 and Figure 3.3-3. The temperature distribution within the impact limiters illustrated in Figure 3.3-2 also reflects the elevation of the payload, plus the upright orientation of the package for NCT conditions in that the inside face of the lower impact limiter experiences the solar loading for a flat horizontal surface, while the same face for the upper impact limiter has a zero solar loading because of its downward orientation.

Figure 3.3-3 illustrates the temperature distribution in the structural shell of the cask. The presence of the impact limiter attachment lugs can be seen by the localized 'cool' spots in the temperature distribution of the outer shell. As noted in the description of the NCT thermal model provided in Appendix 3.5.3, *Analytical Thermal Model*, the NCT Hot results are based on an earlier cask design that used 6 instead of the current 8 attachment lugs per limiter, cask lug plates that are 0.38-inches thick by 2.75-inches wide vs. the current 0.5-inches thick by 3.63-inches wide, and a 0.25-inch vs. 0.125-inch radial gap between the limiter and the cask shell. Since the earlier design version provides slightly conservative results for NCT due to its lower surface area for heat dissipation to the ambient, it is appropriate for predicting the peak NCT temperatures.

Figure 3.3-4 presents the predicted temperature distribution within the MURR fuel basket under the NCT Hot condition.

Evaluation of the package for an ambient air temperature of 100 °F without insolation loads demonstrates that the temperatures of all exterior surfaces of the packaging are below the maximum temperature of 185 °F permitted by 10 CFR §71.43(g) for accessible surface temperature in an exclusive use shipment. The peak accessible surface temperature occurs at the root of the upper impact limiter attachment lugs. A sensitivity analysis, based on the revised lug design, as described in Appendix 3.5.3, *Analytical Thermal Model*, confirms that the peak accessible surface temperature in the vicinity of the upper impact limiter attachment lugs (see temperature distribution in Figure 3.3-5) is 185 °F or less.

### **MITR-II Fuel Basket**

Table 3.3-2 presents the predicted maximum temperature achieved within the MITR-II fuel basket under the NCT Hot condition with a helium gas backfill. The peak temperatures for the BRR packaging components are bounded by those presented in Table 3.3-1. The design basis maximum decay heat loading for the MITR-II fuel elements to be transported is 30 W per element, or 330 W for a payload of eleven (11) fuel elements. The results demonstrate that the design criterion of a maximum fuel plate temperature of 400 °F is met if helium is used as the backfill gas. Figure 3.3-6 presents the predicted temperature distribution within the MITR-II fuel basket under the NCT Hot condition.

### **ATR Fuel Basket**

Table 3.3-3 presents the predicted maximum temperature achieved within the ATR fuel basket under the NCT Hot condition with a helium gas backfill. The peak temperatures for the BRR packaging are again bounded by those presented in Table 3.3-1. The design basis maximum decay heat loading for the ATR fuel elements to be transported is 30 W per element, or 240 W

for a payload of eight (8) fuel elements. Although this level of decay heat loading could be accommodated using air as the backfill gas, a helium gas backfill is to be used to maintain consistency with the loading procedures for the other payloads. Figure 3.3-7 presents the predicted bounding temperature distribution within the ATR fuel basket under the NCT Hot condition.

### **TRIGA Fuel Basket**

Table 3.3-4 presents the predicted maximum temperature achieved within the TRIGA fuel basket under the NCT Hot condition with a helium backfill. The design basis maximum decay heat loading for the TRIGA fuel elements to be transported is 20 W per element, or 380 W for a payload of nineteen (19) fuel elements. As seen from Table 3.3-4, the results demonstrate that the design criterion of a maximum fuel element temperature of 400 °F is met. Figure 3.3-8 presents the predicted bounding temperature distribution within the TRIGA fuel basket under the NCT Hot condition.

#### **3.3.1.2 Minimum Temperatures**

The minimum temperature achieved within each of the fuel baskets would be achieved with a zero decay heat load and an ambient air temperature of -40 °F per 10 CFR §71.71(c)(2). The evaluation of this thermal condition requires no thermal calculation. Instead, all package components will eventually achieve the -40 °F temperature under steady-state conditions. As discussed in Section 3.2.2, *Technical Specifications of Components*, the -40 °F temperature is within the allowable operating temperature range for all package components.

#### **3.3.2 Maximum Normal Operating Pressure**

The cask cavity is to be filled with helium at atmospheric pressure following the draining and drying process. Since the release of fission generated gases from uranium-aluminide and uranium-zirconium hydride based fuel is diffusion-limited as opposed to the direct release mechanism for commercial spent nuclear fuel, the pressurization of the cask cavity due to gaseous release from breached fuel elements will be insignificant [30, 31] and is ignored for this safety evaluation.

The peak pressure developed within the cask cavity under NCT conditions can be conservatively estimated by assuming that the cavity gas reaches a bulk average temperature that is equal to the mean of the average inner shell temperature and the average fuel basket temperature. Under the NCT Hot condition with the MURR fuel payload the average temperature of the inner shell is 225 °F. Combining this temperature with the average fuel basket temperature of 293 °F yields a predicted bulk average backfill gas temperature of 259 °F.

Assuming the backfill gas has an initial temperature of 70 °F at the time of filling and that a fill pressure of one atmosphere is used, the predicted maximum operating pressure within the cask cavity for the transport of the MURR payload can be estimated via:

$$\text{Cavity Pressure} = 14.7 \text{ psia} \frac{(259^\circ\text{F} + 460^\circ\text{F})}{(70^\circ\text{F} + 460^\circ\text{F})} - 14.7 \text{ psia}$$

$$\text{Cavity Pressure} = 5.2 \text{ psig}$$

The equivalent peak bulk average fill gas temperatures for the MITR-II, ATR, and TRIGA baskets are 170, 164, and 174 °F, respectively. As such, the associated peak cask cavity pressures under NCT conditions are 2.8, 2.6, and 2.9 psig, respectively. Based on these NCT pressures, the maximum normal operating pressure (MNOP) within the cask cavity is set at a bounding level of 10 psig.

### 3.3.3 Vacuum Drying Operations

An evaluation of the proposed vacuum drying operation was conducted to ensure that the component temperatures will remain within their normal temperature limits. The vacuum drying operations consist of the following general steps:

- 1) the cask body, without the impact limiters, bottom drain plug, cask lid, and cask shield plug are placed in the reactor pool.
- 2) the fuel elements to be transported are placed in the fuel basket within the cask,
- 3) the shield plug is placed into the cask,
- 4) the loaded cask is lifted above the pool and the enclosed water allowed to drain back into the pool. At this point, the cask cavity is filled with air.
- 5) following decon operations, the loaded cask is moved to the facility work area where the drain port and cask lid is installed. The vent port tool is installed and vacuum drying is initiated.
- 6) the minimum pressure achieved under vacuum drying is 1 to 3 torr.

The transient evaluation of these operations used a modification of the NCT thermal model described in Appendix 3.5.3, *Analytical Thermal Model*. The modifications made for this evaluation consisted of assuming air as the backfill gas. While the impact limiters will not be installed during vacuum drying operations, and the cask lid will not be installed until just before vacuum drying begins, leaving these components in the thermal model greatly simplified the model modifications required and is seen as having no significant impact on the transient temperatures. The effect of being submerged in the reactor pool is addressed by assuming all cask components are at equilibrium with a maximum temperature of 80 °F.

At time = 0, the loaded cask is assumed to be lifted from the pool, the water drained and the cask cavity filled with air, the ambient conditions are conservatively assumed to be 100 °F without insolation. The transient analysis is conducted for a period of 8 hours and followed by a steady-state evaluation to establish the peak temperatures that would occur if the helium backfill is not established. The MURR fuel element payload is selected as a basis for the vacuum drying evaluation since its decay heat loading is over 3 times greater than any of the other potential payloads.

The thermal analysis of vacuum drying assumes that the thermal conductivity of the gas filling the voids of the packaging and the payload remain unchanged from its base value at atmospheric pressure conditions for vacuum pressures of 1 torr or greater. There are two states that define the process by which heat is transferred by a gas [32]:

**viscous state**, in which the totality of molecules is responsible for the heat transfer. The viscous state occurs as long as the pressure is higher than the range in which the

molecular state occurs. Within the viscous state the thermal conductivity of a gas is independent of pressure.

**molecular state**, heat conductivity in the molecular state is when the gas pressure is so low that the molecular mean free path is about equal or greater than the distance between the plates. The thermal conductivity of the gas is no longer characterized by the viscous state for conductivity and therefore the conductivity is dependent on pressure. The heat transfer process under these conditions is called free molecular conduction.

The pressure at which the molecular mean free path is equal to the minimum distance between the surfaces within the packaging is determined below for air as the fill gas. Per [33], the mean free path of the fill gas molecules is computed via:

$$L = \frac{k \times T}{\pi \times \sqrt{2} \times P \times d^2}$$

where:

$k = 1.380658 \times 10^{-23}$  J/K, the Boltzmann constant

P = pressure in Pa

T = temperature in K

d = molecule diameter, in m

At the lowest practical vacuum pressure of 1 torr (133 Pa) used for vacuum drying and a conservatively high gas temperature of 525 °F (547K) based on the hottest fuel element (as determined from the steady-state analysis), the mean free path for air with a molecule diameter of about  $3 \times 10^{-10}$  m (based on oxygen, [33]) is:

$$L = \frac{1.380658 \times 10^{-23} \times 547}{\pi \times \sqrt{2} \times 133 \times (3 \times 10^{-10})^2}$$

$$L = 1.42 \times 10^{-4} \text{ m} = 0.006 \text{ inches}$$

Since this mean free path is much smaller than the smallest significant gap in the model (i.e., the gap between fuel plates), the gas heat transfer everywhere within the model can be characterized as being in the viscous state and independent of the gas pressure.

Figure 3.3-9 illustrates the predicted package heat up following removal from the fuel pool. The illustrated thermal transient conservatively ignores the cooling effect provided by the water remaining in the cask cavity as it evaporates and the increased thermal conductivity provided by moist air over the dry air conductivity assumed by the thermal modeling. As seen by the transient curves presented in Figure 3.3-9, a minimum of 8 hours exists before the peak fuel plate temperature reaches the NCT limit of 400 °F. Since this temperature limit is set by structural considerations for the accident drop events and since no credible drop event exists between the time the cask is placed in the facility work area and the vacuum drying is completed and the cask

is prepared for transportation, the actual temperature limit for the fuel elements under vacuum drying can be higher.

Oxidization of aluminum fuel has been studied for long term exposure to moist air and saturated water vapor at temperatures up to 400 °F (200 °C ) [34, 35]. The results show no significant oxidization and no damage to the fuel cladding as a result of the exposure. As such, no fuel damage is expected for the limited time and exposure temperatures seen under vacuum drying.

In conclusion, the transient results in Figure 3.3-9 demonstrate that adequate time and thermal margin exists to allow the necessary vacuum drying operations to be completed without exceeding the maximum allowable component temperature limits. While even the steady-state temperatures with air as the backfill gas will not result in any damage to the fuel elements, the vacuum drying operations will include a provision to backfill the cask cavity with helium gas if the vacuum drying has not been completed within 8 hours. Once filled with the helium gas, the package temperatures are bounded by those presented in Section 3.3.1.1, *Maximum Temperatures*, for NCT conditions.

**Table 3.3-1 – NCT Temperatures for BRR Packaging with MURR Fuel**

Component	Temperature (°F) <sup>①</sup>		
	NCT Hot <sup>②</sup>	NCT Hot without Solar	Max. Allowable
MURR Fuel Plate	350	331	400
MURR Side Plate	348	329	400
MURR Fuel Basket	334	315	800
Inner Shell	237	216	800
Lead	233	213	620
Outer Shell	216	195	800
Thermal Shield	185	182	800
Lower End Structure	205	184	800
Upper End Structure	220	200	800
Shield Plug	225	205	620 <sup>③</sup>
Cask Lid	216	197	800
Closure/Vent Port Seals	216	197	250
Drain Port Seal	202	181	250
Upper Impact Limiter			
- Max. Foam	215	196	300
- Avg. Foam	146	132	300
- Shell	215	196	250 <sup>④</sup>
Lower Impact Limiter			
- Max. Foam	200	179	300
- Avg. Foam	142	127	300
- Shell	200	179	250 <sup>④</sup>
Max. Accessible Surface	-	185 <sup>⑤</sup>	185
Cask Cavity Bulk Gas	259	239	N/A

Notes: ① Results assume a payload of eight (8) MURR fuel elements dissipating 158 W each and helium as the backfill gas.

② Temperature criterion based on melting point of the enclosed lead shielding.

③ Temperature criterion based on long term temperature limit for shell coating.

④ Results conservatively based on an earlier design for the cask and impact limiter attachment lugs. See Appendix 3.5.3 for a description of the design change and the conservative impact of ignoring the design change for NCT Hot modeling.

⑤ Maximum temperature occurs at the root of the upper cask impact limiter attachment lugs.

**Table 3.3-2 – NCT Hot Temperatures for BRR Packaging with MITR-II Fuel**

Component <sup>⓪</sup>	Temperature (°F)	
	11 Elements @ 30 W Each	Max. Allowable
MITR-II Fuel Plate	263	400
MITR-II Side Plate	262	400
MITR-II Fuel Basket	244	800
Cask Cavity Bulk Gas	170	N/A

Note: <sup>⓪</sup> Temperatures for packaging components bounded by values in Table 3.3-1.

**Table 3.3-3 – NCT Hot Temperatures for BRR Packaging with ATR Fuel**

Component <sup>⓪</sup>	Temperature (°F)	
	8 Elements @ 30 W Each	Max. Allowable
ATR Fuel Plate	197	400
ATR Side Plate	197	400
ATR Fuel Basket	195	800
Cask Cavity Bulk Gas	164	NA

Note: <sup>⓪</sup> Temperatures for packaging components bounded by values in Table 3.3-1.

**Table 3.3-4 – NCT Hot Temperatures for BRR Packaging with TRIGA Fuel**

Component <sup>⓪</sup>	Temperature (°F)	
	19 Elements @ 20 W Each	Max. Allowable
TRIGA Fuel Element	355	400
TRIGA End Fitting	308	400
TRIGA Fuel Basket	287	800
Cask Cavity Bulk Gas	174	NA

Note: <sup>⓪</sup> Temperatures for packaging components bounded by values in Table 3.3-1.



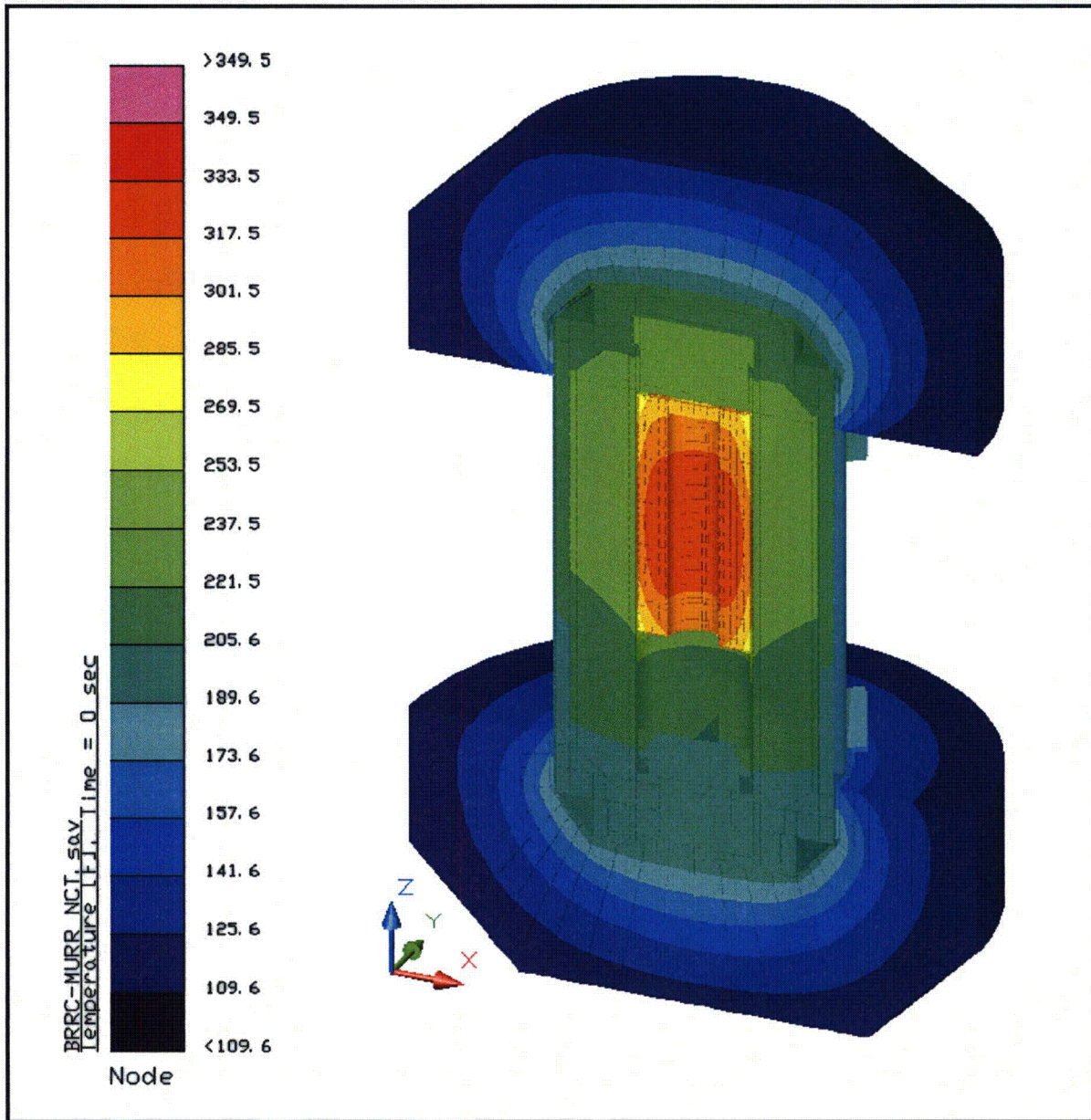
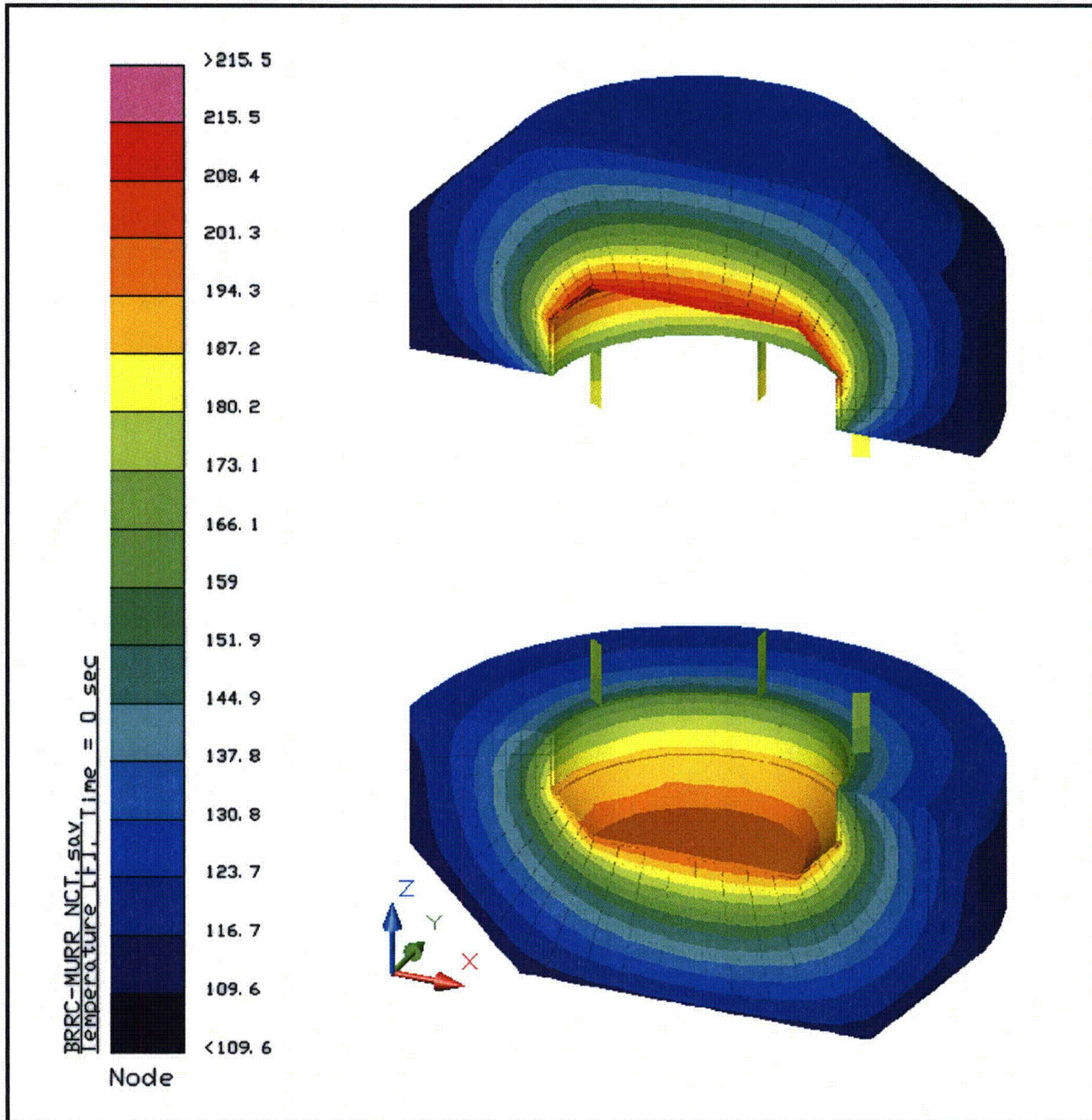


**Figure 3.3-1** – BRR Package Temperature Distribution for NCT Hot Condition with MURR Fuel Basket



Note: Earlier design of 6 vs. 8 attachment lugs per limiter depicted. Results bound the revised design under NCT

**Figure 3.3-2 – Impact Limiter Temperature Distribution for NCT Hot Condition with MURR Fuel Basket**

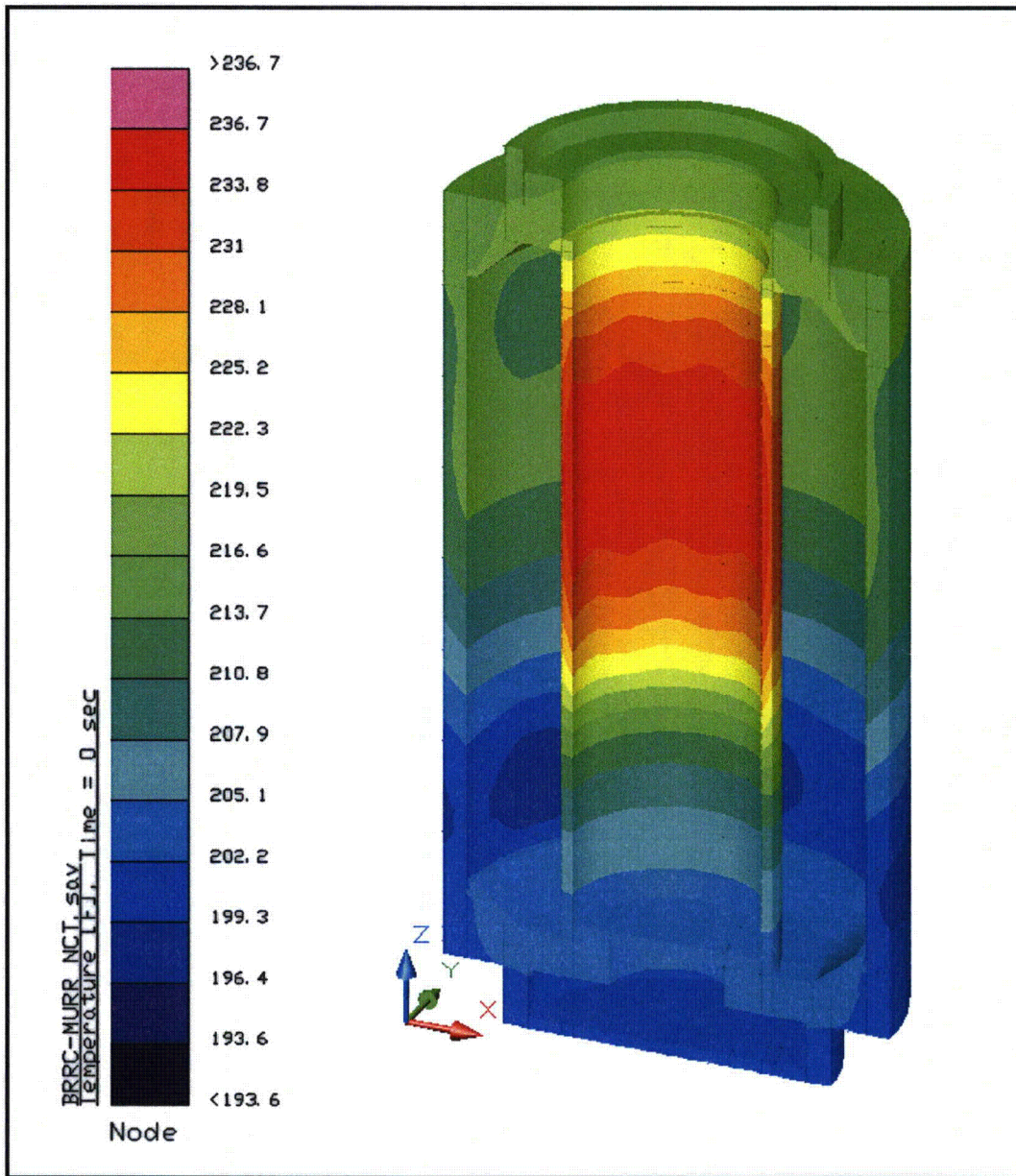


Figure 3.3-3 – Structural Shell Temperature Distribution for NCT Hot Condition with MURR Fuel Basket

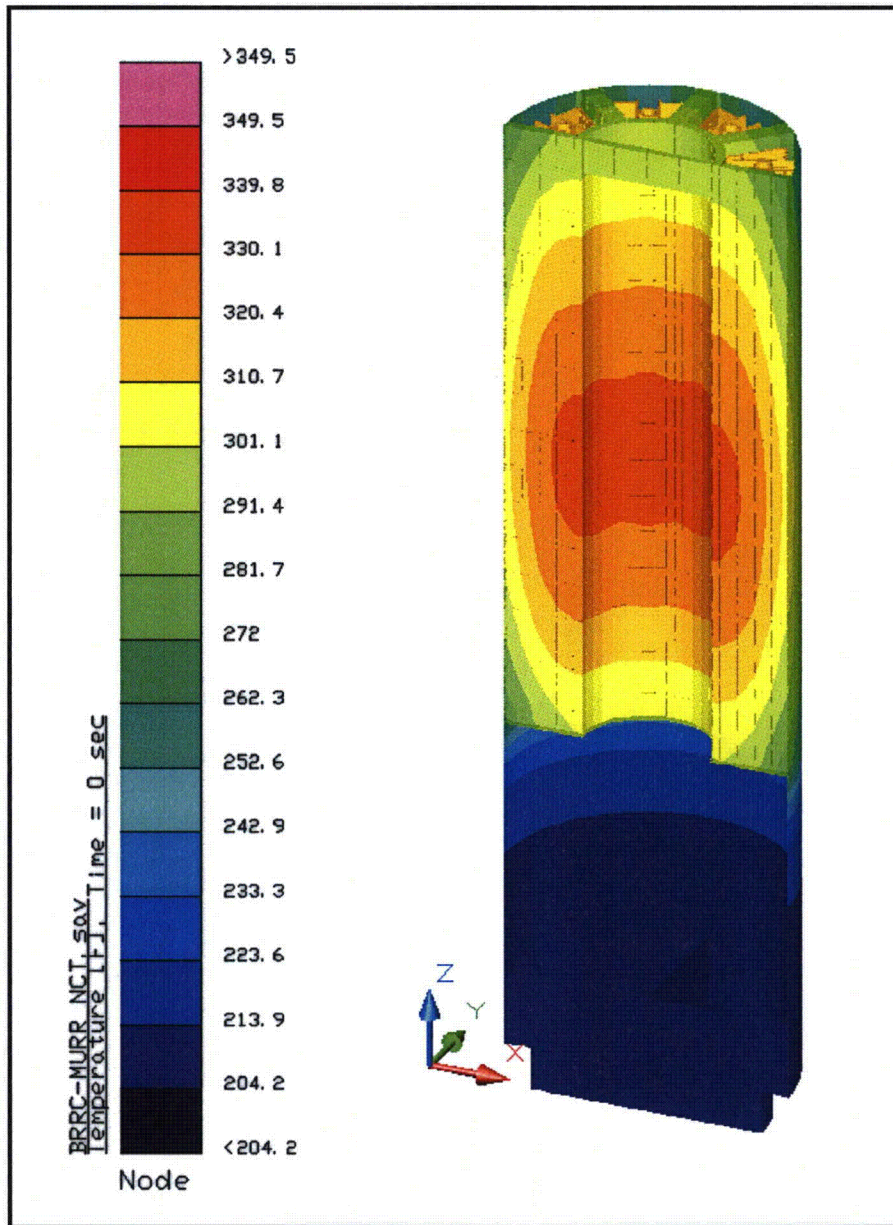
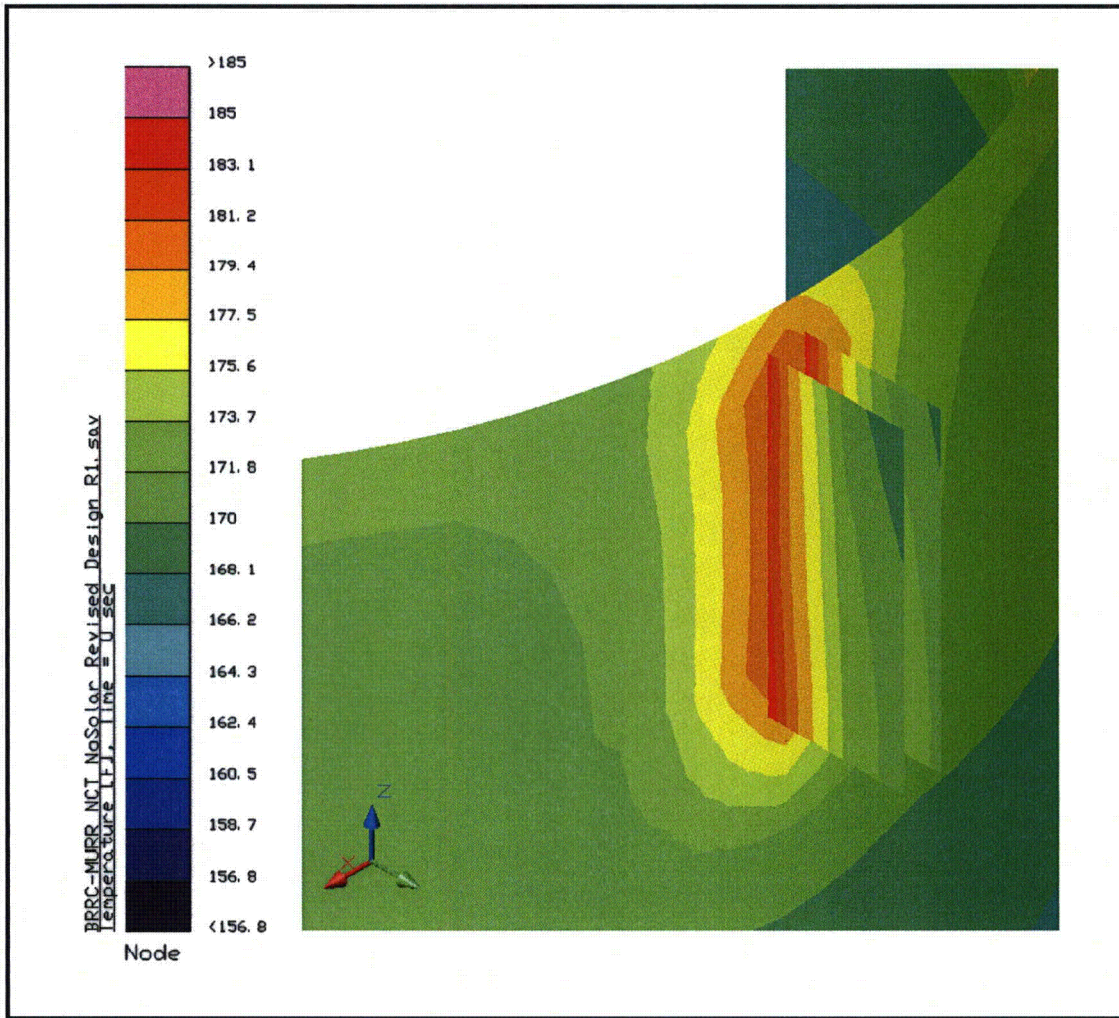
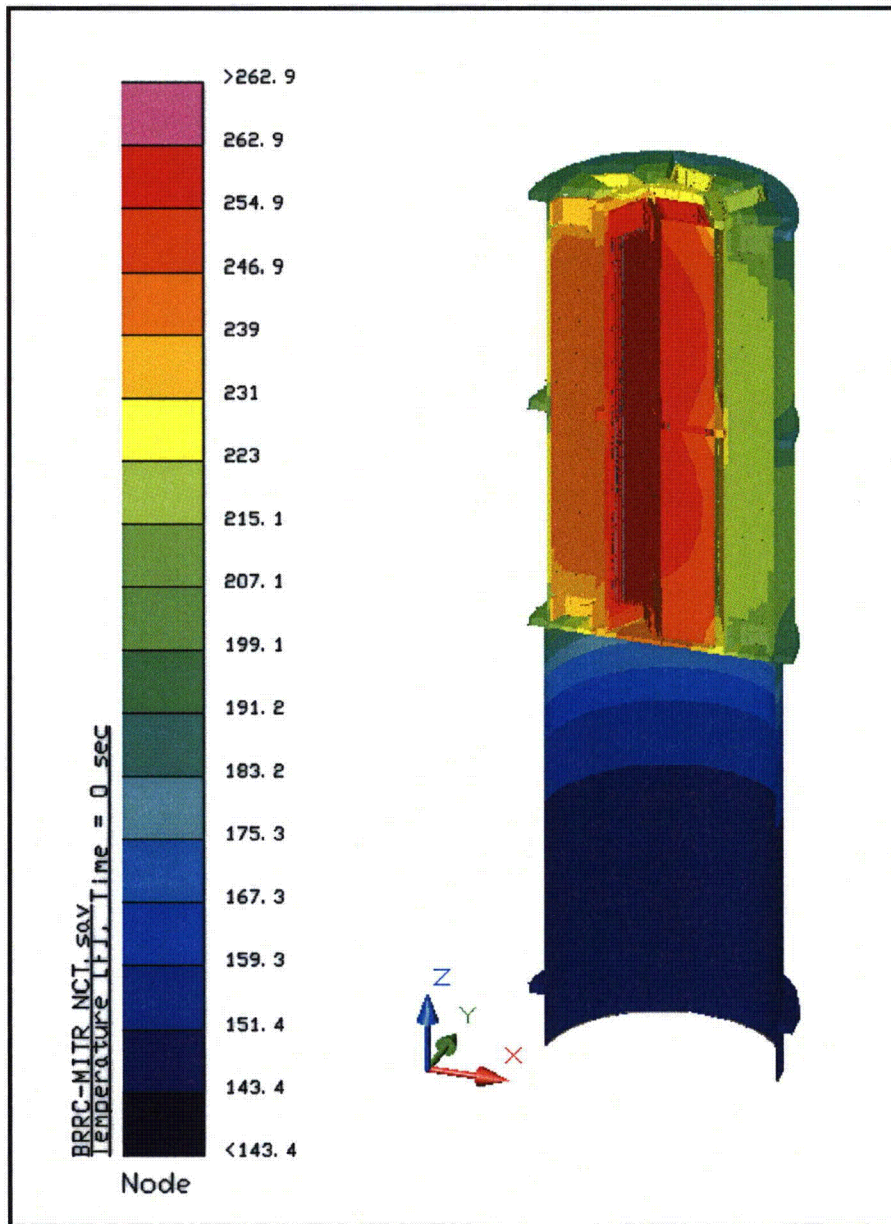


Figure 3.3-4 – MURR Fuel Basket Temperature Distribution for NCT Hot Condition



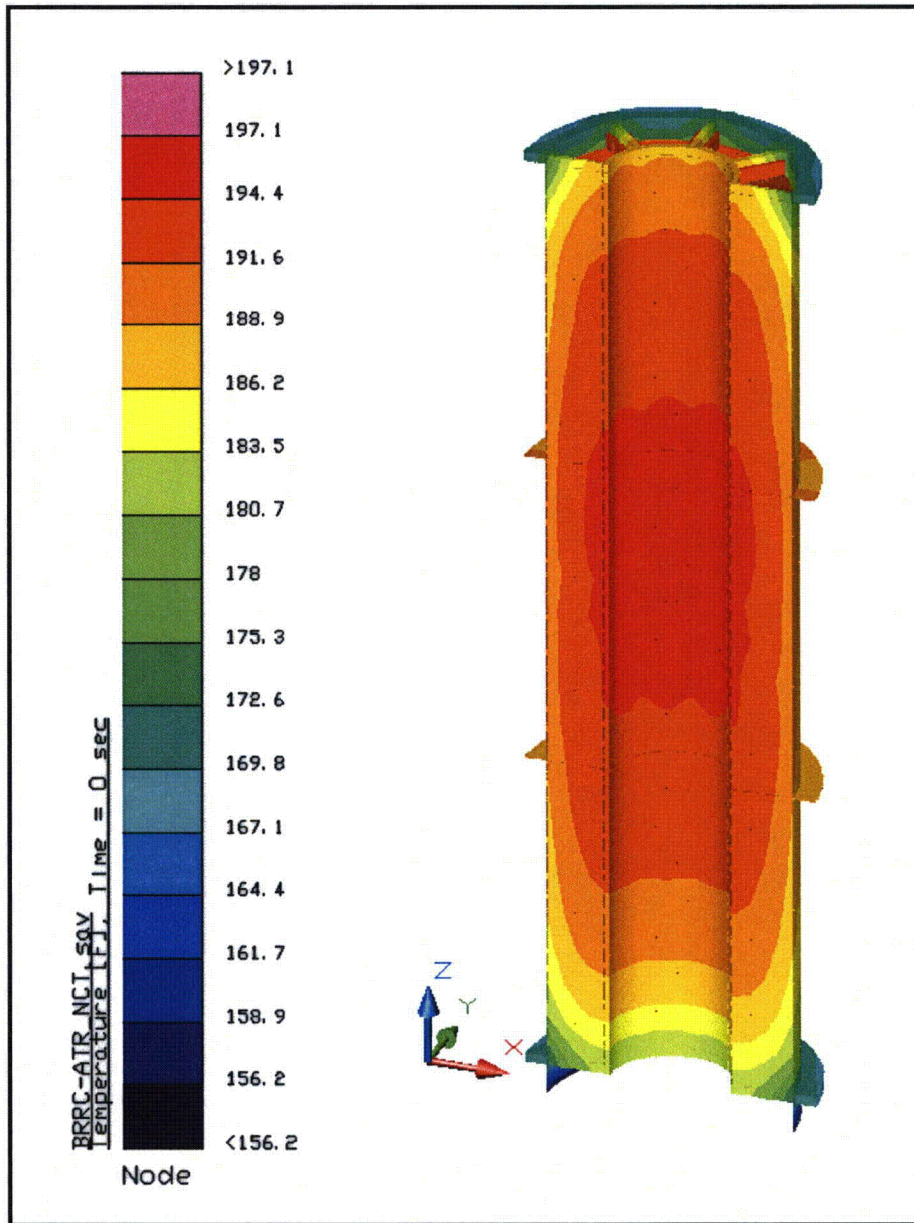
Surface Temperature Distribution in Vicinity of Impact Limiter Attachment Lugs

Figure 3.3-5 – Peak Accessible Surface Temperature for NCT No Solar



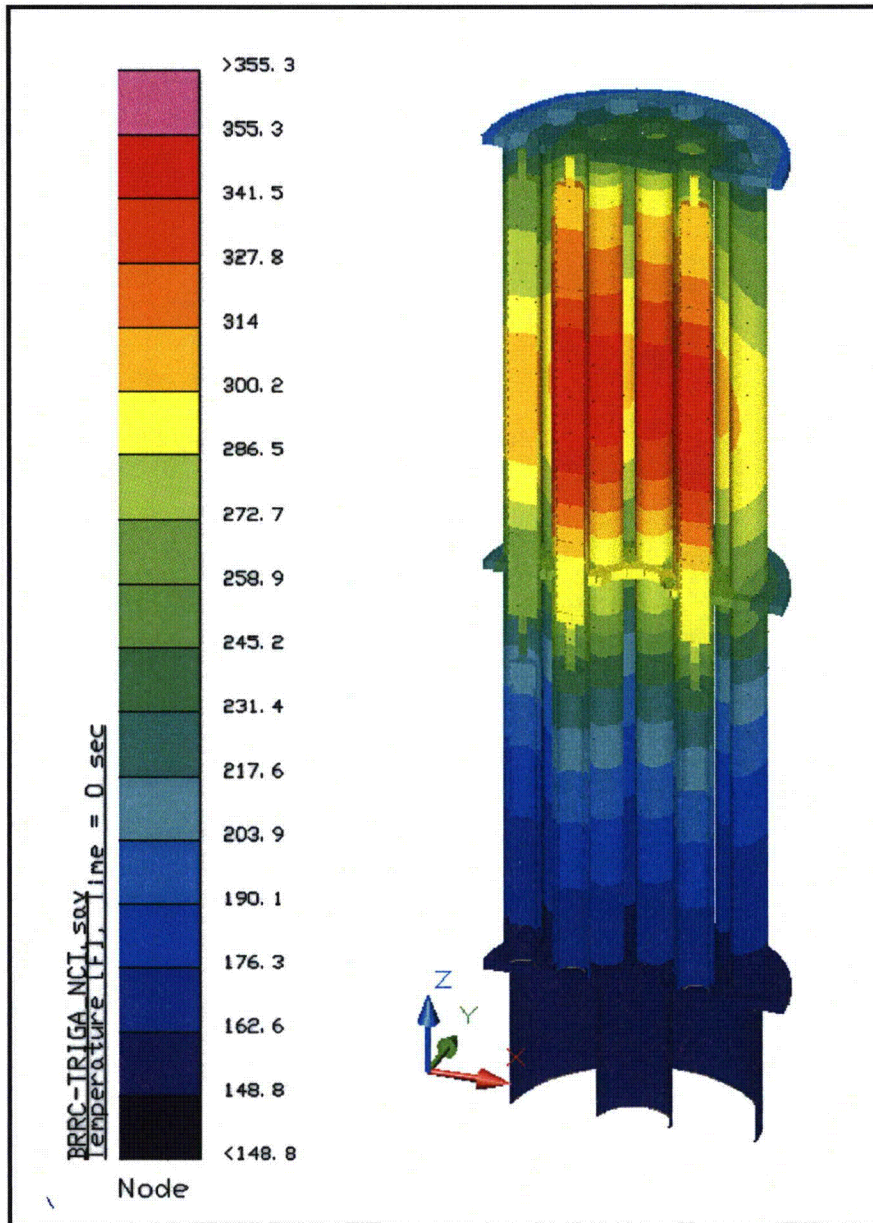
Note: Results are for basket decay heat loading of 330 W

**Figure 3.3-6 – MITR-II Fuel Basket Temperature Distribution for NCT Hot Condition**



Note: Results are for basket decay heat loading of 240 W

**Figure 3.3-7 – ATR Fuel Basket Temperature Distribution for NCT Hot Condition**



Note: Results are for basket decay heat loading of 380 W

**Figure 3.3-8 – TRIGA Fuel Basket Temperature Distribution for NCT Hot Condition**



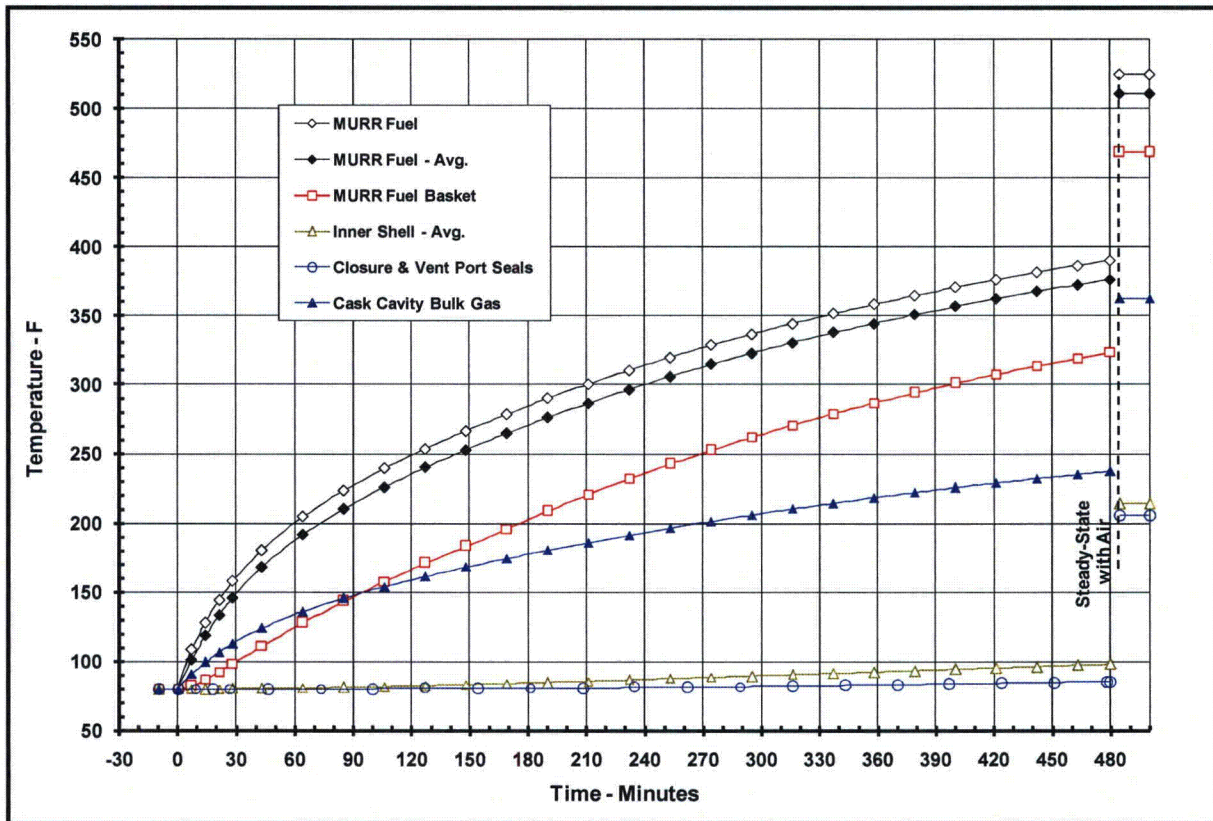


Figure 3.3-9 – Bounding Transient Heat Up During Vacuum Drying

### 3.4 Thermal Evaluation for Hypothetical Accident Conditions

This section presents the thermal evaluation of the BRR package under the hypothetical accident condition (HAC) specified in 10 CFR §71.73(c)(4) based on an analytical thermal model of the BRR. The analytical model for HAC is a modified version of the half symmetry NCT model described in Appendix 3.5.3.1, *Description of BRR Packaging Thermal Model for NCT Conditions*, with the MURR fuel element payload. The MURR payload is selected as a basis for the HAC evaluation since its decay heat loading is more than 3 times greater than any of the other potential payloads.

The principal model modifications made to convert the NCT thermal model to the HAC model consists of modifying the impact limiter attachment thermal model to reflect the design modifications following the drop testing, simulating the expected package damage resulting from the HAC defined drop events, capturing the thermal decomposition of the polyurethane foam under HAC conditions, changing the package surface emissivities to reflect the assumed presence of soot and/or surface oxidization, assumed contact between the thermal shield and the outer shell and zero lead gap to maximize the heat flow into the package, and changing the package orientation from upright to horizontal to reflect its probable orientation following the HAC drop event.

Physical testing using a half scale certified test unit (CTU) is used to establish the expected level of damage sustained by the BRR package from the 10 CFR 71.73 prescribed free and puncture drops that are assumed to precede the HAC fire event. Appendix 2.12.3, *Certification Test Results*, provides the configuration and initial conditions of the test articles, the test facilities and instrumentation used, and the test results. Appendix 3.5.3.7, *Description of Thermal Model for HAC Conditions*, provides an overview of the test results, the rationale for selecting the worst-case damage scenario, and the details of the thermal modeling used to simulate the package conditions during the HAC fire event.

#### 3.4.1 Initial Conditions

The initial conditions assumed for the package prior to the HAC event are described below in terms of the modifications made to the NCT thermal model to simulate the assumed package conditions prior to and during the HAC event. These modifications are:

- Simulated the worst-case damage arising from the postulated HAC free and puncture drops as described in Appendix 3.5.3.7, *Description of Thermal Model for HAC Conditions*,
- Changed the package orientation from upright to horizontal to reflect the assumed position of the package following an HAC accident event,
- Increased the emissivity of all external surfaces to 0.9 and the solar absorptivity to 0.9 to account for possible oxidation and/or soot accumulation on the surfaces,
- Increased the emissivity of the interior surface of the thermal shield from 0.4 to 0.6 to account for oxidization during the HAC event,
- Added heat transfer via radiation within the impact limiter enclosures with an emissivity of 0.95 to account for the potential loss of polyurethane foam from thermal decomposition,

- Assumed an initial temperature distribution equivalent to the package at steady-state conditions with a 100 °F ambient and no insolation. This assumption complies with the requirement of 10 CFR §71.73(b).

Following the free and puncture bar drop events, the BRR package is assumed come to rest in a horizontal position prior to the initiation of the fire event. The MURR basket and the fuel element are predicted to remain intact and experience no significant re-positioning as a result of the drop events. Since the package geometry is essentially axi-symmetrical, the thermal performance under HAC conditions is independent of the rotational orientation of the package.

### 3.4.2 Fire Test Conditions

The fire test conditions analyzed to address the 10 CFR §71.73(c) requirements are as follows:

- The initial ambient conditions are assumed to be 100 °F ambient with no insolation,
- At time = 0, a fully engulfing fire environment consisting of a 1,475 °F ambient with an effective emissivity of 1.0 is used to simulate the average flame temperature of the hydrocarbon fuel/air fire event. The assumption of an average flame emissivity coefficient of 1.0 conservatively bounds the minimum 0.9 flame emissivity specified by 10 CFR Part §71.73(c)(4).
- The convection heat transfer coefficients between the package and the ambient during the 30-minute fire event are based on an average gas velocity of 10 m/sec [29]. Following the 30-minute fire event the convection coefficients are based on still air.
- The ambient condition of 100 °F with insolation is assumed following the 30-minute fire event. A solar absorptivity of 0.9 is assumed for the exterior surfaces to account for potential soot accumulation on the package surfaces.

The transient analysis is continued for 4.5 hours after the end of the 30-minute fire to capture the peak package temperatures.

### 3.4.3 Maximum Temperatures and Pressure

#### 3.4.3.1 Maximum HAC Temperatures

Table 3.4-1 presents the predicted peak temperature for the BRR package with the MURR fuel payload under HAC conditions. Given that the MURR payload dissipates a significantly higher decay heat than the other potential payloads, the presented temperatures are bounding for all payloads. As seen from the table, significant thermal margins exist for all components. The closure and vent/drain port seals remain below their maximum allowable temperature due to a combination of their location, the amount of foam remaining, even after the conservative damage assumptions, and the surrounding thermal mass of the upper and lower end structures. For example, the peak temperature predicted for the vent/drain port seals arises for the improbable condition of the worst case damage described in Appendix 3.5.3.7, *Description of Thermal Model for HAC Conditions*, for the impact limiter aligning directly opposite of the drain port location. Without that conservative assumption, the peak vent/drain port temperature would be approximately 300 °F.

Figure 3.4-1 illustrates the temperature profile within the BRR package at the end of the 30-minute hypothetical fire. The illustrated profile demonstrates the thermal protection afforded to the package by the thermal shield and the polyurethane filled impact limiters since the high temperatures are limited to narrow regions on the exterior of the packaging. This thermal protection occurs despite the conservative level of damage assumed for the impact limiters.

Figure 3.4-2 and Figure 3.4-3 illustrate the temperature response profiles for selected package components. The relatively low temperature rise seen for the fuel elements and the fuel basket over the HAC event further demonstrates the thermal protection afforded by the BRR package design.

### 3.4.3.2 Maximum HAC Pressures

The peak cask cavity pressure under HAC conditions is conservatively estimated in the same manner as for NCT conditions (i.e., the bulk average cavity gas temperature is assumed to be equal to the mean of the average inner shell temperature and the average fuel basket temperature). The potential pressurization of the cask cavity due to failed cladding on the uranium-aluminide and uranium-zirconium hydride based fuel elements is ignored for this safety evaluation since the release of fission generated gases from these fuel types is diffusion-limited as opposed to the direct release mechanism for commercial spent nuclear fuel. At the conditions seen within the BRR package, the pressurization of the cask cavity due to gaseous release from breached fuel elements will be insignificant [30, 31] and is ignored for this safety evaluation.

Under the HAC condition with the MURR fuel payload, the peak bulk average gas temperature achieved during the HAC transient is 388 °F. Based on an assumed backfill gas temperature of 70 °F, the predicted maximum pressure within the cask cavity is computed via:

$$\text{Cavity Pressure} = 14.7 \text{ psia} \frac{(388^\circ \text{F} + 460^\circ \text{F})}{(70^\circ \text{F} + 460^\circ \text{F})} - 14.7 \text{ psia}$$

$$\text{Cavity Pressure} = 8.8 \text{ psig}$$

Given the significantly greater decay heat of the MURR fuel element payload, the computed peak HAC pressure will bound those achieved for the MITR-II, ATR, and TRIGA baskets.

### 3.4.4 Maximum Thermal Stresses

The maximum thermal stresses under the HAC condition are addressed in Section 2.7.4, *Thermal*.

Table 3.4-1 – HAC Temperatures

Component	Temperature (°F) <sup>①</sup>			
	End of Fire	Peak	Post-fire Steady State	Max. Allowable
MURR Fuel Plate	344	451	326	1,100
MURR Side Plate	341	449	324	1,100
MURR Fuel Basket	326	437	310	800
Inner Shell	301	393	211	800
Lead	471	482	207	620
Outer Shell	704	704	200	2,700
Thermal Shield	1,256	1,256	180	2,700
Lower End Structure	318	335	182	800
Upper End Structure	485	485	198	800
Shield Plug	234	317	201	620 <sup>②</sup>
Cask Lid	215	306	196	800
Closure/Vent Port Seals	212	306	196	400
Drain Port Seal	365	373	195	400
Upper Impact Limiter				
- Max. Foam	-	-	-	N/A <sup>③</sup>
- Avg. Foam	-	-	-	N/A <sup>③</sup>
- Shell	1,475	1,475	195	2,700 <sup>③</sup>
Lower Impact Limiter				
- Max. Foam	-	-	-	N/A <sup>③</sup>
- Avg. Foam	-	-	-	N/A <sup>③</sup>
- Shell	1,475	1,475	190	2,700 <sup>③</sup>
Cask Cavity Bulk Gas	305	388	257	N/A

Notes: ① Results assume a payload of eight (8) MURR fuel elements dissipating 158 W each and helium as the backfill gas.

② Temperature criterion based on melting point of the enclosed lead shielding.

③ Temperature criterion based on melting point for the shell. No criteria for the polyurethane foam since its thermal decomposition serves as its principal means of providing thermal protection during the HAC event.

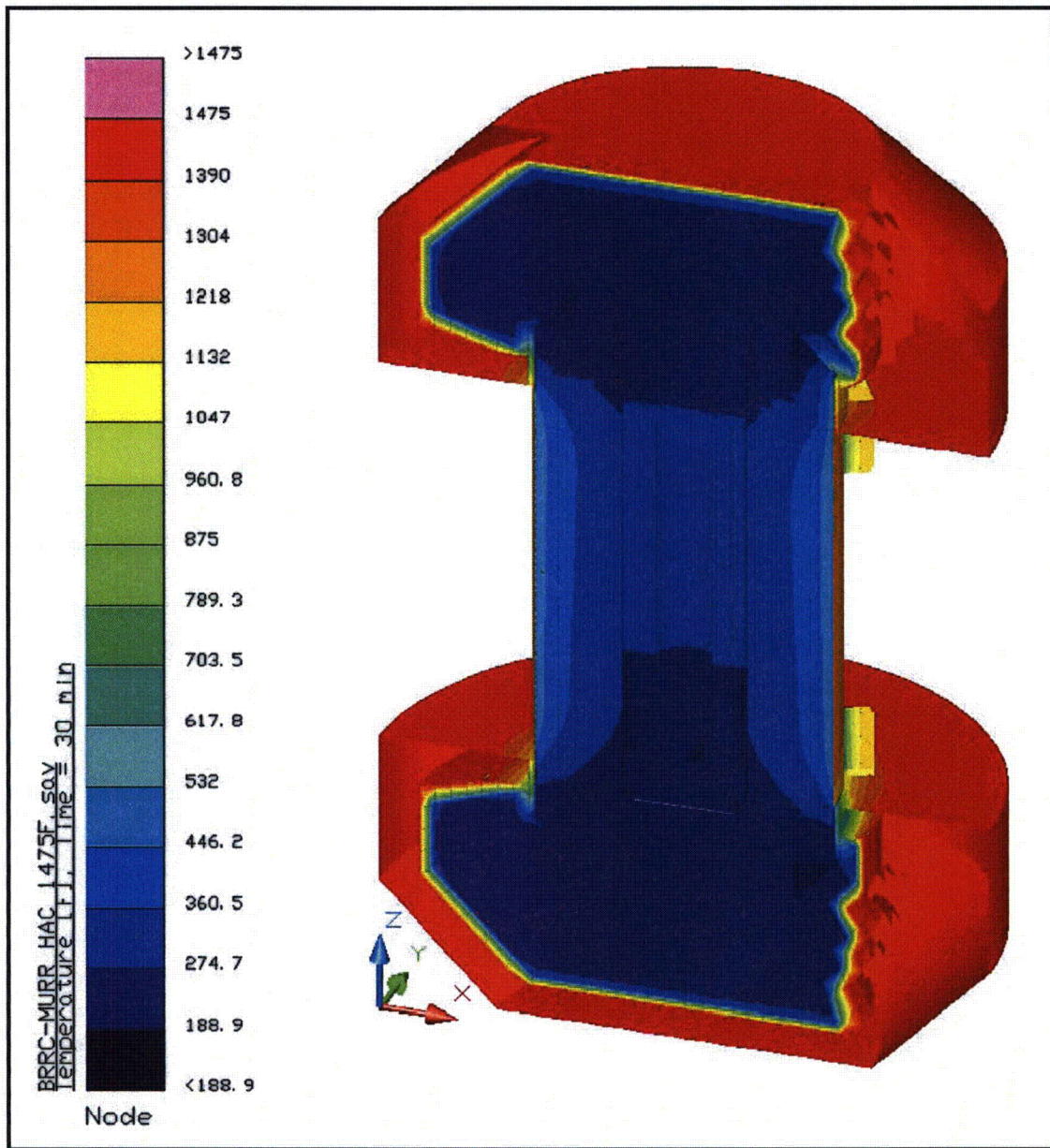


Figure 3.4-1 – BRR Package HAC Temperature Distribution at End of 30 Minute Fire

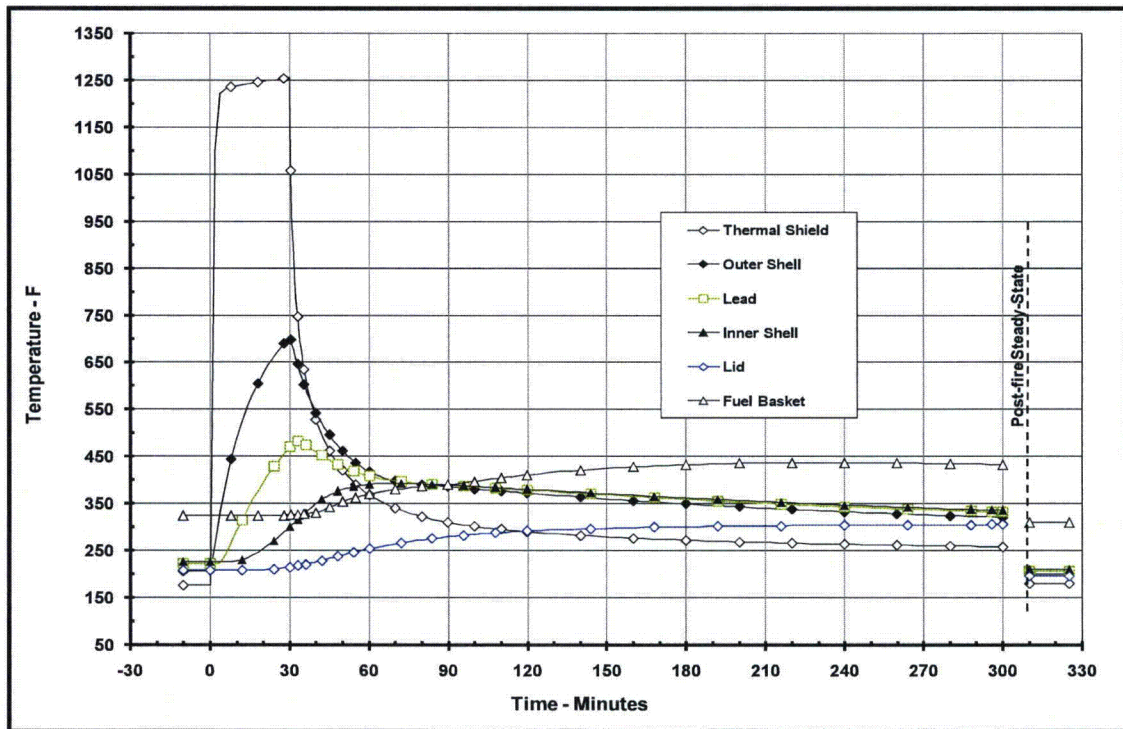


Figure 3.4-2 –Thermal Response to HAC Event, Package Components

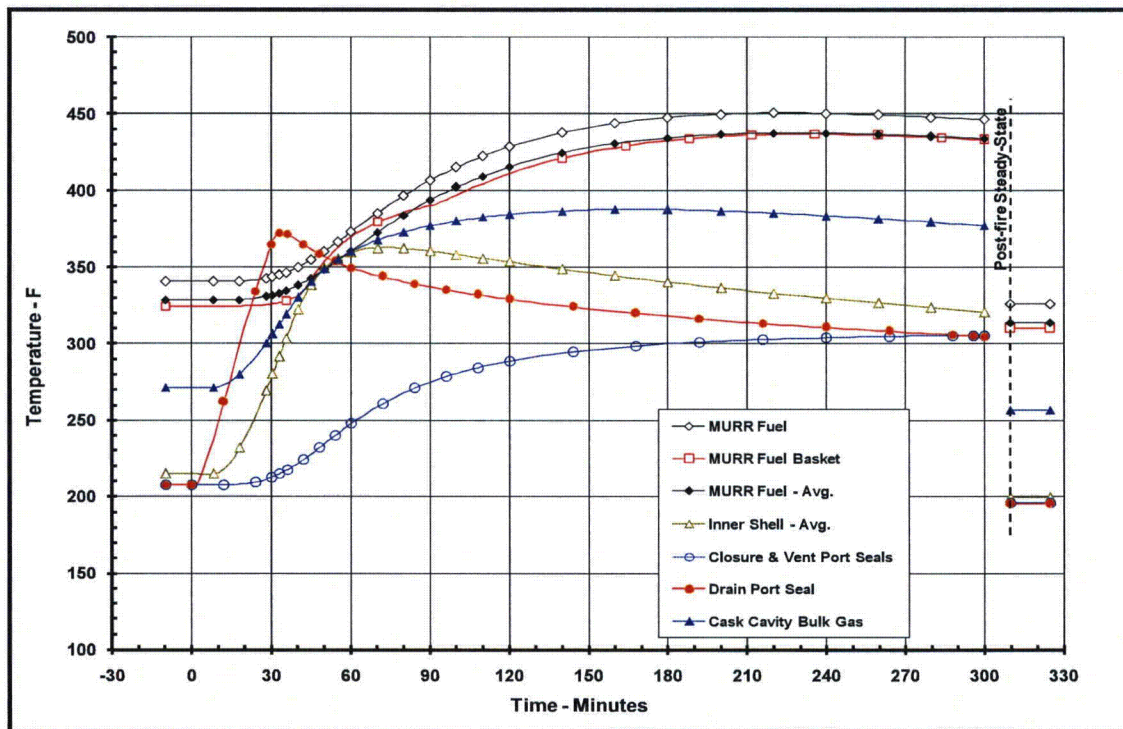


Figure 3.4-3 – Thermal Response to HAC Event, Payload, Seals, and Bulk Gas

19. Rohsenow, Hartnett, and Choi, Handbook of Heat Transfer, 3rd edition, McGraw-Hill, 1998.
20. Rainier Rubber Company, Seattle, WA, [www.rainierrubber.com](http://www.rainierrubber.com).
21. *Parker O-Ring Material Offering Guide*, ORD 5712, August 2002, [www.parkerorings.com](http://www.parkerorings.com).
22. Thermal Desktop<sup>®</sup>, Version 5.1, Cullimore & Ring Technologies, Inc., Littleton, CO, 2007.
23. SINDA/FLUINT, *Systems Improved Numerical Differencing Analyzer and Fluid Integrator*, Version 5.1, Cullimore & Ring Technologies, Inc., Littleton, CO, 2007.
24. AFS Report TR-VV-06-001, Rev. 0, *Thermal Desktop<sup>®</sup> and SINDA/FLUINT Testing and Acceptance Report*, Version 5.1, Areva Federal Services, LLC, 2008.
25. Kreith, Frank, Principles of Heat Transfer, 3rd edition, Harper & Row, 1973.
26. Guyer, Eric, Handbook of Applied Thermal Design, McGraw-Hill, Inc., 1989.
27. Williamson, C., and Iams, Z., *Thermal Assault and Polyurethane Foam - Evaluating Protective Mechanisms for Transport Containers*, General Plastics Manufacturing Company, Tacoma, WA, Waste Management '05 Symposium, Tucson, AZ, 2005.
28. Williamson, C., and Iams, Z., *Thermal Assault and Polyurethane Foam - Evaluating Protective Mechanisms*, General Plastics Manufacturing Company, Tacoma, WA, presented at PATRAM International Symposium, Berlin, Germany, 2004.
29. Schneider, M.E and Kent, L.A., *Measurements of Gas Velocities and Temperatures in a Large Open Pool Fire*, Heat and Mass Transfer in Fire - HTD Vol. 73, 1987, ASME, New York, NY.
30. Vinson, D., Sindelar, R., and Iyer, N., *Containment Evaluation of Breached AL-SNF For Cask Transport*, Savannah River National Laboratory - Materials Science & Technology, Aiken, SC 29808.
31. TRIGA<sup>®</sup> Fuel Description, General Atomics website, <http://triga.ga.com>.
32. Roth A, Vacuum Technology, 2nd Edition, Elsevier Science, 1982.
33. Lide, D., Handbook of Chemistry and Physics, 83rd Edition, The Chemical Rubber Co., 2002-2003.
34. Peacock Jr., H. B., et. al., *Evaluation of Corrosion of Aluminum Based Reactor Fuel Cladding Materials During Dry Storage*, WSRC-TR-95-0345, Westinghouse Savannah River Company.
35. Lam, P, Sindelar, R, and Barrett, K., *Corrosion of Aluminum-Uranium Alloys in Water Vapor at 200°C*, WSRC-MS-98-00858, Westinghouse Savannah River Company.



It should be noted that the NCT thermal model described below is based on an earlier design that used 6 instead of the current 8 attachment lugs per limiter, lug plates that are 0.38-inches thick by 2.75-inches wide vs. the current 0.5-inches thick by 3.63-inches wide, and a 0.25-inch vs. 0.125-inch radial gap between the limiter and the cask shell. Since these variations from the current design result in a lower surface area for heat dissipation to the ambient, the predicted NCT temperatures will be slightly higher than those expected for the current design. Because of this conservatism, the results are valid for the safety evaluations under NCT conditions. The design variations are incorporated for the HAC evaluations.

Figure 3.5-1 to Figure 3.5-5 illustrates 'solid' views of the BRR packaging thermal model. The model is composed of solid and plate type elements representing the various packaging components. Thermal communication between the various components is via conduction, radiation, and surface-to-surface contact. A total of approximately 20,500 nodes, 110 planar elements, and 4,900 solid elements are used to simulate the modeled components. Nearly 80 of the solid elements are finite difference solids (i.e., FD solids), a Thermal Desktop<sup>®</sup> computer program feature that permits a group of solid elements to be represented by a single entity. As such, the number of individual solid 'bricks' utilized in the modeling is actually significantly larger than the 4,900 value indicated above. In addition, one boundary node is used to represent the ambient environment for convection purposes and two boundary nodes is used to represent the ambient temperature for the purpose of radiation heat transfer. The use of separate boundary nodes for radiation heat transfer allows the model to capture the effective emissivity of the ambient environment.

As seen from Figure 3.5-1, the modeling accurately captures the geometry of the various components of the packaging, including the impact limiters, the inner and outer shells, the upper and lower end structures, the closure lid and shield plug, and lead sections. Also captured, but not easily seen in the figure due to the scale of the figures, is the thermal shield and the impact limiter attachment lugs. The minimal spatial resolution provided by the thermal modeling for the cask body components is approximately 1.75 inches in the radial direction, 2 inches in the axial direction, and every 10° in the circumferential direction. Greater spatial resolution (i.e., smaller radial and axial distances) is provided near the cask ends where larger thermal gradients are expected. A slightly lower spatial resolution is provided for the exterior portions of the impact limiters since the relatively low thermal conductivity of the polyurethane foam will yield correspondingly low heat flows.

Figure 3.5-2 illustrates the thermal modeling used for the various stainless steel components of the BRR cask body, while Figure 3.5-3 illustrates the thermal modeling of the lead structures within the cask body. The figures demonstrate that the geometry of the cask components is accurately captured by the thermal modeling.

Figure 3.5-4 illustrates the modeling used for the shell of the shield plug. While the height, radius, and shell thickness of the shield plug are accurately captured, the diagonal pipe and 4° taper are not included for modeling simplicity and because these details have no significant effect on the thermal performance of the packaging. Although the lead sheets used to fill the shield plug cavity are to be oversized and then hammered into place, the thermal modeling conservatively assumes a small (i.e., 0.0625-inch) uniform gap exists between the lead sheets and the shield plug shell.

The thermal modeling of the impact limiters, as illustrated in Figure 3.5-5, accurately captures the compound shape of the limiter's inner shell and the placement of the attachment lugs. Since the fabrication tolerance of the polyurethane foam used to fill the impact limiters can yield foam densities that are  $\pm 15\%$  of the targeted  $9 \text{ lb}_m/\text{ft}^3$  (pcf) foam density and since the foam's conductivity is a function of its density, the thermal modeling conservatively assumes a low tolerance foam density (i.e., 9 pcf less  $15\% \approx 7.65$  pcf) for NCT evaluations and a high tolerance foam density (i.e., 9 pcf plus  $15\% \approx 10.35$  pcf) for HAC evaluations.

### 3.5.3.2 Description of MURR Fuel and Basket Thermal Model

Figure 3.5-6 illustrates the thermal modeling of the MURR fuel basket and fuel element used for this evaluation. Approximately 2,600 nodes, 160 planar elements, and 1,000 solid elements are used to simulate the modeled components of the fuel basket, while approximately 3,300 nodes, 340 planar elements, and 550 solid elements are used to simulate the modeled components of each MURR fuel element.

The fuel basket modeling captures the inner and outer shells, the plates used to section off or divide the basket into compartments to house the individual fuel elements, and the base. While the inner shell and the divider plates are simulated using solid elements, the 0.25-inch thick outer shell and the base plates are represented by planar elements since the temperature difference though their thickness will be small. All of the basket components are assumed to be Type 304 stainless steel. The fuel elements are assumed to be essentially centered within in each compartment with the heat transfer between the fuel elements and the basket assumed to be via conduction and radiation across the separation gap and via contact with the plate supporting the fuel elements.

The fuel element simulation includes separate representation of the twenty-four (24) curved composite fuel plates, the side plates, and the upper and lower end box castings. Heat transfer between the individual fuel plates is simulated via conduction and radiation, while the heat transfer between the fuel plates and the side plates is via radiation and conduction through the crimped edges. The size, curvature, distance between the fuel plates, and the composite thermal properties of the plates are based on the information presented in Appendix 3.5.3.9, *Determination of Composite Thermal Properties for Fuel Plates*. The decay heat loading for the fuel elements is applied as a surface heat flux over the active fuel length of the plates.

Heat transfer between the fuel basket and the BRR packaging is assumed to be via conduction and radiation across the assumed uniform gap between the basket and the inner shell of the packaging. Direct contact is assumed between the base of the fuel basket and the base of the cask cavity. Because of the combination of decay heat and the criterion to limit the maximum fuel plate temperature to  $400 \text{ }^\circ\text{F}$  or less (see Section 3.2.2), the BRR cask cavity is to be filled with helium gas at a pressure of one atmosphere following the draining and drying process.

### 3.5.3.3 Description of MITR-II Fuel and Basket Thermal Model

Figure 3.5-7 illustrates the thermal modeling of the MITR-II fuel basket and fuel element used for this evaluation, while Figure 3.5-8 illustrates the solids modeling used to represent the void spaces between the fuel tubes. Approximately 2,650 nodes, 170 planar elements, and 400 solid elements are used to simulate the modeled components of the fuel basket, while approximately 1,480

nodes, 75 planar elements, and 230 solid elements are used to simulate the modeled components of each MITR-II fuel element.

The fuel basket modeling captures the thin shell tubes used to house the fuel elements, the stiffening ribs/plates, and the base shell. All of the basket components are assumed to be Type 304 stainless steel. The fuel elements are assumed to be essentially centered within in each compartment with the heat transfer between the fuel elements and the basket assumed to be via conduction and radiation across the separation gap and via contact with the plate supporting the fuel elements.

The fuel element simulation includes separate representation of the fifteen (15) composite fuel plates, the side plates, and the upper and lower end box castings. Heat transfer between the individual fuel plates is simulated via conduction and radiation, while the heat transfer between the fuel plates and the side plates is via radiation and conduction through the crimped edges. The size, distance between the fuel plates, and the composite thermal properties of the plates are based on the information presented in Appendix 3.5.3.9, *Determination of Composite Thermal Properties for Fuel Plates*. The decay heat loading for the fuel elements is applied as a uniform surface heat flux over the active fuel length of the plates.

Heat transfer between the fuel basket and the BRR packaging is assumed to be via a combination of conduction and radiation across the gaps between the various basket surfaces and the inner shell of the packaging. The cask cavity is to be filled with helium gas to limit the maximum fuel plate temperature to 400 °F or less (see Section 3.2.2).

#### 3.5.3.4 Description of ATR Fuel and Basket Thermal Model

Figure 3.5-9 illustrates the thermal modeling of the ATR fuel basket and fuel element used for this evaluation. Approximately 3,000 nodes, 50 planar elements, and 90 FD solid elements are used to simulate the modeled components of the fuel basket, while approximately 3,300 nodes, 95 planar elements, and 325 solid elements are used to simulate the modeled components of each ATR fuel element. As previously explained, an FD solid is a Thermal Desktop<sup>®</sup> computer program feature that permits a group of solid elements to be represented by a single entity. As such, the number of individual solid 'bricks' utilized in the modeling of the ATR fuel basket is actually significantly larger than 90.

The fuel basket modeling captures the inner and outer shells, the plates used to section off or divide the basket into compartments to house the individual fuel elements, the stiffening ribs, and the base. All of the basket components are assumed to be Type 304 stainless steel. The fuel elements are assumed to be essentially centered within in each compartment with the heat transfer between the fuel elements and the basket assumed to be via conduction and radiation across the separation gap.

The fuel element simulation includes separate representation of the nineteen (19) curved composite fuel plates and the side plates (including the cutouts). The upper and lower end boxes are to be removed prior to loading of the fuel assemblies within the basket. Heat transfer between the individual fuel plates is simulated via conduction and radiation, while the heat transfer between the fuel plates and the side plates is via radiation and conduction through the crimped edges. The size, curvature, distance between the fuel plates, and the composite thermal properties of the plates are based on the information presented in Appendix 3.5.3.9,

*Determination of Composite Thermal Properties for Fuel Plates* The decay heat loading for the fuel elements is applied as a uniform surface heat flux over the active fuel length of the plates.

Heat transfer between the fuel basket and the BRR packaging is assumed to be via a combination of conduction and radiation across the gaps between the various basket surfaces and the inner shell of the packaging. The thermal evaluations assume the cask cavity is filled with helium gas.

### 3.5.3.5 Description of TRIGA Fuel and Basket Thermal Model

Figure 3.5-10 illustrates the thermal modeling of the TRIGA fuel basket and fuel element used for this evaluation, while Figure 3.5-11 illustrates the solids modeling used to represent the void spaces between the fuel tubes. Approximately 7,500 nodes, 60 planar elements, and 1,000 solid elements are used to simulate the modeled components of the fuel basket, while approximately 1,030 nodes and 7 FD solid elements are used to simulate the modeled components of each TRIGA fuel element. As previously explained, an FD solid is a Thermal Desktop<sup>®</sup> computer program feature that permits a group of solid elements to be represented by a single entity. As such, the number of individual solid 'bricks' utilized in the modeling of each TRIGA fuel element is actually significantly larger than 7.

The fuel basket modeling captures the individual tubes used to house each fuel element, stiffening ribs, and the spacers used to position the shorter length fuel elements within the basket. All of the basket components are assumed to be fabricated of Type 304 stainless steel. The fuel elements are assumed to be essentially centered within in each compartment with the heat transfer between the fuel elements and the basket assumed to be via conduction and radiation across the separation gap and via contact with the plate supporting the fuel elements.

The fuel element simulation includes separate representation of the uranium zirconium hydride metal section, the graphite section, and the upper and lower end fittings. Since the temperature difference across the fuel cladding is small for the decay heats involved, the cladding is not modeled separately. The TRIGA fuel has two design active fuel lengths; 14 and 15 inches. The decay heat loading for the fuel elements is applied as a uniform volumetric heat flux over the active fuel length. The modeling assumes the shorter length to conservatively bound the maximum volumetric heat generation.

Heat transfer between the fuel basket and the BRR packaging is assumed to be via a combination of conduction and radiation across the gaps between the various basket surfaces and the inner shell of the packaging. The thermal evaluations assume the cask cavity is filled with helium.

### 3.5.3.6 Insolation Loads

The insolation loading on the BRR package is based on the 10CFR71.71(c)(1) specified insolation values over a 24-hour period. Since the BRR packaging is characterized by thermally massive shells and large foam filled impact limiters, the interior temperatures of the packaging will be effectively 'decoupled' from the diurnal changes in insolation loading. As such, a steady-state thermal model based on the application of the 10CFR71.71(c)(1) specified insolation values averaged over 24 hours is used to evaluate the design basis package temperatures under NCT conditions.

Subsequent to the drop test, the impact limiter design was modified to improve its performance. These modifications increased the number of attachment lugs from 6 to 8 per limiter, increased the size and thickness of each lug from 0.38-inches thick by 2.75-inches wide to 0.5-inches thick by 3.63-inches wide, increased the size of the attachment pins, reduced the gap between the cask and the impact limiter inner shell from 0.25 to 0.125 inches, and a re-design of the limiter joint that cracked under the side/slap down drop (see Item 1 above).

Besides scaling the noted crush dimensions to the full scale design, the projected damage also needs to reflect the effect of temperature on the polyurethane foam's structural properties since the drop test was conducted under cold conditions and the worst case crush will arise under warm conditions. Figure 3.5-12 depicts the predicted crush depths under hot conditions for the vertical end, C.G. over corner, and side/slap down drop orientations based on an evaluation presented in Section 2.12.5, *Impact Limiter Performance Evaluation*. As seen from the figure, the side/slap down drop orientation is predicted to result in both the greatest crush depth and the closest approach to the inner shell of the limiter. Per Appendix 3.5.4, *'Last-A-Foam' Response under HAC Conditions*, approximately 3.5 to 3.8 inches of the nominally 9 pcf polyurethane foam will decompose during a 30 minute HAC fire event. This foam loss (or recession depth) will be even less for foam in the vicinity of crush damage since its effective density will have increased as a result of the crush damage. Any foam depths greater than 4 inches remaining after the HAC drop events will result in the underlying temperatures rising only marginally during the HAC fire event. Examination of Figure 3.5-12 demonstrates that the vertical end drop and C.G. over corner drops will leave more than 4 inches of foam everywhere, even without credit for increased foam density due to crush. As such, the side/slap down drop event is selected as the controlling scenario for impact limiter damage for the HAC evaluations.

The controlling puncture bar damage is determined from the half-scale drop results described in Section 2.12.3, *Certification Test Results*. Since the polyurethane foam forms an intumescent char that swells and tends to fill voids or gaps created by the puncture bar damage, the level of damage incurred by direct attack to the impact limiter's exterior shell would be thermally insignificant. An untested puncture bar scenario consisting of an impact to the thermal shield of the cask is also considered. This type of impact can be expected to cause a local depression in the thermal shield and potentially a small tear. However, overall, the thermal shield would retain its functionality with the region of elevated temperatures being localized to the size of the puncture bar and similar in temperature level to that seen at the impact limiter attachment lug locations. Therefore, the controlling puncture bar damage is assumed to be an attack on the impact limiter skin joint that tears a flap type opening in the limiter skin (see Item 1 above). While the re-design of the impact limiters following the drop tests is expected to eliminate this type of damage, it is assumed for the HAC evaluation to conservatively bound all other potential puncture bar damage scenarios.

Based on the above observations and the general assumptions for the package condition for the HAC evaluations, the NCT thermal model described above was modified for the HAC evaluations via the following steps:

- 1) Assume the package has been ejected from its support stand and is lying on its side. As such, the convective heat transfer from the package's exterior surfaces is based on a horizontal orientation. In addition, the adiabatic boundary condition assumed for selected surfaces of the lower impact limiter under NCT conditions are switched to active heat transfer surfaces.
- 2) The surface emissivity for all exterior surfaces is assumed to be 0.9 to account for potential oxidation and/or soot accumulation. The emissivity of all inside surfaces of the impact limiter exposed as the result of foam decomposition is assumed to be 0.95 to account for adherence of foam char.
- 3) The small, uniform gap conservatively assumed between the lead and the outer shell under NCT conditions is eliminated to maximize the heat flow into package.
- 4) Thermal conductance via the stand-off strips under the thermal shield is assumed for the HAC condition. Thermal credit for the stand-off strips was conservatively ignored for the NCT evaluations.
- 5) The number and size of the impact limiter attachments are increased for the HAC evaluation to reflect the re-design of the impact limiter following the drop testing. The NCT evaluations ignored this change since neglecting the added surface area yields conservative results.
- 6) A minimum of 3.8 inches of foam is removed from around the perimeter of the impact limiters at the start of the HAC evaluation. This change conservatively bounds the impact of the gradual decomposition of the foam over the 30 minute fire event. The conductivity of the remaining foam is set to that associated with foam fabricated at the high end of the density tolerance range (i.e., 9 pcf + 15%) in order to conservatively bound the heat transfer into the package.
- 7) Simulate the sideways crushing of the upper and lower impact limiters under hot drop conditions. This consisted of removing approximately 15.8 inches from one side of the impact limiters.
- 8) Simulate the conservative assumption that a puncture bar attack tears a flap in the upper impact limiter. This consisted of removing a total of 6.1 inches of foam over a 60° segment of the impact limiter to conservatively capture the additional recession depth over 3.8 inches that may occur due to the direct exposure of the foam surfaces to the flame (see Appendix 3.5.4, *'Last-A-Foam' Response under HAC Conditions*). Added radiation and convection conductors to the exposed region of the impact limiter's inner shell to reflect the conservative assumption that a flap opening has occurred in the upper impact limiter.
- 9) Simulated the possible shifting of the impact limiter by replacing the 0.125 inch nominal gap between the inner shell of the limiters and the cask shell with a direct contact conductance over an approximate 1 inch x 7.2 inch area (i.e., the modeled height of the cylindrical portion of the limiter's inner shell). The contact is placed in the center of the side drop foam crush damage and conservatively bounds the line-contact expected between two cylindrical bodies with no deformation.

Figure 3.5-13 illustrates the revised thermal model of the impact limiters used for the HAC evaluations. All other aspects of the BRR packaging remain the same as used for the NCT thermal evaluations.

**3.5.3.8 Convection Coefficient Calculation**

The BRR package thermal model uses semi-empirical relationships to determine the level of convection heat transfer from the exterior package surfaces under both the regulatory NCT and HAC conditions. The convective heat transfer coefficient,  $h_c$ , has a form of:

$$h_c = Nu \frac{k}{L}$$

where  $k$  is the thermal conductivity of the gas at the mean film temperature and  $L$  is the characteristic length of the vertical or horizontal surface. The convection coefficient is correlated via semi-empirical relationships against the local Rayleigh number and the characteristic length. The Rayleigh number is defined as:

where 
$$Ra_L = \frac{\rho^2 g_c \beta L^3 \Delta T}{\mu^2} \times Pr$$

- $g_c$  = gravitational acceleration, 32.174 ft/s<sup>2</sup>
- $\Delta T$  = temperature difference, °F
- $\mu$  = dynamic viscosity, lb<sub>m</sub>/ft-s
- $L$  = characteristic length, ft
- $c_p$  = specific heat, Btu/ lb<sub>m</sub> -°F
- $\beta$  = coefficient of thermal expansion, °R<sup>-1</sup>
- $\rho$  = density of air at the film temperature, lb<sub>m</sub>/ft<sup>3</sup>
- Pr = Prandtl number =  $(c_p \mu) / k$
- $k$  = thermal conductivity at film temp., Btu/ft-hr-°F
- $Ra_L$  = Rayleigh #, based on length 'L'

Note that  $k$ ,  $c_p$ , and  $\mu$  are each a function of air temperature as taken from Table 3.2-3. Values for  $\rho$  are computed using the ideal gas law,  $\beta$  for an ideal gas is simply the inverse of the absolute temperature of the gas, and Pr is computed using the values for  $k$ ,  $c_p$ , and  $\mu$  from Table 3.2-3. Unit conversion factors are used as required to reconcile the units for the various properties used.

The natural convection from a discrete vertical surface is computed using Equations 4-13, 4-24, 4-31, and 4-33 of reference [19], which is applicable over the range  $1 < \text{Rayleigh number (Ra)} < 10^{12}$ :

$$Nu^T = \bar{C}_L Ra^{1/4}$$

$$\bar{C}_L = \frac{0.671}{\left(1 + (0.492/Pr)^{9/16}\right)^{4/9}}$$

$$Nu_L = \frac{2.0}{\ln(1 + 2.0/Nu^T)}$$

$$Nu_t = C_t^V Ra^{1/3} / \left(1 + 1.4 \times 10^9 Pr/Ra\right)$$

$$C_t^v = \frac{0.13 \text{Pr}^{0.22}}{(1 + 0.61 \text{Pr}^{0.81})^{0.42}}$$

$$\text{Nu} = \frac{h_c L}{k} = [(\text{Nu}_L)^6 + (\text{Nu}_t)^6]^{1/6}$$

The natural convection from a vertical cylindrical surface is computed by applying a correction factor to the laminar Nusselt number ( $\text{Nu}_L$ ) determined using the same methodology and  $\text{Nu}_t$  for a vertical plate (see above). The characteristic dimension,  $L$ , is the height of the vertical cylinder and  $D$  is the cylinder's diameter. The correction factor as defined by Equations 4-44 of reference [19] is:

$$\text{Nu}_{L\text{-Cylinder}} = \frac{\delta}{\ln(1 + \delta)} \text{Nu}_{L\text{-Plate}}$$

$$\delta = \frac{1.8 \times L/D}{\text{Nu}_{\text{Plate}}^T}$$

$$\text{Nu}_{\text{Vert. Cylinder}} = \frac{h_c L}{k} = [(\text{Nu}_{L\text{-Cylinder}})^6 + (\text{Nu}_{t\text{-Plate}})^6]^{1/6}$$

Natural convection from horizontal surfaces is computed from Equations 4-13, 4-25, 4-39, and 4-40 of reference [19], where the characteristic dimension ( $L$ ) is equal to the plate surface area divided by the plate perimeter. For a heated surface facing upwards or a cooled surface facing downwards and  $\text{Ra} > 1$ :

$$\text{Nu} = \frac{h_c L}{k} = [(\text{Nu}_L)^{10} + (\text{Nu}_t)^{10}]^{1/10}$$

$$\text{Nu}_L = \frac{1.4}{\ln(1 + 1.4 / (0.835 \times \bar{C}_L \text{Ra}^{1/4}))}$$

$$\bar{C}_L = \frac{0.671}{(1 + (0.492/\text{Pr})^{9/16})^{4/9}}$$

$$\text{Nu}_t = 0.14 \times \left( \frac{1 + 0.0107 \times \text{Pr}}{1 + 0.01 \times \text{Pr}} \right) \times \text{Ra}^{1/3}$$

For a heated surface facing downwards or a cooled surface facing upwards and  $10^3 < \text{Ra} < 10^{10}$ , the correlation is as follows:

$$\text{Nu} = \text{Nu}_L = \frac{2.5}{\ln(1 + 2.5/\text{Nu}^T)}$$

$$\text{Nu}^T = \frac{0.527}{(1 + (1.9/\text{Pr})^{9/10})^{2/9}} \text{Ra}^{1/5}$$



Calculation of the convection coefficient from a horizontal cylindrical surface is computed using Equation 3-43, Chapter 1, from [26], where the characteristic length,  $D$ , is the outer diameter of the cylinder. This equation, applicable for  $10^{-5} < Ra < 10^{12}$ , is as follows:

$$Nu = \frac{h_c D}{k} = \left\{ 0.60 + \frac{0.387 Ra_D^{1/6}}{\left[ 1 + (0.559/Pr)^{9/16} \right]^{8/27}} \right\}^2$$

The forced convection coefficients applied during the HAC fire event are computed using the relationships in Table 6-5 of reference [25] for a flat surface, where the characteristic dimension ( $L$ ) is equal to the length along the surface and the free stream flow velocity is  $V$ . The heat transfer coefficient is computed based on the local Reynolds number, where the Reynolds number is defined as:

$$Re_L = \frac{V \times \rho \times L}{\mu}$$

$$\text{For } Re < 5 \times 10^5 \text{ and } Pr > 0.1: Nu = 0.664 \times Re_L^{0.5} \times Pr^{0.33}$$

$$\text{For } Re > 5 \times 10^5 \text{ and } Pr > 0.5: Nu = 0.036 \times Pr^{0.33} \times [Re_L^{0.8} - 23,200]$$

Given the turbulent nature of the 30-minute fire event, a characteristic length of 0.25 feet is used for all surfaces to define the probable limited distance for boundary growth. Figure 3.5-14 presents an illustration of the level of convective heat transfer coefficient predicted by the above equation during the HAC transient.

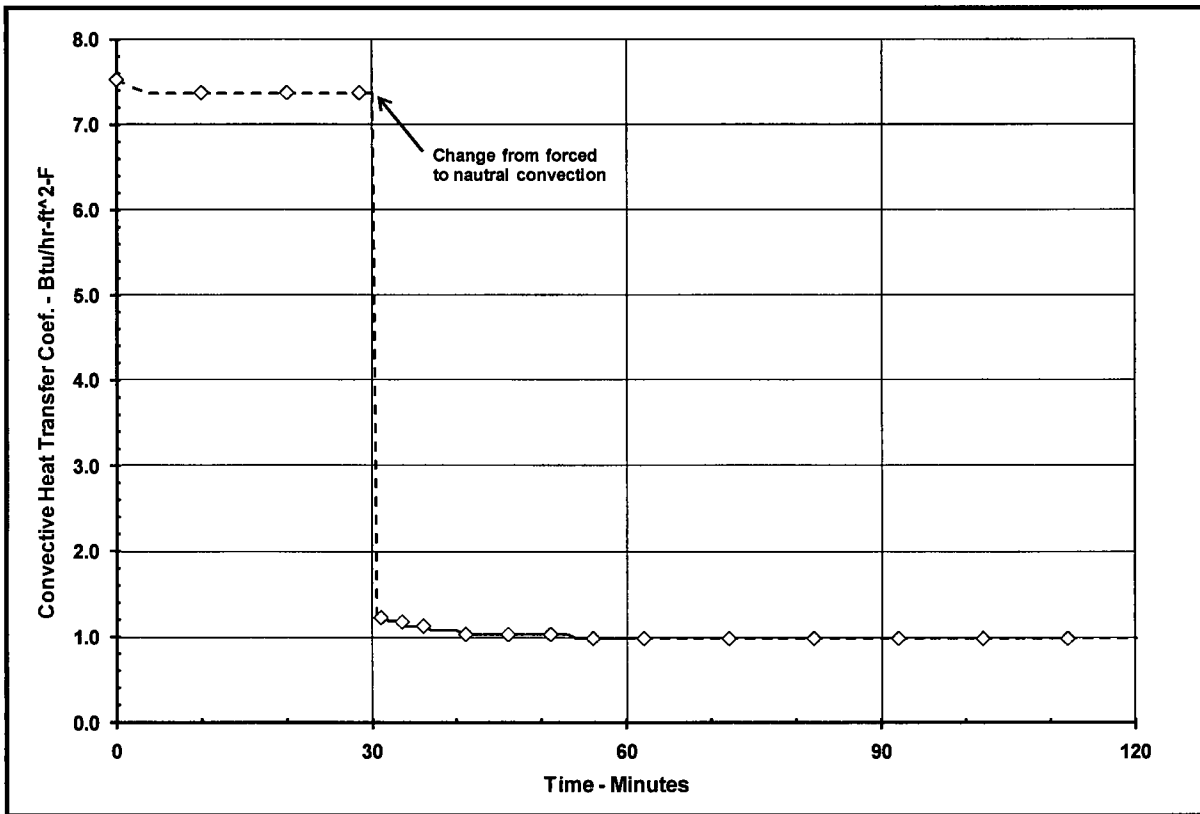
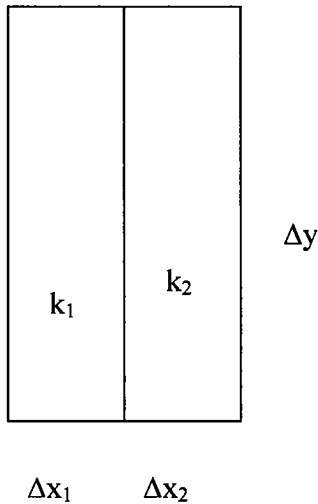


Figure 3.5-14 – Convection Coefficient Variation During HAC Transient

**3.5.3.9 Determination of Composite Thermal Properties for Fuel Plates**

**Thermal Properties for ATR Fuel Plates**

The ATR fuel plates are a composite material consisting of a fissile fuel matrix sandwiched within aluminum cladding. For the purposes of this calculation, the fuel composite is treated as a homogenous material with lumped thermal properties as defined below. This modeling approach is justified since the thermal gradient within the fuel element will be very low given that the un-irradiated fuel has essentially no decay heat.



Because of the thinness of the plates, the average conductivity is required only for the axial and circumferential direction. Conductivity through the plates is not required as this analysis assumes a zero temperature gradient in that direction. Mean density and specific heat values are also defined below.

Circumferential and Axial Conductivity

Ignoring the affect of curvature, the heat flow can be written as,

$$q = -\Delta x \Delta z \bar{k} \frac{\Delta T}{\Delta y} = -\Delta x_1 \Delta z k_1 \frac{\Delta T}{\Delta y} - \Delta x_2 \Delta z k_2 \frac{\Delta T}{\Delta y}$$

where  $\Delta x = \sum_i \Delta x_i$

From which,  $\bar{k} = \frac{\Delta x_1 k_1 + \Delta x_2 k_2}{\Delta x}$

Mean Density

The mean density of the fuel plates is computed from:

$$Mass = \Delta x \Delta y \Delta z \bar{\rho} = \Delta x_1 \Delta y \Delta z \rho_1 + \Delta x_2 \Delta y \Delta z \rho_2, \text{ from which } \bar{\rho} = \frac{\Delta x_1 \rho_1 + \Delta x_2 \rho_2}{\Delta x}$$

Mean Specific Heat

In the same manner used to define the mean density, the mean specific heat for the fuel plates is computed as;

$$\bar{\rho} \bar{c}_p \Delta x \Delta y \Delta z = \rho_1 c_{p_1} \Delta x_1 \Delta y \Delta z + \rho_2 c_{p_2} \Delta x_2 \Delta y \Delta z, \text{ from which, } \bar{c}_p = \frac{\rho_1 c_{p_1} \Delta x_1 + \rho_2 c_{p_2} \Delta x_2}{\bar{\rho} \Delta x}$$

The thermal properties for the individual plates making up the ATR fuel element are computed using the above approach and thermophysical [5] and geometric data [14] for the ATR fuel element.

Based on these data sources, the radius of the inner plate is 3.015 inches, while the radius of the outer plate is 5.44 inches. The gap between the plates is 0.078 inches. The thickness of the aluminum cladding is 0.015 inches.

While the thermal properties for the aluminum cladding and the fissile fuel matrix material will vary with temperature, for the purposes of this evaluation, fixed material properties are assumed in order to simplify the calculation. To provide conservatism for this modeling approach, conservatively low value is assumed for the specific heat for each component, while a conservatively high thermal conductivity value is used. This methodology will result in over-predicting the temperature rise within the composite material during the HAC fire event.

The thermal properties used in this calculation are:

- 1) Aluminum cladding thermal conductivity = 191 W/m-K, conservatively high value from [5], page 18
- 2) Fissile fuel matrix ( $UA_{fx}$ ) = 14.47 W/m-K, conservatively high based on equation 2.3 from [5], at 300K
- 3) Aluminum cladding density = 2702 kg/m<sup>3</sup>, from [5], page 16
- 4) Fissile fuel matrix ( $UA_{fx}$ ) density = 3680 kg/m<sup>3</sup>, from [5], Table 2.5, average density
- 5) Aluminum cladding specific heat = 1034 J/kg-K, from [5], Table 3.2, mean value at 600K
- 6) Fissile fuel matrix ( $UA_{fx}$ ) specific heat = 708 J/kg-K, from [5], Table 2.4, average value at 600K

Table 3.5-1 presents the composite thermal conductivity, specific heat, and density values for each of the nineteen (19) fuel plates making up the ATR fuel element. These composite values are based on the thermal property values given above and the geometry depicted in Figure 3.5-15.

### **Thermal Properties for MIT Fuel Plates**

Like the ATR fuel, the MIT fuel plates are a composite material consisting of a fissile fuel matrix sandwiched within an aluminum cladding. The thermal properties for the plates making up the MIT fuel element are computed using the same approach described above for the ATR fuel and the data contained in [5] and [13]. The plates have a thickness of 0.08 inches and a width of 2.526 inches. The nominal gap between the plates is 0.078 inches. Since the aluminum cladding contains 110 grooves on each side of the plate, the effective thickness of the cladding is reduced from 0.025 inches to 0.02 inches.

Table 3.5-2 presents the composite thermal conductivity, specific heat, and density values for the fifteen (15) fuel plates making up the MIT fuel element. These composite values are based on the thermal property values provided above for the ATR fuel element and the geometry described in Table 3.5-2 and depicted in Figure 3.5-16.

### **Thermal Properties for MURR Fuel Plates**

The MURR fuel plates are also a composite of a fissile fuel matrix sandwiched within an aluminum cladding. The thermal properties for the MURR fuel element are computed using the

same approach described above for the ATR fuel and the data contained in [5] and [12]. The inner plate has an inner radius of 2.77 inches and an arc length of 1.993 inches, while the outer plate has an inner radius of 5.76 inches and an arc length of 4.342 inches. The nominal gap between the plates is 0.08 inches. The thickness of the aluminum cladding is 0.01 inches.

Table 3.5-3 presents the composite thermal conductivity, specific heat, and density values for the twenty four (24) fuel plates making up the MURR fuel element. These composite values are based on the thermal property values provided above for the ATR fuel element and the geometry described in Table 3.5-3 and depicted in Figure 3.5-17.

### **Thermal Properties for TRIGA Fuel Element**

The cladding thickness for the TRIGA fuel is relatively thin and the fuel's thermal properties are dominated by the homogenous properties for the uranium-zirconium hydride fuel and the graphite materials. As such, composite properties are not required. Instead, the thermal properties listed in Table 3.2-2 for the uranium-zirconium hydride fuel and the graphite are used directly in the thermal model.

**Table 3.5-1 – Composite ATR Fuel Plate Thermal Properties**

Plate	Plate Thickness, in	UAlx Thickness, in	Axial & Circumferential Conductivity (W/m-K)	Inner radius, in	Outer radius, in	Mean radius, in	Mean density, kg/m <sup>3</sup>	Mean specific heat, J/(kg K)
1	0.08	0.05	80.7	3.015	3.095	3.055	3313.3	807.7
2	0.05	0.02	120.4	3.173	3.223	3.198	3093.2	878.9
3	0.05	0.02	120.4	3.301	3.351	3.326	3093.2	878.9
4	0.05	0.02	120.4	3.429	3.479	3.454	3093.2	878.9
5	0.05	0.02	120.4	3.557	3.607	3.582	3093.2	878.9
6	0.05	0.02	120.4	3.685	3.735	3.710	3093.2	878.9
7	0.05	0.02	120.4	3.813	3.863	3.838	3093.2	878.9
8	0.05	0.02	120.4	3.941	3.991	3.966	3093.2	878.9
9	0.05	0.02	120.4	4.069	4.119	4.094	3093.2	878.9
10	0.05	0.02	120.4	4.197	4.247	4.222	3093.2	878.9
11	0.05	0.02	120.4	4.325	4.375	4.350	3093.2	878.9
12	0.05	0.02	120.4	4.453	4.503	4.478	3093.2	878.9
13	0.05	0.02	120.4	4.581	4.631	4.606	3093.2	878.9
14	0.05	0.02	120.4	4.709	4.759	4.734	3093.2	878.9
15	0.05	0.02	120.4	4.837	4.887	4.862	3093.2	878.9
16	0.05	0.02	120.4	4.965	5.015	4.990	3093.2	878.9
17	0.05	0.02	120.4	5.093	5.143	5.118	3093.2	878.9
18	0.05	0.02	120.4	5.221	5.271	5.246	3093.2	878.9
19	0.1	0.07	67.4	5.349	5.449	5.399	3386.6	786.0

**Table 3.5-2 – Composite MIT Fuel Plate Thermal Properties**

Plate	Plate Thickness, in	UAlx Thickness, in	Axial and Circumferential Conductivity (W/m-K)	Plate Width, in	Mean density, kg/m <sup>3</sup>	Mean specific heat, J/(kg K)
1 to 15	0.08*	0.03	115.3	2.314	3121.1	869.3

\* - mean plate thickness estimated at 0.07 inches after allowance for ribbing

**Table 3.5-3 – Composite MURR Fuel Plate Thermal Properties**

Plate	Plate Thickness, in	UAix Thickness, in	Axial and Circumferential Conductivity (W/m-K)	Inner radius, in	Outer radius, in	Plate Arc Length, in	Mean density, kg/m <sup>3</sup>	Mean specific heat, J/(kg K)
1	0.05	0.03	85.1	2.77	2.82	1.993	3288.8	815.1
2	0.05	0.03	85.1	2.9	2.95	2.095	3288.8	815.1
3	0.05	0.03	85.1	3.03	3.08	2.197	3288.8	815.1
4	0.05	0.03	85.1	3.16	3.21	2.300	3288.8	815.1
5	0.05	0.03	85.1	3.29	3.34	2.402	3288.8	815.1
6	0.05	0.03	85.1	3.42	3.47	2.504	3288.8	815.1
7	0.05	0.03	85.1	3.55	3.6	2.606	3288.8	815.1
8	0.05	0.03	85.1	3.68	3.73	2.708	3288.8	815.1
9	0.05	0.03	85.1	3.81	3.86	2.810	3288.8	815.1
10	0.05	0.03	85.1	3.94	3.99	2.912	3288.8	815.1
11	0.05	0.03	85.1	4.07	4.12	3.014	3288.8	815.1
12	0.05	0.03	85.1	4.2	4.25	3.116	3288.8	815.1
13	0.05	0.03	85.1	4.33	4.38	3.218	3288.8	815.1
14	0.05	0.03	85.1	4.46	4.51	3.321	3288.8	815.1
15	0.05	0.03	85.1	4.59	4.64	3.423	3288.8	815.1
16	0.05	0.03	85.1	4.72	4.77	3.525	3288.8	815.1
17	0.05	0.03	85.1	4.85	4.9	3.627	3288.8	815.1
18	0.05	0.03	85.1	4.98	5.03	3.729	3288.8	815.1
19	0.05	0.03	85.1	5.11	5.16	3.831	3288.8	815.1
20	0.05	0.03	85.1	5.24	5.29	3.933	3288.8	815.1
21	0.05	0.03	85.1	5.37	5.42	4.035	3288.8	815.1
22	0.05	0.03	85.1	5.5	5.55	4.137	3288.8	815.1
23	0.05	0.03	85.1	5.63	5.68	4.239	3288.8	815.1
24	0.05	0.03	85.1	5.76	5.81	4.342	3288.8	815.1

Figure Withheld Under 10 CFR 2.390

**Figure 3.5-15 – ATR Fuel Element Cross Section**



Figure Withheld Under 10 CFR 2.390

**Figure 3.5-16 – MIT Fuel Element Cross Section**

Figure Withheld Under 10 CFR 2.390

**Figure 3.5-17 – MURR Fuel Element Cross Section**

### 3.5.4 'Last-A-Foam' Response under HAC Conditions

The General Plastics LAST-A-FOAM® FR-3700 rigid polyurethane foam [18] used in the impact limiters has been used for numerous transportation packages. The FR-3700 formulation is specially designed to allow predictable impact-absorption performance under dynamic loading, while also providing a significant level of thermal protection under the HAC conditions. Upon exposure to fire temperatures, this proprietary foam decomposes into an intumescent char that swells and tends to fill voids or gaps created by free drop or puncture bar damage. This thermal decomposition absorbs a significant amount of the heat transferred into the foam, which is then expelled from the impact limiters as a high temperature gas. Because the char has no appreciable structural capacity and will not develop unless there is space available, the char will not generate stresses within the adjacent package components. Without available space the pyrolysis gases developed as a result of the charring process will move excess char mass out through the vent ports and prevent its buildup. Only as the charring process continues and space becomes available will the char be retained, filling the available space and plugging holes at the surface of the impact limiters. The thermal decomposition process does not alter or cause a chemical reaction within the adjacent materials.

The mechanisms behind the observed variations in the thermal properties and behavior of the FR-3700 foam at elevated temperatures are varied and complex. A series of fire tests [27 and 28] conducted on 5-gallon cans filled with FR-3700 foam at densities from 6.7 to 25.8 lb/ft<sup>3</sup> helped define the expected performance of the foam under fire accident conditions. Under the referenced fire tests, one end of the test article was subjected to an open diesel fueled burner flame at temperatures of 980 to 1,200°C (1,800 to 2,200 °F) for more than 30 minutes. A thermal shield prevented direct exposure to the burner flame on any surface of the test article other than the hot face. Each test article was instrumented with thermocouples located at various depths in the foam. In addition, samples of the foam were subjected to thermogravimetric analysis (TGA) to determine the thermal decomposition vs. temperature. The exposure temperatures for the TGA tests varied from 70 to 1,500 °F, and were conducted in both air and nitrogen atmospheres. The result for the nitrogen environment (see Figure 3.5-18) is more representative of the low oxygen environment existing within the impact limiter shells encasing the foam. These test results indicate that the following steps occur in the thermal breakdown of the foam under the level of elevated temperatures reached during the HAC fire event:

- Below 250 °F, the variation in foam thermal properties with temperature is slight and reversible. As such, fixed values for specific heat and thermal conductivity are appropriate.
- Between 250 and 500 °F, small variations in foam thermal properties occur as water vapor and non-condensable gases are driven out of the foam. As such, fixed values for specific heat and thermal conductivity are also appropriate for this temperature range. Further, the observed changes are so slight that the same thermal properties used for temperatures below 250 °F may also be used to characterize the thermal performance of the foam between 250 and 500 °F.
- Irreversible thermal decomposition of the foam begins as the temperature rises above 500 °F and increases non-linearly with temperature. Based on the TGA testing (see

Figure 3.5-18), approximately 2/3's of this decomposition occurs over a narrow temperature range centered about 670 °F.

- The decomposition is accompanied by vigorous out-gassing from the foam and an indeterminate amount of internal heat generation. The internal heat generation arises from the gases generated by the decomposition process that are combustible under piloted conditions. However, since the decomposition process is endothermic, the foam will not support combustion indefinitely. Further, the out-gassing process removes a significant amount of heat from the package via mass transport.
- The weight loss due to out-gassing not only has direct affect on the heat flux into the remaining virgin foam, but changes the composition of the resulting foam char since the foam constituents are lost at different rates. This change in composition affects both the specific heat and the thermal conductivity of the foam char layer.
- As temperature continues to rise, the developing char layer begins to take on the characteristics of a gas-filled cellular structure where radiative interchange from one cell surface to another becomes the dominant portion of the overall heat transfer mechanism. This change in heat transfer mechanisms causes the apparent heat conductivity to take on a highly non-linear relationship with temperature.
- Finally, at temperatures above 1,250 °F, the thermal breakdown of the foam is essentially completed and only about 5 to 10% of the original mass is left. In the absence of direct exposure to a flame or erosion by the channeling of the outgas products through the foam, the char layer will be the same or slightly thicker than the original foam depth. This char layer will continue to provide radiative shielding to the underlying foam material.

Since the thermal decomposition of the foam is an endothermic process, the foam is self-extinguishing and will not support a flame once the external flame source is removed. However, the gases generated by the decomposition process are combustible and will burn under piloted conditions. A portion of these generated gases can remain trapped within the charred layer of the foam after the cessation of the HAC fire event and continue to support further combustion, although at a much reduced level, until a sufficient time has passed for their depletion from the cell structure. This extended time period is typically from 15 to 45 minutes.

The sharp transition in the state of the foam noted in Figure 3.5-18 at or about 670 °F can be used to correlate the observed depth of the foam char following a burn test with the occurrence of this temperature level within the foam. The correlation between the foam recession depth and the foam density, as compiled from a series of tests, is expressed by the relation:

$$y = -0.94581 - 11.64 \times \log_{10}(x)$$

where,  $y$  = the recession depth, cm

$x$  = foam density ( $\text{g/cm}^3$ )

Based on this correlation, the recession depth expected for the nominal 9 pcf density foam used in the packaging is estimated to be 3.5 inches. The loss of foam could increase to a depth of approximately 3.8 inches for foam fabricated at the low end of the density tolerance (i.e., 7.65 pcf).

It should be noted that these results assume that the foam is enclosed within a steel shell with surface openings that are approximately 0.3 ft<sup>2</sup> or smaller. The presence of the steel enclosure helps shield the foam from the heat flux of a HAC fire event and helps contain the foam char that is generated. Test results with and without a steel interface between the foam and the heat source indicates that the foam loss could be an additional 1.5 inches for the 7.65 pcf foam if larger face areas are exposed directly to the fire.

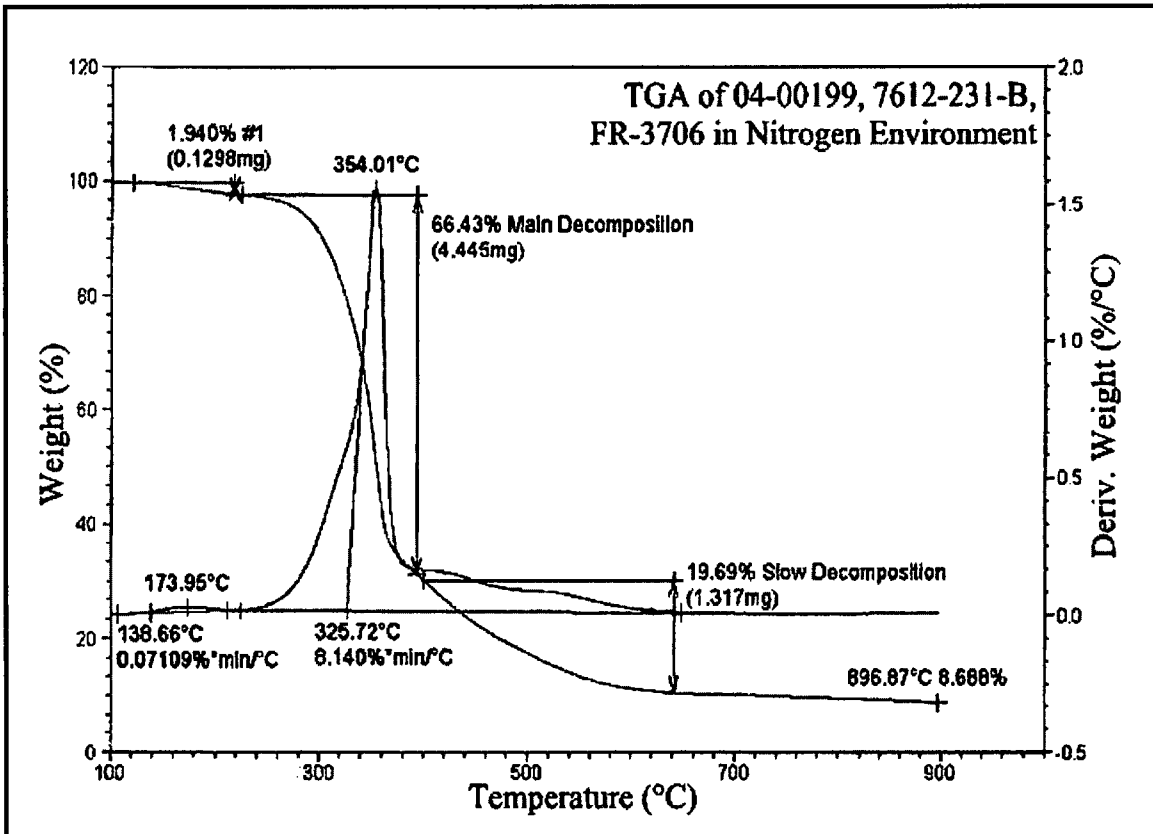


**Figure 3.5-18 – TGA Analysis of Foam Decomposition in Nitrogen Environment**

Two O-ring seals are provided in the closure lid: the inner seal is containment, and the outer forms an annular space for leakage rate testing of the containment seal. The leakage rate tests used for various purposes are summarized in Section 4.4, *Leakage Rate Tests for Type B Packages*, and described in detail in Chapter 8, *Acceptance Tests and Maintenance Program*.

The O-ring containment seal is retained in the closure lid using a dovetail groove having a depth of  $0.284 \pm 0.003$  inches, or  $0.281 - 0.287$  inches. The O-ring has a cross sectional diameter of  $0.375 \pm 0.007$  inches, or  $0.368 - 0.382$  inches. The minimum compression corresponds to the maximum groove depth and the minimum O-ring cross-sectional diameter:

$$C_{\text{Min}} = 100 \times \left( 1 - \frac{G_{\text{Max}}}{D_{\text{Min}}} \right) = 22\%$$

where  $G_{\text{Max}} = 0.287$  inches and  $D_{\text{Min}} = 0.368$  inches. The maximum compression corresponds to the minimum groove depth and the maximum O-ring cross-sectional diameter:

$$C_{\text{Max}} = 100 \times \left( 1 - \frac{G_{\text{Min}}}{D_{\text{Max}}} \right) = 26\%$$

where  $G_{\text{Min}} = 0.281$  inches and  $D_{\text{Max}} = 0.382$  inches. The Parker O-ring Handbook [7] recommends a minimum compression of 16%. The limit for maximum compression is when the O-ring cross-section, adjusted for maximum temperature, fills the cross sectional area of the dovetail groove. This condition occurs for the BRR package closure O-ring at a compression of 31.2%. The compression range of 22% to 26% will therefore provide satisfactory performance of the O-ring during all NCT and HAC.

#### 4.1.4 Welds

All welds used in the containment boundary are full penetration and volumetrically inspected to ensure structural and containment integrity. The welds joining the inner shell to either end structure are ultrasonically inspected in accordance with the ASME Code, Subsection NB, Article NB-5000, and Section V, Article 4 [4]. The weld joining the inner shell and the lower end structure may be optionally radiograph inspected in accordance with the ASME Code, Subsection NB, Article NB-5000, and Section V, Article 2 [3]. All containment boundary welds are inspected by liquid penetrant inspection on the final pass in accordance with the ASME Code, Subsection NB, Article NB-5000, and Section V, Article 6 [5]. All containment boundary welds are confirmed to be leaktight as discussed in Section 8.1.4, *Fabrication Leakage Rate Tests*.

#### 4.1.5 Closure

The closure lid completes the containment boundary, and is attached to the cask body using (12) 1-8 UNC socket head cap screws tightened to  $220 \pm 20$  ft-lb. As shown in Chapter 2, *Structural Evaluation*, the closure lid cannot become detached by any internal pressure, NCT, or HAC events. The closure lid, including the vent port, is completely covered by the upper impact limiter, which is attached to the cask using eight (8) 1-inch diameter ball lock pins. Similarly, the drain port is covered by the lower impact limiter. Thus, the containment openings cannot be inadvertently opened.

## 4.5 Appendix

### 4.5.1 References

1. ANSI N14.5-1997, *American National Standard for Radioactive Materials – Leakage Tests on Packages for Shipment*, American National Standards Institute (ANSI), Inc.
2. Rainier Rubber Company, Seattle, WA.
3. American Society of Mechanical Engineers (ASME) Boiler and Pressure Vessel Code, Section III, *Rules for Construction of Nuclear Facility Components*, Division 1 – Subsection NB, *Class 1 Components*, and Section V, *Nondestructive Examination*, Article 2, *Radiographic Examination*, 2007 Edition.
4. American Society of Mechanical Engineers (ASME) Boiler and Pressure Vessel Code, Section III, *Rules for Construction of Nuclear Facility Components*, Division 1 – Subsection NB, *Class 1 Components*, and Section V, *Nondestructive Examination*, Article 4, *Ultrasonic Examination Methods for Welds*, 2007 Edition.
5. American Society of Mechanical Engineers (ASME) Boiler and Pressure Vessel Code, Section III, *Rules for Construction of Nuclear Facility Components*, Division 1 – Subsection NB, *Class 1 Components*, and Section V, *Nondestructive Examination*, Article 6, *Liquid Penetrant Examination*, 2007 Edition.
6. Title 10, Code of Federal Regulations, Part 71 (10 CFR 71), *Packaging and Transportation of Radioactive Material*, 01-01-08 Edition.
7. Parker O-ring Handbook, ORD-5700, Parker-Hannifin Corporation, Cleveland, OH, © 2007.

Dose rates are very low. Under NCT, the maximum package surface dose rate is 13.4 mrem/hr, the maximum dose rate 2 m from the vehicle surface is 0.3 mrem/hr, and the dose rate in the occupied location is 0.05 mrem/hr. Under HAC, the maximum dose rate at 1 m from the package is 2.8 mrem/hr.

**Table 5.1-1 – Summary of Maximum Total Dose Rates (Exclusive Use)**

NCT	Package Surface (mrem/hr)			Vehicle Surface (mrem/hr)			
	Fuel→	TRIGA	TRIGA	MURR	TRIGA	TRIGA	MURR
	Radiation	Top	Side	Bottom	Top	Side	Bottom
Gamma	8.6	8.5	4.8	8.6	3.5	4.8	
Neutron	0.2	4.9	0.0	0.2	0.1	0.0	
Total	8.8	13.4	4.8	8.8	3.6	4.8	
Limit	200	200	200	200	200	200	

NCT	2 m from Vehicle Surface (mrem/hr)			Occupied Location (mrem/hr)	
	Fuel→	NA	MURR	NA	TRIGA
	Radiation	Top	Side	Bottom	Side
Gamma	NA	0.3	NA	0.04	
Neutron	NA	0.0	NA	0.01	
Total	NA	0.3	NA	0.05	
Limit	10	10	10	2	

HAC	1 m from Package Surface (mrem/hr)			
	Fuel→	TRIGA	TRIGA	MURR
	Radiation	Top	Side	Bottom
Gamma	2.7	2.1	2.0	
Neutron	0.1	0.1	0.0	
Total	2.8	2.2	2.0	
Limit	1000	1000	1000	

## 5.2 Source Specification

The source specification for the four fuel sources are provided in the following sections. Note that the sources for MURR, MITR-II, and ATR fuel were developed and provided by the host reactor staff [9, 10, 11].

### 5.2.1 Gamma Source

#### 5.2.1.1 MURR Fuel

The MURR gamma source term is generated by the ORIGEN 2.2 computer program [4] and is obtained from [9]. The source is based on 775 g U-235 and 57 g U-238 (93% enrichment). The fuel is burned in 21 cycles. The first 20 cycles are 7 days in duration, and the final cycle is 4 days in duration, giving a total irradiation time of 144 days. The element power is 1.25 MW, for a total burnup of 180 MWD (216,346 MWD/MTU, or a U-235 depletion of 28.3%). Two weeks of cooling is assumed between each cycle. The source is allowed to cool 180 days after reactor shutdown.

The ORIGEN 2.2 THERMAL library is used because experience at MURR has shown that this library produces conservative values for the isotopes routinely produced at the reactor. Also, the measured heat dissipation rates are typically less than half of the values computed by ORIGEN 2.2. This indicates that ORIGEN 2.2 generates conservative results for the MURR reactor.

The fuel cycle is modeled as an extreme case of the MURR fuel cycle. Unlike many other research reactors, MURR does not use a once-through fuel cycle. Each fuel element is cycled in and out of the core several times before reaching the final discharge burnup. Typically, a given fuel element is irradiated in several 6.2 to 6.5-day periods with varying cooling (non-irradiation) times in between the irradiation periods. For this calculation, the fuel assembly is irradiated in 7.0-day periods in a one-week-in and two-week-out pattern until the fuel is discharged. This overestimates the source term since MURR fuel elements generally remain outside the core for several weeks at a time during their active life and are never cycled in and out of the core continuously until discharge. Therefore, the irradiation parameters utilized result in a source term that bounds any expected MURR fuel element.

The MURR gamma source is summarized in Table 5.2-1. Note that the MURR basket may transport up to eight fuel elements. A representative axial burnup distribution is provided in Table 5.2-2. This distribution is the ratio of the burnup in each segment to the average burnup.

#### 5.2.1.2 MITR-II Fuel

The MITR-II gamma source term is generated by the ORIGEN 2.2 computer program [4] and is obtained from [10]. The source is based on 508 g U-235, 5 g U-234, and 33.2 g U-238 (93% enrichment). The fuel is burned in one continuous cycle for 900 days. This irradiation time is highly conservative because no credit is taken for down time between cycles. The MITR-II reactor typically operates on a monthly cycle, and operates only 300 days per year. The element power is 0.25 MW (0.01 MW for the first day), for a total burnup of 224.76 MWD (411,498



MWD/MTU, or a U-235 depletion of 55.6%). The source is allowed to cool 30 days after reactor shutdown.

The irradiation time utilized is approximately 10% higher than the maximum expected irradiation time of any fuel element. Because of the lack of standard refueling and shutdown times, no interim shutdowns were modeled. The irradiation parameters utilized result in an average burnup approximately 30% higher than the worst-case element irradiated at MITR-II and is therefore bounding.

The ORIGEN 2.2 PWRUS library is used because experience at MITR-II has shown that this library generates actinide and fission product concentrations that, when input to a criticality program, result in computed reactivities to within 0.2% of measured reactivities. This indicates that ORIGEN 2.2 can accurately predict MITR-II fuel element depletion and fission product buildup, which is the basis of the source term.

The MITR-II gamma source is summarized in Table 5.2-1. Note that the MITR-II basket may transport up to 11 fuel elements.

The axial burnup distribution is provided in Table 5.2-3. This distribution is the ratio of the burnup in each segment to the average burnup. A symmetric distribution is utilized. Because the widths of the distribution are not constant (the end segments are half the width of the remaining segments), the distribution input to MCNP must be divided by 2 for the end regions, as indicated in the last column in the table.

### **5.2.1.3 ATR Fuel**

The ATR gamma source term is generated by the ORIGEN 2.1<sup>1</sup> computer program [3] and is obtained from [11]. The source is based on 1085 g U-235 and 71 g U-238 (94% enrichment). The fuel is burned in one continuous cycle for 35 days. The element power is 10 MW, for a total burnup of 350 MWD (302,768 MWD/MTU, or a U-235 depletion of 40.9%). The source is allowed to cool 1,280 days after reactor shutdown. Fuel elements with burnups that exceed 350 MWD are not allowed. The ATRXS library is used in the calculation, which is a library generated explicitly for use with the ATR.

The fuel cycle modeled is an extreme case of the ATR fuel cycle. Typical fuel element power is in the range 2.25 to 3.25 MW, while 10 MW is modeled. Likewise, a typical cycle length is in the range from 49 to 56 days, while 35 days is modeled. The burnup would also typically be achieved in more than one cycle, and any down time between cycles has been ignored in the calculation. Therefore, the source is bounding for burnups  $\leq$  350 MWD.

The ATR gamma source is summarized in Table 5.2-1. Note that the ATR basket may transport up to eight fuel elements.

The axial burnup distribution provided in Table 5.2-4 is simply assumed based upon a peak of 1.45 at the axial center. This distribution is the ratio of the burnup in each segment to the average burnup. The distribution is divided over 10 segments of equal width over the fuel length of 48-in (121.92 cm).

<sup>1</sup> For ATR fuel, ORIGEN 2.1 and ORIGEN 2.2 generate the same source within 0.1% [11]. Therefore, ORIGEN 2.1 results are used, even though this is an older version of the program.

#### 5.2.1.4 TRIGA Fuel

The TRIGA fuel gamma source term is derived from information in INEL-96/0482 [6]. This report provides detailed activity values for 145 key isotopes as a function of burnup and decay time for four different TRIGA fuel types. These four fuel types are included in Section 1.2.2, *Contents*:

- Type 101 = aluminum-clad standard
- Type 103 = stainless steel-clad standard
- Type 109 = High-enrichment Fuel Life Improvement Program (FLIP)
- Type 117 = Low-enrichment Fuel Life Improvement Program (FLIP-LEU-I)

Key parameters for the four fuel types are summarized in Table 5.2-5. Decay times range from discharge to 20 years. Note that the minimum decay time reported in this table has been selected to be the minimum for transportation purposes.

The models used to generate the source are described in [6]. The TRIGA fuel is modeled with an irradiation time of 4 years. TRIGA reactors tend to run only sporadically rather than continuously, and TRIGA fuel elements often have residence times exceeding 10 years. Therefore, the source is conservative.

For shielding calculations, a bounding source term is selected. The Type 109 fuel has by far the largest burnup of the four candidate TRIGA fuels and hence results in the largest source. It is desired to set a minimum decay time of 1 year for the two higher-burnup fuels (Type 109 and 117) to allow many of the short-lived daughters to decay. For the two standard fuels, a much shorter 28 day decay time is stipulated. It may be demonstrated that the Type 109 fuel is bounding simply by comparing key isotopes (e.g., Co-60, Sr-90, Cm-244, etc.) in the activity tables provided in [6].

A fifth fuel type is included in Section 1.2.2, *Contents*, Type 203 (8.5 wt.% instrumented, stainless steel clad), which is simply a longer, instrumented version of Type 103. The source term for this fuel type is not specifically provided in [6]. However, the source for a Type 203 fuel element would be comparable to a Type 103 element, and the Type 103 element is well-bounded by the high-burnup Type 109 fuel element utilized in the shielding calculations.

However, source term data that could be utilized directly in MCNP are not provided in [6]. Rather, these activities are input into ORIGEN-S [5] to generate a suitable source term that may be used in shielding computations. The source information from Table F.14 of [6] at discharge is input to ORIGEN-S, and then decayed to 1 year. The gamma source for TRIGA fuel is summarized in Table 5.2-6. Note that the TRIGA basket holds 19 fuel elements.

The energy structure of the TRIGA source is slightly different when compared to the MURR, MITR-II, or ATR sources, because it was generated by a different computer program. The TRIGA source is grouped into energy bins, while discrete energy lines are used to characterize the source for the other fuels.

No axial burnup profile is provided for TRIGA fuel, and a flat distribution is utilized.

## 5.2.2 Neutron Source

The neutron sources are extracted from the same output files that define the gamma sources, as described in Section 5.2.1, *Gamma Source*. The neutron source is divided into spontaneous fission and ( $\alpha$ ,n) components. In ORIGEN 2.1, ORIGEN 2.2, and ORIGEN-S, oxygen is used as the target nucleus to generate the ( $\alpha$ ,n) source, although oxygen is not present in the fuel matrix for any of the four fuel types. For the three aluminum matrix fuels, it is assumed that using oxygen as the target nucleus bounds the use of aluminum (aluminum also acts as an ( $\alpha$ ,n) neutron target material). For the TRIGA fuels, no ( $\alpha$ ,n) target nuclides are present in the fuel matrix.

Neutron source terms are provided in Table 5.2-7 through Table 5.2-10 for MURR, MITR-II, ATR, and TRIGA fuel, respectively. Note that for MURR, MITR-II, and ATR fuel, information about the spectral distribution of the neutron source is not provided by the source generation program. Such information is required for input to MCNP. Spontaneous neutron spectra are provided in the MCNP user's manual for the following five isotopes: Pu-240, Pu-242, Cm-242, Cm-244, and Cf-252. Therefore, one of these standard spectra is applied to each neutron source.

For the MURR source, Pu-240 is the largest spontaneous fission source, so the Pu-240 spectrum is utilized. For the MITR-II source, Pu-238 is the largest spontaneous fission source isotope, although no standard spectra is available for this isotope. Therefore, the spectrum of Pu-240 is assumed. For the ATR source, Cm-244 is the largest spontaneous fission source isotope, so the Cm-244 spectrum is utilized. For all three aluminum matrix fuels, the neutron source is rather small and contributes very little to the total dose rate. Therefore, the choice of neutron spectrum has little or no effect on the results.

For the TRIGA neutron source, which is computed by ORIGEN-S, the source is output explicitly in energy groups, so no additional approximations are necessary. This spectrum is input directly to MCNP. To be conservative, the ( $\alpha$ ,n) source is included in the total, although the actual ( $\alpha$ ,n) source would be effectively zero because there is no applicable target nuclide in the fuel matrix. This assumption results in an additional conservatism of 9% in the TRIGA neutron source

The neutron sources for MURR, MITR-II, ATR, and TRIGA fuel is input with the same axial distribution provided in Section 5.2.1, *Gamma Source*.

**Table 5.2-1 – Gamma Source Terms (MURR, MITR-II, ATR)**

	<b>MURR</b>	<b>MITR-II</b>	<b>ATR</b>
<b>Mean Photon Energy (MeV)</b>	<b>Gamma Source (γ/s)</b>	<b>Gamma Source (γ/s)</b>	<b>Gamma Source (γ/s)</b>
1.00E-02	3.322E+14	5.357E+13	8.557E+13
2.50E-02	7.122E+13	1.167E+13	1.868E+13
3.75E-02	8.163E+13	1.335E+13	2.117E+13
5.75E-02	6.650E+13	1.076E+13	1.717E+13
8.50E-02	4.752E+13	7.521E+12	1.200E+13
1.25E-01	7.077E+13	9.086E+12	1.438E+13
2.25E-01	3.866E+13	6.179E+12	9.878E+12
3.75E-01	1.873E+13	3.156E+12	5.090E+12
5.75E-01	6.015E+13	4.251E+13	5.375E+13
8.50E-01	3.184E+14	1.125E+13	8.026E+12
1.25E+00	3.547E+12	1.624E+12	1.711E+12
1.75E+00	4.426E+11	7.615E+10	1.162E+11
2.25E+00	2.282E+12	2.911E+11	4.708E+11
2.75E+00	8.308E+09	1.225E+09	2.057E+09
3.50E+00	5.794E+08	1.266E+08	2.151E+08
5.00E+00	5.166E-01	9.235E+01	1.335E+02
7.00E+00	5.697E-02	9.919E+00	1.506E+01
9.50E+00	6.390E-03	1.093E+00	1.708E+00
Total	1.112E+15	1.710E+14	2.480E+14
Number of Fuel Elements in Basket	8	11	8
Basket Total	8.896E+15	1.881E+15	1.984E+15

**Table 5.2-2 – Axial Burnup Distribution, MURR**

Distance from Bottom of Fuel Element (cm)	Axial Burnup Distribution
5	0.872
10	0.939
15	1.132
20	1.233
25	1.367
30	1.358
35	1.308
40	1.233
45	1.023
50	0.679
55	0.486
60	0.369

**Table 5.2-3 – Axial Burnup Distribution, MITR-II**

Distance from Bottom of Fuel Element (cm)	Axial Burnup Distribution	MCNP Input
2.368	0.999	0.500
4.736	0.788	0.394
9.472	0.788	0.788
14.208	0.901	0.901
18.944	1.042	1.042
23.680	1.140	1.140
28.416	1.253	1.253
33.152	1.267	1.267
37.888	1.112	1.112
42.624	1.028	1.028
47.360	0.901	0.901
52.096	0.774	0.774
54.464	0.802	0.401
56.833	0.999	0.500

**Table 5.2-4 – Axial Burnup Distribution, ATR**

Distance from Bottom of Fuel Element (cm)	Axial Burnup Distribution
12.19	0.50
24.38	0.70
36.58	1.00
48.77	1.30
60.96	1.45
73.15	1.45
85.34	1.30
97.54	1.00
109.73	0.70
121.92	0.50

**Table 5.2-5 – TRIGA Fuel Parameters**

Fuel Type	Enrichment (%)	Maximum U-235 depletion (%)	Maximum Burnup (MWD/MTU)	Minimum Decay Time
Type 101 (Aluminum-clad standard)	20.0	22.42	36,953	28 days
Type 103/203 (Stainless steel-clad standard)	20.0	20.72	34,111	28 days
Type 109 (FLIP)	70.0	59.74	339,368	1 year
Type 117 (FLIP-LEU-I)	20.0	43.81	75,415	1 year

Table 5.2-6 – Gamma Source Term (TRIGA)

Upper Energy Bin (MeV)	Gamma Source ( $\gamma/s$ )
5.00E-02 <sup>ⓐ</sup>	2.601E+13
1.00E-01	8.070E+12
2.00E-01	8.658E+12
3.00E-01	1.952E+12
4.00E-01	1.498E+12
6.00E-01	7.684E+12
8.00E-01	1.928E+13
1.00E+00	3.454E+12
1.33E+00	8.832E+12
1.66E+00	2.637E+12
2.00E+00	2.716E+10
2.50E+00	2.099E+11
3.00E+00	1.065E+09
4.00E+00	8.211E+07
5.00E+00	2.045E+03
6.50E+00	8.196E+02
8.00E+00	1.606E+02
1.00E+01	3.407E+01
Total	8.832E+13
Number of Fuel Elements in Basket	19
Basket Total	1.678E+15

<sup>ⓐ</sup>The lower energy bound for this group is 0.01 MeV.

**Table 5.2-7 – Neutron Source Term, MURR**

Isotope	Spontaneous Fission (n/s)	( $\alpha$ ,n) (n/s)	Total (n/s)
U-235	1.958E-01	4.390E-01	6.348E-01
U-236	1.512E-01	8.800E-01	1.031E+00
U-238	7.222E-01	6.022E-03	7.282E-01
Pu-238	2.695E+00	1.652E+01	1.922E+01
Pu-240	3.623E+00	2.721E+00	6.344E+00
Pu-242	1.332E-02	6.873E-01	7.006E-01
Cm-242	1.071E+00	2.207E-01	1.292E+00
Total	8.474E+00	2.152E+01	2.999E+01
Number of Fuel Elements in Basket	8	8	8
Basket Total	68	172	240
Spectrum: Assume spontaneous fission of Pu-240			

**Table 5.2-8 – Neutron Source Term, MITR-II**

Isotope	Spontaneous Fission (n/s)	( $\alpha$ ,n) (n/s)	Total (n/s)
U-234	1.395E-02	1.297E+01	1.298E+01
U-235	7.951E-02	1.783E-01	2.578E-01
U-236	2.317E-01	1.348E+00	1.580E+00
U-238	4.158E-01	--	4.158E-01
Pu-238	1.112E+03	6.819E+03	7.931E+03
Pu-239	--	9.725E+00	9.725E+00
Pu-240	5.516E+01	1.046E+01	6.562E+01
Pu-242	4.489E+00		4.489E+00
Cm-242	2.491E+01	5.135E+00	3.005E+01
Cm-244	3.293E+02	--	3.293E+02
Cf-252	4.317E-04	--	4.317E-04
Am-241	--	8.287E+00	8.287E+00
Total	1.527E+03	6.867E+03	8.394E+03
Number of Fuel Elements in Basket	11	11	11
Basket Total	1.679E+04	7.554E+04	9.233E+04
Spectrum: Assume spontaneous fission of Pu-240			



**Table 5.2-9 – Neutron Source Term, ATR**

Isotope	Spontaneous Fission (n/s)	( $\alpha$ ,n) (n/s)	Total (n/s)
Pu-238	4.664E+02	2.860E+03	3.326E+03
Pu-239	--	1.203E+02	1.203E+02
Pu-240	3.177E+02	6.027E+01	3.780E+02
Pu-242	4.513E+01	--	4.513E+01
Am-241	--	1.335E+02	1.335E+02
Cm-242	4.093E+00	8.435E-01	4.937E+00
Cm-244	1.854E+03	1.540E+01	1.869E+03
Total	2.687E+03	3.190E+03	5.878E+03
Number of Fuel Elements in Basket	8	8	8
Basket Total	2.150E+04	2.552E+04	4.702E+04
Spectrum: Assume spontaneous fission of Cm-244			

**Table 5.2-10 – Neutron Source Term, TRIGA**

Upper Energy Bin (MeV)	Spontaneous Fission (n/s)	( $\alpha$ ,n) (n/s)	Total (n/s)
3.00E-03 <sup>Ⓞ</sup>	3.241E+00	1.061E-01	3.347E+00
1.70E-02	4.374E+01	1.648E+00	4.539E+01
1.00E-01	6.106E+02	2.350E+01	6.341E+02
4.00E-01	4.148E+03	1.397E+02	4.288E+03
9.00E-01	9.055E+03	2.892E+02	9.344E+03
1.40E+00	9.033E+03	3.985E+02	9.432E+03
1.85E+00	7.179E+03	5.970E+02	7.776E+03
3.00E+00	1.317E+04	2.585E+03	1.576E+04
6.43E+00	1.204E+04	1.715E+03	1.376E+04
2.00E+01	1.155E+03	0.000E+00	1.155E+03
Total	5.644E+04	5.750E+03	6.219E+04
Number of Fuel Elements in Basket	19	19	19
Basket Total	1.072E+06	1.092E+05	1.182E+06

<sup>Ⓞ</sup> The lower energy bound for this group is 5.50E-04 MeV.

### 5.4.3 Flux-to-Dose Rate Conversion

ANSI/ANS-6.1.1-1977 flux-to-dose rate conversion factors are used in this analysis. These are obtained from the MCNP User's Manual [2], Tables H.1 and H.2, although these values have been converted to provide results in mrem/hr rather than rem/hr. These conversion factors are provided in Table 5.4-1.

### 5.4.4 External Radiation Levels

A total of eight input files are developed to compute the NCT and HAC dose rates. A gamma and neutron model is developed for each of the four sources. The files are itemized as follows, where N refers to neutron modeling and G refers to gamma modeling:

- MURR fuel: MURR\_N, MURR\_G
- MITR-II fuel: MIT\_N, MIT\_G
- ATR fuel: ATR\_N, ATR\_G
- TRIGA fuel: TRIGA\_NG, TRIGA\_G

The reported dose rates are the values computed by MCNP, increased an additional 25%. This additional margin compensates for any potential non-conservatism in the ORIGEN2 program used to generate the source.

For exclusive use transport, the following 10 CFR 71.47 dose rates must be met:

- Maximum NCT cask surface dose rate of 200 mrem/hr. The higher 1000 mrem/hr limit is not claimed because the vehicle will be open. The dose rate limit applies at the outer surface of the heat shield, and the outer surface of the impact limiters. These results are summarized in Table 5.4-2 and Table 5.4-3. See also Figure 5.4-1 and Figure 5.4-2 for a graphical depiction of the tally locations.
- Maximum NCT vehicle surface dose rate of 200 mrem/hr. This limit is somewhat redundant because it is the same as the cask surface limit, and the cask surface dose rates are always higher than the vehicle surface dose rates. In this case, the vehicle surface is projected, because the actual vehicle will be open. It is assumed the vehicle is 8 ft wide, and the cask is laterally centered on the vehicle. These results are summarized in Table 5.4-4. See also Figure 5.4-3 and Figure 5.4-4 for a graphical depiction of the tally locations.
- Maximum NCT dose rate 2 m from the vehicle surface of 10 mrem/hr. These results are summarized in Table 5.4-4. See also Figure 5.4-3 and Figure 5.4-4 for a graphical depiction of the tally locations.
- Maximum NCT dose rate in any occupied location of 2 mrem/hr. The only occupied location is the driver of the vehicle, which is assumed to be 25 ft from the centerline of the cask. These results are summarized in Table 5.4-5. See also Figure 5.4-3 and Figure 5.4-4 for a graphical depiction of the tally location.
- Maximum HAC dose rate of 1000 mrem/hr 1 m from the surface of the cask. As the impact limiters will remain attached under HAC, the end dose rates are computed 1 m

from the ends of the impact limiters, assuming 12-in crush on each end. In the radial direction, the dose rates are computed 1 m from the heat shield. These results are summarized in Table 5.4-6 and Table 5.4-7. See also Figure 5.4-3, Figure 5.4-4, and Figure 5.4-5 for a graphical depiction of the tally locations

Dose rates are not constant along the side of the cask. The dose rate is typically at a maximum next to the active fuel, and becomes lower away from this region. Therefore, it is customary to segment the tallies into small regions in order to capture the maximum dose rate. On the side surface of the cask, the tally is divided into 12 equal segments 10.7 cm wide (see Figure 5.4-1). On the cylindrical sides of the impact limiters, the tally is divided into 5 equal segments 17.6 cm wide (see Figure 5.4-2). On the top and bottom impact limiter surfaces, the tally is divided into 9 concentric rings of width 10.2 cm (see Figure 5.4-2).

For the four side tallies (vehicle surface, 2 m from vehicle surface, occupied location, and 1 m HAC), the tallies are segmented into 15 segments 20.3 cm wide (see Figure 5.4-3 and Figure 5.4-4). In addition, the side dose rates above and below the impact limiter surfaces are also reported, although these tallies are approximately 70 cm wide.

The HAC 1 m tallies from the top and bottom of the impact limiters are divided into 11 segments, up to 1 m radially from the surface of the thermal shield (see Figure 5.4-5).

The dose rates reported in the following tables are the summed gamma and neutron dose rates. The maximum dose rates at most locations are computed for TRIGA fuel, although maximum dose rates at some locations occur for MURR fuel. The maximum cask surface dose rate is 13.4 mrem/hr (limit = 200 mrem/hr). The maximum vehicle surface dose rate is 3.6 mrem/hr (limit = 200 mrem/hr). The maximum dose rate 2 m from the surface of the vehicle is 0.3 mrem/hr (limit = 10 mrem/hr), and the maximum dose rate at the occupied location is 0.05 mrem/hr (limit = 2 mrem/hr). Therefore, all of the NCT dose rates are met with large margins.

Note that the maximum dose rate on the vehicle surface occurs at location 1 (see Figure 5.4-4), which is actually above the upper impact limiter. The dose rate is peaking in this region rather than beside the source because the gamma shielding is greatly reduced in the "corners" of the cask. Also, the modeled lead slump in this region could be contributing to this effect.

The maximum HAC dose rate 1 m from the cask is 2.8 mrem/hr (limit = 1000 mrem/hr), and occurs at measured from the top at location 11, for the reasons cited in the previous paragraph. Clearly, the HAC dose rate limit is met with a large margin.

The detailed results from the TRIGA fuel, including statistical uncertainties, are reported in Section 5.5.2, *Detailed TRIGA Results*. Because the TRIGA fuel is bounding at most dose rate locations, detailed results are not provided for the other three fuel types.

Table 5.4-2 – NCT Cask Side Total Dose Rates (mrem/hr)

Location	MURR	MITR-II	ATR	TRIGA
1	2.0	2.3	0.7	8.4
2	5.2	3.4	1.1	12.3
3	9.2	3.9	1.5	13.4
4	12.1	3.7	1.9	11.3
5	12.4	3.0	2.1	7.3
6	9.9	1.8	2.3	4.0
7	5.6	0.8	2.3	2.2
8	1.8	0.3	2.1	1.4
9	0.4	0.1	1.7	0.9
10	0.1	0.1	1.3	0.7
11	0.03	0.05	1.0	0.5
12	0.01	0.03	0.5	0.3
Max	12.4	3.9	2.3	13.4
Limit = 200 mrem/hr				

**Table 5.4-3 – NCT Impact Limiter Total Dose Rates (mrem/hr)**

	Upper Impact Limiter Side				Lower Impact Limiter Side			
Location	MURR	MITR-II	ATR	TRIGA	MURR	MITR-II	ATR	TRIGA
1	2.6	2.6	0.7	7.7	0.1	0.04	0.2	0.2
2	1.9	1.7	0.5	5.4	0.1	0.03	0.2	0.2
3	1.2	1.0	0.3	3.3	0.3	0.04	0.4	0.1
4	0.8	0.7	0.2	2.3	0.4	0.1	0.8	0.1
5	1.1	0.7	0.3	2.3	0.4	0.1	0.9	0.1
Max	2.6	2.6	0.7	7.7	0.4	0.06	0.9	0.2
	Upper Impact Limiter Horizontal				Lower Impact Limiter Horizontal			
Location	MURR	MITR-II	ATR	TRIGA	MURR	MITR-II	ATR	TRIGA
1	2.0	1.0	0.3	2.6	4.5	0.9	1.0	0.4
2	2.2	1.0	0.3	2.8	4.8	0.9	1.0	0.4
3	2.8	1.3	0.4	3.5	3.6	0.8	0.9	0.4
4	2.9	1.5	0.4	3.8	2.3	0.5	0.7	0.3
5	2.4	1.5	0.4	4.3	1.3	0.3	0.5	0.2
6	2.2	1.6	0.5	4.8	0.8	0.1	0.5	0.1
7	2.3	2.0	0.6	6.1	0.5	0.1	0.5	0.1
8	3.1	2.7	0.8	8.4	0.4	0.1	0.6	0.1
9	3.1	2.8	0.8	8.8	0.4	0.1	0.8	0.1
Max	3.1	2.8	0.8	8.8	4.8	0.9	1.0	0.4
Limit = 200 mrem/hr								

**Table 5.4-4 – NCT Vehicle Side and 2 m Total Dose Rates (mrem/hr)**

Location	Vehicle Side				2 m from Vehicle Side			
	MURR	MITR-II	ATR	TRIGA	MURR	MITR-II	ATR	TRIGA
1	1.3	1.2	0.3	3.6	0.2	0.1	0.04	0.3
2	0.9	0.8	0.2	2.5	0.2	0.1	0.05	0.3
3	0.7	0.6	0.2	1.9	0.2	0.1	0.1	0.3
4	0.7	0.5	0.2	1.5	0.2	0.1	0.1	0.3
5	0.8	0.5	0.2	1.5	0.3	0.1	0.1	0.3
6	1.3	0.6	0.3	1.7	0.3	0.1	0.1	0.3
7	1.9	0.7	0.4	1.9	0.3	0.1	0.1	0.3
8	2.1	0.7	0.5	1.7	0.3	0.1	0.1	0.3
9	1.8	0.5	0.5	1.3	0.3	0.1	0.1	0.3
10	1.2	0.3	0.5	0.9	0.3	0.1	0.1	0.2
11	0.7	0.2	0.4	0.5	0.2	0.1	0.1	0.2
12	0.3	0.1	0.3	0.3	0.2	0.1	0.1	0.2
13	0.2	0.1	0.2	0.2	0.2	0.1	0.1	0.2
14	0.1	0.04	0.2	0.2	0.1	0.05	0.1	0.1
15	0.2	0.03	0.2	0.1	0.1	0.04	0.1	0.1
16	0.2	0.04	0.4	0.1	0.1	0.03	0.1	0.1
17	0.2	0.03	0.4	0.1	0.1	0.02	0.05	0.1
Max	2.1	1.2	0.5	3.6	0.3	0.1	0.1	0.3
	Limit = 200 mrem/hr				Limit = 10 mrem/hr			

**Table 5.4-5 – NCT Occupied Location Total Dose Rates (mrem/hr)**

Location	MURR	MITR-II	ATR	TRIGA
1	0.04	0.02	0.01	0.05
2	0.05	0.02	0.01	0.05
3	0.05	0.02	0.01	0.05
4	0.05	0.02	0.02	0.05
5	0.05	0.02	0.02	0.05
6	0.05	0.02	0.02	0.05
7	0.05	0.02	0.02	0.05
8	0.05	0.02	0.02	0.05
9	0.05	0.02	0.02	0.05
10	0.05	0.02	0.02	0.05
11	0.05	0.02	0.02	0.05
12	0.05	0.02	0.02	0.04
13	0.05	0.02	0.02	0.04
14	0.05	0.01	0.02	0.04
15	0.04	0.01	0.01	0.04
16	0.04	0.01	0.01	0.04
17	0.04	0.01	0.01	0.03
Max	0.05	0.02	0.02	0.05
Limit = 2 mrem/hr				

**Table 5.4-6 – HAC 1 m Side Total Dose Rates (mrem/hr)**

<b>Location</b>	<b>MURR</b>	<b>MITR-II</b>	<b>ATR</b>	<b>TRIGA</b>
1	0.8	0.7	0.2	2.2
2	0.5	0.4	0.1	1.4
3	0.5	0.3	0.1	1.2
4	0.6	0.3	0.1	1.1
5	0.7	0.4	0.2	1.1
6	1.0	0.4	0.2	1.2
7	1.3	0.5	0.3	1.3
8	1.4	0.4	0.4	1.2
9	1.3	0.4	0.4	1.0
10	1.0	0.3	0.4	0.7
11	0.6	0.2	0.3	0.5
12	0.4	0.1	0.2	0.3
13	0.2	0.1	0.2	0.2
14	0.2	0.04	0.1	0.2
15	0.1	0.03	0.1	0.1
16	0.2	0.03	0.2	0.1
17	0.2	0.03	0.3	0.1
Max	1.4	0.7	0.4	2.2
Limit = 1000 mrem/hr				



**Table 5.4-7 – HAC 1 m End Total Dose Rates (mrem/hr)**

Location	Upper Impact Limiter				Lower Impact Limiter			
	MURR	MITR-II	ATR	TRIGA	MURR	MITR-II	ATR	TRIGA
1	0.9	0.5	0.1	1.2	1.8	0.3	0.4	0.2
2	0.9	0.5	0.1	1.3	2.0	0.4	0.4	0.2
3	1.1	0.6	0.2	1.5	1.7	0.3	0.4	0.2
4	1.1	0.6	0.2	1.5	1.3	0.3	0.3	0.2
5	1.2	0.6	0.2	1.5	1.0	0.2	0.3	0.1
6	1.0	0.6	0.2	1.6	0.8	0.2	0.3	0.1
7	0.9	0.6	0.2	1.6	0.6	0.1	0.2	0.1
8	0.8	0.6	0.2	1.7	0.4	0.1	0.2	0.1
9	0.8	0.6	0.2	1.7	0.3	0.1	0.2	0.05
10	0.8	0.7	0.2	2.2	0.2	0.04	0.2	0.04
11	1.0	0.9	0.3	2.8	0.1	0.03	0.2	0.04
Max	1.2	0.9	0.3	2.8	2.0	0.4	0.4	0.2
Limit = 1000 mrem/hr								

## 5.5 Appendices

### 5.5.1 References

1. Title 10, Code of Federal Regulations, Part 71 (10 CFR 71), Packaging and Transportation of Radioactive Material, 1-1-09 Edition.
2. MCNP5, "MCNP - A General Monte Carlo N-Particle Transport Code, Version 5; Volume II: User's Guide," LA-CP-03-0245, Los Alamos National Laboratory, April 2003. MCNP5 is distributed by the Radiation Safety Information Computational Center (www-rsicc.ornl.gov), Release C00710MNYCP02 (Windows PC).
3. ORIGEN 2.1, *Isotope Generation and Depletion Code, Matrix Exponential Method*, CCC-371, Oak Ridge National Laboratory, August 1996.
4. ORIGEN 2.2, *Isotope Generation and Depletion Code, Matrix Exponential Method*, CCC-371, Oak Ridge National Laboratory, June 2002.
5. *ORIGEN-S: SCALE System Module to Calculate Fuel Depletion, Actinide Transmutation, Fission Product Buildup and Decay, and Associated Radiation Source Terms*, ORNL/TM-2005/39, Version 5, Vol. II, Book 1, Section F7, Oak Ridge National Laboratory, April 2005.
6. JW Sterbentz, *Radionuclide Mass Inventory, Activity, Decay Heat, and Dose Rate Parametric Data for TRIGA Spent Nuclear Fuels*, INEL-96/0482, Idaho National Engineering Laboratory, March 1997.
7. *Standard Composition Library*, ORNL/TM-2005/39, Version 5, Vol. III, Section M8, April 2005.
8. *Nuclides and Isotopes, Chart of the Nuclides, Fifteenth Edition*, General Electric Co. and KAPL, Inc., 1996.
9. TDR-0119, Rev. 0, *MURR Spent Fuel Source Term Assumptions and Calculations*, University of Missouri Research Reactor, July 2009.
10. SR O-09-1, Rev. 0, *Source Term Specification for the MIT Reactor*, Massachusetts Institute of Technology Research Reactor, July 2009.
11. ECAR-695, Rev. 0, *ORIGEN 2.2 Source Term Calculation for the 30 Watt ATR Fuel Element*, Idaho National Laboratory, July 2009.

### 5.5.2 Detailed TRIGA Results

The following tables provide the detailed results for TRIGA fuel, because this fuel is limiting for most dose rate locations. Capture gamma dose rates are included in the gamma dose rates reported in these tables, although the capture gamma dose rate is essentially zero and could be neglected.

**Table 5.5-1 – TRIGA NCT Cask Side Dose Rates (mrem/hr)**

Location	Gamma	$\sigma$	Neutron	$\sigma$	Total	$\sigma$
1	4.6	0.6%	3.8	0.6%	8.4	0.4%
2	7.7	0.5%	4.7	0.5%	12.3	0.3%
3	8.5	0.4%	4.9	0.5%	13.4	0.3%
4	6.9	0.5%	4.5	0.5%	11.3	0.4%
5	3.7	0.6%	3.6	0.6%	7.3	0.4%
6	1.3	0.9%	2.7	0.7%	4.0	0.6%
7	0.3	1.6%	1.9	0.8%	2.2	0.7%
8	0.1	2.7%	1.3	0.9%	1.4	0.9%
9	0.02	4.1%	0.9	1.1%	0.9	1.1%
10	0.01	4.8%	0.7	1.3%	0.7	1.2%
11	0.005	5.3%	0.5	1.5%	0.5	1.5%
12	0.004	4.2%	0.3	1.9%	0.3	1.9%

**Table 5.5-2 – TRIGA NCT Impact Limiter Dose Rates (mrem/hr)**

Location	Gamma	$\sigma$	Neutron	$\sigma$	Total	$\sigma$
<b>Upper Impact Limiter Side</b>						
1	7.4	1.2%	0.2	1.0%	7.7	1.2%
2	5.1	0.9%	0.3	0.9%	5.4	0.9%
3	2.9	0.7%	0.4	0.7%	3.3	0.7%
4	1.7	0.5%	0.6	0.6%	2.3	0.4%
5	1.5	0.3%	0.8	0.5%	2.3	0.3%
<b>Lower Impact Limiter Side</b>						
1	0.04	0.5%	0.2	1.1%	0.2	0.9%
2	0.03	1.4%	0.1	1.6%	0.2	1.3%
3	0.03	3.6%	0.1	2.0%	0.1	1.8%
4	0.04	5.1%	0.1	2.3%	0.1	2.4%
5	0.03	5.3%	0.05	2.7%	0.1	2.7%
<b>Upper Impact Limiter Horizontal</b>						
1	2.2	0.8%	0.4	3.3%	2.6	0.9%
2	2.4	0.8%	0.4	2.0%	2.8	0.8%
3	3.2	1.0%	0.4	1.6%	3.5	0.9%
4	3.5	0.8%	0.3	1.5%	3.8	0.8%
5	4.0	0.8%	0.3	1.5%	4.3	0.8%
6	4.6	0.8%	0.3	1.4%	4.8	0.8%
7	5.9	1.1%	0.2	1.3%	6.1	1.0%
8	8.2	1.4%	0.2	1.3%	8.4	1.3%
9	8.6	1.4%	0.2	1.3%	8.8	1.4%
<b>Lower Impact Limiter Horizontal</b>						
1	0.4	4.1%	0.1	9.7%	0.4	3.8%
2	0.4	3.8%	0.1	5.5%	0.4	3.4%
3	0.3	4.0%	0.1	4.3%	0.4	3.5%
4	0.2	3.8%	0.04	3.9%	0.3	3.3%
5	0.1	3.6%	0.04	4.4%	0.2	2.9%
6	0.1	3.4%	0.03	3.8%	0.1	2.6%
7	0.04	3.5%	0.03	3.4%	0.1	2.5%
8	0.03	4.6%	0.04	3.1%	0.1	2.7%
9	0.03	6.9%	0.04	3.0%	0.1	3.6%

Table 5.5-3 – TRIGA NCT Vehicle Surface Dose Rates (mrem/hr)

Location	Gamma	$\sigma$	Neutron	$\sigma$	Total	$\sigma$
1	3.5	1.1%	0.1	0.6%	3.6	1.1%
2	2.3	0.8%	0.2	0.8%	2.5	0.8%
3	1.6	0.7%	0.3	0.7%	1.9	0.6%
4	1.2	0.5%	0.4	0.6%	1.5	0.4%
5	1.0	0.3%	0.5	0.5%	1.5	0.3%
6	1.2	0.3%	0.6	0.4%	1.7	0.3%
7	1.3	0.3%	0.6	0.4%	1.9	0.2%
8	1.1	0.3%	0.6	0.4%	1.7	0.3%
9	0.8	0.3%	0.5	0.4%	1.3	0.3%
10	0.4	0.4%	0.4	0.5%	0.9	0.3%
11	0.2	0.4%	0.3	0.6%	0.5	0.4%
12	0.1	0.4%	0.2	0.7%	0.3	0.5%
13	0.1	0.4%	0.2	0.9%	0.2	0.7%
14	0.04	0.8%	0.1	1.2%	0.2	0.9%
15	0.03	1.9%	0.1	1.5%	0.1	1.2%
16	0.03	3.1%	0.1	1.8%	0.1	1.6%
17	0.02	3.6%	0.04	1.4%	0.1	1.6%

**Table 5.5-4 – TRIGA NCT 2 m Vehicle Surface Dose Rates (mrem/hr)**

Location	Gamma	$\sigma$	Neutron	$\sigma$	Total	$\sigma$
1	0.2	0.6%	0.1	0.5%	0.3	0.5%
2	0.2	0.4%	0.1	0.8%	0.3	0.4%
3	0.2	0.4%	0.1	0.8%	0.3	0.3%
4	0.2	0.4%	0.1	0.7%	0.3	0.3%
5	0.2	0.3%	0.1	0.7%	0.3	0.3%
6	0.2	0.3%	0.1	0.7%	0.3	0.3%
7	0.2	0.3%	0.1	0.7%	0.3	0.3%
8	0.2	0.4%	0.1	0.7%	0.3	0.3%
9	0.2	0.4%	0.1	0.7%	0.3	0.3%
10	0.2	0.4%	0.1	0.7%	0.2	0.3%
11	0.1	0.4%	0.1	0.8%	0.2	0.4%
12	0.1	0.4%	0.1	0.8%	0.2	0.4%
13	0.1	0.4%	0.1	0.8%	0.2	0.4%
14	0.1	0.4%	0.1	0.9%	0.1	0.4%
15	0.1	0.4%	0.1	0.9%	0.1	0.5%
16	0.05	0.4%	0.1	0.9%	0.1	0.5%
17	0.03	0.3%	0.04	0.6%	0.1	0.4%

**Table 5.5-5 – TRIGA NCT Occupied Location Dose Rates (mrem/hr)**

Location	Gamma	$\sigma$	Neutron	$\sigma$	Total	$\sigma$
1	0.04	0.4%	0.01	0.6%	0.05	0.3%
2	0.04	0.4%	0.01	1.2%	0.05	0.4%
3	0.04	0.4%	0.01	1.1%	0.05	0.4%
4	0.04	0.4%	0.01	1.1%	0.05	0.4%
5	0.04	0.4%	0.01	1.1%	0.05	0.4%
6	0.04	0.4%	0.01	1.1%	0.05	0.4%
7	0.04	0.4%	0.01	1.1%	0.05	0.4%
8	0.03	0.4%	0.01	1.1%	0.05	0.4%
9	0.03	0.4%	0.01	1.1%	0.05	0.4%
10	0.03	0.5%	0.01	1.1%	0.05	0.5%
11	0.03	0.5%	0.01	1.1%	0.05	0.5%
12	0.03	0.5%	0.01	1.1%	0.04	0.5%
13	0.03	0.5%	0.01	1.1%	0.04	0.5%
14	0.03	0.5%	0.01	1.2%	0.04	0.5%
15	0.03	0.5%	0.01	1.2%	0.04	0.5%
16	0.02	0.5%	0.01	1.2%	0.04	0.5%
17	0.02	0.3%	0.01	0.6%	0.03	0.3%

Table 5.5-6 – TRIGA HAC 1 m Side Dose Rates (mrem/hr)

Location	Gamma	$\sigma$	Neutron	$\sigma$	Total	$\sigma$
1	2.1	1.0%	0.1	0.5%	2.2	1.0%
2	1.2	0.7%	0.2	0.8%	1.4	0.7%
3	0.9	0.6%	0.2	0.7%	1.2	0.5%
4	0.8	0.5%	0.3	0.6%	1.1	0.4%
5	0.8	0.3%	0.3	0.5%	1.1	0.3%
6	0.8	0.3%	0.4	0.5%	1.2	0.3%
7	0.9	0.3%	0.4	0.5%	1.3	0.3%
8	0.8	0.3%	0.4	0.5%	1.2	0.3%
9	0.6	0.3%	0.4	0.5%	1.0	0.3%
10	0.4	0.4%	0.3	0.5%	0.7	0.3%
11	0.2	0.4%	0.3	0.6%	0.5	0.4%
12	0.1	0.4%	0.2	0.7%	0.3	0.4%
13	0.1	0.4%	0.2	0.8%	0.2	0.5%
14	0.1	0.5%	0.1	1.0%	0.2	0.7%
15	0.04	0.8%	0.1	1.1%	0.1	0.8%
16	0.03	1.6%	0.1	1.4%	0.1	1.1%
17	0.02	2.6%	0.04	1.1%	0.1	1.1%



**Table 5.5-7 – TRIGA HAC Impact Limiter 1m End Dose Rates (mrem/hr)**

Location	Gamma	$\sigma$	Neutron	$\sigma$	Total	$\sigma$
<b>1 m from Upper Impact Limiter</b>						
1	1.1	0.8%	0.1	5.9%	1.2	0.9%
2	1.2	0.8%	0.1	3.5%	1.3	0.8%
3	1.4	1.2%	0.1	2.7%	1.5	1.1%
4	1.4	0.8%	0.1	2.3%	1.5	0.8%
5	1.4	0.8%	0.1	2.4%	1.5	0.8%
6	1.5	0.8%	0.1	1.9%	1.6	0.8%
7	1.5	0.8%	0.1	1.9%	1.6	0.8%
8	1.6	0.9%	0.1	1.9%	1.7	0.8%
9	1.6	0.9%	0.1	1.8%	1.7	0.8%
10	2.1	1.1%	0.1	1.0%	2.2	1.0%
11	2.7	1.3%	0.1	1.0%	2.8	1.3%
<b>1 m from Lower Impact Limiter</b>						
1	0.1	5.6%	0.01	16.0%	0.2	5.3%
2	0.2	4.5%	0.02	9.1%	0.2	4.1%
3	0.1	4.2%	0.02	6.9%	0.2	3.9%
4	0.1	4.6%	0.02	6.7%	0.2	4.1%
5	0.1	4.3%	0.02	5.7%	0.1	3.8%
6	0.1	3.9%	0.02	5.0%	0.1	3.3%
7	0.1	3.5%	0.02	4.7%	0.1	2.9%
8	0.04	3.6%	0.02	4.5%	0.1	2.9%
9	0.03	3.1%	0.02	3.8%	0.05	2.4%
10	0.02	2.7%	0.02	2.1%	0.04	1.7%
11	0.02	3.4%	0.03	1.7%	0.04	1.7%

### 5.5.3 Sample Input File

A sample input file is provided for the TRIGA fuel with a gamma source.

```

BRRC
c
c lateral cask wall including Pb shield
c
10 4 -7.94 100 -157 1 -2 imp:p=1 $ SS inner shell split
11 4 -7.94 100 -157 2 -3 imp:p=2 $ SS inner shell split
12 8 -11.35 103 -133 3 -4 imp:p=4 $ Pb gamma shield split
13 8 -11.35 103 -133 4 -5 imp:p=8 $ Pb gamma shield split
14 8 -11.35 103 -133 5 -6 imp:p=16 $ Pb gamma shield split
15 8 -11.35 103 -133 6 -7 imp:p=32 $ Pb gamma shield split
16 8 -11.35 103 -133 7 -8 imp:p=64 $ Pb gamma shield split
17 8 -11.35 103 -133 8 -801 imp:p=128 $ Pb gamma shield split
18 8 -11.35 103 -133 801 -9 imp:p=200 $ Pb gamma shield split
19 4 -7.94 103 300 9 -10 imp:p=256 $ SS
    
```

**BRR Package Safety Analysis Report**

3. 8.5 wt.% uranium, stainless steel clad, high enriched uranium (General Atomics catalog number 109)
4. 20 wt.% uranium, stainless steel clad (General Atomics catalog number 117)
5. 8.5 wt.% uranium, instrumented, stainless steel clad (General Atomics catalog number 203)

The fuel matrix of a TRIGA fuel element consists of a mixture of uranium and zirconium hydride. Therefore, the TRIGA elements contain hydrogen moderator material. Detailed fuel characteristics for the five TRIGA fuel element types are summarized in Table 6.2-7. A schematic of a typical stainless steel clad fuel element is shown in Figure 6.2-8.

TRIGA fuel elements consist of a central active fuel region with graphite axial reflectors above and below the active fuel. Type 101 and 103 TRIGA fuel manufactured prior to 1964 utilizes thin samarium trioxide discs between the active fuel and graphite reflectors. Type 109, 117, and 203 TRIGA fuel utilizes a thin molybdenum disc between the active fuel and lower reflector rather than samarium trioxide. The samarium trioxide discs act as a burnable poison and are conservatively omitted from the models. The molybdenum disc is only 0.031-in thick and has essentially no effect on the reactivity, as demonstrated in Section 6.9.2.4, *TRIGA Fuel Parametric Evaluation*. For this reason, the molybdenum disc is also omitted from the models.

For all TRIGA fuel elements with the exception of Type 101, a solid zirconium rod with an outer diameter of 0.225-in is placed along the active fuel length in the center of the fuel pellet. It is assumed that the inner diameter of the fuel pellet is 0.25-in to allow a small clearance between the rod and the fuel.

The fuel elements are modeled in detail from the bottom of the bottom reflector to the top of the top reflector. The end cap regions are neglected for simplicity. The graphite reflectors are modeled at the same diameter as the fuel pellets for simplicity, although the actual graphite reflectors have a slightly smaller diameter, as shown in Table 6.2-7. The Type 109 and 117 fuel elements contain erbium poison, although this poison is conservatively ignored in the criticality models.

The number densities within the TRIGA fuel elements are computed based upon the information in Table 6.2-7. Because the masses of U-235 and uranium are provided, the uranium number densities in the fuel may be computed based on the known volumes. The uranium is treated as a mix of only U-235 and U-238 for simplicity. The zirconium number density is computed based on the zirconium mass provided, and the hydrogen number density is computed based upon the H/Zr ratio. The fuel number densities for the five fuel types are summarized in Table 6.2-8.

## 6.3 General Considerations

### 6.3.1 Model Configuration

The BRR cask is modeled using conservative simplifying assumptions. The impact limiters are not modeled, and in the single package cases the cask is reflected with 12-in of water. In the array cases, removing the impact limiters conservatively minimizes the separation between the packages and increases the reactivity. The cask body itself is simply modeled as cylinders of steel-lead-steel without modeling the minor cask details, as these minor details have a negligible effect on the system reactivity.

The modeled cask geometry is shown in Figure 6.3-1, and the key model dimensions are provided in Table 6.3-1. Cask dimensions are based on the drawings in Section 1.3.3, *Packaging General Arrangement Drawings*. Note that the cask model in the upper region is simply representative of the shield plug thicknesses and that the 2-in thick steel lid is not included in the model, thereby bring the casks closer together in the array configuration.

Each fuel type has its own unique basket design. The baskets are modeled in sufficient detail to capture the relevant criticality effects, which are primarily of interest near the active fuel region. The key basket dimensions are included in Table 6.3-2, and x-y and x-z views of the four basket designs are provided in Figure 6.3-2 and Figure 6.3-3, respectively. Basket dimensions are based on the drawings in Section 1.3.3, *Packaging General Arrangement Drawings*. Note that the axial and radial fuel positions shown in these figures do not reflect the most reactive configurations, which is determined in Section 6.4, *Single Package Evaluation*.

Minor differences exist between the as-modeled and packaging general arrangement drawing dimensions, as shown in Table 6.3-1 and Table 6.3-2. These differences are small and are within the uncertainty of the Monte Carlo method and may therefore be neglected.

The baskets are modeled as undamaged in all NCT and HAC models. The baskets have been shown to be elastic in all accident scenarios and maintain their geometry (see Section 2.7.1.5, *Fuel Basket Stress Analysis*). The fuel is also modeled as undamaged in all models (with end structures conservatively removed), as it has also been demonstrated that the fuel maintains its structural integrity during accident conditions (see Section 2.7.1.6, *Fuel Impact Deformation*).

In the NCT cases, credit is taken for the leaktight nature of the package, and the cask cavity is modeled as dry (void). Although the package has been shown to be leaktight under accident conditions, in the HAC cases, water is conservatively modeled in the cask cavity at the density that maximizes reactivity. If it is assumed that water is free to flow throughout the cask cavity and fuel elements (as the baskets are designed to drain freely), the moderator water density between the fuel plates may be modeled at the same value as the water density between the fuel elements. This assumption is utilized in all MCNP criticality models. However, it has been shown that when an ATR fuel element is removed from a spent fuel pool and allowed to drip dry, a small volume of water remains between the fuel plates due to the surface tension in the thin channels between the fuel plates. Because the quantity of residual water is relatively small, any minor surface tension effects have been neglected in the MCNP modeling. In addition, no models are developed in which the cask is partially filled with water with some fuel elements

uncovered (such as might be the case if the cask were on its side in an accident), because this scenario would be less reactive due to lack of moderation in the uncovered fuel elements.

In the array cases, a close-packed hexagonal array is modeled by adding a hexagonal reflective boundary condition. The water density between the casks in the array is adjusted to determine the most reactive condition.

### 6.3.2 Material Properties

The fuel meat compositions are provided in Table 6.2-2, Table 6.2-3, Table 6.2-6, and Table 6.2-8 for MURR, MITR-II, ATR, and TRIGA fuel, respectively. For all fuels, aluminum structural material is modeled as pure aluminum with a density of  $2.7 \text{ g/cm}^3$ .

The TRIGA fuel contains materials not found in the aluminum plate fuels, such as stainless steel, graphite, and zirconium. For the stainless steel clad TRIGA fuel, the composition of stainless steel utilized is the standard composition provided in the SCALE material library [4] and is provided in Table 6.3-3. For the TRIGA fuels that contain a zirconium rod in the center of the fuel element, the zirconium is modeled as pure with a density of  $6.5 \text{ g/cm}^3$ . The graphite reflectors in the TRIGA fuel elements is modeled as pure graphite with a density of  $1.6 \text{ g/cm}^3$ . The density is obtained from the TRIGA benchmark experiments (IEU-COMP-THERM-003) listed in the *International Handbook of Evaluated Criticality Benchmark Experiments* [3]. The molybdenum disc is omitted in most models, but when present is modeled as pure molybdenum with a density of  $10.22 \text{ g/cm}^3$ . The material properties of the remaining packaging and moderating materials are described as follows.

The inner and outer tubes of the package are constructed from stainless steel 304. The standard compositions for stainless steel 304 are obtained from the SCALE material library [4], which is a standard set accepted for use in criticality analyses. The stainless steel composition and density utilized in the MCNP models are provided in Table 6.3-3.

Water is modeled with a density ranging up to  $1.0 \text{ g/cm}^3$  and the chemical formula  $\text{H}_2\text{O}$ .

### 6.3.3 Computer Codes and Cross-Section Libraries

MCNP5 v1.30 is used for the criticality analysis [1]. All cross sections utilized are at room temperature (293.6 K). The uranium isotopes utilize preliminary ENDF/B-VII cross section data that are considered by Los Alamos National Laboratory to be more accurate than ENDF/B-VI cross sections. ENDF/B-V cross sections are utilized for chromium, nickel, iron, and lead because natural composition ENDF/B-VI cross sections are not available for these elements. The remaining isotopes utilize ENDF/B-VI cross sections. Titles of the cross sections utilized in the models have been extracted from the MCNP output (when available) and provided in Table 6.3-4. The  $S(\alpha,\beta)$  card LWTR.60T is used to simulate hydrogen bound to water in all models. For the TRIGA models only, the  $S(\alpha,\beta)$  cards H/ZR.60T and ZR/H.60T are used to simulate hydrogen and zirconium in zirconium hydride, respectively.

All cases are run with 2500 neutrons per generation for 250 generations, skipping the first 50. The 1-sigma uncertainty is approximately 0.001 for the HAC cases, and somewhat less for the NCT cases.

Case ID	MITR-II Parametric Study Case Description
PN1	Base MITR-II case
PN2	Decrease active fuel length to minimum value
PN3	Increase active fuel length to maximum value
PN4	Increase channel width to maximum value
PN5	Decrease width of fuel meat to minimum value
PN6	Increase width of fuel meat to maximum value
PN7	Combine cases PN4 and PN6

The geometry of base MITR-II parametric Case PN1 is shown in Figure 6.9-1. The fuel element is reflected with approximately 12-in of water. Note that, like the MURR parametric model, the MITR-II parametric model is an explicit geometrical representation of the MITR-II fuel element.

The results of the parametric analysis are summarized in Table 6.9-7. Because the uncertainty in the calculation is  $\sim 0.001$ , a difference of at least 0.002 (2 milli-k, abbreviated mk) between the various cases is required in order to distinguish a real effect from statistical fluctuation. The variation of the active fuel length has a negligible effect on the results. Although Case PN2 shows a positive reactivity increase when the active fuel height is reduced, because the increase is less than 2 mk, it is concluded that the increase is simply statistical fluctuation. Also, the fuel shows a positive reactivity increase of 11.0 mk when the fuel meat is widened and the channel width is increased (compare Case PN7 with Case PN1). This result is consistent with the results obtained in the ATR and MURR fuel parametric analyses. Therefore, in all MITR-II fuel models, the fuel is modeled with nominal active fuel length, maximum fuel width, and maximum channel width. The maximum channel width is achieved by artificially reducing the cladding thickness.

#### 6.9.2.4 TRIGA Fuel Parametric Evaluation

For the TRIGA fuels, the objective of the parametric analysis is to select the most reactive fuel type for use in the criticality analysis from the five types under consideration. To select the bounding fuel element type, simple moderated pin cell models with infinite square reflection are developed. The lattice pitch is varied for each model by adjusting the location of the reflective surfaces. The pin cell model for each of the fuel element types is shown in Figure 6.9-2. The pin cell models are based upon the data provided in Table 6.2-7. Note that the Type 203 fuel element is not modeled explicitly, since it is essentially the same as Type 103.

The pin cell results are summarized in Table 6.9-8. The most reactive TRIGA fuel type is Type 109 (Case PT20), which is the HEU fuel element. In these cases, the thin molybdenum disc between the fuel and bottom reflector is omitted. In Case PT23, Case PT20 is run with the molybdenum disc modeled explicitly. The reactivity is slightly less, but within the statistical uncertainty of the method. Therefore, this fuel type (without the molybdenum disc) is used for all TRIGA analysis in this calculation.

**Table 6.9-8 – TRIGA Fuel Pin Cell Results**

Case ID	Filename	Pitch (cm)	$k_{\text{eff}}$	$\sigma$	$k_s$ ( $k+2\sigma$ )
<b>Type 101 (8 wt.% aluminum clad)</b>					
PT1	C101_P19	0.38	1.38089	0.00099	1.38287
PT2	C101_P22	0.44	1.31512	0.00086	1.31684
PT3	C101_P25	0.50	1.21166	0.00082	1.21330
<b>Type 103/203 (8.5 wt.% stainless steel clad)</b>					
PT10	C103_P19	0.38	1.31017	0.00085	1.31187
PT11	C103_P22	0.44	1.22796	0.00092	1.22980
PT12	C103_P25	0.50	1.13356	0.00080	1.13516
<b>Type 109 (8.5 wt.% stainless steel clad, HEU)</b>					
<b>PT20</b>	<b>C109_P19</b>	<b>0.38</b>	<b>1.59214</b>	<b>0.00094</b>	<b>1.59402</b>
PT21	C109_P22	0.44	1.55156	0.00095	1.55346
PT22	C109_P25	0.50	1.47780	0.00097	1.47974
PT23	C109_P19M	0.38	1.59058	0.00090	1.59238
<b>Type 117 (20 wt.% stainless steel clad)</b>					
PT30	C117_P19	0.38	1.45689	0.00095	1.45879
PT31	C117_P22	0.44	1.43108	0.00090	1.43288
PT32	C117_P25	0.50	1.36660	0.00093	1.36846

## 7.0 PACKAGE OPERATIONS

### 7.1 Procedures for Loading the Package

This section delineates the procedures for loading a payload from the BRR packaging. Hereafter, reference to specific BRR packaging components may be found in Appendix 1.3.3, *Packaging General Arrangement Drawings*.

#### 7.1.1 Preparation for Loading

1. Remove the BRR package tie-down cover from the upper impact limiter.
2. Attach rigging to the upper impact limiter using the three (3) 1/2-13 UNC threaded holes marked as impact limiter lift points.
3. Remove the (8) eight Ø1-inch ball lock pins from each upper impact limiter attachment.
4. Using an overhead crane (or equivalent), lift and remove the upper impact limiter from the cask body.
5. Secure the lift adaptor to the cask body using the four (4) 1-8UNC bolts. Tighten the bolts to  $220 \pm 20$  ft-lb torque.
6. Remove the (8) eight Ø1-inch ball lock pins from each lower impact limiter attachment.
7. Lift the cask body from the lower impact limiter, and place it on the facility transport equipment.
8. Secure the cask body to the facility transport equipment, and remove the rigging from the lift adaptor.

#### 7.1.2 Loading of Contents

1. Remove the twelve (12) 1-8UNC socket head cap screws (SHCSs) that retain the closure lid.
2. Install three (3) hoist rings (or equivalent) into the three (3) 1/2-13 UNC threaded holes in the closure lid.
3. Lift and remove the closure lid from the cask body. Store the closure lid in a manner to minimize potential damage to the O-ring seals and sealing surfaces.
4. Install and secure the sealing surface protector to the cask body.
5. Using the center 1/2-13 UNC threaded hole in the shield plug as a lift point, remove the shield plug from the cask body.
6. If not previously installed, install the appropriate fuel basket into the cask body cavity as follows:
  - a. For the MURR basket, use the 3/8-16UNC threaded hole.
  - b. For the MITR-II basket, use the two (2) 3/8-16UNC threaded holes.
  - c. For the ATR basket, use the 3/8-16UNC threaded hole.

- d. For the TRIGA basket, use the 3/8-16UNC threaded hole.
7. Remove the drain port dust cover and then the drain port plug. Install an appropriate fitting to the drain port.
8. Using an overhead crane (or equivalent), and attached to the lift adaptor, lift the cask body with the fuel basket from the facility transport equipment and position over the spent fuel pool staging area.
9. Slowly lower the cask body into the pool until the cavity is flooded, and the cask body is secure in the facility fuel loading station.
10. Load a fuel element into each fuel channel in the fuel basket.
  - a. Up to eight (8) MURR fuel elements may be loaded into the basket.
  - b. Up to eleven (11) MITR-II fuel elements may be loaded into the basket.
  - c. Up to eight (8) ATR fuel elements may be loaded into the basket.
  - d. Up to nineteen (19) TRIGA fuel elements may be loaded into the basket.
11. Using the center 1/2-13 UNC threaded hole as a lift point, lower the shield plug into the cask body cavity. Visually verify that the shield plug is properly seated, and reposition if necessary.
12. Install the shield plug restraint, or optionally, install the shield plug restraint once the cask body has been raised to the working level.
13. Lift the loaded cask body from the spent fuel pool while spraying exposed portions with clean demineralized water. Perform a radiological survey of the cask body as it is raised out of the pool.
14. Open the drain fitting to drain the pool water from the cavity. Continue draining the cavity until no appreciable water is noted. Optionally, the cavity may be drained after securing the cask body in the facility work area.
15. Close the drain fitting, and remove the connecting plumbing from the drain fitting.
16. Lift the loaded cask body out of the spent fuel pool area and secure it in the facility work area.
17. Perform a survey of the exterior surfaces of the cask body to determine that smearable surface contamination meets the requirements of 10 CFR §71.87(i) [1] and 49 CFR §173.443 [2]; decontaminate exposed exterior surfaces that exceed the allowable contamination levels.
18. Visually inspect both closure lid main O-ring seals. If necessary, remove the O-ring seal(s) and clean the seal(s) and the sealing surface(s) on the closure lid and cask body to remove contamination. If, during the visual examination, it is determined that damage to the O-ring seal(s) and/or sealing surface(s) is sufficient to impair containment integrity (e.g., cuts, tears, and/or joint separation in O-ring material, or scratches and/or indentations in sealing areas), replace the damaged seal(s) and/or repair the damaged sealing surface(s) per Section 8.2.3.2, *Sealing Area Routine Inspection and Repair*.
19. As an option, remove and sparingly apply vacuum grease to the O-ring seals and/or sealing surfaces. Reinstall O-ring seals into the appropriate seal grooves in the closure lid.



20. Remove the sealing surface protector and shield plug restraint from the shield plug and cask body.
21. Visually inspect the cask body sealing surface, and clean of contamination or water as necessary. If damage sufficient to impair containment integrity is found, repair the damaged surface per Section 8.2.3.2, *Sealing Area Routine Inspection and Repair*.
22. Install the closure lid on the cask body, using the alignment pin to guide the closure lid into position.
23. Visually inspect the closure SHCSs for wear or damage that could impair their function and, if necessary, replace or repair per the requirements of the drawings in Appendix 1.3.3, *Packaging General Arrangement Drawings*.
24. Install the twelve (12) 1-8UNC SHCSs to secure the closure lid to the cask body. Using a star pattern, tighten the closure SHCSs to  $220 \pm 20$  ft-lb torque (lubricated).
25. Remove the vent port dust cover and the vent port plug.
26. Remove the drain port fitting from the drain port.
27. Visually inspect the drain and vent port sealing surfaces and sealing washers. If necessary, clean the sealing surfaces on the drain and vent ports to remove contamination. If, during the visual examination, it is determined that damage to a sealing surface or a sealing washer is sufficient to impair containment integrity (e.g., cuts, tears, and/or joint separation in sealing material, or scratches and/or indentations in sealing areas), repair the damaged sealing surface per Section 8.2.3.2, *Sealing Area Routine Inspection and Repair*, and/or replace the sealing washers.
28. Install the drain port plug and sealing washer in the drain port. Tighten the drain port plug to  $40 \pm 4$  ft-lb torque.
29. Install the vent port plug and sealing washer to the vent port tool, and then install the vent port tool into the vent port.
30. Connect a vacuum pump to the vent port tool and evacuate the cavity until the internal pressure is 1 – 2 torr. Isolate the vacuum pump from the cask body cavity.
31. Monitor the cavity pressure for a minimum of 30 minutes. If the cavity pressure does not exceed 3 torr at the end of the time period, proceed to Step 35.
32. If the pressure exceeds 3 torr, open the port tool to re-pressurize the cask body cavity to atmospheric pressure. Repeat Steps 30 and 31.
33. If after eight (8) hours of vacuum drying with air and the pressure exceeds 3 torr, disconnect the vacuum pump from the vent port tool and connect a source of helium gas.
34. Provide a helium atmosphere inside the cask payload cavity by backfilling with helium gas to a pressure of slightly greater than atmospheric pressure, i.e., +1, -0 psig. Repeat Steps 30 and 31.
35. Disconnect the vacuum pump from the vent port tool and connect a source of helium gas.
36. Provide a helium atmosphere inside the cask payload cavity by backfilling with helium gas to a pressure of slightly greater than atmospheric pressure, i.e., +1, -0 psig.
37. Disconnect the helium gas source from the vent port tool.

38. Using the vent port tool, install the vent port plug and sealing washer in the vent port. Tighten the vent port plug to  $9 \pm 1$  ft-lb torque.
39. Leakage rate testing of the main containment O-ring seal, the drain port sealing washer, and the vent port sealing washer shall be performed based on the following criteria:
  - a. If the inner main O-ring seal (containment), the drain port sealing washer, and/or vent port sealing washer are replaced, or the corresponding sealing surface(s) were repaired, then perform the maintenance/periodic leakage rate test per Section 8.2.2.2, *Helium Leakage Rate Testing the Main Containment O-ring Seal*, Section 8.2.2.3, *Helium Leakage Rate Testing the Drain Port Sealing Washer*, or Section 8.2.2.4, *Helium Leakage Rate Testing the Vent Port Sealing Washer*, as appropriate.
  - b. If the inner main O-ring seal (containment), the drain port sealing washer, and/or vent port sealing washer are not replaced, nor the corresponding sealing surface(s) repaired, then perform preshipment leakage rate testing per Section 7.4, *Preshipment Leakage Rate Test*, or per Section 8.2.2.2, *Helium Leakage Rate Testing the Main Containment O-ring Seal*, or Section 8.2.2.3, *Helium Leakage Rate Testing the Drain Port Sealing Washer*, or Section 8.2.2.4, *Helium Leakage Rate Testing the Vent Port Sealing Washer*, as appropriate.
  - c. At the conclusion of all leakage rate testing, install the drain port dust cover and the vent port dust cover.

### 7.1.3 Preparation for Transport

1. Utilizing the lift adaptor, lift and lower the cask body into the lower impact limiter that is located on the transport trailer. Ensure that the cask body is aligned with the impact limiter alignment stripe for correct circumferential location.
2. Install the (8) eight  $\varnothing 1$ -inch ball lock pins into each lower impact limiter attachment.
3. Remove the (4) four 1 – 8 UNC bolts that attach the lift adaptor to the cask body. Remove the lift adaptor.
4. Lift and lower the upper impact limiter onto the cask body. Ensure that the upper impact limiter is aligned with the cask body stripe for correct circumferential location.
5. Install the (8) eight  $\varnothing 1$ -inch ball lock pins into each upper impact limiter attachment.
6. Install the tamper-indicating device (security seal) in the appropriate upper impact limiter attachment location.
7. Remove the rigging from the upper impact limiter lift points.
8. Install the BRR package tie-down cover over the upper impact limiter, and secure the cover to the semi-trailer using the tie-down attachments.
9. Monitor external radiation for each loaded BRR package per the requirements of 49 CFR §173.441.
10. Determine that surface contamination levels for each loaded BRR package is per the requirements of 49 CFR §173.443.

11. Determine the transport index for each loaded BRR package per the requirements of 49 CFR §173.403.
12. Complete all necessary shipping papers in accordance with Subpart C of 49 CFR 172 [3].
13. BRR package marking shall be in accordance with 10 CFR §71.85(c) and Subpart D of 49 CFR 172. Package labeling shall be in accordance with Subpart E of 49 CFR 172. Package placarding shall be in accordance with Subpart F of 49 CFR 172.